Responsive Coatings Made from Colloidal Building Blocks

DISSERTATION

zur Erlangung des akademischen Grades eines
Doktors der Naturwissenschaften
(Dr. rer. nat.)
an der
Bayreuther Graduiertenschule für Mathematik und Naturwissenschaften
der Universität Bayreuth

vorgelegt von

Inna Dewald

geboren in Komsomolez / Kasachstan

Oktober 2016

Die vorliegende Arbeit wurde in der Zeit von Februar 2013 bis Oktober 2016 am Lehrstuhl Physikalische Chemie II der Universität Bayreuth unter Betreuung von Herrn Prof. Dr. Andreas Fery angefertigt.

Vollständiger Abdruck der von der Bayreuther Graduiertenschule für Mathematik und Naturwissenschaften (BayNat) der Universität Bayreuth genehmigten Dissertation zur Erlangung des akademischen Grades eines Doktors der Naturwissenschaften (Dr. rer. Nat.).

Dissertation eingereicht am:	10.10.2016
Zulassung durch das Leitungsgremium:	18.10.2016
Wissenschaftliches Kolloquium:	31.03.2017

Amtierender Direktor:	Prof. Dr. Stephan Kümmel

Prüfungsausschuss:

Prof. Dr. Andreas Fery	(Erstgutachter)
Prof. Dr. Georg Papastavrou	(Zweitgutachter)
Prof. Dr. Peter Strohriegl	(Vorsitz)
Prof. Dr. Birgit Weber	

“I am just a child who has never grown up.
I still keep asking these 'how' and 'why' questions.
Occasionally, I find an answer.”

Stephen Hawking

Meiner Familie

Table of Contents

Summary

The main scope of this thesis was the investigation of stimuli responsive soft colloidal particles based coating materials. The soft colloids differed in their origin (natural or synthetic), stimulus responsiveness (pH, ionic strength or temperature), and architectural features (patchiness, crosslinking gradient, compartments). The main focus of this study was understanding fundamental aspects of the interplay between the surface, the colloid, and the changes in the environmental conditions, such as pH or ionic strength. Additionally, the collective properties of the coatings with regard to their architectural features were investigated.

The objectives of the thesis are divided in two main parts: (1) the investigation of the interplay between the coating material and the surface under controlled environmental conditions and (2) the collective swelling behavior of mono- and multilayer coatings as a response to external triggers.

In the first part, the stimulus-induced behavior of polyampholytic particles, such as proteins and multicompartment micelles, was investigated at the solid-liquid interface. Specifically, the changes in stimulus response and morphology of the particles and changes in the surface's properties upon particle adsorption were monitored as a function of the external stimulus.

In the case of protein coatings, gold nanoparticles (AuNPs) were used as the model substrates. Due to their plasmonic properties, these particles provide a convenient tool to monitor changes in the environmental conditions. To understand the general trends on the subject of interactions between the AuNPs and proteins, 10 different proteins were used as coating materials, thereby covering a broad range of molecular weights (M_w) and isoelectric points (pI). For the adsorption step both components, proteins and AuNPs, were mixed together. Provided the protein concentration is high enough and the environmental pH is outside the pI range, the coating process results in a complete surface coverage and a stable colloid dispersion of protein coated AuNPs (Au@Protein). Moreover, we found that these systems are very robust, hence stable Au@Protein particles can be recovered even from agglomerated mixtures by changing the pH and removing the excess of protein. Subsequently, the purified Au@Protein particles (no excess of protein) were investigated in terms of their pH-dependent colloidal stability. We discovered that protein-specific shifts in the pI as compared to bare proteins, depend on the availability of acidic and basic functional groups after protein adsorption. Furthermore, the solubility profiles of Au@Protein were of different shape, either U- or S-shaped, depending on the protein's M_w and thereby on the stabilization mechanism, and partially on the starting pH. This study demonstrates

the impact of the particles and the surface on each other's properties under different environmental conditions. This knowledge is crucial for a safe use of hybrid particles in biomedical applications.

Further, to investigate the interplay between soft colloids and an interface for a different system, polyampholytic micelles from an ABC triblock terpolymer were immobilized on a silica surface. The block polyampholyte BMAAD consists of a hydrophobic polybutadiene (B) block, a poly(methacrylic acid) (MAA) middle block, and a poly(2-(dimethylamino)ethyl methacrylate) (D) block. In an aqueous solution at pH 2, the polymer self-assembles into micellar aggregates with a hydrophobic B core, an uncharged / collapsed MAA shell surrounded by a positively charged D corona. Due to their immobilization on the surface and the interpolyelectrolyte complex formation between the polyacid and the polybase at moderate pH values (pH 5-9), the apparent dissociation constants of both polyelectrolyte blocks shifted to higher values, thereby further separating the response of the polyacid (swelling at pH < 5) and the polybase (swelling at pH > 10). In view of future applications, e.g. as charge switchable surfaces, possible p*K* shifts are important because they determine the operation range for the charge inversion. Moreover, a change in pH from pH 2 to pH 11 induced morphological changes in the micellar structure. At pH 11, the repulsive interactions inside the negatively charged shell and those between the micelle and the negatively charged silica surface forced the BMAAD micelles to split into clusters of well-defined submicelles. This phenomenon shows the intricate interplay between competing forces, imposed on the micelles via the environmental conditions and the surface charges. Furthermore, these findings present the first example of surface-assisted formation of colloidal clusters. The in situ approach at the interface opens an avenue toward the formation of hierarchical structures.

In the second part, the collective swelling behavior of particulate mono- and multilayer systems in response to external triggers was investigated for thermoresponsive microgel particles and amphiphilic multicompartment micelles. A special attention was given to the architectural features of the soft colloids, which equip the resulting coatings with enhanced functionality in terms of stimulus response.

Due to a steep crosslinking gradient, and the volume phase transition at ~32 °C, the internal structure of the poly(*N*-isopropylacrylamide) microgel particles allowed to switch the microgel monolayer coatings between a cell-attractive (collapsed) state at 37 °C and a cell-repellent (swollen) state at 25 °C. To prepare cell culture substrates for noninvasive processing of adherent cells, thermoresponsive microgels were immobilized in patterned patches (spots) using inkjet printing and microcontact printing techniques. Furthermore, we demonstrated the applicability of the patterned microgel coatings for wound healing assays and drug screening experiments. For this purpose, patterned substrates were mounted in a microfluidic channel. The cell proliferation, changes in morphology, detachment, and resettlement cycles were monitored in situ for different cell lines, in the presence and absence of a migration-inhibiting compound (locostatin). Our results suggest that the microgel-covered spots provide an excellent platform for various noninvasive cell studies, with high accuracy and reproducibility, rendering quantitative comparison between cell lines possible.

In the next step, multilayer films from triblock terpolymer multicompartment micelles – with a hydrophobic B core, a pH-sensitive MAA shell and a permanently charged corona of quaternized D (i.e., Dq) – and a strong polyanion, poly(sodium 4-styrene sulfonate) (PSS), were assembled in an alternating manner. The complexation of the positively charged Dq corona with the negatively charged PSS provides the resulting films with pH-independent stability. At the same time, the pH-responsive MAA shell, which is not involved in the multilayer assembly, exhibits an enhanced stimulus response due to the spatial confinement between both the micellar core and the multilayer-forming Dq/PSS interpolyelectrolyte complex. Thus, stability and responsiveness are ensured due to decoupling of coherence and functionality via compartmentalization. Moreover, the introduction of a second stimulus, the ionic strength, results in the response of two compartments – the brush-like MAA shell and the Dq/PSS complex. Both compartments can be addressed separately via the choice and the range of the stimulus. Thus, a targeted addressing of different compartments opens new perspectives for surface-mediated drug co-delivery.

In summary, this work presents a broad range of coatings based on soft colloidal particles. The colloidal building blocks from water-soluble and stimuli-responsive macromolecules represent an interesting class of coating materials. Depending on the choice of the particle's internal architecture, the following aspects in the functionality of the resulting coatings can be enhanced: In the case of microgel particles, the density and distribution of the crosslinks determines the range of the phase transition and the mechanical properties of the film. The use of block copolymer micelles as building blocks introduces separate compartments into the coating, thus providing the coating with multifunctionality. The coatings developed in this study are water-based systems with a user-friendly handling. Thus, they meet important requirements for an industrial scale processing and represent the first step toward the development of advanced coatings.

Zusammenfassung

Der Schwerpunkt dieser Doktorarbeit war die Untersuchung von stimuli-responsiven Beschichtungsmaterialen, welche auf weichen kolloidalen Partikeln basieren. Dabei unterscheiden sich die kolloidalen Systeme in ihrer Entstehung (natürlich vorkommend oder synthetisch), ihrer Reaktionsfähigkeit auf einen externen Stimulus (pH, Ionenstärke oder Temperatur) und den, durch ihre interne Architektur bedingten, Besonderheiten (Vernetzungsgradient, Unterteilung in Bereiche bzw. Kompartimente). Im Fokus dieser Untersuchung stand insbesondere das Verständnis fundamentaler Aspekte in Bezug auf die Wechselwirkung zwischen einer Oberfläche und den kolloidalen Partikeln, unter Berücksichtigung der externen Bedingungen wie pH oder Ionenstärke. Zusätzlich wurden die kollektiven Eigenschaften der Oberflächenbeschichtungen hinsichtlich der jeweiligen architektonischen Besonderheiten analysiert.

Die Ziele dieser Arbeit lassen sich in zwei Hauptbereiche unterteilen: (1) Die Untersuchung der wechselseitigen Einflussnahme von Oberfläche und Beschichtungsmaterial unter kontrollierten Bedingungen und (2) das kollektive Quellverhalten von Mono- und Multilagenfilmen als Reaktion auf externe Stimuli.

Der erste Teil dieser Arbeit befasst sich mit der Untersuchung des, durch externe Bedingungen verursachten, Verhaltens von polyamphoteren Partikeln wie Proteinen und Multikompartimentmizellen an der Fest-Flüssig-Grenzfläche. Die Eigenschaften von Oberflächen ließen sich durch Adsorption der responsiven Partikel gezielt modifizieren.

Für die Beschichtung mit Proteinen wurden Goldnanopartikel (AuNPs) als Modelsubstrat verwendet. Aufgrund ihrer optischen (plasmonischen) Eigenschaften stellen die Partikel ein nützliches Werkzeug zur Beobachtung der Änderungen in der näheren Umgebung dar. Um die allgemeinen Trends in Bezug auf die Wechselwirkung zwischen AuNPs und den Proteinen herauszuarbeiten, wurden 10 verschiedene Proteine als Beschichtungsmaterial verwendet. Durch die Wahl der Proteine konnten große Bereiche an Molekulargewichten (M_w) und isoelektrischen Punkten (pI) abgedeckt werden. Für die Adsorption wurden beide Komponenten, das jeweilige Protein und die Goldnanopartikel, gemischt. Unter der Voraussetzung, dass die Proteinkonzentration hoch genug war und der pH außerhalb des pI-Bereichs lag, resultierte der Beschichtungsprozess in einer vollständigen Oberflächenbedeckung und führte zu stabilen Kolloiddispersionen, bestehend aus proteinbeschichteten AuNPs (Au@Protein). Außerdem konnte festgestellt werden, dass diese Systeme sehr robust sind, weshalb durch pH-Änderung und

Entfernung des überschüssigen Proteins aus den agglomerierten Protein-AuNPs-Mischungen stabile Au@Protein Partikel gewonnen werden konnten. Anschließend wurden die aufgereinigten Au@Protein Systeme im Hinblick auf ihre pH-abhängige, kolloidale Stabilität untersucht. Dabei wurden proteinspezifische Verschiebungen des pIs im Vergleich zum freien Protein beobachtet, welche von dem Verhältnis und der Verfügbarkeit von funktionellen Säure- und Basengruppen nach der Proteinadsorption abhängen. Des Weiteren zeigten die Systeme verschiedene Löslichkeitsprofile, die in Abhängigkeit vom M_w und damit vom Stabilisierungsmechanismus, aber auch vom ursprünglichen pH, entweder U- oder S-förmig waren. Diese Ergebnisse demonstrieren welchen Einfluss die Oberfläche und die Partikel unter bestimmten Bedingungen jeweils auf die Eigenschaften des anderen ausüben können. Das Wissen über die dadurch hervorgerufenen Änderungen im resultierenden Hybridsystem ist entscheidend für einen bedenkenlosen Einsatz dieser Systeme in biomedizinischen Anwendungen.

Zur Untersuchung der gegenseitigen Einflussnahme zwischen Oberfläche und Kolloid, wurden polyamphotere Mizellen, bestehend aus einem ABC Triblockterpolymer, auf einer Siliziumoberfläche immobilisiert. Der Blockpolyampholyt BMAAD besteht aus einem hydrophoben Polybutadienblock (B), einem mittleren Polymethacrylsäureblock (MAA) und einem Endblock aus Poly(2-dimethylamino)ethylmethacrylat) (D). In einem wässrigen Medium mit pH 2 aggregieren die Polymerketten zu mizellaren Stukturen mit einem hydrophoben B-Kern, einer ungeladenen und kollabierten MAA-Schale und einer positiv geladenen D-Korona. Infolge der Immobilisierung an der Oberfläche und der Bildung eines Interpolyelektrolytkomplexes zwischen der Polysäure und der Polybase im pH-Bereich 5-9 verschieben sich die apparenten Dissoziationskonstanten beider Blöcke zu höheren Werten. Damit quellen Polysäure (pH < 5) und Polybase (pH > 10) auf der pH-Skala weiter voneinander entfernt auf. Im Hinblick auf zukünftige Anwendungen, z.B. als Oberflächen mit schaltbarer Ladung, müssen solche Verschiebungen der p*K*-Werte berücksichtigt werden, weil sie den Anwendungsbereich maßgeblich beeinflussen. Außerdem konnten bei einem pH-Wechsel von pH 2 zu pH 11 Änderungen der mizellaren Morphologie beobachtet werden. Aufgrund von repulsiven Wechselwirkungen sowohl in der MAA-Schale als auch zwischen den Mizellen und der negativ geladenen Siliziumoberfläche in pH 11, teilten sich die BMAAD Mizellen in Cluster, welche aus definierten Submizellen bestanden. Dieses Phänomen zeigt komplexe Wechselwirkungen zwischen den konkurrierenden Kräften, welche durch die äußeren Bedingungen und den Einfluss der Oberflächenladung auf die Mizellen wirken. Durch dieses Beispiel wurde zusätzlich ein Ansatz zur In-Situ-Herstellung von oberflächenunterstützten kolloidalen Clustern demonstriert und damit ein neuer Weg zur Herstellung von hierarchischen Strukturen geebnet.

Im zweiten Teil der Arbeit wurde das kollektive Quellverhalten von partikulären Mono- und Multilagensystemen von thermoresponsiven Mikrogelpartikeln und amphiphilen Multikompartiment-mizellen als Reaktion auf äußere Einflüsse untersucht. Ein besonderes Augenmerk wurde dabei auf die architekturbedingten Besonderheiten der weichen Kolloide gelegt, welche die resultierenden

Beschichtungen mit einer stärker ausgeprägten Funktionalität in Bezug auf die, durch den Stimulus ausgelöste Reaktion ausstatten.

Aufgrund eines steilen Vernetzungsgradienten und einer Volumenphasenübergangstemperatur bei ~32° C, konnten oberflächenimmobilisierte Poly(*N*-isopropylacrylamid)-Mikrogelmonolagen zwischen einem zellattraktiven (kollabierten) Zustand bei 37 °C und einem zellabweisenden (gequollenen) Zustand bei 25 °C geschaltet werden. Zur Herstellung von Zellkultursubstraten für die nichtinvasive Verarbeitung von adhärenten Zellen wurden die thermoresponsiven Mikrogele, mit Hilfe von Verfahren wie dem Mikrokontaktdruck und dem Tintenstrahldruck, in Form von kreisrunden Strukturen auf der Oberfläche immobilisiert. Des Weiteren wurde die Anwendbarkeit der durch Mikrogelpartikel strukturierten Oberflächen für die Wundheilungsanalyse und das Wirkstoffscreening demonstriert. Hierfür wurden die modifizierten Substrate in einen Mikrofluidikkanal eingebaut und das Zellwachstum, Änderungen in der Zellmorphologie, sowie die Ablösung und Wiederbesiedlung der Zellen in-situ überwacht. Das Experiment wurde sowohl in Anwesenheit, als auch in Abwesenheit eines migrationshemmenden Wirkstoffes (Locostatin) durchgeführt. Unsere Ergebnisse zeigen, dass die mit Mikrogelen beschichteten Oberflächen eine hervorragende Plattform für verschiedene nichtinvasive Zellstudien mit einer hohen Genauigkeit und Reproduzierbarkeit bieten, welche außerdem einen quantitativen Vergleich verschiedener Zelllinien ermöglichen.

Im nächsten Schritt wurden Multilagenfilme, basierend auf der alternierenden Assemblierung von Triblockterpolymermultikompartimentmizellen – bestehend aus einem hydrophoben B-Kern, einer pH-sensitiven MAA-Schale und einer permanent geladenen Korona aus quaternisiertem D (Dq) – und einem starken Polyanion, Natriumpolystyrolsulfonat (PSS) aufgebaut. Die Komplexierung der positiv geladenen Dq-Korona mit negativ geladenem PSS sorgte für eine pH-unabhängige Stabilität der resultierenden Filme. Gleichzeitig konnte durch die Begrenzung der pH-sensitiven MAA-Schale auf den Bereich zwischen dem hydrophoben Kern und dem multilagenbildenden Dq/PSS-Interpolyelektrolytkomplex eine stärker ausgeprägte Reaktion auf einen Stimulus erzielt werden. Durch die interne Kompartimentierung und damit die Entkopplung von Kohärenz und Funktionalität konnten sowohl die Stabilität als auch die Reaktionsfähigkeit der Filme auf Stimuli gewährleistet werden. Ein zusätzlicher Stimulus, die Ionenstärke, führt zur Reaktionsfähigkeit von zwei Kompartimenten – der MAA-Schale und dem Dq/PSS-Komplex. Durch die Wahl des Stimulus und dessen Bereich können beide Regionen unabhängig voneinander angesteuert werden. Diese Funktion ermöglicht das gezielte Schalten verschiedener Bereiche des Films zwischen einem gequollenen und einem kollabierten Zustand und eröffnet damit neue Möglichkeiten für eine oberflächenvermittelte Verabreichung mehrerer Wirkstoffe.

Zusammenfassend präsentiert diese Arbeit verschiedene Ansätze zur Beschichtung von Oberflächen, basierend auf weichen kolloidalen Partikeln. Die kolloidalen Bausteine, bestehend aus wasserlöslichen und stimuli-responsiven Makromolekülen, repräsentieren eine interessante Klasse von

Beschichtungsmaterialien. Durch eine gezielte Wahl ihrer internen Architektur konnten folgende Aspekte der Funktionalität der resultierenden Oberflächen positiv beeinflusst werden: Im Fall von thermoresponsiven Mikrogelen haben die Dichte und die Verteilung der Vernetzungspunkte einen starken Einfluss auf die Breite des Phasenübergangs und die mechanischen Eigenschaften des Polymers. Die Verwendung von Multikompartimentmizellen hat den Vorteil, dass die unterschiedlichen Bereiche des Films unabhängig voneinander geschaltet werden können und damit verschiedene Funktionen in einer Beschichtung vereinen. Die hier entwickelten Oberflächenbeschichtungen sind wasserbasierende Systeme mit einer einfachen Handhabung. Damit erfüllen sie wichtige Voraussetzungen für eine umweltfreundliche Implementierung in industriellen Prozessen und sind der erste Schritt auf dem Weg zur Entwicklung intelligenter Beschichtungen.

List of Publications

1. *Reversible Swelling Transitions in Stimuli-Responsive Layer-by-Layer Films Containing Block Copolymer Micelles.*
   Gensel. J.; **Dewald, I.**; Erath, J.; Betthausen, E.; Müller, A. H. E.; Fery. A., *Chem. Sci.* **2013**, *4* (1), 325-334.

2. *Co-Assemblies of Micelle-Forming Diblock Copolymers and Enzymes on Graphite Substrate for an Improved Design of Biosensor Systems.*
   Sigolaeva, L. V.; Pergushov, D. V.; Synatschke, C. V.; Wolf, A.; **Dewald, I.**; Kurochkin, I. N.; Fery, A.; Müller, A. H. E.; *Soft Matter* **2013**, *9* (10), 2858-2868.

3. *Protein Identity and Environmental Parameters Determine the Final Physico-Chemical Properties of Protein-Coated Metal Nanoparticles.*
   Dewald, I.; Isakin, O.; Schubert, J.; Kraus, T.; Chanana, M.; *J. Phys. Chem. C* **2015**, *119* (45), 25482-25492.

4. *Patterned Thermoresponsive Microgel Coatings for Noninvasive Processing of Adherent Cells.*
   Uhlig, K., Wegener, T.; He, J.; Zeiser, M.; Bookhold, J.; **Dewald, I.**; Godino, N.; Jaeger, M.; Hellweg, T.; Fery, A.; Duschl, C.; *Biomacromolecules* **2016**, *17* (3), 1110-1116.

5. *Splitting of Surface-Immobilized Multicompartment Micelles into Clusters upon Charge Inversion.*
   Dewald, I.; Gensel, J.; Betthausen, E.; Borisov, O. V.; Müller, A. H. E.; Schacher, F. H.; Fery, A.; *ACS Nano* **2016***, 10* (5), 5180-5188.

6. *Polymeric Micelles and Vesicles in Polyelectrolyte Multilayers: Introducing Hierarchy and Compartmentalization.*
   Dewald, I.; Fery, A.; *Adv. Mater. Interfaces* **2017**, *4* (1), 1600317 (1-11).

7. *Impact of Compartmentalization on the Salt-Induced Swelling in Block Copolymer Micelle Multilayers.*
   Dewald, I.; Gensel, J.; Erath, J.; Leluk, A.; Betthausen, E.; Borisov, O. V.; Müller, A. H. E.; Schacher, F. H.; Fery, A.; *to be submitted.*

Awards

- **Outstanding Poster Award**: *Stimuli-Responsive Layer-by-Layer Films Containing Block Copolymer Micelles,* the DPG Spring Meeting 2012, Berlin.

- **Travel Grant** for the Summer School of the Core Facility BioSupraMol (FU Berlin) "Biointerfaces and Surface Characterization" 2015, Berlin.

List of Abbreviations and Symbols

AA	amino acid
AFM	atomic force microscopy
cmc	critical micellization concentration
c_i	concentration of compound i
c_s	salt concentration
D	diffusion coefficient
DLS	dynamic light scatter
dl	double layer
e	elementary charge
F	force
h	separation distance
H	Hamaker constant
I	ionic strength
IPEC	interpolyelectrolyte complex
k_B	Boltzmann constant
k_BT	thermal energy
l_B	Bjerrum length
LbL	layer-by-layer
LCST	lower critical solution temperature
LCSC	lower critical solution concentration
l_e	distance between elementary charges
l_{eff}	effective charge distance
LSPR	localized surface plasmon resonance

m-IEP	micellar isoelectric point
M_w	molecular weight
N_A	Avogadro's number
NP(s)	nanoparticle(s)
P	packing parameter
RSA	random sequential adsorption
PE	polyelectrolyte
PEM	polyelectrolyte multilayer
pI	isoelectric point
pK_a, pK_b	logarithmic dissociation constants
PEO	poly(ethylene oxide)
PNIPAM	poly(*N*-isopropylacrylamide)
PDMAEMA	poly(2-(dimethylamino)ethyl methacrylate)
q_s	salt valence
P	packing parameter
R	radius
t	time
T	temperature
V	volume
vdW	van der Waals
VPTT	volume phase transition temperature
W	energy
α, α'	degree of dissociation, degree of neutralization
ε	dielectric constant
ε_0	permittivity of vacuum
θ	surface coverage
κ^{-1}	Debye screening length
χ	(Flory-Huggins) interaction parameter
ψ	electric potential

1 Introduction / Motivation

It is well known that coatings cover virtually every surface in our surroundings. Examples of objects covered merely with lacquers and paints are automobiles, planes, ships, buildings, furniture, magazines and data storage devices.[1] Furthermore, edible coatings are widely applied in food industry where they are used for preservation of taste, texture, and appearance during handling, storage, and transportation, resulting in shelf life prolongation.[2] For example, wax coatings have been applied to fruits for centuries, in order to prevent loss of moisture and provide a shiny gloss. Other prominent fields of applications are cosmetics, pharmaceuticals, and textiles. More generally, coatings protect vulnerable material's surface from environmental influences, hence contributing to the overall resource conservation and cost reduction.

The earliest reported paints date back to ~20 000 years B.C. and were mainly used for decorative purposes.[3] As early as ~2 500 B.C., Egyptians developed and applied cedar oil-based varnishes and paints to buildings, sculptures and coffins. As an evidence, well preserved Egyptian artifacts contained very durable coatings fulfilling their purpose beyond simple decoration. For the caulking wooden ships, ancient Egyptians, Greeks, and Romans used substances such as asphalt, pitch, and tar to seal ship timbers. Except for additional metal sheathing for protective reasons, this method remained almost unchanged until steel hulls came into use in 1800s.[4] By that time paints and varnishes have reached the industrial production scale and were the coating of choice.[3, 5]

Even though traditionally, coatings were applied mainly for a decorative and / or protective purpose, for many applications the method of simple passivation of the surface remains insufficient. For example, in the case of sailing vessels, even after several thousand years of experience in trying to prevent the attachment and accumulation of marine organisms, biofouling continues to pose a severe problem.[4-5] The exposure of a chemically inert surface, e.g. a ship hull, to seawater entails almost immediate accumulation of organic compounds at the interface. Their presence encourages the attachment of bacteria, and the resulting biofilm in turn attracts barnacles, algae and other macrofoulers. Both, the additional mass and the increased surface roughness add to ship's hydrodynamic drag, which increases the fuel consumption and leads to increased costs. Initially, to reduce biofouling paints containing copper, tin, or other toxic ingredients were applied. Despite their efficacy, due to ecological concerns, alternative rather non-toxic strategies were employed instead, such as slippery non-stick surfaces based on fluoropolymers and silicones. However, the tenacity of biofilm requires high velocities to dislodge the foulers, which means the coating is practically useless when the ship is in dock or moving slowly.

Today, the problem of biofouling has not been completely resolved, therefore the development of antifouling coatings remains an active area of research.[6]

In recent years, challenges such as biofouling triggered a considerable progress in material and polymer science. The growing demand for functional and *smart* coatings, lead to the development of a broad range of stimuli-responsive materials for various applications.[7] Today numerous surface coatings with different architectures and compositions have been proposed and are available. For instance, self-healing and anti-corrosion films were introduced,[8] as well as substrates for tissue engineering,[9] or materials with sensing abilities.[10]

The key challenge of the development of smart, multifunctional coatings is the introduction of multiple complementary or even synergistic attributes to the surface.[11] Currently, many research projects in the field are driven by requirements for specific applications such as self-cleaning surfaces or surface-mediated targeted drug co-delivery. Thus, there is an increasing demand for versatile coatings, which are biocompatible and stimuli-responsive, and respond to environmental signals in a completely reversible fashion.[12] However, considering that responsiveness for external triggers is coupled with conformational and chemical changes, combining qualities such as structural integrity, stability, and reversible responsiveness is not trivial.

The vital question is: How to equip surface coatings with all the desired attributes – stability, reversible stimulus response, and multifunctionality – all at once?

The answer can be found in nature's ability to secure biological function by spatial separation in highly organized constructs, for example the different organelles in a cell which fulfill different functions. Following nature's lead in compartmentalization, stimuli-responsive colloidal building blocks with internal architectures are used as coating material.

In general, the coatings from colloidal building blocks provide several advantages in terms of stability and functionality, and are the central point of this thesis. The study focuses on the investigation of the soft colloids with respect to stability, changes in their functionality upon adsorption to the surface, as well as the correlation between their architectural features and the stimulus response at the solid-liquid interface. In the first part of the thesis, mainly the mutual influences of polyampholytic colloidal building blocks and the surface on each other's properties are examined under various environmental conditions. In the second part, collective swelling behavior of colloidal mono- and multilayers are investigated. The soft colloids used in this work represent different classes of stimuli-responsive coating materials, such as proteins, thermoresponsive microgel particles, and triblock terpolymer micelles. They differ in terms of their origin, architecture, and stimulus response, providing the resulting coatings with superior properties and performance with respect to specific applications as compared to conventional coatings. The aim of this work is to demonstrate several strategies for the design of novel functional coatings

based on soft colloidal building blocks which would open new perspectives for their potential applications.

References

1. Umweltbundesamt, Use of Nanomaterials in Coatings. *Fact Sheet* **2014**, 1-18.
2. Pavlath, A. E.; Orts, W., Edible Films and Coatings: Why, What, and How? In *Edible Films and Coatings for Food Applications*, Huber, C. K.; Embuscado, E. M., Eds. Springer New York: New York, NY, 2009; pp 1-23.
3. Gooch, J. W., History of Paint and Coatings Materials. In *Lead-Based Paint Handbook*, Springer US: Boston, MA, 2002; pp 13-35.
4. Winner, C., To Banish Biofouling - Can a New Approach Help Sailors Prevent Barnacles and Algae from Coating Ship Hulls? *Oceanus Magazine* **2013,** *50*, 8-11.
5. Chambers, L. D.; Stokes, K. R.; Walsh, F. C.; Wood, R. J. K., Modern Approaches to Marine Antifouling Coatings. *Surface & Coatings Technology* **2006,** *201*, 3642-3652.
6. Nurioglu, A. G.; Esteves, A. C. C.; de With, G., Non-Toxic, Non-Biocide-Release Antifouling Coatings Based on Molecular Structure design for Marine Applications. *J. Mater. Chem. B* **2015,** *3*, 6547-6570.
7. Stuart, M. A. C.; Huck, W. T. S.; Genzer, J.; Müller, M.; Ober, C.; Stamm, M.; Sukhorukov, G. B.; Szleifer, I.; Tsukruk, V. V.; Urban, M.; Winnik, F.; Zauscher, S.; Luzinov, I.; Minko, S., Emerging Applications of Stimuli-responsive Polymer Materials. *Nature Materials* **2010,** *9*, 101-113.
8. Andreeva, D. V.; Skorb, E. V.; Shchukin, D. G., Layer-by-Layer Polyelectrolyte/Inhibitor Nanostructures for Metal Corrosion Protection. *ACS Appl. Mater. Interfaces* **2010,** *2*, 1954-1962.
9. Nakayama, M.; Okano, T.; Winnik, F. M., Poly(*N*-isopropylacrylamide)-based Smart Surfaces for Cell Sheet Tissue Engineering. *Material Matters* **2010,** *5.3*, 56.
10. Bünsow, J.; Erath, J.; Biesheuvel, P. M.; Fery, A.; Huck, W. T. S., Direct Correlation between Local Pressure and Fluorescence Output in Mechanoresponsive Polyelectrolyte Brushes. *Angewandte Chemie-International Edition* **2011,** *50*, 9629-9632.
11. Shchukin, D.; Möhwald, H., A Coat of Many Functions. *Science* **2013,** *341*, 1458-1459.
12. Dewald, I.; Fery, A., Polymeric Micelles and Vesicles in Polyelectrolyte Multilayers: Introducing Hierarchy and Compartmentalization. *Adv. Mater. Interfaces* **2017**, *4*, 1600317 (1-11).

2 Theory / Status of the Field

The present chapter provides the theoretical background in the area of responsive polymers, colloidal particles, and adsorption mechanisms necessary to understand this work. The theoretical introduction is limited to systems in aqueous solution relevant for this thesis. Additionally, a short comparison of colloidal coatings to conventional molecular coatings is provided based on their properties and performance.

2.1 Classification of Hydrophilic Responsive Polymers

Macromolecules exhibiting solubility in aqueous solutions represent a diverse class of polymers ranging from natural to synthetic ones.[1-2] Thereby, the key for water solubility is the possession of a sufficiently high number of hydrophilic, i.e. polar or charged, functional groups along the polymer backbone. In this chapter water-soluble and stimuli-responsive polymers have been divided into three categories: nonionic polymers, polyelectrolytes, and polyampholytes, according to their key structural features.

2.1.1 Thermoresponsive Polymers

Polymers that respond to temperature changes in aqueous solution with a solubility transition are called thermoresponsive.[3-4] Due to the miscibility gap in the phase diagram, the binary polymer-solvent mixture undergoes a temperature-induced phase separation from a one-phase system to a two-phase system (Figure 2.1a). At the lower critical solution temperature (LCST), the polymer changes its conformation from a hydrophilic coil to a hydrophobic globule. In this process, hydrogen bonds between polymer and surrounding water molecules break and polymer-polymer interactions become more favorable. As a result, the collapsed polymer chains agglomerate under water expulsion, thereby leading to an endothermic and entropically driven phase separation and precipitation (Figure 2.1b).

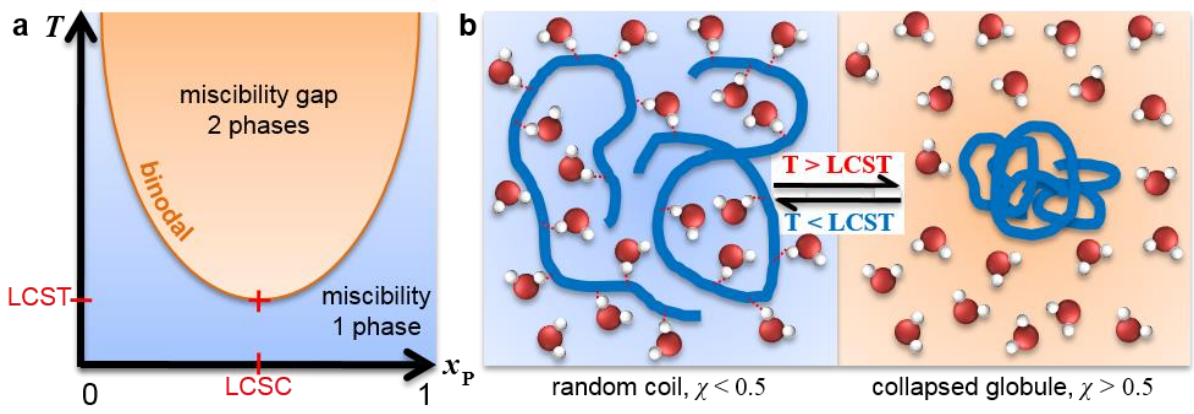

Figure 2.1. Phase diagram of a binary polymer-solvent mixture for a polymer exhibiting LCST behavior (a). Coil-to-globule transition of a thermoresponsive LCST polymer in an aqueous solution (b). Red dotted lines represent H-bonds between water molecules and polymer segments. Reproduced from ref 3, 5.

Thermoresponsive polymers are classified in 3 types according to their critical miscibility with water.[4, 6] Type I polymers, such as poly(ethylene oxide) (PEO) and poly(2-(dimethylamino)ethyl methacrylate) (PDMAEMA), show a classical Flory-Huggins behavior. Thus, the LCST depends on the molecular weight and shifts to lower temperatures with increasing M_w. The LCST of type II polymers, such as poly(*N*-isopropylacrylamide) (PNIPAM), is almost independent of polymer's molar mass. Phase diagrams of type III polymers are bimodal and exhibit two LCSTs at low and high concentrations corresponding to type I and II behaviors, respectively.

The dependence of the coil-to-globule transition on the overall hydrophilic-hydrophobic balance allows a tuning of thermoresponsive properties, e.g. by copolymerization or use of additives. The LCST behavior of copolymers is a function of comonomer composition and can be adjusted within the temperature range between the LCSTs of the homopolymers. In detail, hydrophobic comonomers tend to decrease and hydrophilic comonomers tend to increase the LCST.[7-9] The introduction of additives, such as salts, surfactants, or organic compounds, into the polymer-water mixture induces a shift in the phase transition temperature, as well.[10-12]

2.1.2 Polyelectrolytes

Polyelectrolytes (PEs) are macromolecules that carry ionizable or ionic groups along the polymeric backbone with counterions securing electroneutrality.[13-15] Depending on the type of functional groups, PEs are classified as cationic and anionic polyions. In terms of charge density and acidity they can be divided into weak (annealed) and strong (quenched) PEs. The behavior of PEs in dilute solution is governed by their charge density and may be quantified by the effective charge distance between elementary charges l_{eff} along the chain. At low charge densities, in the Debye-Hückel regime l_{eff} corresponds to the actual distance between elementary charges l_e as depicted in Figure 2.2a.

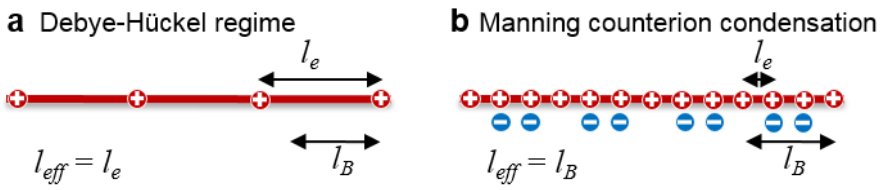

Figure 2.2. Schematic illustration of the relationship of effective charge distance l_{eff}, Bjerrum length l_B, and the distance between elementary charges l_e for a polyelectrolyte with a low (a) and a high (b) charge density.

In contrast, a high charge density of a polyelectrolyte leads to strong binding of counterions to the chain. This effect has been described by Manning as counterion condensation,[16] whereby charges of neighboring functional groups are screened (Figure 2.2b) by condensed counterions. In that case, the l_{eff} equals the Bjerrum length l_B,

$$l_B = \frac{e^2}{\varepsilon \cdot k_B T} \tag{2.1}$$

which is defined as the distance between two elementary charges e, at which their Coulombic interaction energy in a medium with the dielectric constant ε equals the thermal energy $k_B T$. In an aqueous solution with $T \sim 20$ °C, l_B corresponds to ~0.7 nm.[14]

The effect of electrostatic interactions between counterions and added salt ions is taken into account by the concentration dependence of the Debye screening length κ^{-1},

$$\kappa^2 = 4\pi \cdot l_B \sum_s c_s q_s^2 \tag{2.2}$$

with c_s as the concentration of salt ions and q_s as their valence. Basically, κ^{-1} describes the exponential decay of electrostatic interactions due to screening by electrolytes.

Strong Polyelectrolytes

Strong polyelectrolytes are permanently charged regardless of solution pH. However, they are sensitive to the ionic strength of the environment. As depicted in Figure 2.3a, at low ionic strength the PE assumes a stretched conformation due to repulsive interactions between neighboring charges. With increasing salt concentration charges along the PE chain are progressively screened from each other. Above a certain ionic strength, the PE assumes a globular conformation.

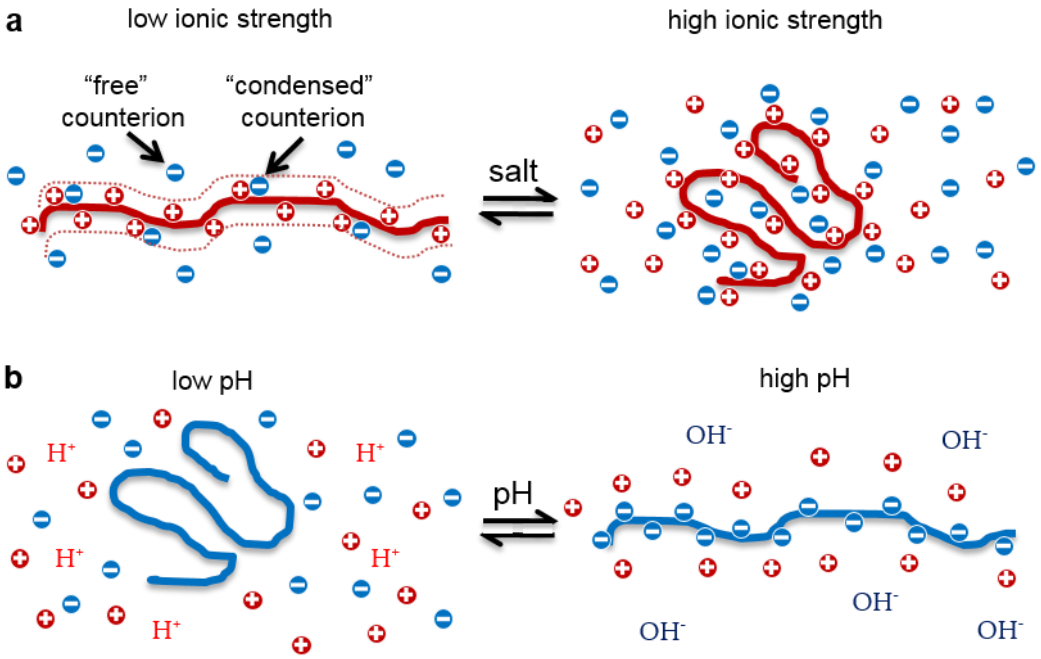

Figure 2.3. Effect of counterion condensation and screening of charges by salt ions on the conformation of a strong polycation (a). Illustration of changes in charge density of a weak polyacid as a function of pH (b).

Weak Polyelectrolytes

In contrast to strong PEs, the charge density of weak PEs depends on solution pH (Figure 2.3b).[13] In analogy to low molecular acids, the logarithmic dissociation constant pK_a of a polyacid can be calculated by the Henderson-Hasselbalch equation:

$$pK_{a,app} = pH + \log\frac{(1-\alpha)}{(\alpha)} \tag{2.3}$$

As opposed to low molecular compounds, pK_a is an apparent value ($pK_{a,app}$) and depends on the degree of dissociation α instead of the degree of neutralization α', whereby $\alpha = \alpha' + (c_{H^+} / c_{PE})$ with c_{H^+} and c_{PE} being the molar concentrations of H^+ ions and PE, respectively.

The relationship between the experimentally accessible pH and the intrinsic pK_a^0 of polyelectrolytes has been described by Overbeek.[17]

$$pH = pK_a^0 - \log\frac{(1-\alpha)}{(\alpha)} + 0.4343\frac{\Delta G_{el}}{RT} \tag{2.4}$$

Thereby, ΔG_{el} is the change in free electrostatic energy or the work necessary to remove a proton from the PE chain against the electrostatic attraction of the polyion. By applying eq 2.3 the apparent pK_a can be written as a function of the intrinsic pK_a^0:

$$pK_{a,app} = pK_a^0 + 0.4343\frac{\Delta G_{el}}{RT} \qquad (2.5)$$

In contrast to pK_a^0, the $pK_{a,app}$ of a polyacid depends strongly on environmental parameters such as the presence of a polybase and / or salt ions, e.g. in polyelectrolyte multilayers.[18] In addition, shifts in the apparent dissociation constants (Figure 2.4) in respect to a linear polyelectrolyte were reported for star polymers, block copolymer micelles, and surface-attached brushes.[6, 19-23] The extent of this effect depends on the confinement of the polyelectrolyte chains in a certain architecture. Particularly strong shifts were observed for an increased number of arms, chains per area, or grafting density.[24]

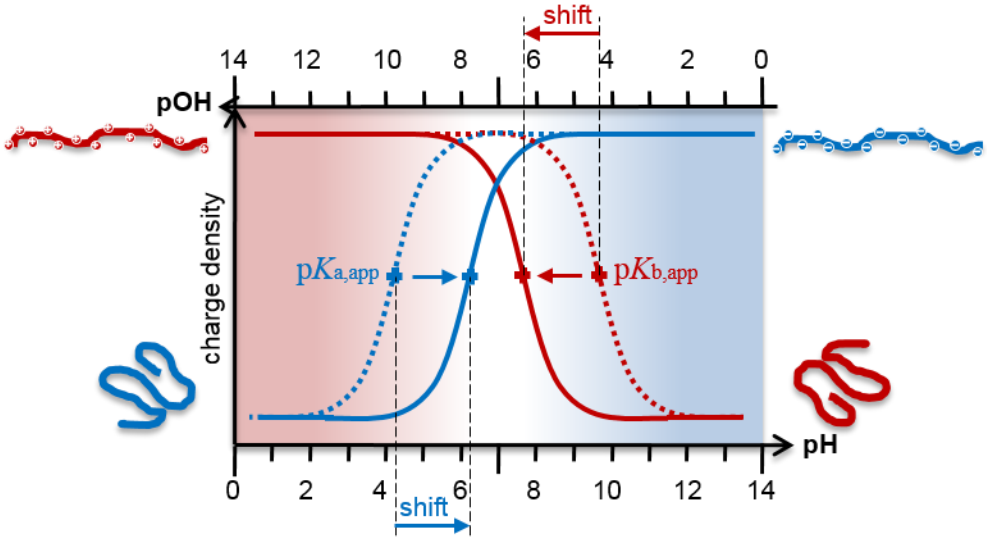

Figure 2.4. Charge density as a function of pH for weak polyelectrolytes and the corresponding shifts in the apparent dissociation constants, e.g. due to architecture, with respect to the linear PE in solution.

Interpolyelectrolyte Complex

Mixing of two oppositely charged polyelectrolytes results in the formation of interpolyelectrolyte complexes (IPECs).[13, 25-26] Though, polyion condensation is induced by strong Coulombic interactions, secondary interactions such as hydrogen bonding, van der Waals forces, hydrophobic and dipole interactions are involved as well. The driving force for the assembly is the gain in entropy, due to the release of counterions (Figure 2.5a). The process of IPEC formation is very fast and predominantly controlled by the counterion diffusion.

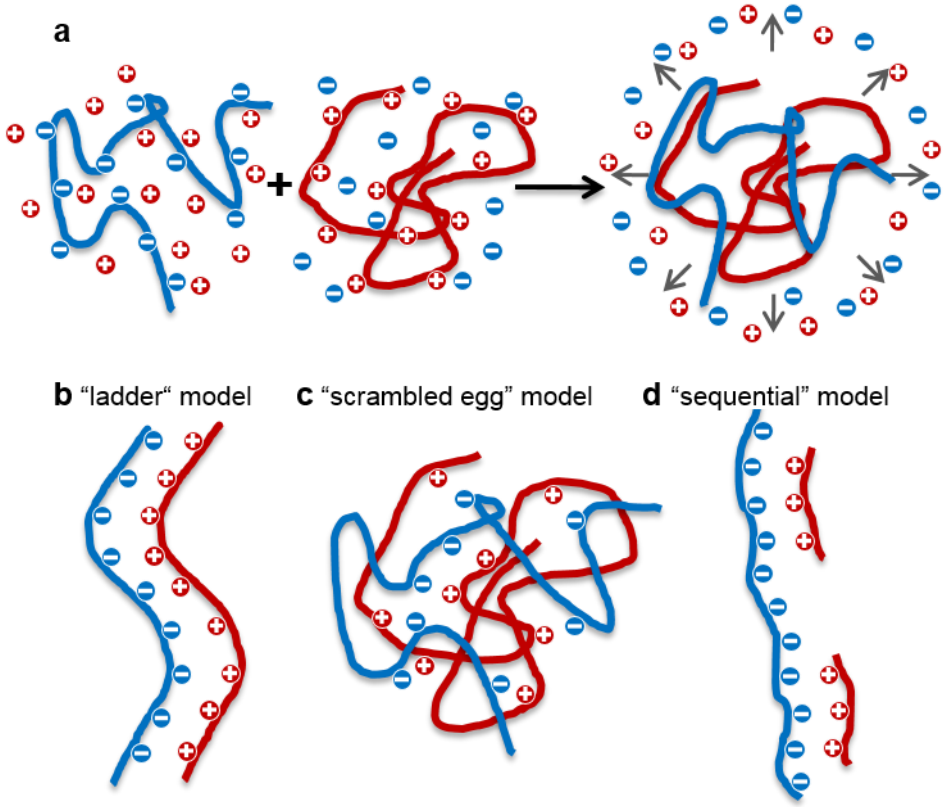

Figure 2.5. Polyion condensation accompanied by the release of low molecular weight counterions (a). Polyelectrolyte complex models for ordered (b) and disordered (c) stoichiometric complexes according to Michaels and Miekka,[27] and non-stoichiometric soluble complexes according to Kabanov (d).[28] Reproduced from ref 25.

Depending on M_w, ionic strength of functional groups, and the stoichiometry in the mixture, different complex structures can occur (Figure 2.5b-d). For strong polyelectrolytes with similar molar mass and a stoichiometry of 1:1 the structure can be described by two borderline models introduced by Michaels and Miekka.[27] In contrast, non-stoichiometric association of PEs of different M_w results in water-soluble complexes between a long host molecule and shorter guest molecules introduced by Kabanov and Zezin.[28]

2.1.3 Polyampholytes

Polyampholytes are classified as charged macromolecules carrying both acidic and basic functional groups.[29-31] Examples include natural polymers, such as proteins and nucleic acids, and synthetic copolymers from either acidic and basic, or zwitterionic monomers. Different types of synthetic polyampholytes are available with statistical, alternating, graft, and block structures, depending on the connectivity of the monomer units. In the following paragraphs important features of polyampholytes are introduced for two special cases, namely block copolymers and proteins.

Block Polyampholytes

Amphoteric block copolymers consist of at least two oppositely charged polyelectrolytes connected via a covalent bond. In aqueous solution their behavior is mainly governed by Coulombic interactions, similar to the behavior of homopolyelectrolytes described in the previous section (2.1.2). The type of behavior depends on environmental parameters (pH, ionic strength), copolymer composition, and the relative strength of the acidic and basic groups.[32] Polyampholytes containing both, a weak polyacid and a weak polybase, possess an isoelectric point (pI). At the pI the net charge of the copolymer is zero (Figure 2.6).

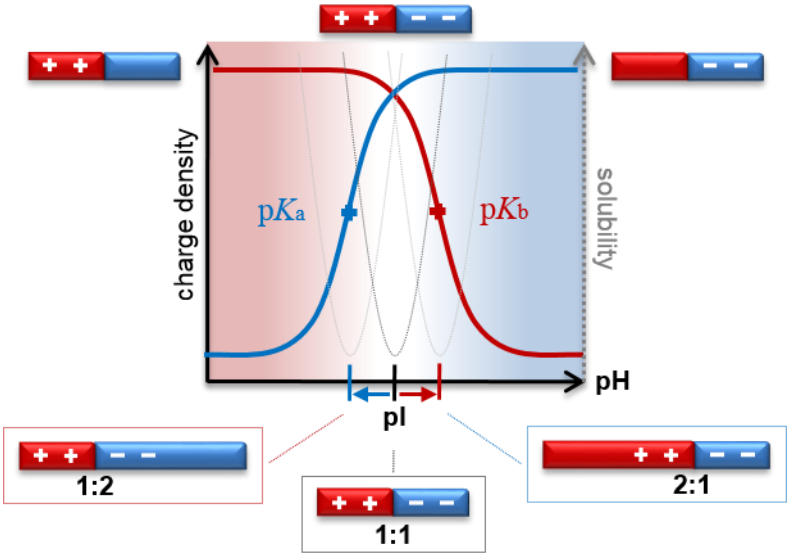

Figure 2.6. Charge density profiles of the weak polyacid and the weak polybase block, and the shifts in the isoelectric point (pI) of the corresponding block polyampholytes with respect to relative block lengths.

In contrast to statistical copolymers, block polyampholytes are soluble only at pH values below and above the pI. At the isoelectric point they tend to precipitate due to the formation of insoluble complexes between acid and amine sequences, similar to IPEC formation in polyelectrolyte blends.[29] The pI of the polyampholyte depends on the acid to base molar ratio and the dissociation constants. Knowing the polymer composition and the respective pK values, the isoelectric point can be estimated.[32] In the symmetric case, the pI equals the arithmetic average of the pK_a and pK_b values. In the case of charge asymmetry, e.g. if the ratio is 1:2 or 2:1 (Figure 2.6), the pI shifts to the pK value of the longer block. The addition of salt may have two opposite consequences on the solubility of the polyampholyte: depending on the starting situation in terms of pH and charge density, salt can either increase or decrease the solubility.[33] At the pH range close to pI the additional salt loosens the ionic bonds in the complex leading to a redissolution of the block copolymer. Above a critical salt concentration, the screening of electrostatic charges dominates, resulting in polymer precipitation.

Above the so called critical micellization concentration and pH far from pI, the ampholytic diblock copoloymers phase separate into supramolecular structures with different morphologies (cf. section

2.2.2), whereby the uncharged block forms hydrophobic domains surrounded by the soluble corona of the charged block. Increasing the number of blocks results in richer phase behavior and higher variety in terms of different morphologies. In the case of amphiphilic triblock terpolymers carrying both polycationic and polyanionic blocks, the formation of IPECs enables compartmentalization and provides the resulting aggregates with structural diversity.[34-35]

Proteins

Another, special type of polyampholytes are proteins. They represent the most abundant class of water-soluble and stimuli-responsive biopolymers. They consist of amino acids (AA) carrying different residues (> 20 in total), which are connected via peptide bonds to a linear chain.[36-37] The resulting AA sequence is defined as the primary structure of the protein (Figure 2.7).

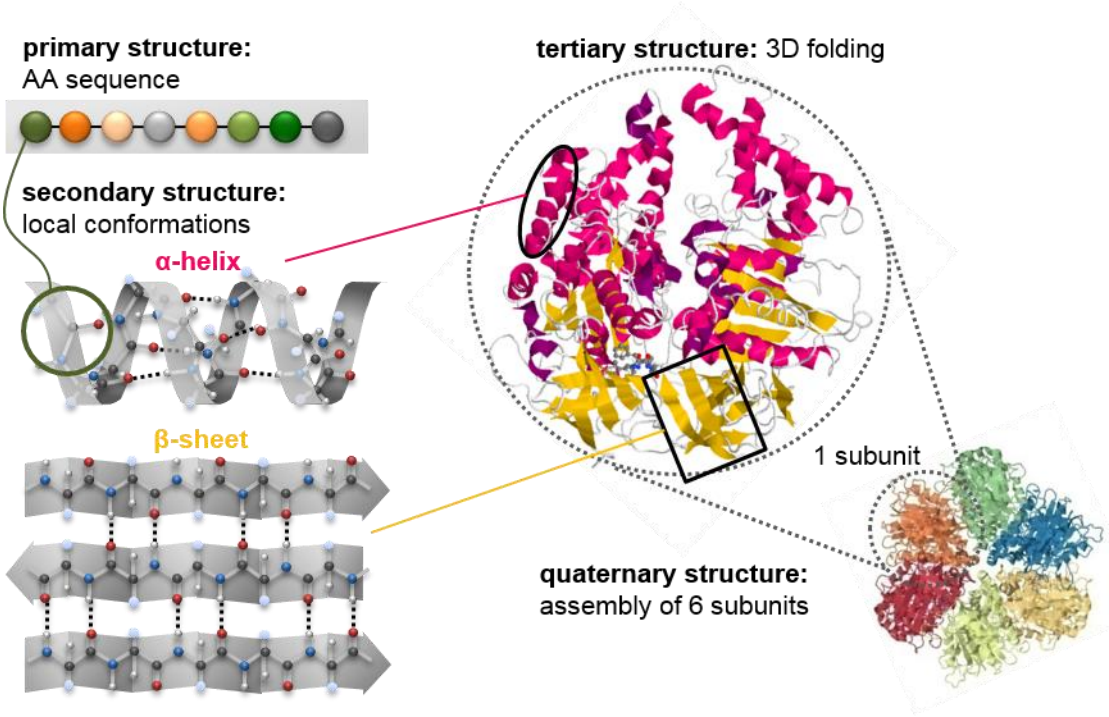

Figure 2.7. Structural features of proteins exemplarily shown for a *spinach chloroplast F1-ATPase*. 3D structures of the protein are from the RCSB protein data bank (1KMH). Illustration of secondary structures reproduced from ref 38.

Beside random coils, AA segments may adopt regular folding patterns, such as α-helices and β-sheets, called secondary structure.[36-37] These local conformations are stabilized via hydrogen bonds between amino and carboxyl groups along the peptide backbone. The tertiary structure corresponds to the 3D structure in the native folded state, whereby the AA sequence dictates the final conformation of a functional protein. The folding is mainly driven by the entropy of released structured water, resulting in formation of intramolecular interactions, thereby easily counterbalancing the loss of conformational entropy. Except for a few disulfide bridges, the tertiary structure is mainly stabilized by many weak non-covalent interactions between AA residues, such as H-bonds, hydrophobic, and ionic interactions. To avoid the contact with water molecules, hydrophobic AAs form hydrophobic domains and are

preferentially located in the inner part of the protein. In contrast, hydrophilic AAs are located at the outer regions, facing aqueous medium. The quaternary structure describes the spatial assembly of subunits (i.e., separately folded polypeptide chains) of a protein relative to each other.

As a consequence of such a chemical and structural diversity, protein solubility is a function of pH, temperature, salt concentration, and other factors.[37, 39-42] As a function of pH, the proteins exhibit a U-shaped solubility profile with a minimum at the pI (Figure 2.8a). At low ionic strength most proteins, especially when close to their pI, are poorly soluble. Elevated salt concentrations initially induce a rise in solubility ("salting in" effect) until an optimum (~150 mM) is reached (Figure 2.8b). However, further increase in ionic strength decreases the solubility ("salting out" effect). The reason for these effects is the displacement of water molecules in the protein's hydration shell. Low ion concentrations and pH close to pI lead to formation of highly ordered layers of water molecules around the mainly hydrophobic proteins. This state is energetically unfavorable. Thus, proteins agglomerate in order to gain entropy by releasing structured water. Additional salt ions distort the order in the hydration shell, thereby removing the source of agglomeration. A complete water displacement at higher salt concentrations results in the exposure of hydrophobic patches, which in turn facilitates agglomeration. Furthermore, some ions have the ability to enhance these effects. These ions are ordered in the so-called Hofmeister series according to their ability to influence the hydrophobic interactions between proteins. Depending on their ability to enhance or decrease the protein solubility, these ions are called chaotropes or kosmotropes, respectively.

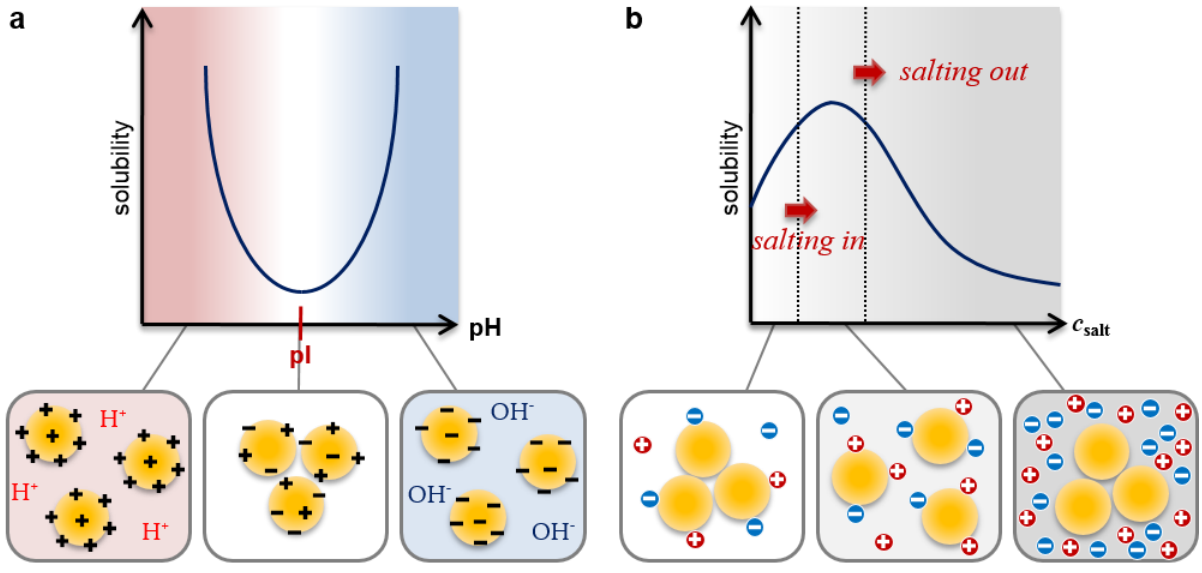

Figure 2.8. Typical solubility profiles of proteins as a function of pH (a) and salt concentration (b) with the corresponding pictograms illustrating the charge density and solubility of the protein in a certain region of pH or salt concentration. Reproduced from ref 43-44.

In contrast to synthetic homopolymers, proteins provide several advantages, such as the precise composition (AA sequence) and M_w. Furthermore, naturally occurring proteins are biocompatible and biodegradable. Their biological relevance (e.g., as enzymes) renders proteins interesting as coating

material for biological and biomedical applications. Proteins are on the boundary between macromolecules and colloids. Thus, their behavior can be described using both, the macromolecular and colloidal concepts. Their structural diversity presents highly tailored colloidal building blocks, which are available to choose from nature's toolbox.

2.2 Colloidal Particles

The colloidal domain covers a size range from 1 nm to several μm, thereby spanning the dimensions from "simple" biological molecules, such as DNA or proteins, to more complex and sophisticated constructs, such as blood cells or human hair.[45-46] One key feature of colloidal particles is the high surface to volume ratio. Consequently, surface properties dominate the behavior of colloidal particles rendering the interaction forces between particles and with surrounding molecules more important than for macroscopic objects.

DLVO Theory

In order to describe the forces acting between colloidal particles Derjaguin, Landau, Verwey, and Overbeek introduced the DLVO theory in the 1940s.[47-49] Basically, the theory explains the stability of colloidal particles by providing a quantitative relationship between the attractive van der Waals (vdW) forces, which favor particle aggregation, and repulsive electric double layer (dl) forces, which favor colloidal stability.[46, 50-53]

The force $F(h)$ acting between two colloidal particles at a separation distance h can be related to the (theoretically accessible) energy per unit area between two planar surfaces $W(h)$ using the Derjaguin approximation:

$$F(h) = 2\pi R_{eff} W(h) \tag{2.6}$$

with $R_{eff} = \frac{R_1 R_2}{R_1 + R_2}$ being the effective radius, which can be simplified to $R_{eff} = R/2$ for a symmetrical system of two identical spheres ($R_1 = R_2 = R$).

According to the DLVO theory, the free energy per unit area is a superposition of two contributions:

$$W(h) = W_{vdW}(h) + W_{dl}(h) \tag{2.7}$$

The attractive van der Waals forces arise from interactions of rotating and fluctuating dipoles of atoms. Their strength is summarized in the Hamaker constant H. In a sphere-sphere geometry the corresponding van der Waals interaction free energy is directly proportional to the particle radius R and scales with $1/h$ (eq 2.8).

$$W_{vdW}(h) = -\frac{HR}{12h} \tag{2.8}$$

In aqueous solution, colloidal particles carrying ionizable groups dissociate into charged particles and counterions. Thermal fluctuations tend to drive these counterions away from the surface, against the drive to keep the electroneutrality of the system, thereby forming an electric double layer around the particle (Figure 2.9a).

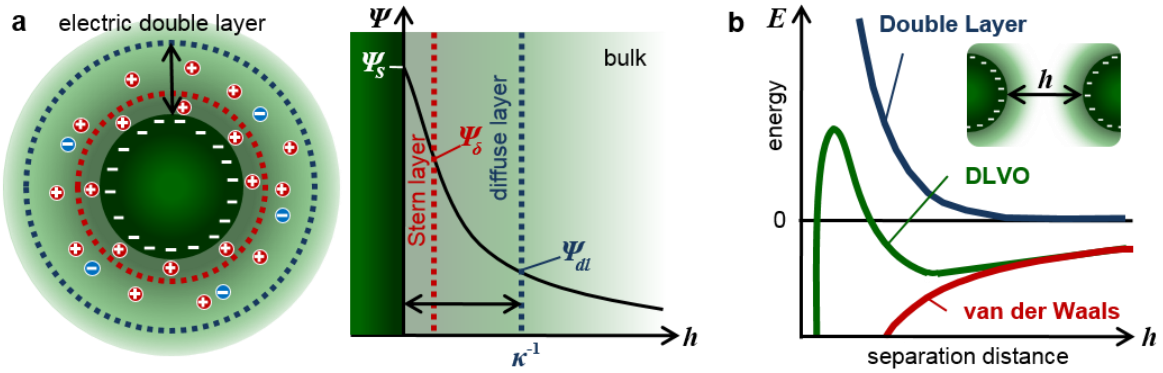

Figure 2.9. Counterion distribution in a double layer of a negatively charged colloidal particle and the corresponding electric potential Ψ as a function of the distance h (a). Subscripts s, δ, and dl denote surface, Stern, and double layer potential, respectively. A typical energy-distance plot that shows the contribution of the van der Waals and double layer interactions between two colloidal particles described by the DLVO theory (b). Reproduced from ref 51, 53.

The electric double layer consists of an inner Stern layer and an outer Gouy-Chapman or diffuse layer. The Stern layer contains immobile ions which adsorb directly onto the surface. In contrast, the ions in the diffuse layer are mobile and their distribution obeys Poisson-Boltzmann statistics. As shown in Figure 2.9a the electric potential ψ decays exponentially as a function of the distance h from the surfaces

$$\psi(h) = \psi_s \cdot e^{-\kappa h} \tag{2.9}$$

with a characteristic decay length, the Debye length κ^{-1}, which corresponds to the thickness of the electric double layer:

$$\kappa^{-1} = \left(\frac{k_B T \varepsilon_0 \varepsilon}{2e^2 N_A I} \right)^{1/2} \cong \frac{0.3nm}{\sqrt{I}} \tag{2.10}$$

ε_0 is the permittivity of vacuum, ε the dielectric constant of water, e the elementary charge, N_A Avogadro's number, and I the ionic strength. Thus, at a given temperature (e.g. 25 °C) κ^{-1} depends solely on solution properties, such as type and concentration of ions, and not on particle properties.

When two charged particles come close, their ionic clouds overlap and the resulting differences in ion concentration, between the overlap region and the bulk, result in an osmotic pressure which leads to repulsive interactions. For distances $h << R$, the corresponding double layer interaction free energy can be described as

$$W_{dl}(h) = 2\pi\varepsilon\varepsilon_0 R\psi^2 \cdot e^{-\kappa \cdot h} \tag{2.11}$$

In addition to the dependency on particle size, the repulsive dl term depends strongly on the particle surface potential and on the ionic strength.

The characteristic profiles of both contributions and the resulting DLVO interaction energy as a function of the separation distance are illustrated in Figure 2.9b. At large and small separations the DLVO profile is defined by attractive vdW forces. At intermediate distances repulsive dl forces dominate interparticle interactions, thereby introducing a maximum to the curve. The maximum represents the activation energy for aggregation and determines the colloidal stability. In order to provide a significant level of stability over an extended period of time, the maximum must be at least 20 $k_B T$.[46]

Colloidal Stability

In addition to the attractive vdW and the repulsive dl forces (Figure 2.10a-b), non-DLVO interactions arise in systems containing polymers (Figure 2.10c-d).[46, 53-56] In the presence of a polymer in a colloidal dispersion, the interparticle interactions depend mainly on the adsorption behavior and the properties of the polymer. If the polymer adsorbs favorably to the particle, resulting in a saturated surface, the colloids are stabilized by steric repulsion due to the elastic recoil at shorter distances. In contrast, low surface coverages due to long polymer chains or low particle concentrations result in attractive interactions via bridging flocculation. In the presence of non-adsorbing polymers or smaller particles, depletion attraction sets in if the space between the colloids becomes smaller than the size of the depletant. The origin of depletion forces is the osmotic pressure imbalance inside and outside the gap between the particles and the gain in conformational entropy in the case of polymers.

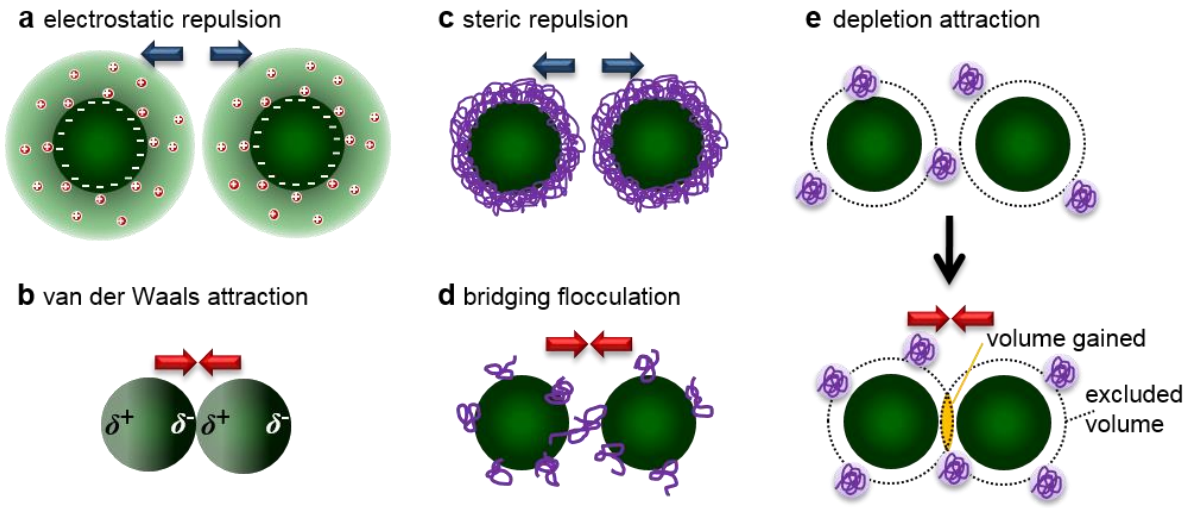

Figure 2.10. Attractive and repulsive interactions which facilitate aggregation or stabilization of colloidal particles in the absence (a-b) and in the presence of polymers or other particles (c-e). Reproduced from ref 54-55, 57.

Apart from polymer-mediated interactions, other non-DLVO surface forces may also contribute significantly to the interaction behavior of colloidal particles.[46, 50] These forces can be repulsive (e.g., Born and hydration forces), attractive (e.g., capillary and hydrophobic forces), or oscillatory (e.g., structural forces). Nevertheless, despite the simple superposition of vdW and dl forces, the DLVO theory successfully predicts basic features of colloidal stability and particle deposition phenomena on flat surfaces in the presence of monovalent salts.[58] Furthermore, the experimental data obtained for bare colloidal particles (hard spheres),[59] and under certain conditions even for proteins[55] and other soft colloids,[60] are consistent with the simple DLVO picture.

2.2.1 Thermoresponsive Microgels

In general, gels are defined as non-fluid networks that are expanded throughout their whole volume by a fluid, thus combining properties of a solid (polymer network) and a liquid (solvent).[5, 61] Thermally sensitive microgels are microscopic 3D networks in the size range of nm - µm.[62-65] The chemically (covalently) crosslinked macromolecular chains provide the colloidal particles with structural integrity. In addition to steric stabilization, electrostatic stabilization is provided by ionic initiator residues, and further increased by the use of surfactant molecules or charged comonomers during polymerization.

In response to temperature variations, the microgels undergo a phase transition from a highly swollen to a collapsed state at the volume phase transition temperature (VPTT) (Figure 2.11a). In line with thermoresponsive linear polymers, the VPTT of microgels depends on the balance of hydrophilic-hydrophobic interactions between polymer segments and between the polymer and water molecules. Besides the comonomer composition and external factors such as ionic strength,[66] the phase transition of microgels can be tuned by microgel architecture, e.g. by introducing a more complex core-shell morphology.[67]

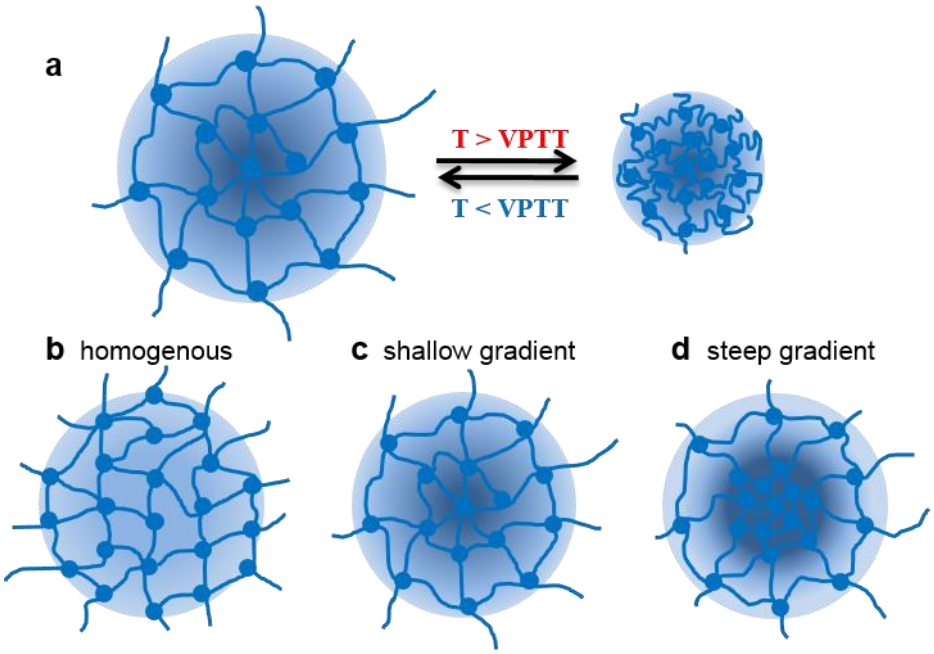

Figure 2.11. Schematic illustration of a temperature-induced volume phase transition (VPTT) in thermoresponsive microgel particles (a). Microgel particles with different distributions of crosslinks (b-d).

The swelling or shrinking of a microgel is caused by conformational changes of the subchains between two neighboring crosslinking points, and depend on the density and distribution of the crosslinks.[68-70] Since the length (M_w) of subchains has a substantial impact on the transition temperature, gels with a high polydispersity of subchains and microgels with a shallow gradient exhibit a continuous phase transition in a broad temperature range due to a superposition of phase transitions of all chain segments. In contrast, gels with a homogenous distribution of chain segments or lightly crosslinked microgels with a steep gradient show a sharp (discontinuous) phase transition in a narrow temperature range Figure 2.11b-d). A quantitative description of the swelling behavior of microgels is provided by the Flory-Rehner theory.[71]

To meet the requirements of desired applications a considerable number of possibilities is available for the design of suitable microgel particles with tailored size, architecture, charge density, and stimulus response.[64, 72-73] The incorporation of inorganic nanoparticles provides the microgels additionally with optical or catalytic properties.[74-76]

2.2.2 Self-Assembly of Amphiphilic Block Copolymers

Amphiphiles are molecules carrying covalently linked hydrophilic and hydrophobic units. Well-known examples for surface active amphiphiles are surfactants, lipids and block copolymers. Conceptually, the self-assembly process of block copolymers to micellar aggregates – a thermodynamically stable morphology – is similar to the assembly of low M_w amphiphiles.[14, 77-80] The self-assembly is driven by weak and noncovalent interactions favored by chemical complementarity and structural compatibility.[81] In a selective solvent for block B (Figure 2.12a), the insoluble block A undergoes a microphase

separation, forming the micellar core, which is surrounded by an extended corona. Depending on relative block lengths in an AB diblock copolymer, micellar aggregates are divided into two limiting structures: star-like (compact core and long corona) and crew-cut (large core and short corona) micelles (Figure 2.12b).

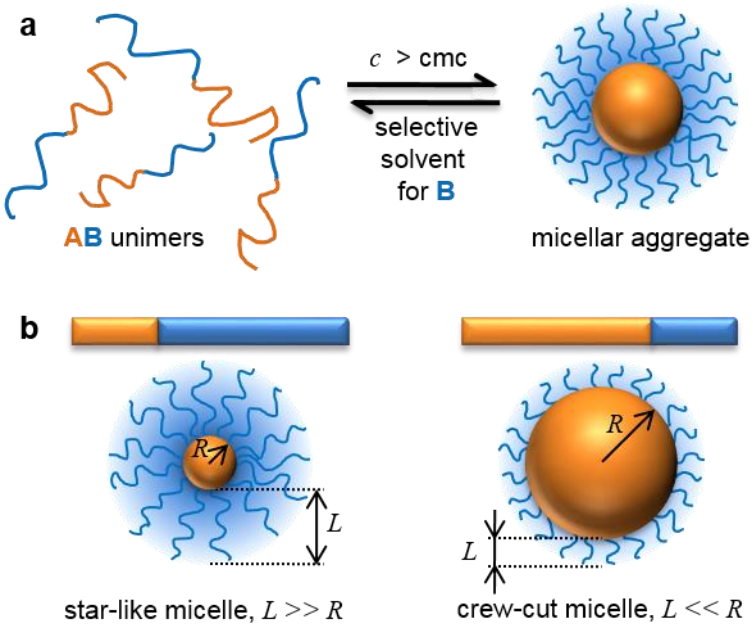

Figure 2.12. Micellization of an AB diblock copolymer in a selective solvent for block B (a). Schematic representation of "star-like" and "crew-cut" micelles with core radius *R*, and shell thickness *L* (b). Reproduced from ref 82.

Owing to their high M_w, block copolymers have strongly reduced lower critical micellization concentrations and higher stability of the aggregates, compared to low M_w assemblies.[79, 82-83] The dependence of the free energy of micellization (transfer of a polymer from unimers to micellar aggregates) on the molecular weight strongly favors the micellar state as compared to free polymer in solution. Ideally, the final size of block copolymer micelles represents the optimum thermodynamic state, whereby the free energy is determined by the interfacial energy of the core/shell interface, the stretching energy of polymer chains, and the repulsive interactions among corona chains.

The geometry and degree of order in the block copolymer aggregates depends mainly on the concentration and the volume ratio between soluble and insoluble block.[84-85] In analogy to low molecular weight amphiphiles, the resulting morphology (Figure 2.13) can be predicted using the concept of the dimensionless packing parameter *P*.[84, 86-87]

$$P = \frac{V}{a_0 l} \tag{2.12}$$

Thereby, V is the volume and l is the length of the hydrophobic block. a_0 is the interface between hydrophobic and hydrophilic blocks. The size of the interface is governed by the interactions between the two blocks and can be tuned via the properties of the hydrophilic block. In the case of short soluble

blocks a lamellar structure is preferred.[14] In contrast, long soluble blocks introduce repulsion between soluble chains in favor of a curved surface of spherical or cylindrical aggregates. In addition, stimuli-responsive blocks provide a means to control the aggregation process and the resulting morphology as a response to chemical (pH, salt) or physical (*T*) signals.[35]

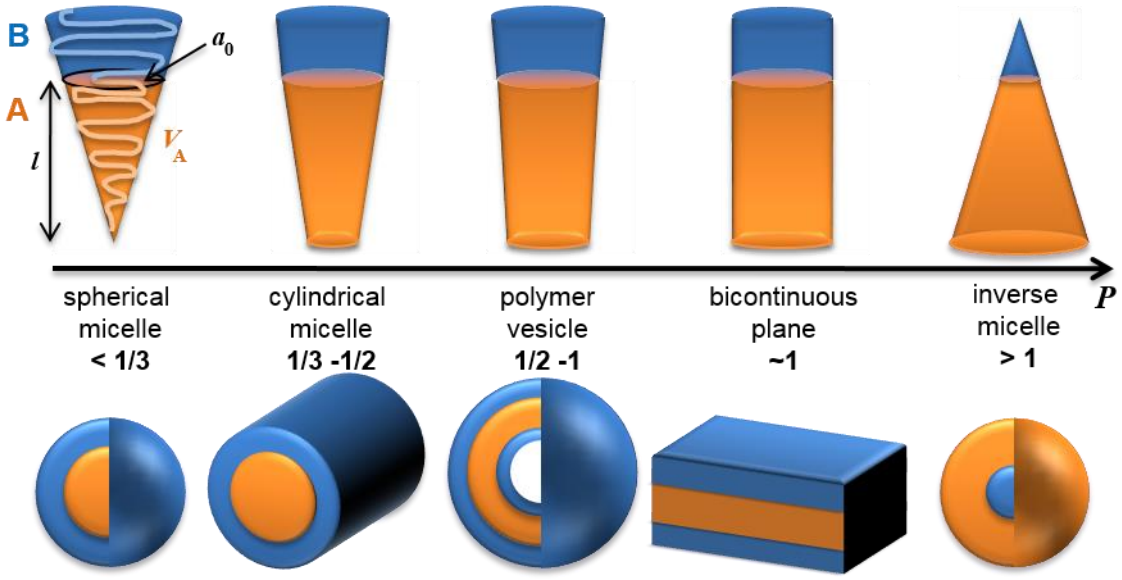

Figure 2.13. Dependence of the morphology on the packing parameter *P* schematically shown for a linear AB block copolymer in aqueous solution, i.e. selective solvent for the hydrophilic block B. In contrast, the inverse micelles are formed in a selective solvent for the hydrophobic block A. Reproduced from ref 86, 88.

Although the schematic depiction in Figure 2.13 may suggest otherwise, cylindrical and planar morphologies are of finite dimensions. Due to thermal fluctuations and the fluid-like nature, the aggregates form end-caps or curved edges. Block copolymers comprised of three or more blocks give rise to a seemingly unlimited number of morphologies in terms of structure and architecture.[89-92]

In contrast to surfactant aggregates,[77, 93-95] block copolymer's M_w is several orders of magnitude higher, which causes a much slower dynamic.[80, 83, 96] In addition, a distinction has to be made between equilibrium (dynamic) micelles and non-equilibrium (kinetically trapped / frozen) ones. For dynamic systems, there are two possible mechanisms for the exchange kinetics at steady state: insertion and expulsion of single chains or merging and subsequent splitting of the micelles. Thereby, parameters such as glass transition temperature (T_g) of the hydrophobic block, interfacial tension between hydrophobic block and solvent, temperature, length of the hydrophobic block and steric hindrance due to corona or core block architecture have to be taken into account. In the case of changes in the environmental conditions, dynamic systems may adapt by changes in aggregation number, morphology, and structure according to unimer exchange or merging/splitting processes. However, elevated temperatures or the presence of a plasticizer (e.g. good solvent for the hydrophobic block) may trigger the response of micellar aggregates that are kinetically trapped at ambient conditions.[97-98] In order to suppress changes

in micellar morphology and aggregation number, or even prevent a complete dissolution into unimers, strategic crosslinking of the micellar core or corona provides the assembly with sufficient stability.[99-100]

The chemical versatility and advances in synthetic polymer chemistry provide almost unlimited diversity of block copolymer structural complexity, especially in terms of block properties (M_w, functionality), sequence and connectivity.[101] The variety of molecular architectures, offers the opportunity to generate highly tailored materials with control over domain size and geometry, symmetry and chemical composition, thereby giving rise to a plethora of colloidal building blocks with complex internal hierarchy.[102-103]

2.3 Adsorption on Solid Substrates

2.3.1 Adsorption of Polymers

The adsorption onto a surface is generally defined as an accumulation of solute at the interface.[14, 52, 104] Roughly, there are two modes of adsorption: chemisorptions and physisorption. Polymers adsorb via physisorption if the adsorption is governed by physical interactions with interaction energies on the order of k_BT. In contrast, interaction energies for chemisorption are several orders of magnitude larger than k_BT and involve the formation of a covalent bond. Polymers mainly adsorb via physisorption as a result of attractive interactions with the surface and / or unfavorable interactions with the solvent.

The kinetics of polymer adsorption depends on three parameters: the mass transport toward the surface (via diffusion or convection), the rate of attachment to the surface, and reconformation of the adsorbed macromolecule, which involves a relaxation from a random coil conformation to a train-loop-tail structure (Figure 2.14).[14, 105]

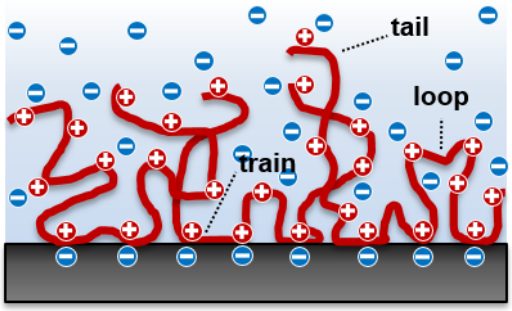

Figure 2.14. Schematic illustration of the train-loop-tail structure of a polyelectrolyte adsorbed on a charged surface, accompanied by charge compensation at the liquid-solid interface and counterion release. Reproduced from ref 14.

The adsorption of neutral polymers is governed by the adsorption energy parameter χ_s and the solvency parameter χ.[14, 59] In the case of polyelectrolytes, electrostatic interactions such as mutual repulsion between polymer segments, and attraction between oppositely charged polymer and surface, play an important role in the adsorption process. These interactions depend on the charge density of both, the surface and the polymer, and can be tuned by salt concentration c_s between charge compensation at low

c_s and screening at high c_s. However, due to the hydrophobicity of the PE backbone attractive van der Waals and hydration forces are important as well. In contrast, weak PEs are able to adjust their degree of dissociation to compensate surface charges, and for that reason are less affected by ionic strength. In general, the adsorbed amount depends on parameters such as molecular weight, polymer concentration, the overall charge balance and ionic strength.

In analogy to IPEC formation, the adsorption of PEs onto an oppositely charged substrate is governed by the gain in entropy from counterion release and displacement of water molecules.[106-107] The contribution of secondary interactions leads to a charge reversal (charge overcompensation),[108] thereby allowing an alternating deposition of oppositely charged PEs to form polyelectrolyte multilayer films.[109-110]

2.3.2 Adsorption of Colloidal Particles

In analogy to polymers, the adsorption of particles corresponds to their accumulation at the surface performed in two basic steps: the transport of particles from the bulk toward the surface and the subsequent adhesion.[111] In the absence of a hydrodynamic flow and negligible impact of gravity (valid for colloidal systems), the initial adsorption kinetics for short adsorption times are controlled by a diffusive flux of particles to the surface.[112] The corresponding time-dependent particle surface concentration $c_s(t)$ is a function of the particle concentration in the bulk c_b and the diffusion coefficient D:

$$c_s(t) = 2c_b\sqrt{Dt/\pi} \tag{2.13}$$

In addition, unscreened electrostatic inter-particle repulsion in the bulk may enhance the diffusivity of particles toward an oppositely charged surface.[112-113]

For longer adsorption times blocking effects (i.e., surface exclusion effects), described by the theoretical model of random sequential adsorption (RSA),[114-115] become dominant.[116-117] The particles are assumed to attach successively and irreversibly to the surface at random adsorption sites, whereby geometrical overlap between incoming and adsorbed particles is prohibited. The time-dependent surface coverage $\theta(t)$ asymptotically approaches a jamming limit for $t \to \infty$ (saturation) according to eq 2.14 (Figure 2.15a).

$$\theta(\infty) - \theta(t) \propto t^{-1/2} \tag{2.14}$$

For N spherical objects with a radius R, the surface coverage corresponds to $\theta(t) = N\pi R^2$. For the adsorption of non-interacting monodisperse spheres a jamming limit of 0.547 has been predicted.[114] In

the case of charged particles, the influence of electrostatics in terms of the classical DLVO theory has to be taken into account.[58, 118]

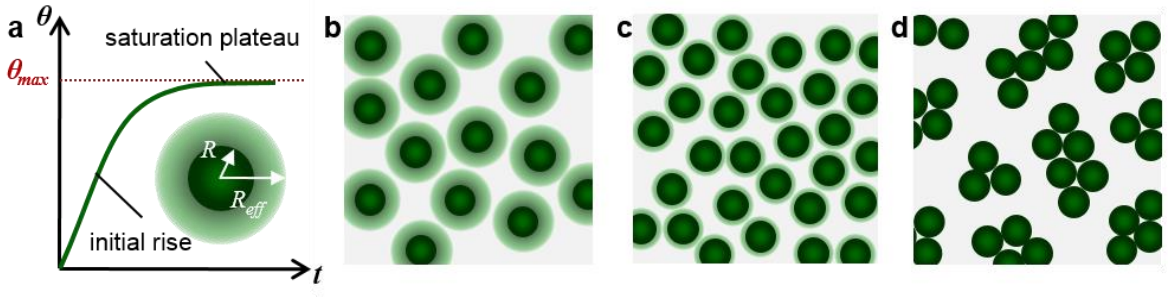

Figure 2.15. A typical increase in surface coverage as a function of time for the RSA model (a). Schematic illustration of differences in surface coverage for charged particles at low (b) and high (c) ionic strength, and the impact of capillary forces on the microstructure (d). Reproduced from ref 59, 119.

The long-ranged repulsive interactions between particles generally result in a larger effective radius R_{eff} , and thereby in a lower maximum surface coverage $\theta_{\max}$ with respect to the jamming limit θ_{jam} (Figure 2.15b-c).

$$\theta_{\max} = \theta_{jam}(R / R_{eff})^2 \qquad (2.15)$$

On account of R_{eff} being a function of ionic strength, the repulsive interactions are screened at high salt concentrations, whereby non-specific interactions, such as vdW or hydrophobic interactions, become dominant. The result is a higher surface coverage and a gradual loss of substrate selectivity to the point where adsorption on both oppositely and like-charged substrates occurs.[112, 120] In the case of weak or sufficiently screened particle-surface interactions, attractive capillary forces dominate the surface morphology. Instead of randomly distributed particles, particle islands or 2D clusters are formed due to lateral mobility upon drying (Figure 2.15d). Although the RSA model does not account for any lateral movement, provided the desorption can be neglected during drying, the surface coverage is still RSA-like.

In general, the RSA model is very versatile in terms of the adsorbate, covering the whole range from single macromolecules[59, 113] to different types of hard and soft colloidal particles.[112, 114, 120-121] In any case, the adsorption is limited to a sub-monolayer. For higher surface coverages, convective and capillary assembly provide a means to direct particle assembly, resulting in dense hexagonally packed mono- and multilayers.[122] To account for the impact of gravity on the adsorption behavior of particles, which exceed the colloidal domain, the Ballistic deposition model has been developed.[123]

2.4 Conventional (Molecular) vs. Colloidal Surface Coatings

Having defined possible components of a coating and discussed their adsorption behavior, the next logical step is the comparison of different systems with regard to their properties and their performance.

Usually, the purpose of the coating dictates the desirable properties. In order to facilitate a task-independent comparison, general key features or requirements have to be defined. Therefore, the concept of *smart coatings* and their key properties are used as a *bench mark* (Figure 2.16a).[124-125]

The Concept of Smart Coatings

The term *smart coating* is not well-defined and various, sometimes conflicting definitions are present in literature.[124] Generally, coatings are regarded as *smart* if they have one or more of the features schematically shown in Figure 2.16a.

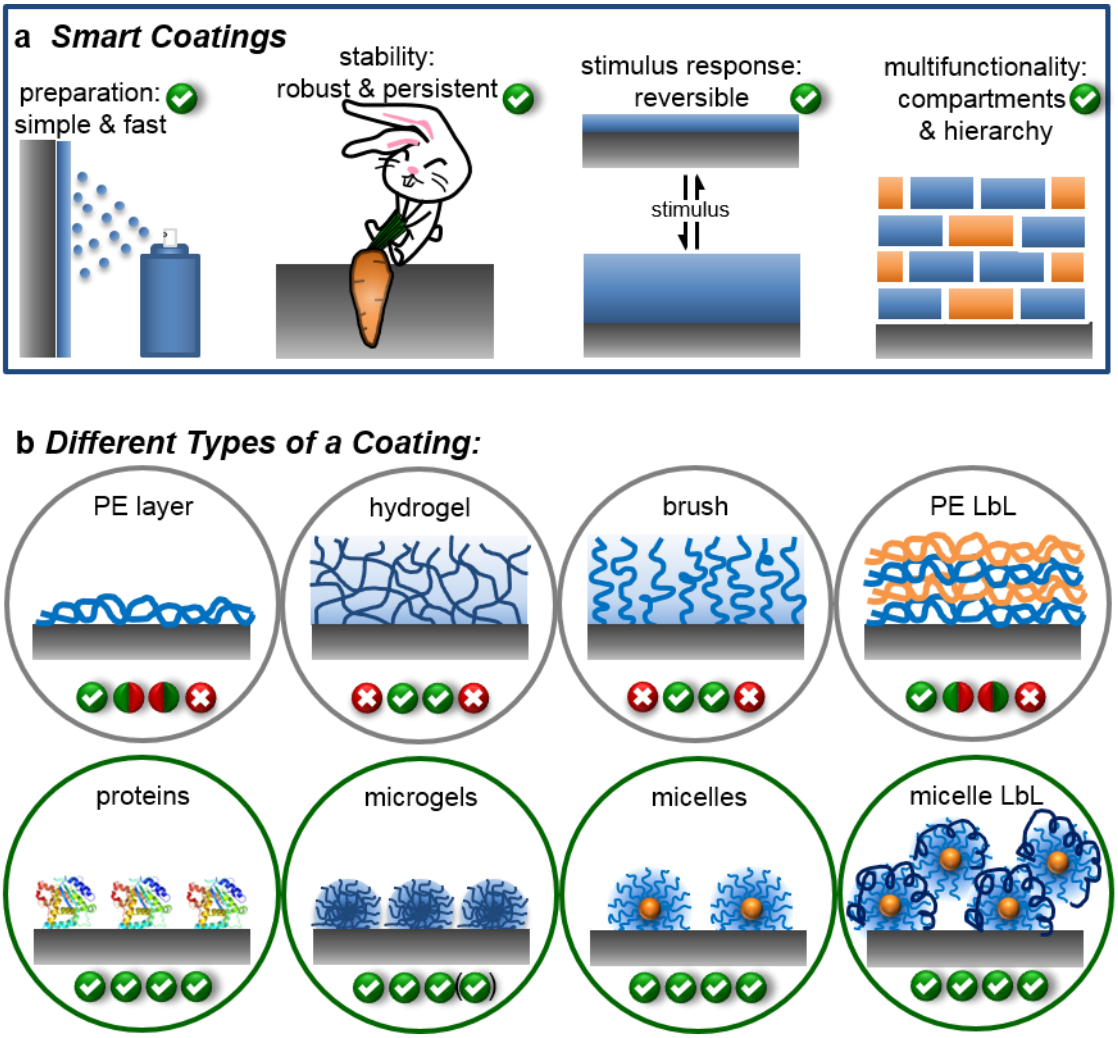

Figure 2.16. The concept of smart coatings and graphical illustrations of their key properties (a). 8 examples of different coatings (b), with top row showing conventional coatings and bottom row showing soft colloidal coatings. Their ability to meet the requirements of a smart coating are indicated by ticks and crosses. Thereby the order corresponds to the order of the properties in (a). For polyelectrolyte mono- and multilayers the stability and stimulus are co-dependent. Depending on whether the polyelectrolyte (PE) is weak or strong, the resulting layers are responsive or stable, respectively.

First, the application of the coating to the surface has to be simple and fast (i.e., user-friendly), independent of the actual synthesis process. After the attachment, the coating material should display a certain degree of persistence under altering environmental conditions. Beside their traditional purpose

as a passive barrier between a surface and its environment, functional coatings have to be active. As active coatings, they respond reversibly to subtle changes in the environment by changing their properties, such as charge density, water content, and mechanical properties. Moreover, smart coatings are also multifunctional, i.e. they respond separately to different stimuli, which require different levels of hierarchy and compartmentalization. A direct comparison based on these four key features provides a good insight in terms of the properties and performance of a coating.

Due to the relative simplicity in terms of synthesis and availability, the most common coatings are molecular polymer coatings. Probably the most known examples are polyelectrolyte mono-and multilayers, surface-grafted brushes and surface-anchored hydrogel networks (Figure 2.16b). Starting with the simplest one – the polyelectrolyte (PE) layer(s), the attachment of a linear PE to an oppositely charged surface is performed in a simple physisorption process via spin, dip or spray coating.[109, 126] Thereby, multiple attachment points along the chain provide the coating with sufficient stability and resilience on the surface. Depending on the nature of the PE, whether it is weak or strong, the layer is either pH-responsive or stable. Strong PEs provide the films with stability, and weak PEs ensure the stimulus response, but may detach from the surface under unfavorable pH conditions. The same restrictions apply to PE multilayers.[127-128]

At the cost of a simple sample preparation, covalent attachment provides brush layers and hydrogel films with considerable stability. Polymer brushes are usually end-grafted to or from the surface, rendering an additional modification of the polymer and / or the surface necessary.[129] The advantage of this approach is the preservation of the stimulus response, since the functional groups of the polymer do not participate in the attachment to the surface.[130-132] Similar to brush layers, anchoring a hydrogel film to the surface requires an additional layer of adhesion-promoting molecules.[133-134]

All four coatings share a major drawback, the lack of multifunctionality by means of hierarchy and compartmentalization, thereby fulfilling only ~50% of the requirements. Though the PE multilayers are hierarchically structured due to the layer-by-layer (LbL) approach, layer interdiffusion impedes the formation of distinct compartments.[135-136] However, there are many ways to improve these coatings, in order to satisfy the requirements for an intelligent coating, such as using block copolymers,[137-138] hydrogels with complex architectures,[139-141] block copolymer or mixed brushes,[131, 142] or via incorporation of colloidal objects into LbL films.[81, 143] Another, and in some cases even simpler approach to reach this particular goal is the use of soft colloidal building blocks as coating material.

In terms of the smart coating concept, soft colloidal coatings, such as proteins, microgels or block copolymer micelle mono- and multilayers (Figure 2.16c), are usually superior in their properties compared to the simpler variants of conventional coatings. Their attachment is generally performed by simple adsorption (via chemi- or physisorption) with several chains (synthetic polymers) or different functional groups (proteins) participating in the anchoring process, with still enough non-attached

chains / groups to secure responsiveness. The main advantage is the simplicity of this approach, but also the possibility to cover large areas of virtually any surface. Furthermore, the internal architecture of the colloidal building blocks provides the coatings with a superior stimulus response compared to simple molecular coatings. In addition to a compartmentalization of the coating by the particulate character, the internal compartmentalization of the colloidal building blocks, e.g. hydrophobic and hydrophilic patches of a protein, or core-shell structures of microgel particles and block copolymer micelles, provides the coatings with multifunctionality on a single particle level. Basically, coatings from soft colloids meet the four major requirements of a smart coating, thereby providing a foundation for intelligent application-targeted solutions.

Aside from the smart coating concept, soft colloidal building blocks provide further advantages with respect to their applications. For instance, proteins profit from the diversity of functional groups and the huge number of different AA combinations and sequences.[37] Due to the biological integrity, some proteins are widely used in biomedical applications, e.g. as coatings for biomedical devices and implants.[144-145] These proteins introduce biologically relevant properties to inert materials, mediate the material-cell interactions and trigger specific biological responses. The capping of nanoparticles with proteins results in highly efficient vehicles with the potential for site-specific / targeted drug delivery.[146]

Equally interesting for biomedical applications are stimuli-responsive microgel particles.[147] Due to structural heterogeneity of the polymer network in terms of mesh size distribution, surface-anchored hydrogel films suffer from a continuous swelling over a broad temperature range.[148] Thereby, the swelling is restricted to one dimension, perpendicular to the surface, and the equilibration may take days.[68] In contrast, microgel particles with a steep crosslinking gradient exhibit a sharp phase transition in a narrow temperature range.[70] The particles expand in all three dimensions with an equilibration in the range of milliseconds.[68] The fast response and a sharp transition are important aspects for biomedical engineering, specifically in the manipulation of cell attachment and proliferation.[149-150]

The diversity in block copolymer's structural complexity, especially in terms of functionality and architecture, gives rise to a great number of potential building blocks for smart coatings.[101-103] Kinetic constraints due to a high number of attachment sites provide surface-immobilized micelles with an excellent resilience on the surface, e.g. against dilution.[151] In contrast, their dynamic nature in terms of stimulus response often compromises the structural integrity. Especially diblock copolymer micelles often respond irreversibly to external triggers, either by partial desorption,[152-155] or by changes in their morphology to brush-like layers[156-157] or smaller micelles.[157] In contrast, triggering these changes in a controlled manner provides new possibilites for lithography free surface patterning and in situ formation of surface-immobilized colloidal molecules.[24] Furthermore, a wise choice of the block copolymer system (e.g. ABC triblock terpolymer),[121, 158] the substrate,[151] and other parameters[99-100, 159] allows the formation of smart micellar coatings with a reversible stimulus response or even multifunctionality on a single particle level.

Another approach to enhance the functionality and stability of block copolymer micelle layers is their incorporation into LbL films.[81, 160] Thereby, the complexation of the micellar corona with a linear PE provides the micelles with stability and introduces compartments to the film. In the case of diblock copolymer micelles a pH-responsive[161-164] or *T*-responsive[153-154, 157, 165-167] core, which does not participate in the multilayer buildup, secures the responsiveness of the LbL film. In triblock copolymer micelles, either the core[166-167] or the shell[168] may be responsive. The main advantage of this approach is the achievement of architectures with decoupled responsiveness and cohesion. Furthermore, the addition of another level of hierarchy beyond molecular scale provides the classical LbL architectures with reservoirs for controlled retention and release of functional cargo in response to environmental triggers.[153, 165] In any respect, the incorporation of supramolecular polymeric aggregates into multilayer films offers qualitatively novel opportunities.

As discussed above, a large number of materials and methods is available to functionalize a surface. Depending on the targeted application, even simple coatings may be sufficient to provide the desired functionality. Yet, in many aspects the colloidal coatings are still distinctly superior. Application of soft colloidal particles are gaining interest in life science, increasing importance in biotechnological and medical applications. Considering their promising properties, they are still subject to active research.

References

1. McCormick, C. L., Structural Design of Water-Soluble Copolymers. *ACS Symp. Ser.* **1991,** *467*, 2-24.
2. McCormick, C. L.; Lowe, A. B.; Ayres, N., Water-Soluble Polymers. In *Encyclopedia of Polymer Science and Technology*, John Wiley & Sons, Inc.: 2002.
3. Weber, C.; Hoogenboom, R.; Schubert, U. S., Temperature Responsive Bio-Compatible Polymers Based on Poly(ethylene oxide) and Poly(2-oxazoline)s. *Prog. Polym. Sci.* **2012,** *37*, 686-714.
4. Aseyev, V. O.; Tenhu, H.; Winnik, F. M., Temperature Dependence of the Colloidal Stability of Neutral Amphiphilic Polymers in Water. In *Conformation-Dependent Design of Sequences in Copolymers II*, Khokhlov, A. R., Ed. Springer-Verlag Berlin: Berlin, 2006; Vol. 196, pp 1-85.
5. Nayak, S.; Lyon, L. A., Soft Nanotechnology with Soft Nanoparticles. *Angew. Chem. Int. Ed.* **2005,** *44*, 7686-7708.
6. Plamper, F. A.; Ruppel, M.; Schmalz, A.; Borisov, O.; Ballauff, M.; Müller, A. H. E., Tuning the Thermoresponsive Properties of Weak Polyelectrolytes: Aqueous Solutions of Star-Shaped and Linear Poly(*N,N*-dimethylaminoethyl methacrylate). *Macromolecules* **2007,** *40*, 8361-8366.
7. Liu, H. Y.; Zhu, X. X., Lower Critical Solution temperatures of *N*-Substituted acrylamide Copolymers in Aqueous Solutions. *Polymer* **1999,** *40*, 6985-6990.
8. Nichifor, M.; Zhu, X. X., Copolymers of *N*-Alkylacrylamides and Styrene as New Thermosensitive Materials. *Polymer* **2003,** *44*, 3053-3060.
9. Bailey, F. E.; Callard, R. W., Some Properties of Poly(ethylene oxide)[1] in Aqueous Solution. *J. Appl. Polym. Sci.* **1959,** *1*, 56-62.
10. Louai, A.; Sarazin, D.; Pollet, G.; François, J.; Moreaux, F., Effect of Additives on Solution Properties of Ethylene oxide - Propylene oxide Statistical Copolymers. *Polymer* **1991,** *32*, 713-720.

11. Benkhira, A.; Bagassi, M.; Lachhab, T.; Rudatsikira, A.; Reibel, L.; François, J., Interactions of Ethylene Oxide/Methylene Oxide Copolymers with Sodium Dodecyl Sulphate. *Polymer* **2000,** *41*, 7415-7425.
12. Benkhira, A.; Lachhab, T.; Bagassi, M.; François, J., Interactions of Polyethers with a Cationic Surfactant. *Polymer* **2000,** *41*, 2471-2480.
13. Dautzenberg, H.; Jaeger, W.; Kötz, J.; Philipp, B.; Seidel, C.; Stscherbina, D., *Polyelectrolytes: Formation, Characterization and Application*. Carl Hanser Verlag: München, 1994.
14. Fleer, G. J.; Cohen Stuart, M. A.; Scheutjens, J. M. H. M.; Cosgrove, T.; Vincent, B., *Polymers at Interfaces*. Chapman & Hall: London, 1998.
15. Dobrynin, A. V.; Rubinstein, M., Theory of Oolyelectrolytes in Solutions and at Surfaces. *Prog. Polym. Sci.* **2005,** *30*, 1049-1118.
16. Manning, G. S., Limiting Laws and Counterion Condensation in Polyelectrolyte Solutions. I. Colligative PRoperties. *J. Chem. Phys.* **1969,** *51*, 924-933.
17. Overbeek, J. T. G., The Dissociation and Titration Constants of Polybasic Acids. *Bull. Soc. Chim. Belg.* **1948,** *57*, 252-261.
18. Rmaile, H. H.; Schlenoff, J. B., "Internal pK(a)'s" in Polyelectrolyte Multilayers: Coupling Protons and Salt. *Langmuir* **2002,** *18*, 8263-8265.
19. Currie, E. P. K.; Sieval, A. B.; Fleer, G. J.; Stuart, M. A. C., Polyacrylic Acid Brushes: Surface Pressure and Salt-Induced Swelling. *Langmuir* **2000,** *16*, 8324-8333.
20. Tomlinson, M. R.; Cousin, F.; Geoghegan, M., Creation of Dense Polymer Brush Layers by the Controlled Deposition of an Amphiphilic Responsive Comb Polymer. *Polymer* **2009,** *50*, 4829-4836.
21. Plamper, F. A.; Becker, H.; Lanzendorfer, M.; Patel, M.; Wittemann, A.; Ballauff, M.; Müller, A. H. E., Synthesis, Characterization and Behavior in Aqueous Solution of Star-Shaped Poly(acrylic acid). *Macromol. Chem. Phys.* **2005,** *206*, 1813-1825.
22. Parnell, A. J.; Martin, S. J.; Dang, C. C.; Geoghegan, M.; Jones, R. A. L.; Crook, C. J.; Howse, J. R.; Ryan, A. J., Synthesis, Characterization and Swelling Behaviour of Poly(methacrylic acid) Brushes Synthesized Using Atom Transfer Radical Polymerization. *Polymer* **2009,** *50*, 1005-1014.
23. Burkhardt, M.; Martinez-Castro, N.; Tea, S.; Drechsler, M.; Babin, I.; Grishagin, I.; Schweins, R.; Pergushov, D. V.; Gradzielski, M.; Zezin, A. B.; Müller, A. H. E., Polyisobutylene-*block*-Poly(methacrylic acid) Diblock Copolymers: Self-Assembly in Aqueous Media. *Langmuir* **2007,** *23*, 12864-12874.
24. Dewald, I.; Gensel, J.; Betthausen, E.; Borisov, O. V.; Müller, A. H. E.; Schacher, F. H.; Fery, A., Splitting of Surface-Immobilized Multicompartment Micelles into Clusters upon Charge Inversion. *ACS Nano* **2016,** *10*, 5180-5188.
25. Koetz, J.; Kosmella, S., *Polyelectrolytes and Nanoparticles*. Springer: Berlin, 2007.
26. *Polyelectrolytes: Thermodynamics and Rheology*. Springer International Publishing: Switzerland, 2014.
27. Michaels, A. S.; Miekka, R. G., Polyction-Polyanion Complexes - Preparation and Properties of Poly-(vinylbenzyltrimethylammonium) Poly-(styrenesulfonate). *J. Phys. Chem.* **1961,** *65*, 1765-1773.
28. Kabanov, V. A.; Zezin, A. B., Soluble Interpolymeric Complexes as a New Class of Synthetic Poly-Electrolytes. *Pure Appl. Chem.* **1984,** *56*, 343-354.
29. Bekturov, E. A.; Kudaibergenov, S. E.; Rafikov, S. R., Synthetic Polymeric Ampholytes in Solution. *Journal of Macromolecular Science-Reviews in Macromolecular Chemistry and Physics* **1990,** *C30*, 233-303.
30. Kudaibergenov, S. E., Behavior of Polyampholytes in Solutions. In *Polyampholytes: Synthesis, Characterization and Application*, Springer US: Boston, MA, 2002; pp 43-89.
31. Dobrynin, A. V.; Colby, R. H.; Rubinstein, M., Polyampholytes. *Journal of Polymer Science Part B-Polymer Physics* **2004,** *42*, 3513-3538.

32. Lowe, A. B.; McCormick, C. L., Synthesis and Solution Properties of Zwitterionic Polymers. *Chem. Rev.* **2002,** *102*, 4177-4189.
33. Gohy, J. F.; Creutz, S.; Garcia, M.; Mahltig, B.; Stamm, M.; Jérôme, R., Aggregates Formed by Amphoteric Diblock Copolymers in Water. *Macromolecules* **2000,** *33*, 6378-6387.
34. Pergushov, D. V.; Müller, A. H. E.; Schacher, F. H., Micellar Interpolyelectrolyte Complexes. *Chem. Soc. Rev.* **2012,** *41*, 6888-6901.
35. Gohy, J.-F., Stimuli-Responsive Block Copolymer Assemblies. In *Block Copolymers in Nanoscience*, Wiley-VCH Verlag GmbH & Co. KGaA: 2008; pp 91-116.
36. Cozzone, A. J., Proteins: Fundamental Chemical Properties. In *eLS*, John Wiley & Sons, Ltd: 2001.
37. Nelson, D. L.; Cox, M. M., *Lehninger Principles of Biochemistry*. 4th ed.; W.H. Freeman and Company: New York, 2005.
38. Reece, J. B.; Urry, L. A.; Cain, M. L.; Wasserman, S. A.; Minorsky, P. V.; Jackson, R. B., *Campbell Biology*. 9th ed.; Pearson Education, Inc.: 2011.
39. van Oss, C. J.; Good, R. J.; Chaudhury, M. K., Solubility of Proteins. *J. Protein Chem.* **1986,** *5*, 385-405.
40. Zayas, J. F., Solubility of Proteins. In *Functionality of Proteins in Food*, Springer Berlin Heidelberg: Berlin, Heidelberg, 1997; pp 6-75.
41. Pace, C. N.; Trevino, S.; Prabhakaran, E.; Scholtz, J. M., Protein Structure, Stability and Solubility in Water and Other Solvents. *Philos. Trans. R. Soc. London, Ser. B* **2004,** *359*, 1225-1234.
42. Zhang, J., Protein-Protein Interactions in Salt Solutions. In *Protein-Protein Interactions - Computational and Experimental Tools*, Cai, W.; Hong, H., Eds. InTech Europe: Rijeka, 2012.
43. Low-Resolution, Large-Scale Protein Fractionation: http://elte.prompt.hu/sites/default/files/tananyagok/IntroductionToPracticalBiochemistry/ch05s04.html (last access: July 2016).
44. Hydrophobic Interaction Chromatography: http://nptel.ac.in/courses/102103045/module5/lec31/2.html (last access: July 2016).
45. Evans, D. F.; Wennerström, H., *The Colloidal Domain - Where Physics, Chemistry, Biology, and Thechnology Meet*. 2nd ed.; Wiley-VCH: New York, 1999.
46. Bartlett, P.; Briscoe, W.; Cosgrove, T.; Davis, S.; Eastman, J.; Eastoe, J.; Fermin, D.; Hughes, R.; Kwamena, N.-O. A., .; Reid, J. P.; Reynolds, P.; Richardson, R.; Riley, J.; van Duijneveldt, J.; Vincent, B., *Colloid Science Principles, Methods and Applications*. 2nd ed.; John Wiley & Sons Ltd: Chichester, 2010.
47. Derjaguin, B., A Theory of Interaction of Particles in Presence of Electric Double-Layers and the Stability of Lyophobe Colloids and disperse Systems. *Acta Phys. Chim.* **1939,** *10*, 333-346.
48. Derjaguin, B.; Landau, L. D., Theory of the Stability of Strongly Charged Lyophobic Sols and of the Adhesion of Strongly Charged Particles in Solutions of Electrolytes *Acta Phys. Chim.* **1941,** *14*, 633-662.
49. Verwey, E. J. W.; Overbeek, J. T. G., *Theory of Stability of Lyophobic Colloids*. Elsevier: Amsterdam, 1948.
50. Israelachvili, J. N., *Intermolecular and Surface Forces*. 3rd ed.; Elsevier: Academic Press London, 2011.
51. Trefalt, G.; Borkovec, M. Overview of DLVO Theory. 2014, www.colloid.ch/dlvo (last access: July 2016).
52. Butt, H.-J.; Graf, K.; Kappl, M., *Physics and Chemistry of Interfaces*. WILEY-VCH: Weinheim, 2003.
53. Polte, J., Fundamental Growth Principles of Colloidal Metal Nanoparticles - A New Perspective. *CrystEngComm* **2015,** *17*, 6809-6830.

54. Gong, X. J.; Wang, Z. H.; Ngai, T., Direct Measurements of Particle-Surface Interactions in Aqueous Solutions with Total Internal Reflection Microscopy. *Chem. Commun.* **2014,** *50*, 6556-6570.
55. Moore, T. L.; Rodriguez-Lorenzo, L.; Hirsch, V.; Balog, S.; Urban, D.; Jud, C.; Rothen-Rutishauser, B.; Lattuada, M.; Petri-Fink, A., Nanoparticle Colloidal Stability in Cell Culture Media and Impact on Cellular Interactions. *Chem. Soc. Rev.* **2015,** *44*, 6287-6305.
56. Fleer, G.; Cohen Stuart, M.; Leermakers, F., Effect of Polymers on the Interaction between Colloidal Particles. In *Fundamentals of Interface and Colloid Science: Soft Colloids*, Lyklema, J., Ed. Elsevier Ltd.: 2005; Vol. V.
57. Bishop, K. J. M.; Wilmer, C. E.; Soh, S.; Grzybowski, B. A., Nanoscale Forces and Their Uses in Self-Assembly. *Small* **2009,** *5*, 1600-1630.
58. Adamczyk, Z., Particle Adsorption and Deposition: Role of Electrostatic Interactions. *Adv. Colloid Interface Sci.* **2003,** *100*, 267-347.
59. Szilagyi, I.; Trefalt, G.; Tiraferri, A.; Maroni, P.; Borkovec, M., Polyelectrolyte adsorption, Interparticle Forces, and Colloidal Aggregation. *Soft Matter* **2014,** *10*, 2479-2502.
60. Heyes, D. M.; Brańka, A. C., Interactions Between Microgel Particles. *Soft Matter* **2009,** *5*, 2681-2685.
61. Jones, R. G.; Kahovec, J.; Stepto, R.; Wilks, E. S.; Hess, M.; Kitayama, T.; Metanomski, W. V., *Compendium of Polmer Terminology and Nomenclature: IUPAC Recommendations* RSC Publishing: 2008.
62. Hertle, Y.; Hellweg, T., Thermoresponsive Copolymer Microgels. *J. Mater. Chem. B* **2013,** *1*, 5874-5885.
63. Albrecht, K.; Arndt, K.-F.; Ballauff, M.; Groll, J.; Krahl, F.; Landfester, K.; Lu, Y.; Moeller, M.; Musyanovych, A.; Pich, A.; Richtering, W.; Welsch, N., *Chemical Design of Responsive Microgels*. Springer: Berlin Heidelberg, 2011.
64. Pelton, R., Temperature-Sensitive Aqueous Microgels. *Adv. Colloid Interface Sci.* **2000,** *85*, 1-33.
65. Saunders, B. R.; Vincent, B., Microgel Particles as Model Colloids: Theory, Properties and Applications. *Adv. Colloid Interface Sci.* **1999,** *80*, 1-25.
66. Wedel, B.; Zeiser, M.; Hellweg, T., Non NIPAM Based Smart Microgels: Systematic Variation of the Volume Phase Transition Temperature by Copolymerization. *Z. Phys. Chem.* **2012,** *226*, 737-748.
67. Zeiser, M.; Freudensprung, I.; Hellweg, T., Linearly Thermoresponsive Core-Shell Microgels: Towards a New Class of Nanoactuators. *Polymer* **2012,** *53*, 6096-6101.
68. Cheng, H.; Zhang, G., Thermally Sensitive Microgels: From Basic Science to Applications. In *Hydrogel Micro and Nanoparticles*, Lyon, L. A.; Serpe, M. J., Eds. Wiley-VCH Verlag GmbH & Co. KGaA: 2012; pp 1-32.
69. Wu, C.; Zhou, S. Q., Volume Phase Transition of Swollen Gels: Discontinuous or Continuous? *Macromolecules* **1997,** *30*, 574-576.
70. Wedel, B. Thermoresponsive Mikrogele auf *N*-Alkylacrylamidbasis: Einfluss der chemischen Struktur der Monomere auf die Partikelbildung sowie die strukturellen und thermischen Eigenschaften von Homopolymer- und Copolymersystemen. Universität Bielefeld, Bielefeld, 2015.
71. Fernandes, P. A. L.; Schmidt, S.; Zeiser, M.; Fery, A.; Hellweg, T., Swelling and Mechanical Properties of Polymer Gels with Cross-Linking Gradient. *Soft Matter* **2010,** *6*, 3455-3458.
72. Das, M.; Zhang, H.; Kumacheva, E., Microgels: Old Materials with New Applications. In *Annual Review of Materials Research*, 2006; Vol. 36, pp 117-142.
73. Wellert, S.; Richter, M.; Hellweg, T.; von Klitzing, R.; Hertle, Y., Responsive Microgels at Surfaces and Interfaces. *Z. Phys. Chem.* **2015,** *229*, 1225-1250.
74. Karg, M., Multifunctional Inorganic/Organic Hybrid Microgels. *Colloid. Polym. Sci.* **2012,** *290*, 673-688.

75. Karg, M.; Hellweg, T., New "Smart" Poly(NIPAM) Microgels and Nanoparticle Microgel Hybrids: Properties and Advances in Characterisation. *Curr. Opin. Colloid Interface Sci.* **2009,** *14*, 438-450.
76. Karg, M.; Hellweg, T., Smart Inorganic/Organic Hybrid Microgels: Synthesis and Characterisation. *J. Mater. Chem.* **2009,** *19*, 8714-8727.
77. Israelachvili, J. N., *Intermolecular and Surface Forces*. 2nd ed.; Academic Press: San Diego, **1992**.
78. Gao, Z. S.; Eisenberg, A., A Model of Micellization for Block-Copolymers in Solutions. *Macromolecules* **1993,** *26*, 7353-7360.
79. Alexandridis, P.; Lindman, B., *Amphiphilic Block Copolymers - Self-Assembly and Applications*. Elsevier Science B. V.: Amsterdam, 2000.
80. Nicolai, T.; Colombani, O.; Chassenieux, C., Dynamic Polymeric Micelles *versus* Frozen Nanoparticles Formed by Block Copolymers. *Soft Matter* **2010,** *6*, 3111-3118.
81. Dewald, I.; Fery, A., Polymeric Micelles and Vesicles in Polyelectrolyte Multilayers: Introducing Hierarchy and Compartmentalization. *Adv. Mater. Interfaces* **2017**, *4*, 1600317 (1-11).
82. Hamley, I. W., *Block Copolymers in Solution: Fundamentals and Applications*. John Wiley & Sons Ltd.: Chichester, 2005.
83. Gohy, J. F., Block Copolymer Micelles. In *Block Copolymers II*, Abetz, V., Ed. Springer: Berlin, 2005; Vol. 190, pp 65-136.
84. Smart, T.; Lomas, H.; Massignani, M.; Flores-Merino, M. V.; Perez, L. R.; Battaglia, G., Block Copolymer Nanostructures. *Nano Today* **2008,** *3*, 38-46.
85. Mai, Y.; Eisenberg, A., Self-assembly of Block Copolymers. *Chem. Soc. Rev.* **2012,** *41*, 5969-5985.
86. Blanazs, A.; Armes, S. P.; Ryan, A. J., Self-Assembled Block Copolymer Aggregates: From Micelles to Vesicles and their Biological Applications. *Macromol. Rapid Commun.* **2009,** *30*, 267-277.
87. Le Meins, J. F.; Sandre, O.; Lecommandoux, S., Recent Trends in the Tuning of Polymersomes' Membrane Properties. *Eur. Phys. J. E* **2011,** *34*, 1-17.
88. Ramanathan, M.; Shrestha, L. K.; Mori, T.; Ji, Q.; Hill, J. P.; Ariga, K., Amphiphile Nanoarchitectonics: From Basic Physical Chemistry to Advanced Applications. *PCCP* **2013,** *15*, 10580-10611.
89. Fustin, C. A.; Abetz, V.; Gohy, J. F., Triblock Terpolymer Micelles: A Personal Outlook. *Eur. Phys. J. E* **2005,** *16*, 291-302.
90. Löbling, T. I.; Borisov, O.; Haataja, J. S.; Ikkala, O.; Gröschel, A. H.; Müller, A. H. E., Rational Design of ABC Triblock Terpolymer Solution Nanostructures with Controlled Patch Morphology. *Nat. Commun.* **2016,** *7*, 12097-12097.
91. Bates, F. S.; Fredrickson, G. H., Block Copolymers - Designer Soft Materials. *Physics Today* **1999,** *52*, 32-38.
92. Moughton, A. O.; Hillmyer, M. A.; Lodge, T. P., Multicompartment Block Polymer Micelles. *Macromolecules* **2012,** *45*, 2-19.
93. Rharbi, Y.; Winnik, M. A., Salt Effects on Solute Exchange in Sodium Dodecyl Sulfate Micelles. *J. Am. Chem. Soc.* **2002,** *124*, 2082-2083.
94. Pool, R.; Bolhuis, P. G., Sampling the Kinetic Pathways of a Micelle Fusion and Fission Transition. *J. Chem. Phys.* **2007,** *126*, 244703-(1-9).
95. Sammalkorpi, M.; Karttunen, M.; Haataja, M., Micelle Fission through Surface Instability and Formation of an Interdigitating Stalk. *J. Am. Chem. Soc.* **2008,** *130*, 17977-17980.
96. Borisov, O. V.; Zhulina, E. B.; Leermakers, F. A. M.; Müller, A. H. E., Self-Assembled Structures of Amphiphilic Ionic Block Copolymers: Theory, Self-Consistent Field Modeling and Experiment. In *Self Organized Nanostructures of Amphiphilic Block Copolymers I*, Müller, A. H. E.; Borisov, O., Eds. 2011; Vol. 241, pp 57-129.

97. Mok, M. M.; Lodge, T. P., Temperature-Based Fluorescence Measurements of Pyrene in Block Copolymer Micelles: Probing Micelle Core Glass Transition Breadths. *J. Polym. Sci., Part B: Polym. Phys.* **2012,** *50*, 500-515.
98. van Stam, J.; Creutz, S.; De Schryver, F. C.; Jérôme, R., Tuning of the Exchange Dynamics of Unimers between Block Copolymer Micelles with Temperature, Cosolvents, and Cosurfactants. *Macromolecules* **2000,** *33*, 6388-6395.
99. Betthausen, E.; Drechsler, M.; Förtsch, M.; Pergushov, D. V.; Schacher, F. H.; Müller, A. H. E., Stimuli-Responsive Micellar Interpolyelectrolyte Complexes - Control of Micelle Dynamics *via* Core Crosslinking. *Soft Matter* **2012,** *8*, 10167-10177.
100. O'Reilly, R. K.; Hawker, C. J.; Wooley, K. L., Cross-Linked Block Copolymer Micelles: Functional Nanostructures of Great Potential and Versatility. *Chem. Soc. Rev.* **2006,** *35*, 1068-1083.
101. Bates, F. S.; Hillmyer, M. A.; Lodge, T. P.; Bates, C. M.; Delaney, K. T.; Fredrickson, G. H., Multiblock Polymers: Panacea or Pandora's Box? *Science* **2012,** *336*, 434-440.
102. Gröschel, A. H.; Müller, A. H. E., Self-Assembly Concepts for Multicompartment Nanostructures. *Nanoscale* **2015,** *7*, 11841-11876.
103. Liu, Y.; Liu, B.; Nie, Z., Concurrent Self-Assembly of Amphiphiles into Nanoarchitectures with Increasing Complexity. *Nano Today* **2015,** *10*, 278-300.
104. O'Shaughnessy, B.; Vavylonis, D., Non-Equilibrium in Adsorbed Polymer Layers. *J. Phys.: Condens. Matter* **2005,** *17*, R63-R99.
105. Motschmann, H.; Stamm, M.; Toprakcioglu, C., Adsorption-Kinetics of Block Copolymers from a Good Solvent - A 2-Stage Process. *Macromolecules* **1991,** *24*, 3681-3688.
106. Bucur, C. B.; Sui, Z.; Schlenoff, J. B., Ideal Mixing in Polyelectrolyte Complexes and Multilayers: Entropy Driven Assembly. *J. Am. Chem. Soc.* **2006,** *128*, 13690-13691.
107. Schlenoff, J. B.; Rmaile, A. H.; Bucur, C. B., Hydration Contributions to Association in Polyelectrolyte Multilayers and Complexes: Visualizing Hydrophobicity. *J. Am. Chem. Soc.* **2008,** *130*, 13589-13597.
108. Schlenoff, J. B.; Dubas, S. T., Mechanism of Polyelectrolyte Multilayer Growth: Charge Overcompensation and Distribution. *Macromolecules* **2001,** *34*, 592-598.
109. Decher, G., Fuzzy Nanoassemblies: Toward Layered Polymeric Multicomposites. *Science* **1997,** *277*, 1232-1237.
110. Decher, G.; Hong, J. D.; Schmitt, J., Buildup of Ultrathin Multilayer Films by a Self-Assembly Process. 3. Consecutive Adsorption of Anionic and Cationic Polyelectrolytes on Charged Surfaces. *Thin Solid Films* **1992,** *210*, 831-835.
111. Pagonabarraga, I.; Rubí, J. M., Adsorption of Colloidal Particles: Influence of Transport (Hydrodynamic Interactions). *Colloids Surf., A* **1997,** *127*, 249-255.
112. Johnson, C. A.; Lenhoff, A. M., Adsorption of Charged Latex Particles on Mica Studied by Atomic Force Microscopy. *J. Colloid Interface Sci.* **1996,** *179*, 587-599.
113. Pericet-Camara, R.; Papastavrou, G.; Borkovec, M., Atomic Force Microscopy Study of the Adsorption and Electrostatic Self-Organization of Poly(amidoamine) Dendrimers on Mica. *Langmuir* **2004,** *20*, 3264-3270.
114. Feder, J., Random Sequential Adsorption. *J. Theor. Biol.* **1980,** *87*, 237-254.
115. Schaaf, P.; Talbot, J., Kinetics of Random Sequential Adsorption. *Phys. Rev. Lett.* **1989,** *62*, 175-178.
116. Schaaf, P.; Talbot, J., Surface Exclusion Effects in Adsorption Processes. *J. Chem. Phys.* **1989,** *91*, 4401-4409.
117. Pomeau, Y., Some Asymptotic Estimates in the Random Parking Problem. *J. Phys. A: Math. Gen.* **1980,** *13*, L193-L196.
118. Adamczyk, Z.; Zembala, M.; Siwek, B.; Warszyński, P., Structure and Ordering in Localized Adsorption of Particles. *J. Colloid Interface Sci.* **1990,** *140*, 123-137.

119. Borkovec, M. Adsorption of Dendrimers on Oppositely Charged Solid Substrates. 2012, www.colloid.ch/dendrimers (last access: August 2016).
120. Hanske, C.; Schneider, C.; Drechsler, M.; Wittemann, A.; Fery, A., Salt-Regulated Attraction and Repulsion of Spherical Polyelectrolyte Brushes Towards Polyelectrolyte Multilayers. *PCCP* **2012,** *14*, 4196-4203.
121. Gensel, J.; Betthausen, E.; Hasenöhrl, C.; Trenkenschuh, K.; Hund, M.; Boulmedais, F.; Schaaf, P.; Müller, A. H. E.; Fery, A., Surface Immobilized Block Copolymer Micelles with Switchable Accessibility of Hydrophobic Pockets. *Soft Matter* **2011,** *7*, 11144-11153.
122. Malaquin, L.; Kraus, T.; Schmid, H.; Delamarche, E.; Wolf, H., Controlled Particle Placement Through Convective and Capillary Assembly. *Langmuir* **2007,** *23*, 11513-11521.
123. Schaaf, P.; Voegel, J. C.; Senger, B., From Random Sequential Adsorption to Ballistic Deposition: A General View of Irreversible Deposition Processes. *J. Phys. Chem. B* **2000,** *104*, 2204-2214.
124. Challener, C., The Intelligence Behind Smart Coatings. *JCT CoatingsTech* **2006,** *3*, 50-55.
125. Shchukin, D.; Möhwald, H., A Coat of Many Functions. *Science* **2013,** *341*, 1458-1459.
126. Decher, G., Layer-by-Layer Assembly (Putting Molecules to Work). In *Multilayer Thin Films*, Wiley-VCH Verlag GmbH & Co. KGaA: 2012; pp 1-21.
127. Sukhishvili, S., Responsive Layer-by-Layer Assemblies: Dynamics, Structure and Function. In *Multilayer Thin Films*, Wiley-VCH Verlag GmbH & Co. KGaA: 2012; pp 337-362.
128. Glinel, K.; Déjugnat, C.; Prevot, M.; Schöler, B.; Schönhoff, M.; Klitzing, R. V., Responsive polyelectrolyte multilayers. *Colloids Surf., A* **2007,** *303*, 3-13.
129. Barbey, R.; Lavanant, L.; Paripovic, D.; Schuwer, N.; Sugnaux, C.; Tugulu, S.; Klok, H. A., Polymer Brushes via Surface-Initiated Controlled Radical Polymerization: Synthesis, Characterization, Properties, and Applications. *Chem. Rev.* **2009,** *109*, 5437-5527.
130. Brittain, W. J.; Minko, S., A structural definition of polymer brushes. *J. Polym. Sci., Part A: Polym. Chem.* **2007,** *45*, 3505-3512.
131. Minko, S., Responsive Polymer Brushes. *Polym. Rev.* **2006,** *46*, 397-420.
132. Rühe, J.; Ballauff, M.; Biesalski, M.; Dziezok, P.; Gröhn, F.; Johannsmann, D.; Houbenov, N.; Hugenberg, N.; Konradi, R.; Minko, S.; Motornov, M.; Netz, R. R.; Schmidt, M.; Seidel, C.; Stamm, M.; Stephan, T.; Usov, D.; Zhang, H., Polyelectrolyte Brushes. In *Polyelectrolytes with Defined Molecular Architecture I*, Schmidt, M., Ed. Springer: Berlin Heidelberg, 2004; Vol. 165.
133. Mateescu, A.; Wang, Y.; Dostalek, J.; Jonas, U., Thin Hydrogel Films for Optical Biosensor Applications. *Membranes* **2012,** *2*, 40-69.
134. Navarro, R.; Perrino, M. P.; Prucker, O.; Rühe, J., Preparation of Surface-Attached Polymer Layers by Thermal or Photochemical Activation of alpha-Diazoester Moieties. *Langmuir* **2013,** *29*, 10932-10939.
135. Picart, C.; Mutterer, J.; Richert, L.; Luo, Y.; Prestwich, G. D.; Schaaf, P.; Voegel, J. C.; Lavalle, P., Molecular basis for the explanation of the exponential growth of polyelectrolyte multilayers. *Proc. Natl. Acad. Sci. U. S. A.* **2002,** *99*, 12531-12535.
136. Soltwedel, O.; Ivanova, O.; Nestler, P.; Müller, M.; Köhler, R.; Helm, C. A., Interdiffusion in Polyelectrolyte Multilayers. *Macromolecules* **2010,** *43*, 7288-7293.
137. Luo, M.; Epps, T. H., Directed Block Copolymer Thin Film Self-Assembly: Emerging Trends in Nanopattern Fabrication. *Macromolecules* **2013,** *46*, 7567-7579.
138. Segalman, R. A., Patterning with block copolymer thin films. *Mater. Sci. Eng., R* **2005,** *48*, 191-226.
139. Tokarev, I.; Minko, S., Stimuli-Responsive Hydrogel Thin films. *Soft Matter* **2009,** *5*, 511-524.
140. White, E. M.; Yatvin, J.; Grubbs, J. B.; Bilbrey, J. A.; Locklin, J., Advances in smart materials: Stimuli-responsive hydrogel thin films. *J. Polym. Sci., Part B: Polym. Phys.* **2013,** *51*, 1084-1099.

141. Chollet, B.; Li, M.; Martwong, E.; Bresson, B.; Fretigny, C.; Tabeling, P.; Tran, Y., Multiscale Surface-Attached Hydrogel Thin Films with Tailored Architecture. *ACS Appl. Mater. Interfaces* **2016,** *8*, 11729-11738.
142. Synytska, A.; Stamm, M.; Diez, S.; Ionov, L., Simple and Fast Method for the Fabrication of Switchable Bicomponent Micropatterned Polymer Surfaces. *Langmuir* **2007,** *23*, 5205-5209.
143. Rubner, M. F.; Cohen, R. E., Layer-by-Layer Processed Multilayers: Challenges and Opportunities. In *Multilayer Thin Films*, Wiley-VCH Verlag GmbH & Co. KGaA: 2012; pp 23-41.
144. Ferreira, P.; Alves, P.; Coimbra, P.; Gil, M. H., Improving Polymeric Surfaces for Biomedical Applications: A Review. *J. Coat. Technol. Res.* **2015,** *12*, 463-475.
145. Uquillas Paredes, J. A.; Polini, A.; Chrzanowski, W., Protein-Based Biointerfaces to Control Stem Cell Differentiation. In *Biointerfaces: Where Material Meets Biology*, Hutmacher, D.; Chrzanowski, W., Eds. The Royal Society of Chemistry: Cambridge, 2014; pp 1-29.
146. Chanana, M.; Rivera_Gil, P.; Correa-Duarte, M. A.; Liz-Marzán, L. M.; Parak, W. J., Physicochemical Properties of Protein-Coated Gold Nanoparticles in Biological Fluids and Cells before and after Proteolytic Digestion. *Angew. Chem. Int. Ed.* **2013,** *52*, 4179-4183.
147. Peppas, N. A.; Hilt, J. Z.; Khademhosseini, A.; Langer, R., Hydrogels in Biology and Medicine: From Molecular Principles to Bionanotechnology. *Adv. Mater.* **2006,** *18*, 1345-1360.
148. Di Lorenzo, F.; Seiffert, S., Nanostructural heterogeneity in polymer networks and gels. *Polymer Chemistry* **2015,** *6*, 5515-5528.
149. Uhlig, K.; Wegener, T.; He, J.; Zeiser, M.; Bookhold, J.; Dewald, I.; Godino, N.; Jaeger, M.; Hellweg, T.; Fery, A.; Duschl, C., Patterned Thermoresponsive Microgel Coatings for Noninvasive Processing of Adherent Cells. *Biomacromolecules* **2016,** *17*, 1110-1116.
150. Schmidt, S.; Zeiser, M.; Hellweg, T.; Duschl, C.; Fery, A.; Möhwald, H., Adhesion and Mechanical Properties of PNIPAM Microgel Films and Their Potential Use as Switchable Cell Culture Substrates. *Adv. Funct. Mater.* **2010,** *20*, 3235-3243.
151. Webber, G. B.; Wanless, E. J.; Armes, S. P.; Tang, Y.; Li, Y.; Biggs, S., Nano-Anemones: Stimulus-Responsive Copolymer-Micelle Surfaces. *Adv. Mater.* **2004,** *16*, 1794-1798.
152. Webber, G. B.; Wanless, E. J.; Bütün, V.; Armes, S. P.; Biggs, S., Self-Organized Monolayer Films of Stimulus-Responsive Micelles. *Nano Lett.* **2002,** *2*, 1307-1313.
153. Zhu, Z. C.; Sukhishvili, S. A., Temperature-Induced Swelling and Small Molecule Release with Hydrogen-Bonded Multilayers of Block Copolymer Micelles. *ACS Nano* **2009,** *3*, 3595-3605.
154. Erel, I.; Zhu, Z. C.; Zhuk, A.; Sukhishvili, S. A., Hydrogen-Bonded Layer-by-Layer Films of Block Copolymer Micelles with pH-Responsive Cores. *J. Colloid Interface Sci.* **2011,** *355*, 61-69.
155. Mahltig, B.; Müller-Buschbaum, P.; Wolkenhauer, M.; Wunnicke, O.; Wiegand, S.; Gohy, J. F.; Jérôme, R.; Stamm, M., Highly Regular Polyampholytic Structures Adsorbed Directly from Solution. *J. Colloid Interface Sci.* **2001,** *242*, 36-43.
156. Sakai, K.; Smith, E. G.; Webber, G. B.; Baker, M.; Wanless, E. J.; Bütün, V.; Armes, S. P.; Biggs, S., Characterizing the pH-Responsive Behavior of Thin Films of Diblock Copolymer Micelles at the Silica/Aqueous Solution Interface. *Langmuir* **2006,** *22*, 8435-8442.
157. Xu, L.; Zhu, Z. C.; Sukhishvili, S. A., Polyelectrolyte Multilayers of Diblock Copolymer Micelles with Temperature-Responsive Cores. *Langmuir* **2011,** *27*, 409-415.
158. Gensel, J.; Borke, T.; Pazos-Pérez, N.; Fery, A.; Andreeva, D. V.; Betthausen, E.; Müller, A. H. E.; Möhwald, H.; Skorb, E. V., Cavitation Engineered 3D Sponge Networks and Their Application in Active Surface Construction. *Adv. Mater.* **2012,** *24*, 985-989.
159. Webber, G. B.; Wanless, E. J.; Armes, S. P.; Biggs, S., Tunable Diblock Copolymer Micelles-Adapting Behaviour *via* Subtle Chemical Modifications. *Faraday Discuss.* **2005,** *128*, 193-209.
160. Zhu, Z. C.; Sukhishvili, S. A., Layer-by-layer Films of Stimuli-Responsive Block Copolymer Micelles. *J. Mater. Chem.* **2012,** *22*, 7667-7671.

161. Biggs, S.; Sakai, K.; Addison, T.; Schmid, A.; Armes, S. P.; Vamvakaki, M.; Bütün, V.; Webber, G., Layer-by-layer formation of smart particle coatings using oppositely charged block copolymer micelles. *Adv. Mater.* **2007,** *19*, 247.

162. Sakai, K.; Webber, G. B.; Vo, C.-D.; Wanless, E. J.; Vamvakaki, M.; Bütün, V.; Armes, S. P.; Biggs, S., Characterization of layer-by-layer self-assembled multilayer films of diblock copolymer micelles. *Langmuir* **2008,** *24*, 116-123.

163. Addison, T.; Cayre, O. J.; Biggs, S.; Armes, S. P.; York, D., Polymeric Microcapsules Assembled from a Cationic/Zwitterionic Pair of Responsive Block Copolymer Micelles. *Langmuir* **2010,** *26*, 6281-6286.

164. Addison, T.; Cayre, O. J.; Biggs, S.; Armes, S. P.; York, D., Incorporation of Block Copolymer Micelles into Multilayer Films for Use as Nanodelivery Systems. *Langmuir* **2008,** *24*, 13328-13333.

165. Zhu, Z. C.; Gao, N.; Wang, H. J.; Sukhishvili, S. A., Temperature-triggered on-demand drug release enabled by hydrogen-bonded multilayers of block copolymer micelles. *J. Controlled Release* **2013,** *171*, 73-80.

166. Tan, W. S.; Cohen, R. E.; Rubner, M. F.; Sukhishvili, S. A., Temperature-Induced, Reversible Swelling Transitions in Multilayers of a Cationic Triblock Copolymer and a Polyacid. *Macromolecules* **2010,** *43*, 1950-1957.

167. Tan, W. S.; Zhu, Z.; Sukhishvili, S. A.; Rubner, M. F.; Cohen, R. E., Effect of Block Copolymer Architecture on the Thermally Induced Swelling of Micelle-Containing Multilayer Thin Films. *Macromolecules* **2011,** *44*, 7767-7774.

168. Gensel, J.; Dewald, I.; Erath, J.; Betthausen, E.; Müller, A. H. E.; Fery, A., Reversible Swelling Transitions in Stimuli-Responsive Layer-by-Layer Films Containing Block Copolymer Micelles. *Chemical Science* **2013,** *4*, 325-334.

3 Overview of the Thesis

3.1 Objectives of the Thesis

The key objectives of the thesis are summarized schematically in Figure 3.1. The reported findings are focused on the understanding of the interplay between the three major components: the substrate, the soft colloidal particles, and their environment.

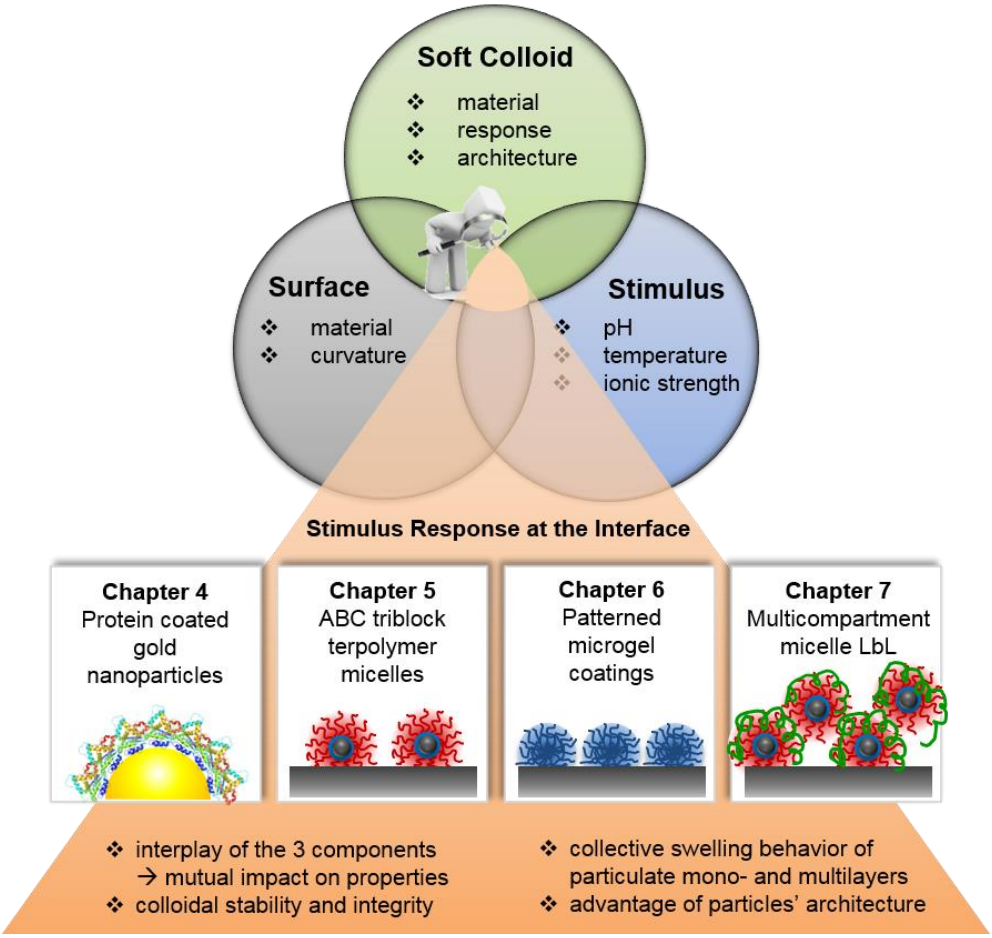

Figure 3.1. Interplay of the three components, surface, stimulus, and type of soft colloids, and its impact on the coatings' stimulus response at the interface. The main findings are summarized below the according depiction of the investigated system.

The comprehensive investigation of different colloidal particles and their interactions with the environment at a solid-liquid interface was performed in view of the possible applications. The findings of this study represent the basis for future advances in the field of colloidal coatings and are expected to promote their application. The application of soft colloidal building blocks as coating material is based

on the benefits discussed in Chapter 2. Especially the mutual influence between the particles and the surface upon adsorption, stimuli-triggered changes in surface morphology, and collective swelling of particulate mono- and multilayers were investigated.

3.2 Content of the Individual Chapters

This thesis consists of four projects. Chapters 4 to 6 are individual publications. Chapter 7 is a manuscript prepared for future publication. The scientific studies presented in this thesis are generally targeted at the design and characterization of stimuli-responsive surface coatings made from soft colloidal particles as building blocks.

The first part (Chapter 4-5) of the thesis deals with the preparation and characterization of polyampholytic colloidal objects. The main focus is given to the investigation of interplay between the three components – the surface, the soft colloids and their environment – and the resulting mutual impact on each other's properties. In Chapter 4 protein-coated gold nanoparticles are used as a model system to study the impact of parameters such as coating material (different proteins) and environmental triggers (pH, ionic strength) on the responsiveness and colloidal stability of the resulting hybrid system. In Chapter 5 a similarly intricate interplay is examined for pH-responsive multicompartment micelles from a linear ABC triblock terpolymer. In contrast to micelles in solution, the surface-immobilized micelles respond to pH changes by splitting into well-defined clusters of submicelles.

In the second part (Chapter 6-7), the collective swelling behavior of surface-immobilized soft colloidal particle layers, more specifically mono- and multilayer systems, is investigated. Firstly (Chapter 6), the thermoresponsive properties of microgel monolayers were studied. The microgel-covered substrates are reversibly and repeatedly switchable between a cell-attractive and a cell-repellent state, thus providing the substrate with control over cell adhesion and cell cultivation. Secondly (Chapter 7), highly swellable multilayer films were constructed using multicompartment micelles from ABC triblock terpolymers. The strong response to changes in pH and / or ionic strength is a result of the hierarchical assembly of building blocks with internal architecture.

The summary of the main results is presented below.

3.2.1 Protein-Coated Gold Nanoparticles

The central point of Chapter 4 is the investigation of the influence of environmental conditions and material properties of the coating and the surface on the final physicochemical properties of coated objects. To study the interplay between the three parameters, gold nanoparticles (AuNPs) were used as a model surface. They are particularly well suited for studying such interactions owing to their plasmonic properties. Depending on the size and shape they exhibit a typical localized surface plasmon resonance (LSPR) band in the UV–vis–NIR spectral range. In addition, the LSPR is highly sensitive to the

interparticle distance and the refractive index of the surrounding media. Thus, it is considered to be a useful optical tool for detection of adsorption and aggregation events caused by the coating material. Furthermore, there is an increasing interest in inorganic NPs for biomedical applications.[1] Their application as drug delivery vehicles brings the NPs inevitably into contact with biological environments. The exposure to protein rich liquids induces immediate adsorption of different proteins, which results in the formation of an undefined protein corona altering particle's properties. To study the impact of the protein properties (M_w and pI) and the environmental conditions (pH and ionic strength) on the final physicochemical properties and colloidal stability of AuNPs under controlled conditions, 10 different proteins – one at a time – were used as coating material.

To demonstrate the effect of the interplay, spherical AuNPs of an average size of ~15 nm in diameter were mixed with proteins of different pI and M_w dissolved in water of different pH (2, 7, 12) and salinity (no salt, PBS buffer) (Figure 3.2a). The stability and the degree of agglomeration in the mixture were judged from the red-shift of the plasmon peak via UV–vis, the hydrodynamic size via DLS, and surface charge via zeta-potential measurements as shown exemplarily for pepsin-coated AuNPs in Figure 3.2b.

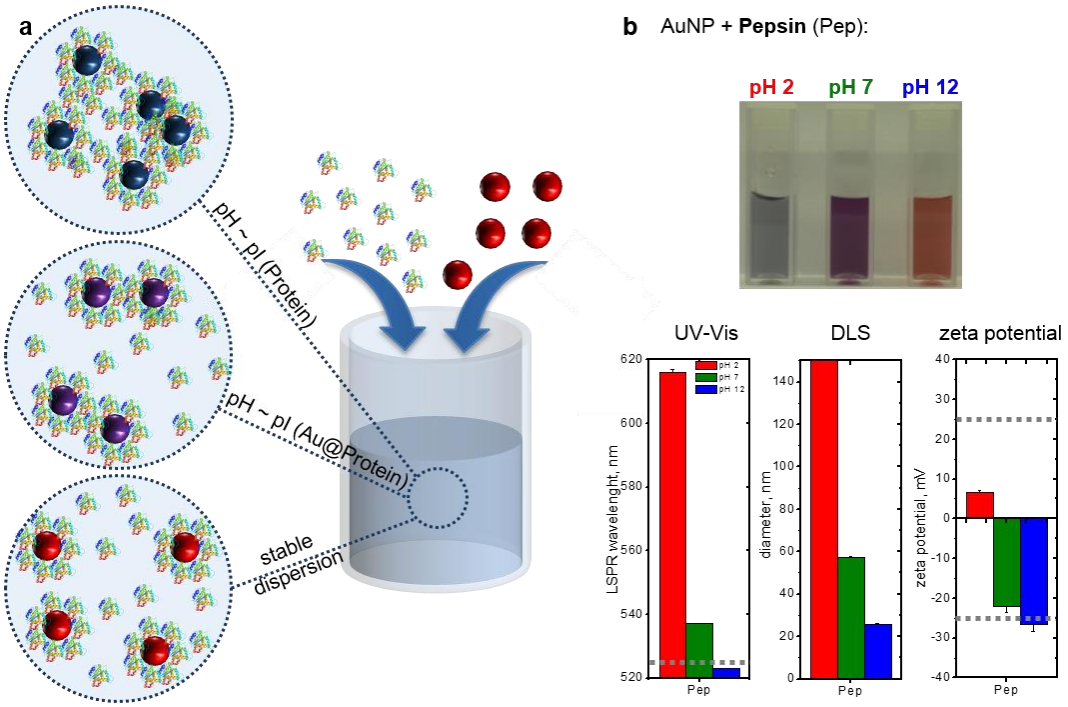

Figure 3.2. Schematic illustration of mixing gold nanoparticles (AuNPs) with proteins (a). Data obtained from mixing AuNPs with pepsin (Pep) at different pH conditions (pH 2, 7 and 12) (b). The dotted gray lines represent the stability thresholds (UV–vis: 525 nm; ζ-potential: ±25 mV).

Depending on the availability of ionizable residues and the environmental conditions, the proteins may bind to the metal surface with both negatively or positively charged functional groups, which become then unavailable for the interactions with water. Changes in the ratio between positively and negatively charged groups upon binding leads to a measurable shift in pI, as compared to bare proteins. Consequently, there are two sources of agglomeration during the mixing of gold NPs with proteins that

correlate with the pH of the mixture: (1) the insolubility of the excess protein and (2) the instability of the resulting protein coated AuNPs (Au@Protein). In both cases, the agglomeration was found to be reversible if the environmental pH was changed to a value far away from the respective pI, and the excess protein was removed from the mixture.

The final protein coated nanoparticles exhibit specific stabilities and surface charges that depend on protein type and the conditions during its adsorption. To understand the effect of the environmental pH on the stability of the purified Au@Protein NPs systems, we studied the pH-dependent colloidal stability profiles over the pH range between pH 2 and 12, covering also a broad pI and M_w range of proteins from acidic (pepsin: 2.8)[2] to basic (lysozyme: 11.0)[3-4] and from 5.8 kDa (insulin)[5] to 34.6 kDa (pepsin),[6] respectively. Exemplarily, the results for lysozyme-coated particles (Au@LYZ) are shown in Figure 3.3.

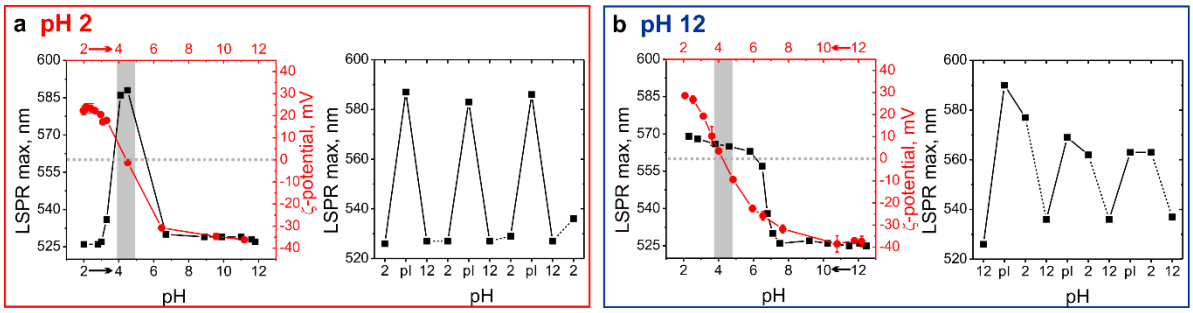

Figure 3.3. The direction-dependent stability profiles for the lysozyme coated AuNPs (Au@LYZ) and the corresponding pH-responsive reversible aggregation/disaggregation cycles. Prior to the measurements Au@LYZ were purified either in pH 2 (a) or pH 12 (b). The pI of the Au@LYZ NPs and the pH stability range of the NPs were determined by measuring the ζ-potential (red) and LSPR maximum, λ_{max} (black) as a function of solution pH. The gray stripes indicate the region of the pI (±0.5 pH units).

We found that the resulting Au@Protein particles exhibit extremely high colloidal stability indicated by the reversible agglomeration/disagglomeration behavior. Depending on their M_w and the starting pH, Au@Protein particles show two types of solubility profiles, U-shaped or sigmoidal, which determine the stability range of the system. Proteins with high M_w exhibit a U-shaped profile similar to bare proteins. In contrast, small proteins show sigmoidal profiles. We found that these differences arise from different stabilization mechanisms, the availability of charged residues, and in the case of middle sized proteins, such as lysozyme (Figure 3.3), the starting / purification pH. In a first approximation, the knowledge of the stability range of a hybrid system allows the estimation of its behavior under similar biological conditions.

The results obtained in this study demonstrate the importance of all three factors for the adjustment of the properties and performance of the coated material. We showed the mutual influence of the surface and coating material under controlled environmental conditions. On the one hand, the coating provides the surface with a protective layer and introduces functionality, but may also alter the surface's (optical) properties. On the other hand, the immobilization of soft particles on a surface can lead to changes in

their shape (conformation, unfolding) and / or the response to external triggers (accessibility of functional groups, shifts in pI).

3.2.2 Morphological Changes in Polyampholyte Micelles

In Chapter 5 the investigation of the interplay between a surface, a colloidal coating, and the environmental conditions was performed using polyampholytic micelles from an ABC triblock terpolymer. The block polyampholyte BMAAD consists of a hydrophobic polybutadiene (B) block, a poly(methacrylic acid) (MAA) middle block, and a poly(2-(dimethylamino)ethyl methacrylate) (D) block. Both, MAA and D are weak polyelectrolytes, rendering the polymer pH-sensitive (Figure 3.4a). The polymer was synthesized by Felix H. Schacher and Eva Betthausen in the group of Prof. Axel H. E. Müller (during cooperation University of Bayreuth, now Johannes Gutenberg University Mainz).

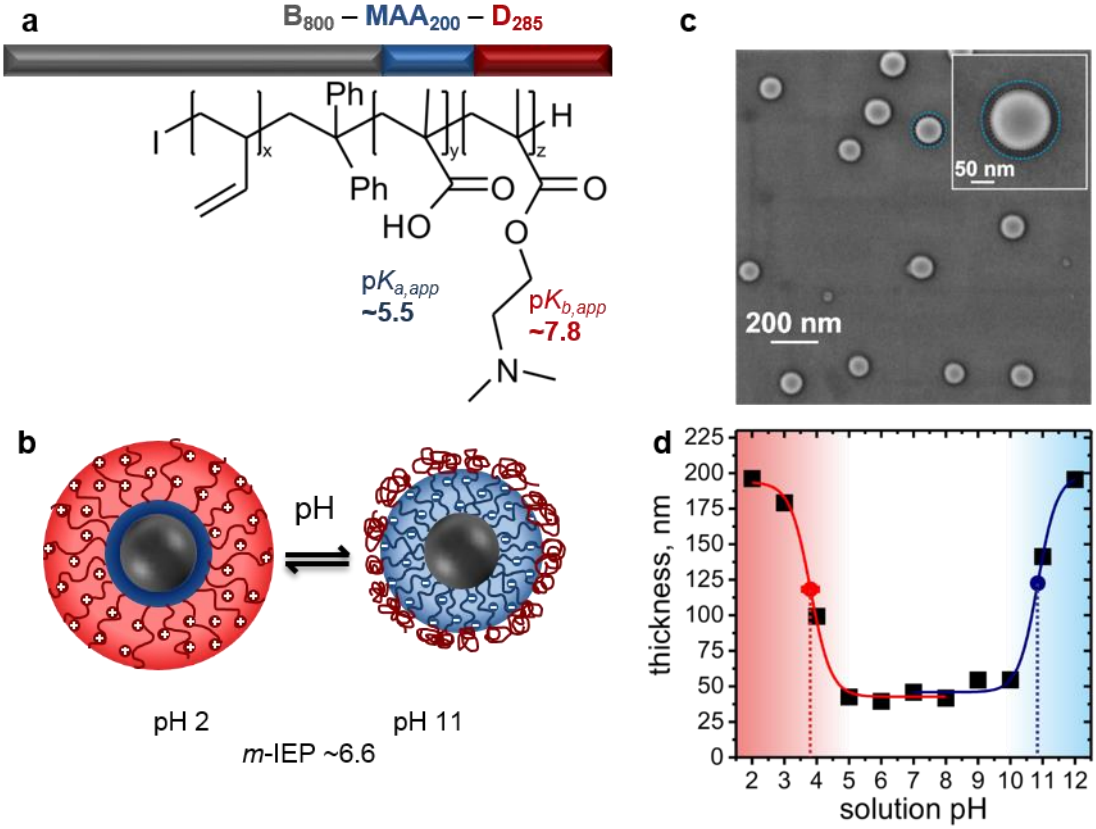

Figure 3.4. Chemical structure of the BMAAD triblock terpolymer with the corresponding dissociation constants of the pH-responsive blocks (a). Schematic illustration of micellar aggregates in aqueous solution below and above the micellar isoelectric point (m-IEP) (b). SEM image showing the surface-immobilized micelles (B core: black dashed line, MAA shell: blue dashed line) (c). The pH response of a BMAAD monolayer as a function of pH measured using in situ ellipsometry (d).

In aqueous solution the triblock terpolymer self-assembles into core-shell-corona micelles with B block in the micellar core.[7] The composition of the shell and the corona depends on solution pH. As shown in Figure 3.4b, at both strongly acidic and strongly basic pH star-like micelles are formed. At low pH the hydrophobic core is surrounded by the collapsed / uncharged MAA shell and a positively charged D corona. In contrast, at high pH values the MAA block is negatively charged, whereas the D block is

uncharged, but remains soluble. At intermediate pH, closer to the micellar isoelectric point (m-IEP), the oppositely charged blocks form an intramicellar interpolyelectrolyte complex (im-IPEC) which results in a compact structure and nearly neutral net charges.

To study the impact of a flat substrate with a pH-dependent charge density on the micellar morphology, the BMAAD micelles were immobilized on a silica surface via dip coating from a pH 2 solution. We found that upon adsorption the micelles retain their spherical shape and their stimulus response, as indicated by the scanning electron microscopy images and the in situ ellipsometry measurements (Figure 3.4c,d). The swelling observed in strong acidic and strong basic pH is a consequence of the stretching of either the D or the MAA block, with increasing charge density. In the range of moderate pH values, the film thickness decreases due to the formation of the im-IPEC between the two PEs. The strong shifts in the apparent dissociation constants are attributed to the interaction between weak polybase and weak polyacid blocks and the confinement at the interface.

Moreover, we found that an abrupt change in the environmental conditions from pH 2 to pH 11 has a major impact on the morphology of surface-immobilized BMAAD micelles. Within 1 h of exposure to pH 11, the initial micelles undergo a complete splitting process into clusters of well-defined spherical subunits (submicelles) as shown in Figure 3.5. Thereby, the ex situ AFM measurements on the same spot allowed us to track the changes in morphology on a single particle level.

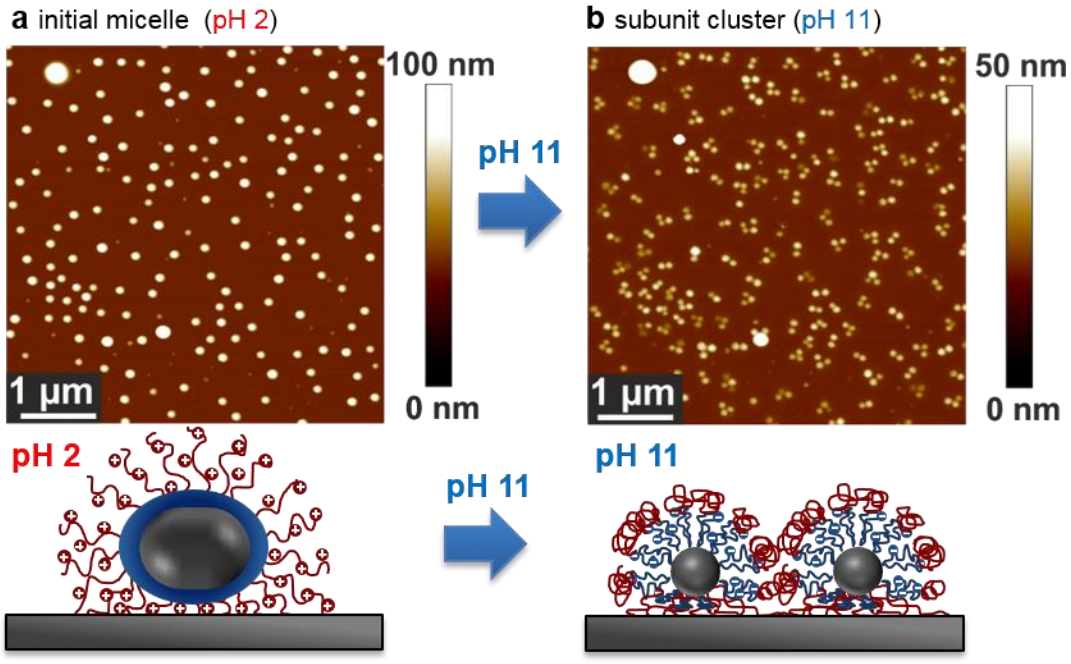

Figure 3.5. Ex situ AFM measurements on the same spot of the sample (in dry state) performed after adsorption from pH 2 solution (a) and after incubation in pH 11 for 1 h (b). Schematic illustration of the BMAAD micelle indicates the structural rearrangements of the triblock terpolymer in the splitting process.

We found that the pH-induced structural rearrangements of the BMAAD micelles into subunits are the result of an intricate interplay between polymer characteristics, such as nature, length and sequence of

each block, micelle immobilization on a pH-sensitive surface, and the solution pH. A pH-switch from pH 2 to pH 11 leads to a fast charge reversal inside the micelle from positive to negative. Simultaneously, the density of negative charges increases on the silica surface. Due to the internal osmotic pressure inside the charged MAA shell and the overall repulsive interactions, the micelles become unstable, rupture, and ~60% of the polymer is desorbed from the surface. The remaining ~40% are retained due to secondary interactions between D block and silica and are subject to subsequent rearrangements with the aim to minimize the total free energy of the system. Thereby, the hydrophobic B core is forced to adjust to the pH response of the shell.

These results suggest that the splitting is a compromise between the hydrophobicity of B, aiming at the minimization of the B/water interface, and the repulsion of negatively charged MAA chains, attempting to increase the distance between neighboring charged groups. Hence, the pH-induced splitting of BMAAD micelles provides an insight into the delicate balance between competing forces at the interface and opens new perspectives to surface-assisted cluster formation.

3.2.3 Thermoresponsive Microgel Coatings

In Chapter 6 the fabrication of thermoresponsive coatings based on colloidal crosslinked microgel particles is presented for noninvasive processing of adherent cells. In this study, microgels from poly(*N*-isopropylacryamide) (PNIPAM) with a volume phase transition temperature (VPPT) of ~32 °C and a steep crosslinking gradient were used. These properties are advantageous with regard to biomedical applications, allowing for reversible switching between a cell-attractive and cell-repellent state of surface-immobilized mocrogel monolayers in a biologically relevant temperature range (Figure 3.6). The microgel particles were synthesized by Michael Zeiser and Johannes Bookhold in the group of Prof. Thomas Hellweg (University of Bielefeld).

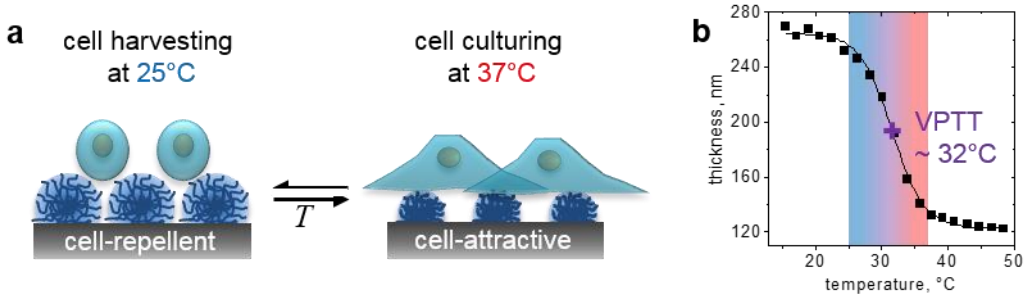

Figure 3.6. Schematic illustration of cell behavior on microgel-coated substrates at 25 °C and 37 °C (a). A plot of the temperature-dependent swelling of microgel monolayers with a complete phase transition within the relevant temperature range (b).

In this context, patterned surfaces with microgel-covered spots and microgel-free areas were produced by inkjet printing and microcontact printing. The printing experiments were performed by Thomas Wegener and Jian He (GeSiM mbH). Depending on the concentration of the microgel dispersion, spots

with different surface coverages and interparticle distances were found. Using cell tests and AFM measurements (Figure 3.7a) we correlated the microgel density with cell detachment functionality. Thereby, a higher surface coverage and smaller interparticle distances, as a consequence of a higher microgel concentration during printing, inhibited cell-surface interactions and facilitated cell detachment upon cooling to room temperature.

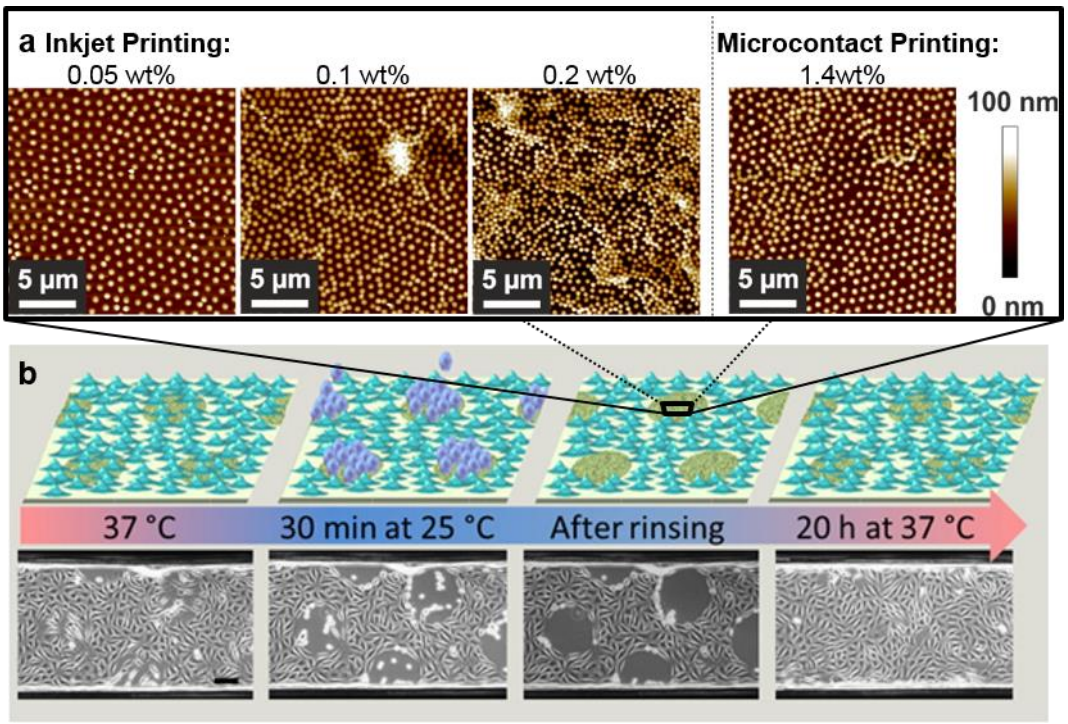

Figure 3.7. AFM height images of microgel-covered spots produced via Inkjet Printing or Microcontact Printing using different dispersion concentrations (a). Schematic illustration and phase contrast images of a wound healing experiment performed on microgel spots in a microfluidic channel (b). Therefore, L929 mouse fibroblasts were first cultivated at 37 °C. After the temperature decrease to 25 °C, the rounded cells were rinsed from the microgel spots only. The following increase to 37 °C facilitated the resettlement of cells inside the spots.

To demonstrate the broad applicability of patterned thermoresponsive coatings, the microgel-coated substrates were integrated into a microfluidic cell assay as shown in Figure 3.7b. First, L929 mouse fibroblasts were grown at 37 °C until the surface was covered by a monolayer of spread cells. At 25 °C the cells located on microgel spots assumed a rounded shape and were flushed away via a laminar shear flow, leaving cell-free areas. After ~20 h at 37 °C the cells resettled the cell-free microgel spots. The microgel-covered patches are reversibly and repeatedly switchable between a cell-attractive and a cell-repellent state, thus providing the substrate with localized control over cell adhesion and cell cultivation. The cell experiments were performed by Dr. Katja Uhlig in the group of Prof. Claus Duschl (Fraunhofer Institute for Cell Therapy and Immunology).

As a future perspective, the combination of soft thermoresponsive colloids as coating material and the controlled environment of a microfluidic chamber provides a powerful tool for drug screening experiments, in terms of efficacy and toxicity toward different cell lines.

3.2.4 Stimuli Responsive Micelle Multilayer Films

Chapter 7 addresses the incorporation of polymeric micelles into multilayer structures and the resulting advantages which arise from the hierarchical assembly and the internal architecture of the micellar aggregates. For this purpose, micelles from an ABC triblock terpolymer, BMAADq, were used. BMAADq consists of a hydrophobic polybutadiene (B) block, a poly(methacrylic acid) (MAA) middle block, and a quaternized poly(2-(dimethylamino)ethyl methacrylate) (Dq) block (Figure 3.8a). The polymer was synthesized by Felix H. Schacher and Eva Betthausen in the group of Prof. Axel H. E. Müller (during cooperation University of Bayreuth, now Johannes Gutenberg University Mainz). At pH 4 the triblock terpolymer aggregates to micellar structures with a hydrophobic B core, a collapsed / uncharged MAA shell, and a positively charged Dq corona as shown in Figure 3.8b.

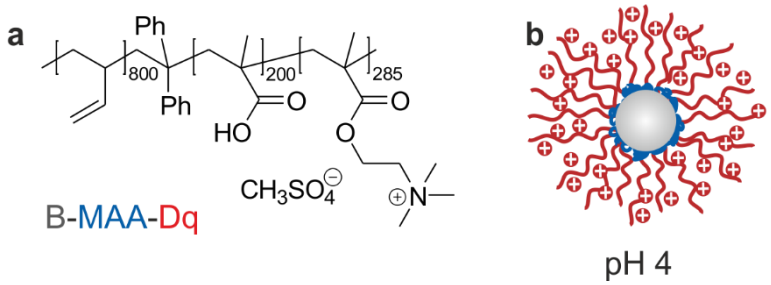

Figure 3.8. Chemical structure of the BMAADq triblock terpolymer (a) and the schematic illustration of the micellar structure in pH 4 (b).

For the multilayer formation at pH 4, BMAADq micelles were assembled with poly(sodium 4-styrene sulfonate) (PSS) – a strong polyanion – in an alternating manner using the layer-by-layer[8] approach. A schematic illustration of the resulting structures is given in Figure 3.9a. As we found in our previous work, the high stability and the pronounced swelling of BMAADq/PSS films are the result of decoupling the functionality and the cohesion.[9] The stability of the multilayer structure is provided by the complex between two strong polyelectrolytes – Dq corona and PSS. The pronounced swelling was attributed to the brush-like nature of the pH-sensitive MAA shell.

The aim of the study in Chapter 7 was the investigation of the swelling behavior of BMAADq/PSS multilayer films with regard to the anomalous salt effect (non-monotonous swelling)[10-11] known for weak PE brush systems, and the contribution of the Dq/PSS complex to the overall swelling. We found that the swelling of the micelle/PSS multilayers can be decoupled under appropriate conditions (Figure 3.9b).

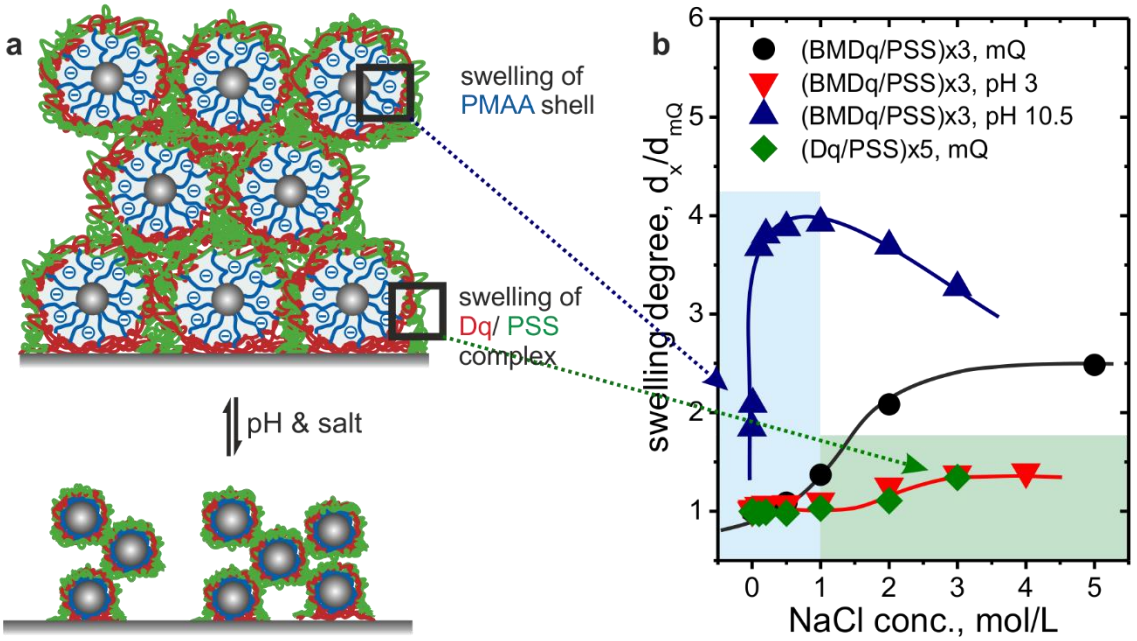

Figure 3.9. Schematic illustration of the BMAADq/PSS multilayer film in collapsed (uncharged MAA block) and swollen (charged MAA shell) state (a). Swelling degree of $(BMAADq/PSS)_3$ in different pH and $(Dq/PSS)_5$ film plotted as a function of salt concentration (b). The blue background in the plot indicates the contribution of MAA shell to the swelling. The green background highlights the contribution of the Dq/PSS complex.

A control experiment with Dq/PSS multilayer films showed a remarkable correlation with the swelling of BMAADq/PSS films at pH 3 – well below the $pK_{a,app}$~9.5[9] of the incorporated micelles. In both cases, the swelling occurs at salt concentrations of ≥1 M. In contrast, at pH values above the $pK_{a,app}$ the already swollen films swell even further with increasing salt concentration until a maximum at 1 M is reached. Since no contribution of the complex is expected at low salt concentrations, the swelling is attributed solely to the brush-like behavior of the MAA shell. For intermediate pH conditions and salt concentrations the contribution of both the shell and the PE complex is expected.

The decoupling of the swelling behavior in two compartments, in addition to the decoupling of functionality and stability, opens new perspectives for the surface-mediated drug co-delivery.

3.3 Individual Contributions to Joint Publications

The results presented in this thesis were obtained in collaboration with others. In the following the contributions of each co-author are specified. The asterisks denote the corresponding authors.

Chapter 4

This work was published in *The Journal of Physical Chemistry C* **2016**, *199* (45), 25482-25492 under the title:

"Protein Identity and Environmental Parameters Determine the Final Physicochemical Properties of Protein-Coated Metal Nanoparticles"

by Inna Dewald, Olga Isakin, Jonas Schubert, Tobias Kraus, and Munish Chanana*

I was involved in the initial experiments, evaluated the data and wrote the manuscript. Olga Isakin performed the experiments within the scope of her master thesis under my guidance. Jonas Schubert assisted with literature research and was involved in correcting the manuscript. Tobias Kraus was involved in scientific discussions. Munish Chanana wrote the manuscript, was involved in scientific discussions and corrected the manuscript.

Chapter 5

This work was published in *ACS Nano* **2016**, *10* (5), 5180-5188 under the title:

"Splitting of Surface-Immobilized Multicompartment Micelles into Clusters upon Charge Inversion"

by Inna Dewald, Julia Gensel, Eva Betthausen, Oleg V. Borisov, Axel H.E. Müller, Felix H. Schacher, Andreas Fery*

I performed the experiments, evaluated the data and wrote the manuscript. Julia Gensel was involved in the initial experiments and scientific discussions. Felix H. Schacher and Eva Betthausen conducted the synthesis of the polymer. Eva Betthausen was involved in correcting the manuscript. Oleg V. Borisov wrote the theoretical part of the manuscript, was involved in scientific discussions and correcting the manuscript. Axel. H.E. Müller and Felix. H. Schacher were involved in scientific discussions and correcting the manuscript. Andreas Fery supervised the project, wrote a part of the manuscript and was involved in scientific discussions.

Chapter 6

This work was published in *Biomacromolecules*, **2016**, *17* (3), 1110-1116 under the title:

"Patterned Thermoresponsive Microgel Coatings for Noninvasive Processing of Adherent Cells"

by Katja Uhlig*, Thomas Wegener, Jian He, Michael Zeiser, Johannes Bookhold, Inna Dewald, Neus Godino, Magnus Jaeger, Thomas Hellweg, Andreas Fery, and Claus Duschl

I performed AFM measurements and wrote a part of the manuscript. Katja Uhlig performed cell culture tests and wrote the manuscript. Michael Zeiser and Johannes Bookhold conducted the synthesis of the microgels. Thomas Wegener and Jian He performed the printing experiments. Neus Godino assisted with microfluidic setups. Thomas Hellweg, Andreas Fery, Magnus Jaeger and Claus Duschl were involved in scientific discussions and corrected the manuscript.

Chapter 7

This chapter is unpublished work prepared for future publication under the title:

"Impact of Compartmentalization on the Salt-Induced Swelling in Block Copolymer Micelle Multilayers"

by Inna Dewald, Julia Gensel, Johann Erath, Alexandra Leluk, Eva Betthausen, Oleg V. Borisov, Axel H.E. Müller, Felix H. Schacher, Andreas Fery*

I performed most of the experiments and wrote the manuscript. Julia Gensel was involved in project development and scientific discussions. Johann Erath performed Colloidal Probe AFM measurements. Alexandra Leluk performed measurements on polyelectrolyte multilayer films within the scope of her lab course under my guidance. Felix H. Schacher and Eva Betthausen synthesized the polymer used. Oleg V. Borisov wrote the theoretical part of the manuscript and was involved in scientific discussions. Axel H.E. Müller and Felix H. Schacher were involved in scientific discussions. Andreas Fery supervised the project and was involved in scientific discussions.

References

1. Conde, J.; Dias, J. T.; Grazú, V.; Moros, M.; Baptista, P. V.; de la Fuente, J. M., Revisiting 30 Years of Biofunctionalization and Surface Chemistry of Inorganic Nanoparticles for Nanomedicine. *Frontiers in Chemistry* **2014,** *2*.
2. Malamud, D.; Drysdale, J. W., Isoelectric Points of Proteins - Table. *Anal. Biochem.* **1978,** *86*, 620-647.
3. Lauer, H. H.; McManigill, D., Capillary Zone Electrophoresis of Proteins in Untreated Fused-Silica Tubing. *Anal. Chem.* **1986,** *58*, 166-170.
4. Wetter, L. R.; Deutsch, H. F., Immunological Studies on Egg White Proteins. 4. Immunochemical and Physical Studies of Lysozyme. *J. Biol. Chem.* **1951,** *192*, 237-242.
5. Ui, N., Isoelectric Points and Conformation of Proteins. 1. Effect of Urea on Behavior of Some Proteins in Isoelectric Focusing. *Biochim. Biophys. Acta* **1971,** *229*, 567-581.
6. Sepulveda, P.; Marciniszyn, J.; Liu, D.; Tang, J., Primary Structure of Porcine Pepsin. 3. Amino-Acid Sequence of a Cyanogen-Bromide Fragment, CB2A, and Complete Structure of Porcine Pepsin. *J. Biol. Chem.* **1975,** *250*, 5082-5088.
7. Betthausen, E.; Drechsler, M.; Förtsch, M.; Schacher, F. H.; Müller, A. H. E., Dual Stimuli-Responsive Multicompartment Micelles from Triblock Terpolymers with Tunable Hydrophilicity. *Soft Matter* **2011,** *7*, 8880-8891.
8. Decher, G., Fuzzy Nanoassemblies: Toward Layered Polymeric Multicomposites. *Science* **1997,** *277*, 1232-1237.
9. Gensel, J.; Dewald, I.; Erath, J.; Betthausen, E.; Müller, A. H. E.; Fery, A., Reversible Swelling Transitions in Stimuli-Responsive Layer-by-Layer Films Containing Block Copolymer Micelles. *Chemical Science* **2013,** *4*, 325-334.
10. Biesalski, M.; Johannsmann, D.; Rühe, J., Synthesis and Swelling Behavior of a Weak Polyacid Brush. *J. Chem. Phys.* **2002,** *117*, 4988-4994.
11. Bhat, R. R.; Tomlinson, M. R.; Wu, T.; Genzer, J., Surface-Grafted Polymer Gradients: Formation, Characterization, and Applications. In *Surface-Initiated Polymerization II*, Springer: Berlin, 2006; Vol. 198, pp 51-124.

4 Protein Identity and Environmental Parameters Determine the Final Physicochemical Properties of Protein-Coated Metal Nanoparticles*

Reprinted with permission from

Protein Identity and Environmental Parameters Determine the Final Physicochemical Properties of Protein-Coated Metal Nanoparticles, Inna Dewald, Olga Isakin, Jonas Schubert, Tobias Kraus, and Munish Chanana,

The Journal of Physical Chemistry C **2015** *119* (45), 25482-25492

DOI: 10.1021/acs.jpcc.5b06266

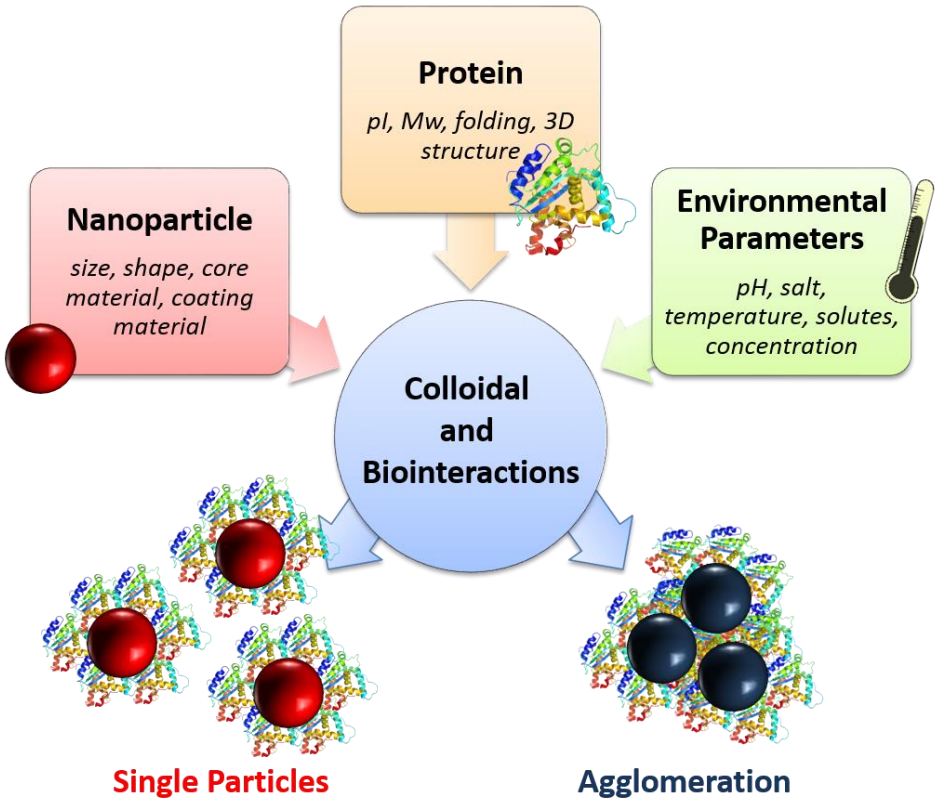

* Inna Dewald and Olga Isakin contributed equally

Abstract

When a nanomaterial enters a biological system, proteins adsorb onto the particle surface and alter the surface properties of nanoparticles, causing drastic changes in physicochemical properties such as hydrodynamic size, surface charge and aggregation state, thus giving a completely new and undefined physicochemical identity to the nanoparticles. In the present work, we study the impact of the protein identity (molecular weight and isoelectric point) and the environmental conditions (pH and ionic strength) on the final physicochemical properties of a model nanoparticle system, i.e. gold nanoparticles. Gold nanoparticles either form stable dispersions or agglomerate spontaneously when mixed with protein solutions, depending on the protein and the experimental conditions. Strikingly, the agglomerates redisperse to individually dispersed and colloidally stable nanoparticles, depending on the purification pH. The final protein coated nanoparticles exhibit specific stabilities and surface charges that depend on protein type and the conditions during its adsorption. By understanding the interactions of nanoparticles with proteins under controlled conditions, we can define the protein corona of the nanoparticles and thus their physicochemical properties in various media.

Introduction

Safe use of nanomaterials in industrial and life science applications requires to fundamentally understand and to control the interactions of nanomaterials with biological systems.[1-7] These interactions strongly depend on the physicochemical properties of the nanomaterial (including colloidal stability, surface charge, and wettability) and the physiological parameters in the biological system. In cells and organisms, the situation becomes complex because the environmental conditions (such as pH, ionic strength, and temperature) and composition (presence of various solutes and biomolecules) can differ from compartment to compartment.[7] When a nanomaterial enters a biological system, its surface is immediately covered by biomatter, usually proteins.[1, 2] Proteins adsorb onto the particle surface forming an undefined protein "corona".[3-6] The adsorbed proteins alter the surface properties of nanoparticles (NPs) and cause drastic changes in the physicochemical properties such as hydrodynamic size, surface charge, and aggregation state and give a new and unknown physicochemical identity to the NPs. This physicochemical identity determines the particles' fate in biological systems mediated by their interaction with biomolecules and membranes in various physiological environments.[7] Deeper understanding of the nuances of NP bonding within biological environments is required not only to advance their applicability in life science applications but also to foresee their long-term fate in human body and environment.[2] Here, we investigate the interactions of NPs with proteins under controlled conditions to ultimately describe, explain, and control the protein corona of the NPs and thus their final physicochemical properties.

Gold NPs in combination with proteins have been used as colorimetric detectors of proteins[8-10] to study proteins' structural conformation,[9, 11] protein kinetics,[10, 12] and their chemical modifications.[9, 13] In terms

of medical applications, they have been used as specific targets and for the delivery of drugs and biomolecules.[14-16] In all of these applications, it is paramount to maintain the stability of colloidal gold solutions by suppressing aggregation. Stability depends on the interplay of (a) the nanoparticle surface chemistry (*nanoparticle identity*), (b) the properties of the protein (*protein identity*, i.e., molecular composition, molecular weight (MW), isoelectric point (pI), folding), and (c) environmental parameters (*environmental identity*, i.e., solvent, pH, ionic strength, temperature). For example, gold NPs have been mixed with proteins such as bovine serum albumin (BSA), human serum albumin (HSA), ovalbumin (Ova), insulin (Ins), β-lactoglobulin (BLG), lysozyme (LYZ), and trypsinogen (Tg).[17-19] Depending on the protein identity (pI and MW) and the experimental conditions (*environmental identity*: pH, concentrations, ionic strength), either stable particle dispersions[18-20] or particle aggregates[17-19, 21, 22] are obtained, which can easily be demonstrated in the case of gold NPs by the color change of dispersions. The aggregation process can be easily monitored by the shift and broadening of the LSPR band.

Proteins are usually dissolved in pH-controlled buffer solutions (phosphate,[17, 23, 24] TRIS,[23] borate,[23] hepes,[24] or at physiological conditions (pH 7.4)), and effects of the ionic strength and pH of the media have to be considered. For example, Chen et al.[18] mixed a series of proteins such as ribonuclease A (Rib), cytochrome c (cyt C), Tg, α-chymotrypsinogen A (α-Chy), myoglobin (Myo), hemoglobin (Hb), conalbumin (CA), α-lactalbumin (α-Lac), Ova, BSA, β-casein (β-Cas), glucose oxidase (GO), and Ins with citrate-coated gold NPs (Au@Citrate) in 10 mM glycin at pH 7 and observed immediate aggregation for all the high-pI proteins, including Hb. They suggested the electrostatic interactions between the positively charged proteins and the negatively charged NPs to cause agglomeration. On the other hand, Garabagiu et al.[19] mixed Hb with Au@Citrate NPs in 100 mM phosphate buffer and observed strong binding of Hb without signs of aggregation. Hydrophobic interactions were invoked to explain adsorption. A recent study[25] revealed that Au@Citrate NPs agglomerate in the presence of Hb at acidic pH (pH 4), but in different manners, depending on the ratio between the NPs and the protein. Depending on the concentration ratio [Hb]/[Au@Citrate], the mixture remained stable, agglomerated, and precipitated or formed stable dispersions of hybrid AuNP:Hb clusters. It was suggested that agglomeration was caused either by particle bridging or by electrostatic destabilization from the oppositely charged Hb and sufficiently high protein concentrations lead to the formation of stable particles and clusters.[25]

We previously reported on extremely stable, protein-coated gold NPs (Au@Protein NPs)[26-28] and gold nanorods.[29] We were able to adsorb moderate-pI proteins such as Ins, BSA, BLG, and Ova onto gold NPs of different surface chemistries.[26-29] The resulting particles exhibited extremely high colloidal stability, and reversible agglomeration/disagglomeration behavior indicated strong binding of proteins to the gold surface. Although indications about the interrelationship between the *nanoparticle identity*, *protein identity* and the *environmental identity* exist,[23, 30] a systematic study of the interactions between Au(metal) NPs and proteins has not been reported so far. In this study, we seek to understand what

governs the interactions of proteins with AuNPs, to describe and explain the mechanisms of protein corona formation, and to ultimately control the physicochemical properties of Au@Protein NPs.

Nanoparticle identity comprises the particle size, shape, core material, and coating material. The first two can be adjusted precisely during the synthesis of the nanomaterials. Core material and coating material define the surface chemistry and the interfacial properties of the particles that are relevant for the interactions between proteins and particles and the adsorption of proteins to the particle surface. From the plethora of various types of organic and inorganic particles consisting of polymers such as latex,[31] hydrogels,[32] oxides (Fe_3O_4, SiO_2),[33] sulfides (CdTe/CdS, ZnS),[34] or metal NPs, AuNPs qualify particularly well for studying such interactions because of their plasmonic properties. They exhibit a localized surface plasmon resonance (LSPR) band that can be excited in the UV–vis–NIR spectral range. The LSPR is highly sensitive to size, shape, and interparticle distance and depends on the refractive index of the surrounding media. The sensitivity of the NPs to the changes in surrounding medium and the interparticle distance has been used as optical tool for detecting material adsorption events[35, 36] and aggregation events induced by the material adsorption to particles.[25]

Nearly all types of NPs bear organic coatings during and after the synthesis, such as small charged molecules, surfactants, or polymers, which are essential not only for the size and shape control but also for their colloidal stability. For studying the adsorption interactions of proteins onto NPs, it is reasonable to use NPs that bear neither stealth coatings (e.g., PEG)[37] nor coatings such as surfactants (e.g., CTAB)[38] that interact with proteins and thus distort the protein–particle interactions ambiguously. Citrate has proven to be a versatile and simple stabilizing agent for various types of NPs, including metal and metal oxide NPs. The negatively charged citrate shell with its large, negative ζ-potential (−35 mV) sufficiently stabilizes the particles via electrostatic repulsion, preventing particle aggregation. Citrate binds weakly enough to the particle surface and therefore can be easily replaced with macromolecules, allowing for subsequent surface functionalization with surfactants, polymers, and even proteins.

The *protein identity* is the other essential component in the interactions of proteins with NPs. The intrinsic properties of proteins differ from species to species, depending on their biological function. Proteins differ in their molecular weights and isoelectric points and display different domains, which can be negatively or positively charged or even hydrophobic, depending on their chemical composition and 3D structure. Thus, different proteins may interact differently with the same kinds of NPs.

The charges of protein and NPs play a significant role in their electrostatic interaction. They depend on environmental parameters such as pH, ionic strength, and temperature of the dispersion media. Hence, for properly studying the protein particle interactions, the *environmental identity* of the system has to be carefully selected as well.

Herein, we systematically studied the impact of two parameters, *protein identity* and *environmental identity*, on the colloidal stability of protein-coated NPs and on the robustness of the final protein corona, while keeping the third parameter, *nanoparticle identity*, constant.

Experimental Section

Chemicals. Gold(III) chloride trihydrate (≥99.9%), trisodium citrate dihydrate (≥99.9%), phosphate buffered saline (PBS), conalbumin type I from chicken egg white (CA), β-lactoglobulinfrom bovine milk (BLG), lysozyme from chicken egg white (LYZ), pepsin from porcine gastric mucosa (Pep), bovine serum albumin (BSA), human hemoglobin (Hb), ovalbumin from chicken egg white (Ova), cytochrome c from bovine heart (cyt C), recombinant human insulin (Ins), and trypsinogen from bovine pancreas (Tg) were purchased from Sigma-Aldrich. All chemicals were used as received. Milli-Q water (18.2 MΩ·cm) was used in all aqueous solutions. The pH was adjusted using 0.1 or 1 M HCl and NaOH from Grüssing.

Synthesis of Au@Protein NPs. Citrate-coated gold NPs (Au@Citrate) were synthesized by the Turkevich method[39] and used as synthesized. The average particle size was d_{TEM} ~ 15 nm, (λ_{max} = 520 nm; d_{DLS} ~ 19 nm; ζ-potential ~ −35 mV). The NPs were functionalized with proteins by a ligand exchange reaction as previously reported.[26-28] Typically, 20 mg of a protein were dissolved in 2 mL of a 1 wt % citrate solution (pH ~ 7.4). The pH was adjusted to 2 and 12 with 1 M HCl and NaOH, respectively. Subsequently, 20 mL of citrate-coated gold NPs solution ([Au] = 0.26 mM) were added to the protein solution in a shot. The mixture was stirred overnight (ca. 16 h) at room temperature. Finally, the protein-coated gold NPs (Au@Protein) were purified and concentrated via 3-fold centrifugation (10 000 rcf, 20–30 min) using Milli-Q water with pH adjusted to 2, 7 and 12 and stored in the fridge at ~7 °C.

Characterization Techniques. All gold NP dispersions were characterized by means of the following techniques: UV–vis absorption spectra were measured with a Specord 250 Plus spectrophotometer (Analytik Jena), the NP diameter (average of 3 measurements and 15 runs each), and ζ-potential (from the electrophoretic mobility at 25 °C, average of at least 5 measurements and 10–50 runs each) were monitored using a Nano-Zetasizer (Malvern Instruments Co, Worcestershire, UK). Transmission electron microscopy (TEM) was carried out on EM 922 Omega (Zeiss) transmission electron microscope. The average NP size was calculated from at least 150 particles. In addition, cryo-TEM measurements were performed at −179 °C and a pressure of 10^{-7}–10^{-8} hPa using a Zeiss/LEO EM 922 Omega (Zeiss NTS GmbH, Oberkochen, Germany). The pH values were measured by a digital pH meter Lab 850 (Schott Instrument, SI Analytics GmbH).

Results and Discussion

In order to demonstrate the effect of the interplay of the three parameters, spherical Au@Citrate NPs of an average size of ~15 nm in diameter (Figure S4.1 in the Supporting Information) were mixed with proteins of different pI and molecular weights dissolved in water (Milli-Q, no salt, pH 5–6) and in phosphate buffer saline (PBS, ionic strength 150 mM, pH 7.4). The Au@Citrate NP dispersions were added in one shot to relatively highly concentrated protein solutions (10 mg/mL, i.e., 1 wt %) in a volume ratio of 10:1, resulting in a final protein concentration of 1 mg/mL in the mixture. High protein concentrations were chosen to avoid particle aggregation due to bridging interactions, which usually occur at low protein or polymer concentrations.[25, 33, 40] All experiments were performed at room temperature. The stability and the degree of agglomeration were judged from the red-shift of the plasmon peak via UV–vis and from hydrodynamic size measurements via DLS.

Figure 4.1 illustrates the protein-dependent behavior of the AuNPs dispersions. In water (Figure 4.1A), the very low-pI protein pepsin (Pep, negatively charged), the very high-pI proteins such as Tg, cyt C, and LYZ[41] (positively charged), and the neutral-pI proteins such as CA and Hb caused a spontaneous agglomeration (Figure 4.1C) and fast precipitation (within 3 h, data shown after 24 h) of the NPs upon mixing. Stable NP dispersions are only achieved for intermediate pI proteins (Figure 4.1A,C) such as Ova,[42] BSA,[43, 44] and BLG[45] (negatively charged at the given pH values), except Ins.

The reason for the fast agglomeration of the negatively charged Au@Citrate NPs with the positively charged high-pI proteins (Tg, cyt C, and LYZ) is assumed to be the strong electrostatic attraction forces between the NPs and the proteins.[17, 18, 25] For the neutral-pI proteins (CA and Hb) and Ins the effect may originate from the low solubility of the proteins in the absence of salt or due to the slightly acidic pH of the Milli-Q water (pH 5–6), which is close to the pI of the proteins (Ins, CA). The increased solubility of proteins in the presence of salt at an optimum of salt concentration is known as the "salting in" effect.[46, 47] The effect of salt concentration can be seen in Figure 4.1B. The proteins Ins, CA, Tg, and cyt C yielded stable dispersions in PBS, while they caused precipitation in Milli-Q water. It is unclear why the NPs agglomerate in the case of Pep, but form stable dispersions with Ova, BSA, and BLG, although these proteins are all negatively charged in Milli-Q and PBS. But it becomes obvious that the *protein identity* and the *environmental identity* of the system are significant parameters for the colloidal stability of the resulting NPs.

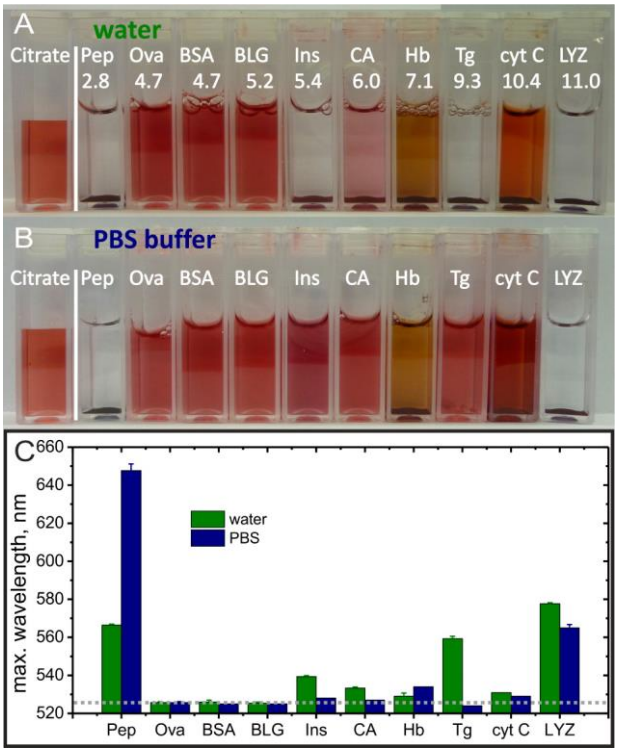

Figure 4.1. Functionalization of Au@Citrate by protein adsorption resulting in Au@Protein NPs. The photographs show the resulting protein–gold NP mixtures (A) in water (pH 5–6) and (B) in PBS buffer (pH 7.4), 24 h after mixing protein solution with Au@Citrate NPs. The vials in (A) and (B) are arranged according to the isoelectric point of the proteins[48-53] increasing from left to right. (C) LSPR peak shifts of AuNPs dispersions (shaken) 24 h after mixing with proteins. The value of 520 nm corresponds to LSPR maximum of the original Au@Citrate NPs. The dotted gray line indicates the LSPR maximum value for the stable protein-coated NPs. The shift of 3–4 nm was caused by refractive index changes due to protein coating.

We studied the influence of the pH on the colloidal stability of NPs when they were exposed to proteins of different pI as shown in Figure 4.2. The pH of the protein solutions was adjusted to three different pH values, namely highly acidic, neutral, and highly basic and mixed with Au@Citrate NPs, giving final pH values of pH 2, 7, and 12, respectively. As shown in Figure 4.2A–C, the AuNP dispersions exhibited different colors and precipitation behavior depending on the protein and the environmental pH.

Mixing Au@Citrate NPs with Proteins. At pH 2 (Figure 4.2A and red bars in Figure 4.2D–F), all investigated proteins were positively charged (all pI > 2). Upon fast addition of Au@Citrate NPs to the acidic protein solutions, stable protein-coated NPs were obtained for all proteins except for Pep and Ins (Figure 4.2A), which was surprising. The fact that the colloidal stability of the AuNPs is not affected during the coating process at pH 2, although the citrate molecules should be fully protonated and uncharged at this pH, and also the initially negatively charged Au@Citrate NPs do not aggregate with most of the positively charged proteins upon contact suggests fast protein adsorption on the particle surface with full coverage[54] and rapid charge inversion (Figure 4.2F). Please note that stable LYZ-coated gold NPs (Au@LYZ) can be obtained by functionalizing the NPs at pH 2. To the best of our knowledge, this is the first time that stable LYZ-coated NPs have been reported. In the case of Pep, the NPs agglomerate very strongly and precipitate completely in a short time (within ~3 h). The LSPR exhibits

a pronounced red-shift of ca. 100 nm (Figure 4.2D), and the hydrodynamic size of the agglomerates reaches into the micron range (Figure 4.2E), making DLS measurements difficult (Figure S4.2). The reason for the NP agglomeration with Pep is likely to be the environmental pH in the reaction mixture, which is too close to the pI of pepsin (pI = 2.8). Pep itself is not stable at this pH and therefore cannot stabilize the NPs. The ζ-potential of the final particles is around +6 mV, which is not enough to stabilize the NPs (Figure 4.2F). Ins, on the other hand, induces NP agglomeration even though it is sufficiently positively charged at pH 2. The final agglomerates are small in size (~43 ± 1 nm), with a weak LSPR shift; they bear sufficient surface charges and are therefore stable over longer time periods (several days). The reason for the agglomeration with insulin at this pH is most probably the molecular weight of insulin (MW ~ 5.8 kDa[51]), which is low in comparison to the other investigated proteins. This result is consistent with our previous report on Ins-coated NPs.[28]

At pH 7 (Figure 4.2B and green bars in Figure 4.2D–F), the colloidal stability behavior of the NPs can be divided into two groups. Proteins with pI < 7 result in stable Au@Protein NPs, whereas agglomeration is observed for proteins with pI ≥ pH 7 NP. Pep, a very low-pI protein, is an exception and leads to NP agglomeration. The NPs agglomerated weakly in the presence of Pep, which lead to a color change to purple (Figure 4.2B) and an LSPR red-shift of only ca. 20 nm (Figure 4.2D). The agglomerates were in the size range of 50–60 nm (Figure 4.2E) with a negative ζ-potential of around −20 mV (Figure 4.2F, green). Small agglomerate sizes and relatively high surface charge make these agglomerates stable over time; they do not precipitate for several days. Please note that in the presence of salt or at lower pH values the NPs agglomerate stronger and precipitate (Figure 4.1). Weakly acidic pI proteins (4.5 ≳ pI ≲ 7) such as Ova, BSA, BLG, and Ins yielded stable NPs at pH 7, which is far enough from the protein pIs. The resulting Au@Protein NPs bear sufficient surface charge at this pH (Figure 4.2F, green) and therefore remain stable. Another exception are CA-coated gold NPs at pH 7. Because of the proximity of the pI of CA (6.0–6.6)[55, 56] to pH 7, the surface charge of the particles is around −10 mV (Figure 4.2F), which is below the stability threshold of (±25 mV). Nevertheless, the particles remained stable even after 24 h incubation time according to UV–vis and DLS data (Figure 4.2D,E). The reason for the stability of NPs with CA at this pH is most probably the high molecular weight of CA (MW = 77.8 kDa),[56] which provides steric stabilization to the coated NPs. Neutral-pI (Hb, pI ~ 6.6–7.4)[49, 51, 52] and high-pI proteins (pI > 9) such as Tg, cyt C, and LYZ caused the NPs to agglomerate and sediment completely. For Hb (pI ~ 6.6–7.4),[49, 51, 52] the NPs agglomerated fast, probably due to the strong hydrophobic interactions of the protein at this pH that is close to its pI. With Tg, cyt C, and LYZ, the NPs agglomerated and precipitated as well, probably due to Coulomb attraction between the positively charged proteins and the negatively charged Au@Citrate NPs at pH 7. The ζ-potential of the NPs was within the range of −10 to 0 mV (Figure 4.2F), which is insufficient to electrostatically stabilize the protein-coated NPs.

At pH 12 (Figure 4.2C and blue bars in Figure 4.2D–F), the general trend was toward stable Au@Protein NPs. All the proteins were negatively charged at pH 12 and therefore compatible to the negatively charged Au@Citrate NPs in terms of surface charge. The proteins adsorbed onto the NPs without inducing Coulomb attraction and agglomeration.

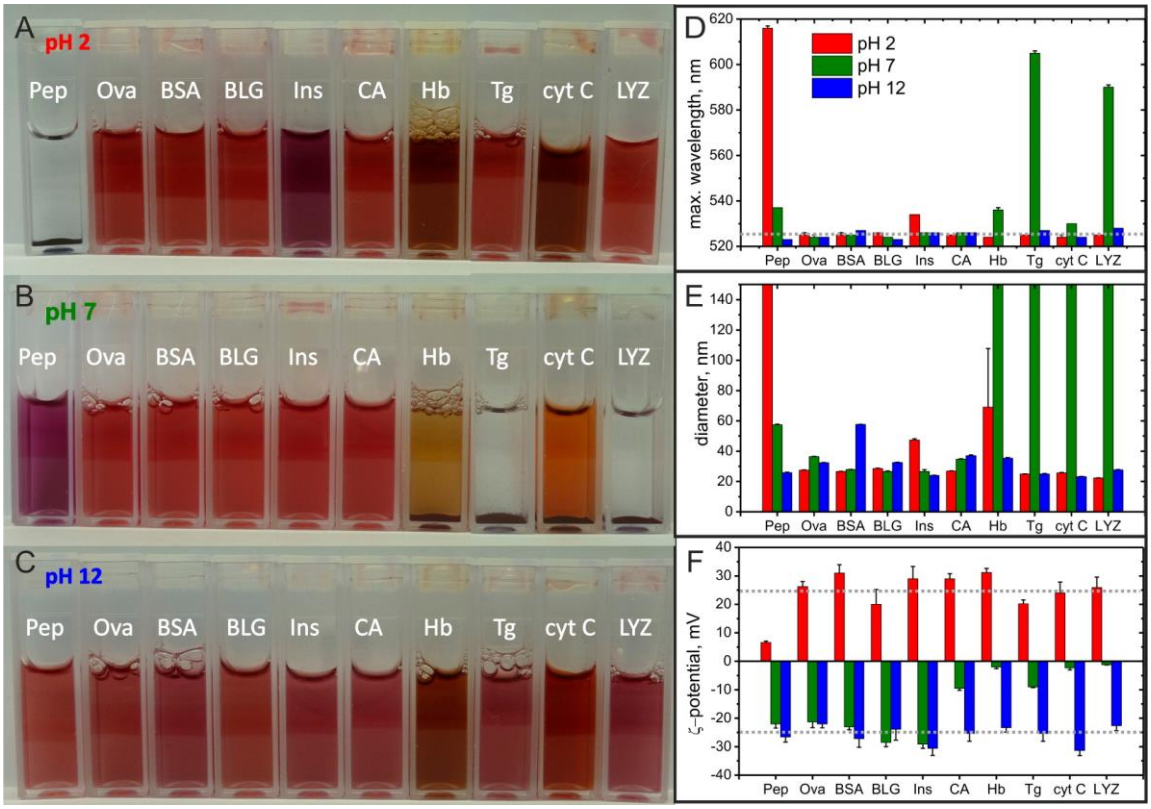

Figure 4.2. Functionalization of Au@Citrate by protein adsorption at different pH resulting in Au@Protein NPs of different stability. The images show the resulting protein–gold NP mixtures after 24 h at (A) pH 2, (B) pH 7, and (C) pH 12. The order of the cuvettes corresponds to an increasing isoelectric point of the proteins. The bar charts show the corresponding data of the (D) LSPR peak, (E) the hydrodynamic diameter (see Figure S4.2), and (F) ζ-potential of these systems. The color code corresponds to the pH (red = pH 2, green = pH 7, blue = pH 12), and the dotted gray lines represent the stability thresholds (UV–vis: 525 nm; ζ-potential: ±25 mV).

We assume that there are two sources of agglomeration during the mixing of gold NPs with proteins that correlate with the pH of the mixture: (1) the insolubility of the excess protein and (2) the instability of the resulting Au@Protein NPs. The first case occurs if the environmental pH is close to pI of excess protein. The second case occurs if the pH is close to pI of the resulting Au@Protein system that differs from that of pure protein. It is known from literature (Au@BSA,[27] Au@Ins[28]) that the pI of a protein shifts upon adsorption onto gold NPs. If one of the two components that coexist in the mixture (Au@Protein or excess protein) has a pI close to the environmental pH, the entire dispersion agglomerates and sediments. For example, the pI of Au@Pep formed at pH 2 was shifted to ~5.5 from the pI (Pep) ~ 2.8[48] (Figure 4.4). The Au@Pep NPs themselves were actually stable in pH 2 (Figure 4.4A) and should not agglomerate. The low solubility and the high concentration of the excess protein with a pI close to pH 2 caused flocculation and removed the stable gold NPs from the dispersion,

corresponding to the first case. An example for the second case is the functionalization of gold NPs with Pep at pH 7 (Figure 4.2B). In this case, the protein Pep is highly soluble at pH 7; however, the Au@Pep NPs are unstable at pH 7 with ζ-potentials between 0 and 10 mV, which are below the stability threshold (Figure 4.4A,E). The high protein concentrations in our experiments largely suppressed contact between the NPs and protein-induced bridging.[40] Bridging aggregation would prevent redispersion of Au@Pep NPs from agglomerates (formed at pH 2) via purification (in pH 12) (Figure 4.3A,E–G).

Surprisingly, dispersions formed with LYZ at pH 12 were stable over time, although the pH is close to the pI of LYZ (~11)[50, 57] (Figure 4.2C). The surface charge of the LYZ-coated NPs at pH 12 was high enough to provide colloidal stability. A weak red-shift of the LSPR peak for dispersions containing LYZ, BSA, and Tg (Figure 4.2D) at pH 12 indicates a weak agglomeration of NPs. These small agglomerates did not precipitate over time and were redispersed upon purification. Purification conditions, in particular the pH of the purification media, are critical for the colloidal stability of the Au@Protein NPs, and therefore their impact was studied systematically in the following.

Purification of AuNPs after Protein Adsorption. After mixing the NPs with proteins at different pH, the dispersions were washed three times with water at acidic, neutral, and basic pH values via centrifugation and redispersion (see Experimental Section). The behavior of Au@Protein NPs after purification conditions is shown in Figure 4.3. We studied four different Au@Protein NP systems with a protein from each pI regime: low pI (Pep), intermediate pI (BLG), and high pI (LYZ). We studied Ins as a low molecular weight protein with an intermediate pI to assess the effect of the molecular weight when keeping the pI similar (Ins: pI 5.3,[58] MW 5.8 kDa; BLG: pI 5.2,[49] MW 18.4 kDa).

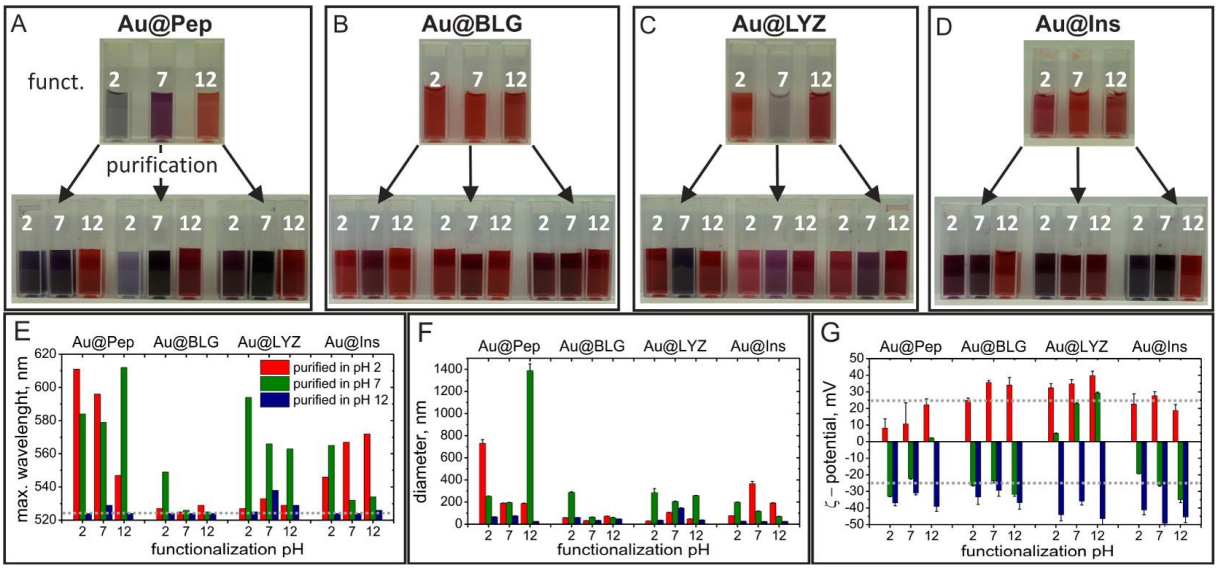

Figure 4.3. Purification can reverse NP agglomeration during the protein functionalization. Au@Citrate functionalized with Pep (A), BLG (B) LYZ (C), and Ins (D) at pH 2, 7, and 12 were purified at three different pH values. NPs that agglomerated during the functionalization (gray/blue and purple dispersions) were redisperse to individual NPs and regained their colloidal stability as indicated by the red color when purified at the right pH. The dotted gray lines (E, G) represent the stability thresholds (UV–vis: 525 nm; ζ-potential: ±25 mV).

The purified Au@Protein NP dispersions exhibited different stability behavior depending on the purification conditions, clearly seen by the different colors and LSPR shifts of the dispersions (Figure 4.3A–E). The Au@Pep system was only stable at pH 12, during both functionalization and purification (Pep and Au@Pep are both stable at pH 12). Remarkably, the NP dispersions that were not stable and aggregated during the functionalization at pH 2 and 7 were redispersed completely upon purification at pH 12 as evidenced by UV–vis and DLS measurements (Figure 4.3E,F). At pH 7, the purified Au@Pep NPs were not stable. At pH 2, the Au@Pep NPs became stable with increasing incubation time at this pH only when the NPs had been functionalized with Pep at pH 12 (see also Figure 4.4A and Supporting Information Figure S4.3).

The Au@BLG system (with intermediate pI) was functionalized (Figure 4.2) and purified at all three pH values (Figure 4.3) without affecting the colloidal stability of the dispersions. Only in the case of dispersions functionalized at pH 2 and purified at pH 7 did the NPs agglomerate upon purification as seen by the purple color of the dispersion and proven by UV–vis and DLS. All three selected pH values (i.e., pH 2, 7, and 12) appear to be far enough from the pI of BLG and render Au@Protein NP systems stable.

The Au@LYZ system was functionalized at pH 2 (Figure 4.2) and then purified at pH 2 and pH 12 without destabilizing the NPs (Figure 4.3). At pH 7, the Au@LYZ NPs were unstable during both functionalization and purification. The NPs disaggregated to a certain extent when purified at pH 2 or 12, but not entirely, as indicated by plasmon peak shift (UV–vis) and DLS. When functionalized at pH 12, Au@LYZ showed slight aggregation with a small red-shift of the plasmon peak (Figure 4.2) that remained when purified at pH 2 and pH 12 and increased when purified at pH 7.

The Au@Ins system was functionalized at pH 7 and 12 but could only be purified and completely redispersed at pH 12. At pH 7, the NPs did not fully redisperse during purification (Figure 4.3E,F). At pH 2, the Au@Ins NPs were not stable at all, which is consistent with previous studies.[28] The ζ-potentials for Au@Ins NPs at pH 2 are not high enough to electrostatically stabilize the NPs. Ins also is smaller than BLG (or BSA[27]) that does not provide additional steric stabilization to the NPs. Although the pI's of the Ins and BLG are similar, there are clear differences in their stability behavior, most likely due to the differences in their molecular weights.

It is worth noting that all AuNPs that agglomerated when mixed with proteins (Figure 4.2A–C) were fully recovered and stabilized again by purifying the agglomerated NPs at pH values far from the pI of the respective protein system (Figure 4.3). This indicates that when NPs meet proteins, reversible agglomeration can occur. Among all proteins that we studied, stable Au@Protein formed only when functionalization was done at pH values far from the pI of the proteins. The same trend existed for the purification of the NPs, but we find that the optimal pH conditions for the functionalization step can differ from that for purification. For example, for Au@LYZ, pH 2 was the optimum pH for

functionalization, but pH 12 was optimal for purification. Surprisingly, pH 7 was not optimal for purification for the four Au@Protein systems (Figure 4.3).

pH-Dependent Colloidal Stability of Different Au@Protein NPs. To understand the effect of the environmental pH on the stability of the different Au@Protein NPs, we studied the pH-dependent colloidal stability profiles for Au@Pep, Au@BLG, Au@LYZ, and Au@Ins (Figure 4.4) over the pH range between pH 2 and 12, covering also a broad pI and MW range of proteins from acidic (Pep: 2.8)[48] to basic (LYZ: 11.0)[50, 57] and from 5.8 kDa (Ins)[51] to 34.6 kDa (Pep),[59] respectively. The NPs were functionalized with the proteins under the conditions that lead to the most stable Au@Protein NPs, i.e., Au@Pep in pH 12, Au@LYZ in pH 2; Au@BLG and Au@Ins in pH 7. The stability profiles were assessed by measuring the LSPR shifts and ζ-potentials at different pH values. Furthermore, since the colloidal stability of Au@Protein NPs strongly depends on the surface charge of the NPs and thus, on the pH of the medium and the pI of the protein, the direction of the pH change played a significant role in the stability of the NPs and the redispersibility of their agglomerates. Moving from basic pH (pH 12), where all Au@Protein NPs were stable, to acidic pH, the NPs started aggregating at neutral pH values and did not redisperse at extreme acidic pH values. Coming from acidic pH (pH 2) however, where the Au@Protein NPs were stable too (except Au@Ins), the NPs aggregated at neutral pH values, but redispersed completely at pH 12. To better understand the effect of pH and the direction of pH changes, we investigated the colloidal stability behavior of the four Au@Protein systems from both directions. Therefore, each system was purified in pH 2 and pH 12, setting the starting pH.

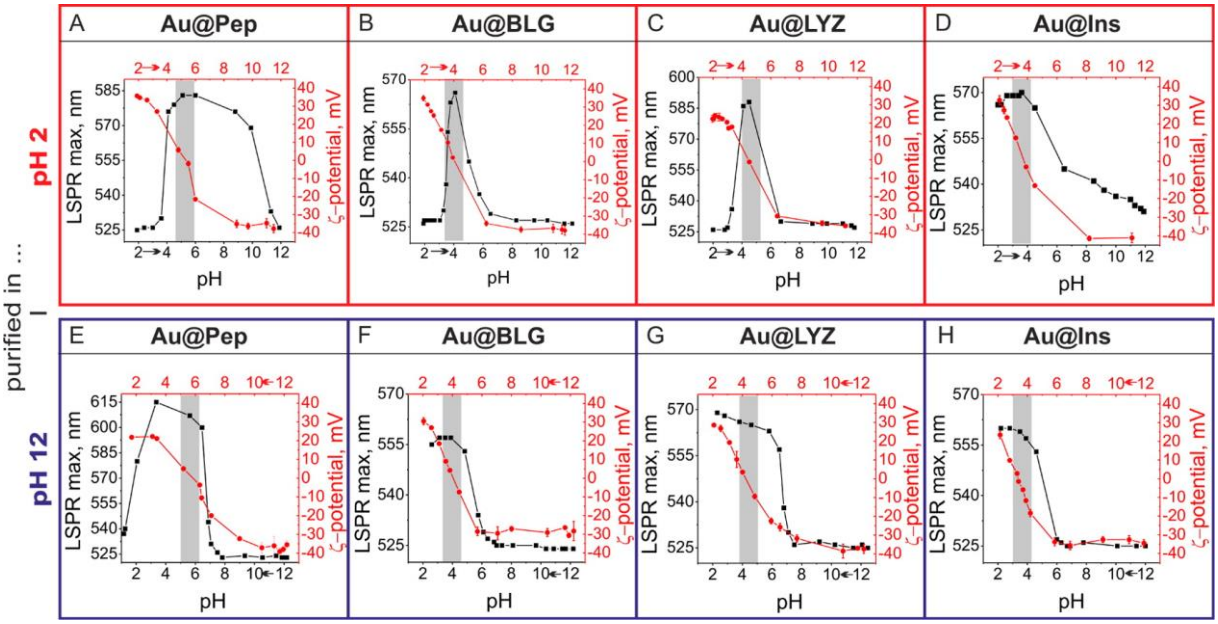

Figure 4.4. Effect of the pH of the purification medium on the pH stability range of the Au@Protein NPs. Au@Pep, Au@BLG, Au@Ins, and Au@LYZ were functionalized under stable conditions and purified in pH 2 and pH 12, respectively. The pI of the Au@Protein NPs and the pH stability range of the NPs were determined by measuring the ζ-potential (red) and LSPR maximum, λ_{max} (black) and as a function of solution pH. The gray stripes indicate the region of the pI of the respective Au@Protein system (±0.5 pH units).

In systems purified at pH 2, Au@Pep, Au@BLG, and Au@LYZ were stable with the LSPR peak around 525 nm and ζ-potentials ≥+30 mV. Although they exhibit a ζ-potential of ∼+30 mV, the Au@Ins NPs were in an aggregated state with an LSPR peak beyond 565 nm, which has also been reported before.[28] The pH of the dispersions was then increased stepwise from pH 2. The surface charge of the Au@Protein NPs decreased from values well below +25 mV to zero, favoring hydrophobic interactions and leading to agglomeration of the Au@Pep (Figure S4.4), Au@BLG (Figure S4.5), Au@LYZ (Figure S4.6), and Au@Ins (Figure S4.7) systems. The agglomeration caused their color to change from ruby red to blue/gray (Figures S4.4–S4.7). Further pH increase above the pI of Au@Protein NPs lead to charge inversion due to deprotonation of carboxyl and amino groups and to an increase of negatively charged groups. The ζ-potential of the NPs decreased below the stability threshold of −25 mV and the electrostatic repulsion between charged NPs increased, leading to complete redispersion of the NPs (LSPR ∼ 525 nm). The three protein systems Au@Pep, Au@BLG, and Au@LYZ exhibited U-shaped stability profiles and were stable in both acidic and basic conditions. The Au@BLG and Au@LYZ showed a sharp transition between stable and unstable regime; the Au@Pep system showed a much broader instability regime. Although the ζ-potential values were beyond −25 mV at pH 8–9, the system fully recovered its LSPR peak only at pH 12. The disaggregation of the Au@Pep NPs was much slower than that of Au@BLG and Au@LYZ. A different stability behavior was observed for Au@Ins system. Increase of the pH caused charge inversion of this aggregated dispersion (Figure 4.4D), but redispersion was possible only at highly basic pH values.

All Au@Protein systems purified at pH 12 (Figure 4.4E–H) were highly stable with negative surface charges beyond −30 mV and LSPR absorption maxima at 525 nm. Upon decreasing the pH, the particles remained stable up to pH 7, and the LSPR maximum remained at 525 nm (Figure 4.4E–H). The ζ-potentials of the NPs also remained beyond −30 mV until pH 7. Only Au@Pep showed an increase of ζ-potential to −20 mV but remained stable. Further pH decrease (pH < 7) caused all Au@Protein systems to start agglomerating and the LSPR peaks to shift to higher wavelengths. The NPs crossed the point of zero charge and inverted their surface charge to positive ζ-potentials. Only the Au@Pep system redispersed to a great extent at pH values below pH 2 and the LSPR maximum recovered from 620 to 538 nm. The other three protein systems did not redisperse at acidic pH values (pH 2), although the surface charges reached high positive values beyond +30 mV. The pH-dependent stability of Au@Protein NPs strongly depended on the purification medium: the same Au@Protein systems (Figure 4.4) purified in different pH values, i.e., acidic (Figure 4.4A–D) and basic (Figure 4.4E–H), behaved entirely different.

The Au@BLG and Au@LYZ systems showed a pronounced influence of the purification pH on their colloidal stability behavior. Both NP systems were functionalized at optimal pH, i.e., Au@BLG at pH 7 and Au@LYZ at pH 2. When the NPs were purified at acidic pH (Figure 4.4B,C), they exhibited a U-shaped pH stability profile that was similar to the bare proteins. The NPs were stable at pH values far

below and above the pI of the Au@Protein system and unstable at pH close to pI. When the dispersions were purified at basic pH, the NPs were stable at pH values above the pI, but unstable at pH values below the pI, exhibiting a sigmoidal stability profile (Figure 4.4F,G). This pH-dependent stability profile was confirmed via DLS and cryo-TEM measurements, which is shown exemplarily for the Au@LYZ system in Figure 4.5 (and for the Au@BLG system, Figure S4.8). The Au@LYZ system was synthesized in pH 2 and purified in pH 2 (Figure 4.5A–D) and pH 12 (Figure 4.5E–H), yielding stable Au@LYZ NP dispersions of ruby red color and hydrodynamic sizes around 23 ± 0.3 nm. The cryo-TEM images confirmed individually dispersed NPs for both cases (pH 2, Figure 4.5B, and pH 12, Figure 4.5F). When increasing or decreasing the pH toward the pI of the Au@LYZ system (i.e., ~4.3), the NPs started to agglomerate as seen from the color of the dispersion (purple, blue, gray). The hydrodynamic size of the agglomerates started increasing from hundreds of nanometers to micrometers. Loose flocs and 3D networks of NP agglomerates formed (Figure 4.5C,G). Figure 4.4 illustrates how the Au@LYZ NPs behave differently for the two systems. When purified at pH 2, the agglomerates redispersed again to individual NPs (Figure 4.5A,D) at basic pH values. When purified at pH 12, the NP agglomerates formed at pH = pI that grew in size and density (Figure 4.5E,H) upon further pH decrease down to pH 2.

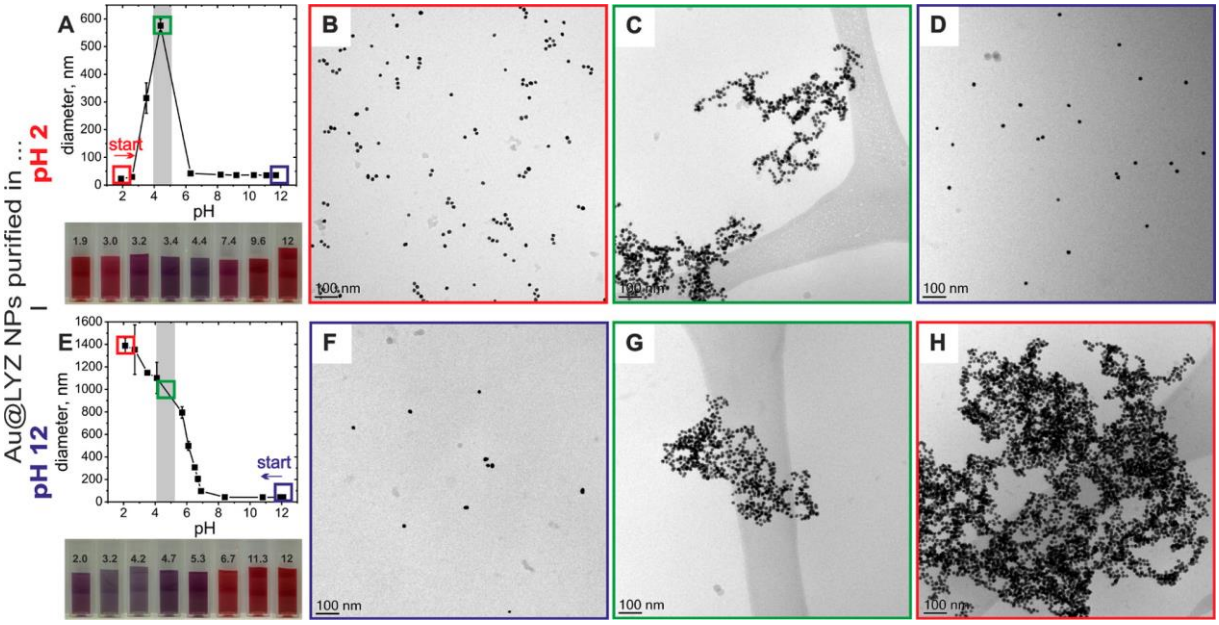

Figure 4.5. pH-dependent agglomeration behavior of colloidally stable Au@LYZ NPs purified at pH 2 (A–D) and pH 12 (E–H) measured with dynamic light scattering (A, E) and cryo-TEM (B–D and F–H). Starting at pH 2, the Au@LYZ NPs are red in color and individually dispersed with small hydrodynamic sizes (A: red box), confirmed with cryo-TEM (B). When increasing the pH, the NPs aggregated at the pI of Au@LYZ (A: green box, and C) and redispersed at pH 12 (A: blue box, and D). Starting at pH 12, the Au@LYZ NPs were red in color and individually dispersed with small hydrodynamic sizes (E: blue box), confirmed with cryo-TEM (F). When decreasing the pH, the NPs aggregated at the pI of Au@LYZ (E: green box, and G) and aggregate further to bigger aggregates at pH 2 (E: red box, and H).

Au@Pep and Au@Ins systems showed similar profiles for both purification pH. The Au@Pep system showed a U-shaped stability profile, with a large instability range (>6 pH units) in the medium pH region that slightly shifted depending on the direction of the pH change. The Au@Ins system exhibited a

sigmoidal-shaped stability profile for both cases, being stable at basic pH values and instable at acidic pH values.

Stability profiles of the Au@Protein NPs are surprisingly sensitive to different purification conditions even when the NPs, the proteins, and the synthesis conditions (coating procedure) are the same. The Au@Protein NPs behave differently from the pure proteins. Bare proteins usually exhibit a U-shaped solubility profile with high solubility at pH values below and above the pI and a low solubility at pH = pI. The pI of proteins depends on the ratio of the negatively and positively charged amino acid residues. When proteins adsorb or bind onto metal surfaces, they may bind with both negatively or positively charged functional groups, which become then unavailable for the interactions with outer medium, i.e., water. The ratio between these charged groups changes upon binding, which leads to a measurable shift in pI. Depending on the functional groups that are available on the protein and bind to the gold surface, the pI can be shifted toward lower or higher pH values compared to the original pI of the protein. When a protein binds to the NP with basic (positively charged) groups, such as amino, imidazole, or guandino groups, the pI of the resulting Au@Protein system shifts to lower pH values. If the protein binds with the carboxylic (negatively charged) groups to the surface, the pI shift is expected to be toward higher pH values. In the case of NPs being coated with BLG, Ins, and LYZ, the pI shifted toward lower pH values. We assume that these proteins adsorb onto gold surfaces preferentially via basic groups. The pI of Au@Protein systems containing proteins with intermediate proteins, such as Au@BLG and Au@Ins, was measured to be 4.1 (BLG: 5.2[49]) and 3.5 (Ins: 5.3[58]), which is consistent with literature.[27, 28] High-pI proteins such as LYZ (pI: 11.0[50, 57]) exhibited a pronounced pI shift toward pH ~ 4.3) when adsorbed onto the AuNPs. This suggests that the main binding groups also for Au@LYZ are the basic functional groups. In contrast, the low-pI protein pepsin (2.8[48]) exhibits a pI shift to higher pH values with a pI ~ 5.5. This indicates that pepsin binds to the gold NP surface to a larger part via carboxyl groups, which are indeed abundant in the protein. Furthermore, pepsin has relatively low amount of positively charged groups (4 in total, i.e., 2 Arg, 1 His, and 1 Lys).[59, 60] Nevertheless, it is remarkable that the pI shifts for all Au@Protein systems investigated in this study were independent of the purification medium (pH 2 or 12, see Figure 4.4). In fact, this behavior is plausible, since the proteins were adsorbed (functionalization step) under same conditions. Hence, we assume that protein adsorption occurred onto gold surface via same sites, leaving same functional groups available toward the solvent (water). This would lead to the same final pI of an Au@Protein system, which is independent of the purification conditions.

The proteins' molecular weight also affected the stability of Au@Protein. Proteins with high molecular weight contributed to the stability of the proteins coated NPs with steric stabilization additional to the electrostatic stabilization.[26, 27] From the four investigated proteins, Ins with its 5.8 kDa[51] molecular weight was the smallest, BLG (18.4 kDa[49]) and LYZ (14.3 kDa[50, 61]) were in the middle range, and Pep (34.6 kDa[59]) was the largest. Large proteins have many acidic and basic functional groups that probably

provide enough electrostatic repulsion on the Au@Protein surface upon pH change. Additionally, their size provides steric repulsion. The Au@Pep system's U-shaped stability profile can be attributed to the electrosteric stabilization mechanism. Smaller proteins have less functional groups and provide less steric repulsion. The Au@Ins system for example is stable at basic pH but instable at acidic pH independent of the purification pH. Insulin is a very small protein and cannot provide steric repulsion to disagglomerate the system completely. In the case of the middle-sized proteins, both Au@BLG and Au@LYZ systems are sensitive to the direction of pH change, but it is not clear yet what causes the direction-dependent stabilities of the systems.

Remarkably, the stability profiles of all Au@Protein systems were highly consistent over multiple aggregation/disaggregation cycles. Figure 4.6 shows three-point pH switching cycles for all four protein coated NP systems purified at pH 2 and pH 12, in analogy to Figure 4.4. The purification pH served as starting point as shown in Figure 4.6. The reversible agglomeration and disagglomeration was followed by recording the LSPR peak maximum of the dispersions at different pH values via UV–vis spectroscopy. All Au@Protein systems maintained their original stability profiles (Figure 4.4) at least over three pH cycles. For example, Au@Pep (both purification pH, Figure 4.6A,E) and Au@BLG and Au@LYZ (pH 2 purification, Figure 4.6B,C) were highly stable at extreme pH values and aggregated at pH = pI (U-shaped profile), recovering completely after each cycle. Upon a sudden pH change from one extreme to other extreme pH, e.g., from pH 12 to pH 2 (Figure 4.6A–C,E, at the end of a cycle) the particles remained stable. The reason for this is that the pH change is fast and the particles undergo an immediate charge inversion, without agglomerating, while going through the point of zero charge. Au@Ins (Figure 4.6D,H) and Au@BLG and Au@LYZ (pH 12 purification, Figure 4.6F,G), on the other hand, exhibited sigmoidal stability profiles, being stable only at basic pH values, in analogy to Figure 4.4.

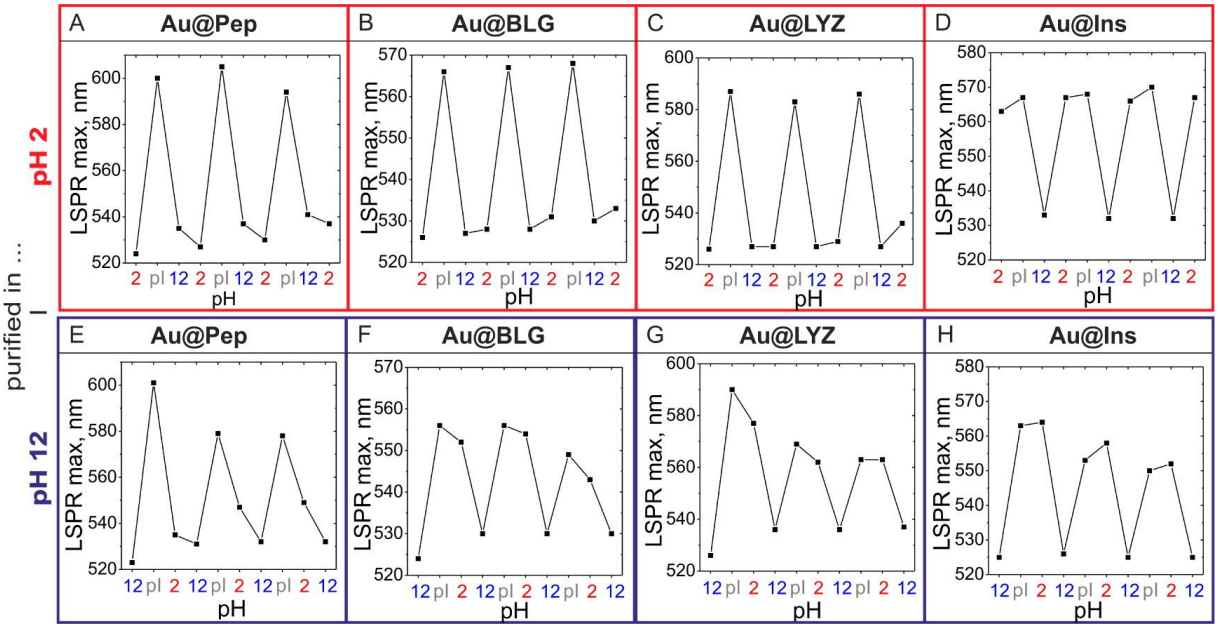

Figure 4.6. pH-responsive reversible aggregation–disaggregation cycles of four representative protein-coated gold NPs. The Au@Pep (A, E), Au@BLG (B, F), Au@LYZ (C, G), and Au@Ins (D, H) NPs were functionalized under stable conditions and purified in pH 2 (A–D) and pH 12 (E–H). The pH of the dispersions was changed from pH 2 to pH 12 (A–D) or vice versa (E–H) going over the pI of the protein-coated NPs. The reversible aggregation of the different Au@Protein NPs was followed via UV–vis spectroscopy, by measuring the LSPR maximum λ_{max}.

Conclusions

The behavior of Au@Protein dispersions strongly depends on three parameters: (a) *nanoparticle identity*, (b) *protein identity*, and (c) *environmental identity*. The present study reveals the importance of the *protein identity* and the environmental conditions on the final physicochemical properties of metal nanoparticle systems stabilized by small charged molecules such as citrate. The NPs either formed stable dispersions or agglomerated spontaneously when mixed with protein solutions, depending on the pI of the protein and pH of the mixture. The agglomerates redispersed when purified under suitable conditions. The final Au@Protein NPs exhibited a stability regime and stability profile that strongly depended on the adsorbed protein and the environmental conditions. The surface charge of the Au@Protein NPs also depended on the pI and the pH.

Controlling the environmental parameters and adjusting them to the physicochemical properties of the proteins and of NPs allowed us to create highly stable Au@Protein NPs with a defined protein corona and thus, with a defined biointerface. Understanding the interactions of nanomaterials with individual proteins in regard of their abundance, composition, and physicochemical properties would allow us to decipher the formation of the new physicochemical identity upon protein adsorption in complex biological systems and fluids.

Acknowledgment

This study was funded by the German Research Foundation (DFG) within the collaborative research center SFB 840. J.S. was supported and funded by a grant for PhD candidates of the German Federal Environmental Foundation (DBU). The authors thank Markus Drechsler for cryo-TEM, Carmen Kunert for TEM measurements, and Corinna Link for proofreading. T.K. thanks Eduard Arzt for his continuing support. M.C. thanks Andreas Fery for his broad support and scientific discussions on this paper.

References

1. Walczyk, D.; Bombelli, F. B.; Monopoli, M. P.; Lynch, I.; Dawson, K. A., What the Cell "Sees" in Bionanoscience. *J. Am. Chem. Soc.* **2010**, *132*, 5761-5768.
2. Kelly, P. M.; Åberg, C.; Polo, E.; O'Connell, A.; Cookman, J.; Fallon, J.; Krpetić, Ž.; Dawson, K. A., Mapping Protein Binding Sites on the Biomolecular Corona of Nanoparticles. *Nat. Nano* **2015**, *10*, 472-479.
3. Lynch, I.; Dawson, K. A., Protein-Nanoparticle Interactions. *Nano Today* **2008**, *3*, 40-47.
4. Nel, A. E.; Madler, L.; Velegol, D.; Xia, T.; Hoek, E. M.; Somasundaran, P.; Klaessig, F.; Castranova, V.; Thompson, M., Understanding Biophysicochemical Interactions at the Nano-Bio Interface. *Nat. Mater.* **2009**, *8*, 543-57.
5. Yan, Y.; Gause, K. T.; Kamphuis, M. M. J.; Ang, C.-S.; O'Brien-Simpson, N. M.; Lenzo, J. C.; Reynolds, E. C.; Nice, E. C.; Caruso, F., Differential Roles of the Protein Corona in the Cellular Uptake of Nanoporous Polymer Particles by Monocyte and Macrophage Cell Lines. *ACS Nano* **2013**, *7*, 10960-10970.
6. Wei, Q.; Becherer, T.; Angioletti-Uberti, S.; Dzubiella, J.; Wischke, C.; Neffe, A. T.; Lendlein, A.; Ballauff, M.; Haag, R., Protein Interactions with Polymer Coatings and Biomaterials. *Angew. Chem. Int. Ed.* **2014**, *53*, 8004-8031.
7. Bertoli, F.; Davies, G.-L.; Monopoli, M. P.; Moloney, M.; Gun'ko, Y. K.; Salvati, A.; Dawson, K. A., Magnetic Nanoparticles to Recover Cellular Organelles and Study the Time Resolved Nanoparticle-Cell Interactome Throughout Uptake. *Small* **2014**, *10*, 3307-3315.
8. Zakaria, H. M.; Shah, A.; Konieczny, M.; Hoffmann, J. A.; Nijdam, A. J.; Reeves, M. E., Small Molecule- and Amino Acid-Induced Aggregation of Gold Nanoparticles. *Langmuir* **2013**, *29*, 7661-7673.
9. Chah, S.; Hammond, M. R.; Zare, R. N., Gold Nanoparticles as a Colorimetric Sensor for Protein Conformational Changes. *Chem. Biol.* **2005**, *12*, 323-328.
10. Pavlov, V.; Xiao, Y.; Shlyahovsky, B.; Willner, I., Aptamer-Functionalized Au Nanoparticles for the Amplified Optical Detection of Thrombin. *J. Am. Chem. Soc.* **2004**, *126*, 11768-11769.
11. Bhattacharya, J.; Jasrapuria, S.; Sarkar, T.; GhoshMoulick, R.; Dasgupta, A. K., Gold Nanoparticle-Based Tool to Study Protein Conformational Variants: Implications in Hemoglobinopathy. *Nanomed. Nanotechnol. Biol. Med.* **2007**, *3*, 14-19.
12. Wang, Z.; Lee, J.; Cossins, A. R.; Brust, M., Microarray-Based Detection of Protein Binding and Functionality by Gold Nanoparticle Probes. *Anal. Chem.* **2005**, *77*, 5770-5774.
13. Kerman, K.; Chikae, M.; Yamamura, S.; Tamiya, E., Gold Nanoparticle-Based Electrochemical Detection of Protein Phosphorylation. *Anal. Chim. Acta.* **2007**, *588*, 26-33.
14. Albanese, A.; Chan, W. C. W., Effect of Gold Nanoparticle Aggregation on Cell Uptake and Toxicity. *ACS Nano* **2011**, *5*, 5478-5489.

15. Ghosh, P.; Han, G.; De, M.; Kim, C. K.; Rotello, V. M., Gold Nanoparticles in Delivery Applications. *Adv. Drug Del. Rev.* **2008**, *60*, 1307-1315.
16. Duncan, B.; Kim, C.; Rotello, V. M., Gold Nanoparticle Platforms as Drug and Biomacromolecule Delivery Systems. *J. Control. Release* **2010**, *148*, 122-127.
17. Zhang, D. M.; Neumann, O.; Wang, H.; Yuwono, V. M.; Barhoumi, A.; Perham, M.; Hartgerink, J. D.; Wittung-Stafshede, P.; Halas, N. J., Gold Nanoparticles Can Induce the Formation of Protein-Based Aggregates at Physiological pH. *Nano Lett.* **2009**, *9*, 666-671.
18. Chen, Y. M.; Yu, C. J.; Cheng, T. L.; Tseng, W. L., Colorimetric Detection of Lysozyme Based on Electrostatic Interaction with Human Serum Albumin-Modified Gold Nanoparticles. *Langmuir* **2008**, *24*, 3654-3660.
19. Garabagiu, S., A Spectroscopic Study on the Interaction between Gold Nanoparticles and Hemoglobin. *Mater. Res. Bull.* **2011**, *46*, 2474-2477.
20. Horovitz, O.; Tomoaia, G.; Mocanu, A.; Yupsanis, T.; Tomoaia-Cotisel, M., Protein Binding to Gold Colloids. *Gold Bull.* **2007**, *40*, 213-218.
21. Lacerda, S. H. D. P.; Park, J. J.; Meuse, C.; Pristinski, D.; Becker, M. L.; Karim, A.; Douglas, J. F., Interaction of Gold Nanoparticles with Common Human Blood Proteins. *ACS Nano* **2010**, *4*, 365-379.
22. Tom, R. T.; Pradeep, T., Interaction of Azide Ion with Hemin and Cytochrome C Immobilized on Au and Ag Nanoparticles. *Langmuir* **2005**, *21*, 11896-11902.
23. Thobhani, S.; Attree, S.; Boyd, R.; Kumarswami, N.; Noble, J.; Szymanski, M.; Porter, R. A., Bioconjugation and Characterisation of Gold Colloid-Labelled Proteins. *J. Immunol. Methods* **2010**, *356*, 60-69.
24. Yang, Y.; Burkhard, P., Encapsulation of Gold Nanoparticles into Self-Assembling Protein Nanoparticles. *J. Nanobiotechnol.* **2012**, *10*, 42-53.
25. Moerz, S. T.; Kraegeloh, A.; Chanana, M.; Kraus, T., Formation Mechanism for Stable Hybrid Clusters of Proteins and Nanoparticles. *ACS Nano* **2015**, *9*, 6696-6705.
26. Chanana, M.; Gil, P. R.; Correa-Duarte, M. A.; Liz-Marzan, L. M.; Parak, W. J., Physicochemical Properties of Protein-Coated Gold Nanoparticles in Biological Fluids and Cells before and after Proteolytic Digestion. *Angew. Chem. Int. Ed.* **2013**, *52*, 4179-4183.
27. Strozyk, M. S.; Chanana, M.; Pastoriza-Santos, I.; Perez-Juste, J.; Liz-Marzan, L. M., Protein/Polymer-Based Dual-Responsive Gold Nanoparticles with pH-Dependent Thermal Sensitivity. *Adv. Funct. Mater.* **2012**, *22*, 1436-1444.
28. Chanana, M.; Correa-Duarte, M. A.; Liz-Marzan, L. M., Insulin-Coated Gold Nanoparticles: A Plasmonic Device for Studying Metal-Protein Interactions. *Small* **2011**, *7*, 2650-2660.
29. Tebbe, M.; Kuttner, C.; Mannel, M.; Fery, A.; Chanana, M., Colloidally Stable and Surfactant-Free Protein-Coated Gold Nanorods in Biological Media. *ACS Appl. Mater. Interfaces* **2015**, *7*, 5984-91.
30. Rayavarapu, R. G.; Petersen, W.; Ungureanu, C.; Post, J. N.; van Leeuwen, T. G.; Manohar, S., Synthesis and Bioconjugation of Gold Nanoparticles as Potential Molecular Probes for Light-Based Imaging Techniques. *Int. J. Biomed. Imaging* **2007**, *2007*, 29817-29827.
31. Welsch, N.; Lu, Y.; Dzubiella, J.; Ballauff, M., Adsorption of Proteins to Functional Polymeric Nanoparticles. *Polymer* **2013**, *54*, 2835-2849.
32. Zustiak, S. P.; Wei, Y.; Leach, J. B., Protein-Hydrogel Interactions in Tissue Engineering: Mechanisms and Applications. *Tissue Eng. Part B Rev.* **2013**, *19*, 160-171.
33. Bharti, B.; Meissner, J.; Findenegg, G. H., Aggregation of Silica Nanoparticles Directed by Adsorption of Lysozyme. *Langmuir* **2011**, *27*, 9823-9833.
34. Schmidtke, C.; Lange, H.; Tran, H.; Ostermann, J.; Kloust, H.; Bastús, N. G.; Merkl, J.-P.; Thomsen, C.; Weller, H., Radical Initiated Reactions on Biocompatible CdSe-Based Quantum Dots: Ligand Cross-Linking, Crystal Annealing, and Fluorescence Enhancement. *J. Phys. Chem. C* **2013**, *117*, 8570-8578.

35. Ament, I.; Prasad, J.; Henkel, A.; Schmachtel, S.; Sonnichsen, C., Single Unlabeled Protein Detection on Individual Plasmonic Nanoparticles. *Nano Lett.* **2012**, *12*, 1092-1095.
36. Ahijado-Guzman, R.; Prasad, J.; Rosman, C.; Henkel, A.; Tome, L.; Schneider, D.; Rivas, G.; Sonnichsen, C., Plasmonic Nanosensors for Simultaneous Quantification of Multiple Protein-Protein Binding Affinities. *Nano Lett.* **2014**, *14*, 5528-5532.
37. Kinnear, C.; Dietsch, H.; Clift, M. J.; Endes, C.; Rothen-Rutishauser, B.; Petri-Fink, A., Gold Nanorods: Controlling Their Surface Chemistry and Complete Detoxification by a Two-Step Place Exchange. *Angew. Chem. Int. Ed.* **2013**, *52*, 1934-1938.
38. Mahmoudi, M.; Lohse, S. E.; Murphy, C. J.; Fathizadeh, A.; Montazeri, A.; Suslick, K. S., Variation of Protein Corona Composition of Gold Nanoparticles Following Plasmonic Heating. *Nano Lett.* **2014**, *14*, 6-12.
39. Turkevich, J.; Stevenson, P. C.; Hillier, J., A Study of the Nucleation and Growth Processes in the Synthesis of Colloidal Gold. *Discuss. Faraday Soc.* **1951**, 55-75.
40. Bharti, B.; Meissner, J.; Klapp, S. H.; Findenegg, G. H., Bridging Interactions of Proteins with Silica Nanoparticles: The Influence of pH, Ionic Strength and Protein Concentration. *Soft Matter* **2014**, *10*, 718-728.
41. Kuehner, D. E.; Engmann, J.; Fergg, F.; Wernick, M.; Blanch, H. W.; Prausnitz, J. M., Lysozyme Net Charge and Ion Binding in Concentrated Aqueous Electrolyte Solutions. *J. Phys. Chem. B* **1999**, *103*, 1368-1374.
42. Delahaije, R. J.; Wierenga, P. A.; van Nieuwenhuijzen, N. H.; Giuseppin, M. L.; Gruppen, H., Protein Concentration and Protein-Exposed Hydrophobicity as Dominant Parameters Determining the Flocculation of Protein-Stabilized Oil-in-Water Emulsions. *Langmuir* **2013**, *29*, 11567-11574.
43. Salis, A.; Bostrom, M.; Medda, L.; Cugia, F.; Barse, B.; Parsons, D. F.; Ninham, B. W.; Monduzzi, M., Measurements and Theoretical Interpretation of Points of Zero Charge/Potential of BSA Protein. *Langmuir* **2011**, *27*, 11597-11604.
44. Jachimska, B.; Pajor, A., Physico-Chemical Characterization of Bovine Serum Albumin in Solution and as Deposited on Surfaces. *Bioelectrochemistry* **2012**, *87*, 138-146.
45. Engelhardt, K.; Lexis, M.; Gochev, G.; Konnerth, C.; Miller, R.; Willenbacher, N.; Peukert, W.; Braunschweig, B., pH Effects on the Molecular Structure of Beta-Lactoglobulin Modified Air-Water Interfaces and Its Impact on Foam Rheology. *Langmuir* **2013**, *29*, 11646-11655.
46. Arakawa, T.; Timasheff, S. N., Mechanism of Protein Salting in and Salting out by Divalent Cation Salts: Balance between Hydration and Salt Binding. *Biochemistry* **1984**, *23*, 5912-5923.
47. Zhang, F.; Skoda, M. W. A.; Jacobs, R. M. J.; Martin, R. A.; Martin, C. M.; Schreiber, F., Protein Interactions Studied by SAXS: Effect of Ionic Strength and Protein Concentration for BSA in Aqueous Solutions. *J. Phys. Chem. B* **2007**, *111*, 251-259.
48. Malamud, D.; Drysdale, J. W., Isoelectric Points of Proteins: A Table. *Anal. Biochem.* **1978**, *86*, 620-647.
49. Righetti, P. G.; Caravaggio, T., Isoelectric Points and Molecular-Weights of Proteins - a Table. *J. Chromatogr.* **1976**, *127*, 1-28.
50. Lauer, H. H.; McManigill, D., Capillary Zone Electrophoresis of Proteins in Untreated Fused-Silica Tubing. *Anal. Chem.* **1986**, *58*, 166-170.
51. Ui, N., Isoelectric Points and Conformation of Proteins .1. Effect of Urea on Behavior of Some Proteins in Isoelectric Focusing. *Biochim. Biophys. Acta* **1971**, *229*, 567-581.
52. Righetti, P. G.; Tudor, G.; Ek, K., Isoelectric Points and Molecular-Weights of Proteins - a New Table. *J. Chromatogr.* **1981**, *220*, 115-194.
53. Walsh, K. A.; Neurath, H., Trypsinogen and Chymotrypsinogen as Homologous Proteins. *Proc. Natl. Acad. Sci. USA* **1964**, *52*, 884-889.
54. Casals, E.; Pfaller, T.; Duschl, A.; Oostingh, G. J.; Puntes, V., Time Evolution of the Nanoparticle Protein Corona. *ACS Nano* **2010**, *4*, 3623-3632.

55. Jeltsch, J. M.; Chambon, P., The Complete Nucleotide-Sequence of the Chicken Ovotransferrin Messenger-RNA. *Eur. J. Biochem.* **1982**, *122*, 291-295.

56. Williams, J.; Elleman, T. C.; Kingston, I. B.; Wilkins, A. G.; Kuhn, K. A., The Primary Structure of Hen Overtransferrin. *Eur. J. Biochem.* **1982**, *122*, 297-303.

57. Wetter, L. R.; Deutsch, H. F., Immunological Studies on Egg White Proteins. 4. Immunochemical and Physical Studies of Lysozyme. *J. Biol. Chem.* **1951**, *192*, 237-242.

58. Fischel-Ghodsian, F.; Brown, L.; Mathiowitz, E.; Brandenburg, D.; Langer, R., Enzymatically Controlled Drug Delivery. *Proc. Natl. Acad. Sci. USA* **1988**, *85*, 2403-2406.

59. Sepulveda, P.; Marciniszyn, J.; Liu, D.; Tang, J., Primary Structure of Porcine Pepsin. *J. Biol. Chem.* **1975**, *250*, 5082-5088.

60. Tang, J.; Sepulved.P; Marcinis.J; Chen, K. C. S.; Huang, W. Y.; Tao, N.; Liu, D.; Lanier, J. P., Amino-Acid Sequence of Porcine Pepsin. *Proc. Natl. Acad. Sci. USA* **1973**, *70*, 3437-3439.

61. Canfield, R. E., Amino Acid Sequence of Egg White Lysozyme. *J. Biol. Chem.* **1963**, *238*, 2698-2707.

Supporting Information

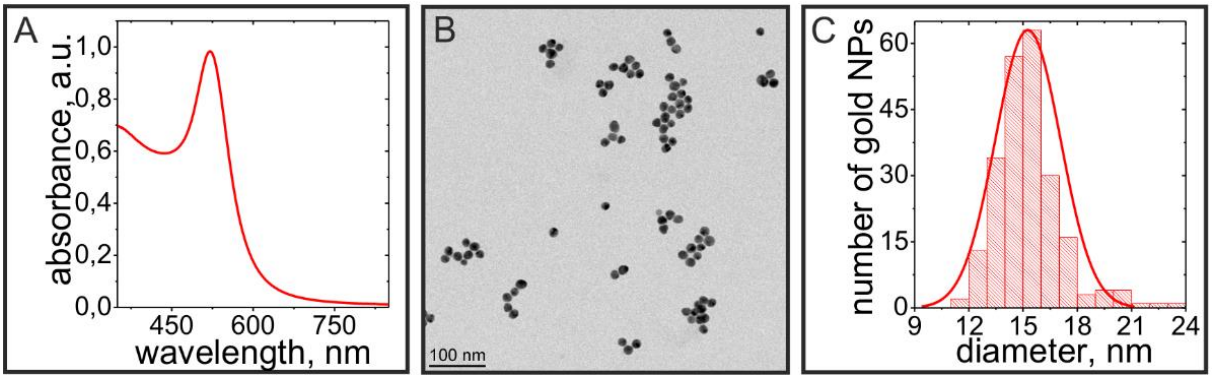

Figure S4.1. (A) representative UV-vis spectrum with λ_{max} = 520 nm, (B) TEM image, and the corresponding size distribution of Au@Citrate NPs (C) calculated from TEM images, which results in a mean diameter of (15 ± 2) nm.

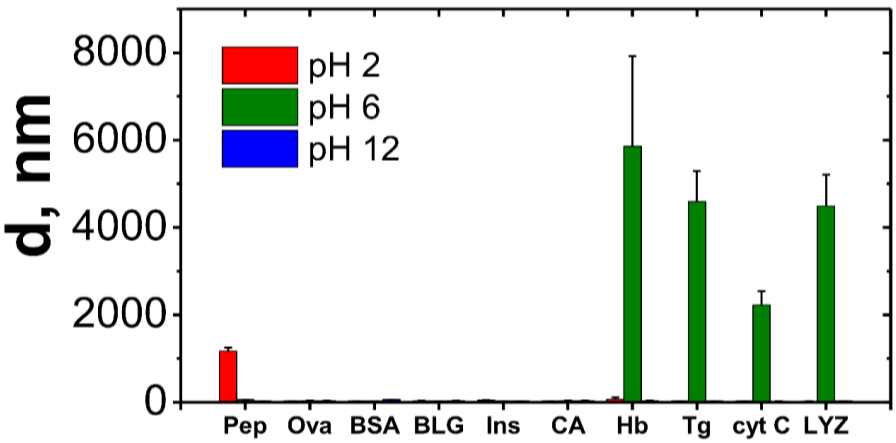

Figure S4.2. Overview of the hydrodynamic diameter of the functionalization of Au@Citrate by protein adsorption at different pH resulting in Au@Protein NPs of different stability. A zoom-in to the region of 0-150 nm is displayed in Figure 4.2E.

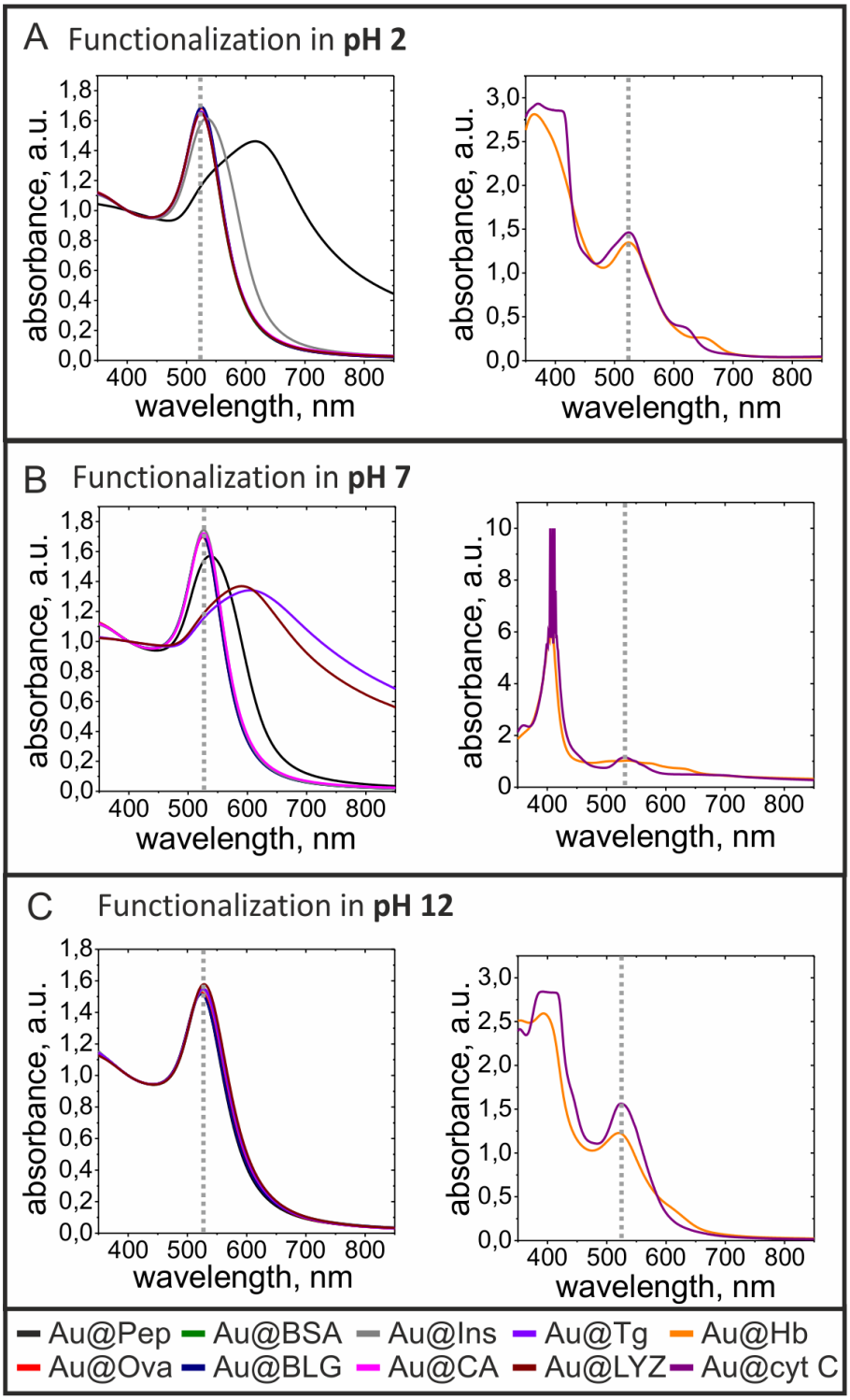

Figure S4.3. UV-Vis spectra of Au@Protein for pH 2 (A), 7 (B), and 12 (C), measured 24 hours after functionalization. The spectra are normalized at 400 nm, except for Au@Hb and Au@cyt C as these proteins exhibit a high absorption band in the visible region. The spectra correspond to the values and cuvettes shown in Figure 4.2.

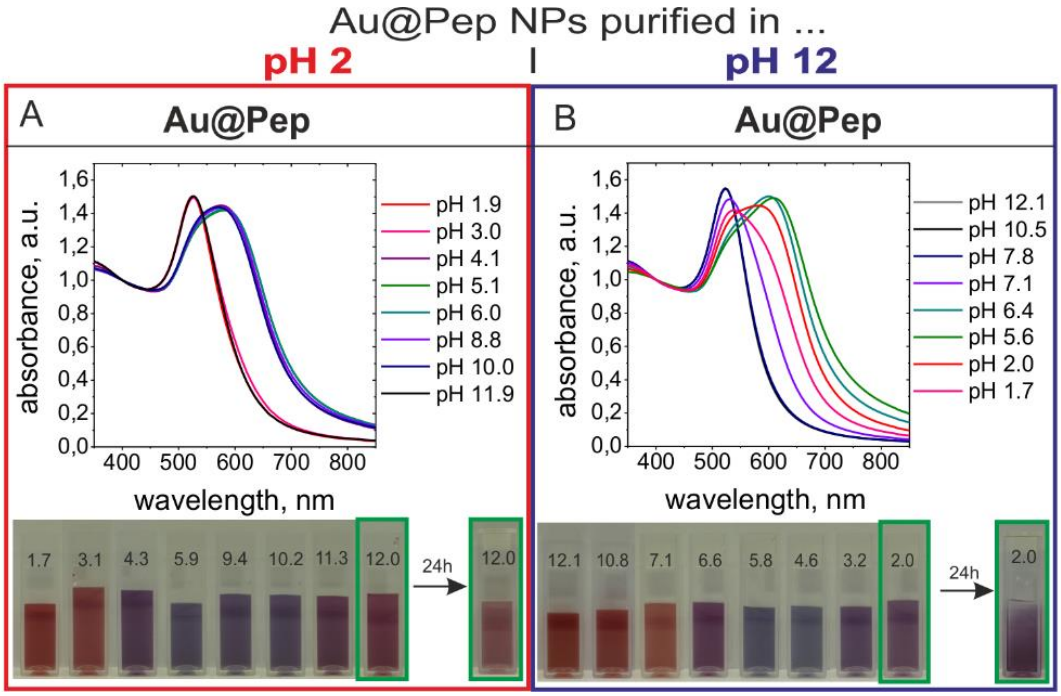

Figure S4.4. UV-Vis spectra and dispersions colors of Au@Pep at different pH values, after purification in (A) pH 2 and (B) in pH 12. Also the dispersion color at the final pH values (pH 12, and pH 2) after 24 h incubation are shown. The spectra are normalized at 400 nm. The spectra and cuvettes correspond to the values shown in Figure 4.4.

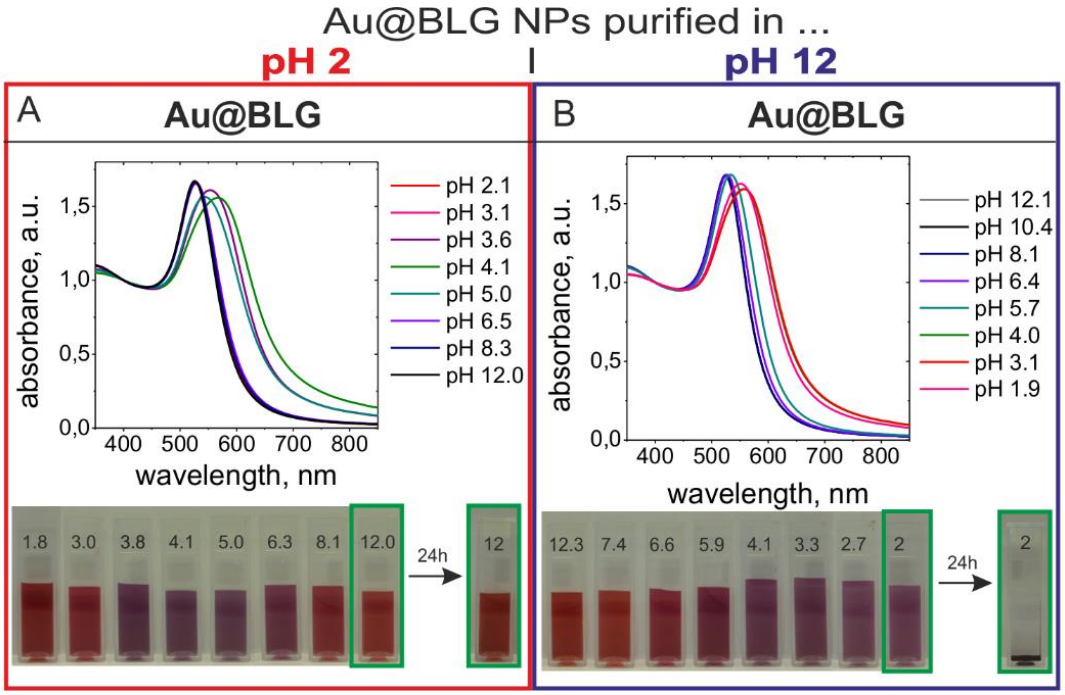

Figure S4.5. UV-Vis spectra and dispersions colors of Au@BLG at different pH values, after purification in (A) pH 2 and (B) in pH 12. Also the dispersion color at the final pH values (pH 12, and pH 2) after 24 h incubation are shown. The spectra are normalized at 400 nm. The spectra and cuvettes correspond to the values shown in Figure 4.4.

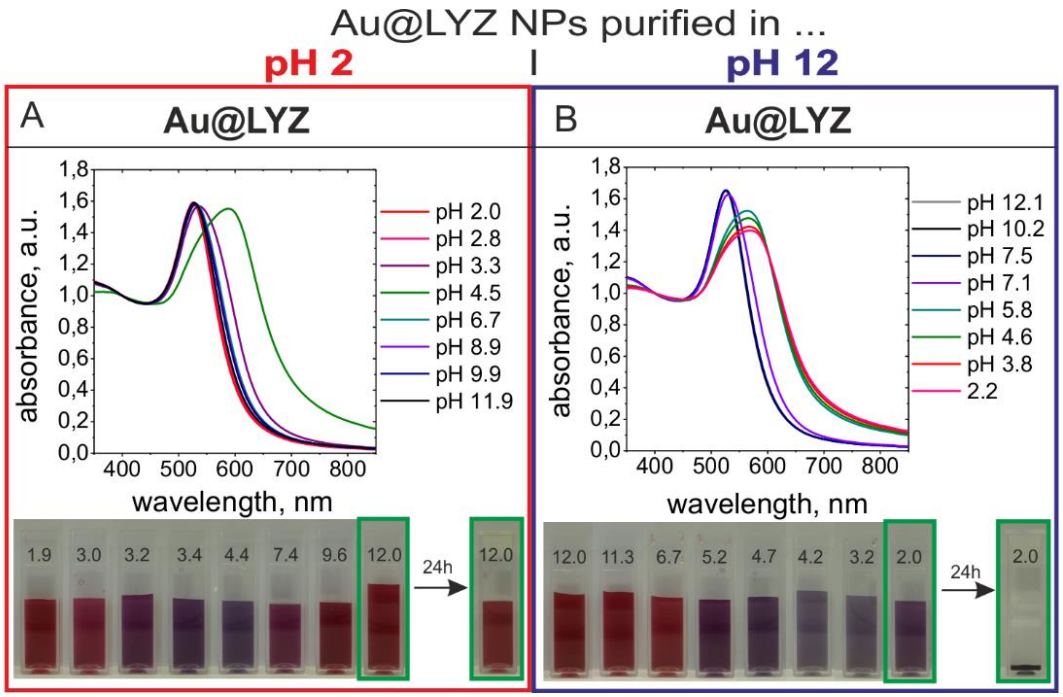

Figure S4.6. UV-Vis spectra and dispersions colors of Au@LYZ at different pH values, after purification in (A) pH 2 and (B) in pH 12. Also the dispersion at the final pH values (pH 12, and pH 2) after 24 h incubation are shown. The spectra are normalized at 400 nm. The spectra and cuvettes correspond to the values shown in Figure 4.4.

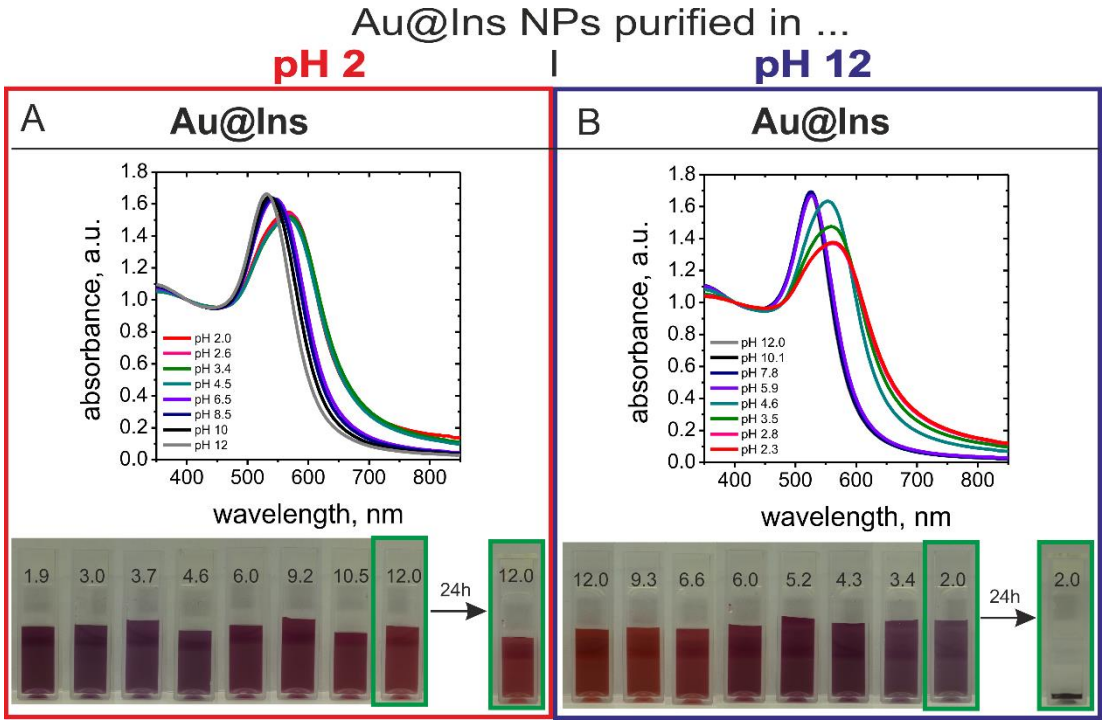

Figure S4.7. UV-Vis spectra and dispersions colors of Au@Ins at different pH values, after purification in (A) pH 2 and (B) in pH 12. Also the dispersion at the final pH values (pH 12, and pH 2) after 24 h incubation are shown. The spectra are normalized at 400 nm. The spectra and cuvettes correspond to the values shown in Figure 4.4.

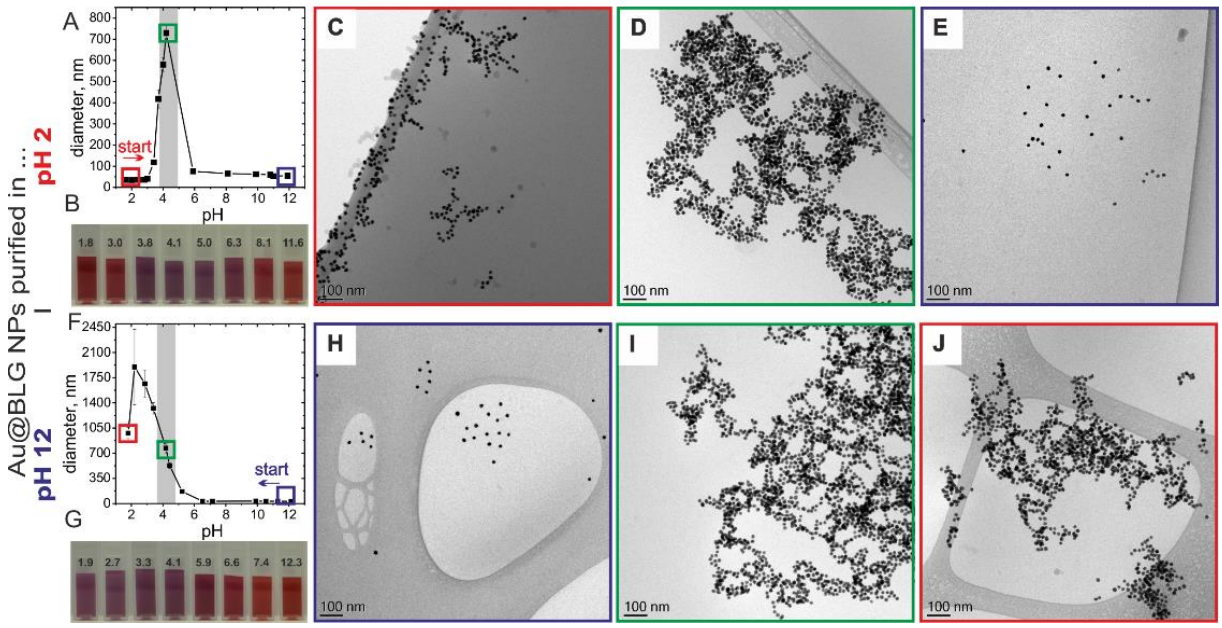

Figure S4.8. pH-dependent agglomeration behavior of colloidally stable Au@BLG NPs purified in pH 2 (A-E) and pH 12 (F-H) measured with dynamic light scattering (A, F) and Cryo-TEM (C-E and H-J). Starting at pH 2, the Au@BLG NPs are red in color and individually dispersed with small hydrodynamic sizes (A red box), confirmed with Cryo-TEM (C). By increasing the pH, the NPs aggregate at the pI of Au@BLG (A green box, and D) and redisperse at pH 12 (A blue box, and E). Starting at pH 12, the Au@BLG NPs are red in color and individually dispersed with small hydrodynamic sizes (F blue box), confirmed with Cryo-TEM (H). By decreasing the pH, the NPs aggregate at the pI of Au@LYZ (F green box, and G) but cannot redispersed competely at pH 2 (F red box, and F).

5 Splitting of Surface-Immobilized Multicompartment Micelles into Clusters upon Charge Inversion

Reprinted with permission from

Splitting of Surface-Immobilized Multicompartment Micelles into Clusters upon Charge Inversion, Inna Dewald, Julia Gensel, Eva Betthausen, Oleg V. Borisov, Axel H. E. Müller, Felix H. Schacher, and Andreas Fery, *ACS Nano* **2016** *10* (5), 5180-5188

DOI: 10.1021/acsnano.6b00670

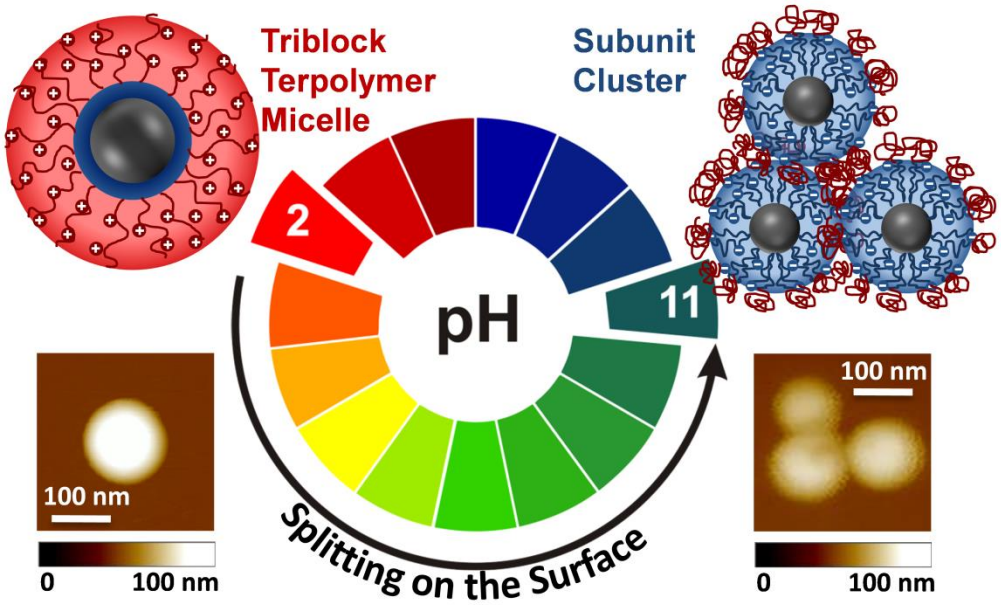

Abstract

We investigate a morphological transition of surface-immobilized triblock terpolymer micelles: the splitting into well-defined clusters of satellite micelles upon pH changes. The multicompartment micelles are formed in aqueous solution of ABC triblock terpolymers consisting of a hydrophobic polybutadiene block, a weak polyanionic poly(methacrylic acid) block, and a weak polycationic poly(2-(dimethylamino)ethyl methacrylate) block. They are subsequently immobilized on silicon wafer surfaces by dip-coating. The splitting process is triggered by a pH change to strongly basic pH, which goes along with a charge reversal of the micelles. We find that the aggregation number of the submicelles is well-defined and that larger micelles have a tendency to split into a larger number of submicelles. Furthermore, there is a clear preference for clusters consisting of doublets and triplets of submicelles. The morphology of surface-immobilized clusters can be "quenched" by returning to the original pH. Thus, such well-defined micellar clusters can be stabilized and are available as colloidal building blocks for the formation of hierarchical surface structures. We discuss the underlying physicochemical principles of the splitting process considering changes in charge and total free energy of the micelles upon pH change.

Introduction

Block copolymers are one of the most successfully and abundantly used class of molecular building blocks for soft nanotechnology.[1-8] This is due to their ability to form supramolecular structures on different length scales[9-11] and due to their pronounced responsiveness toward environmental parameters[12, 13] such as solvent composition, pH, temperature and others. While pioneering work focused on diblock copolymers, in recent years, progress in macromolecular synthesis greatly expanded the range of monomer combinations and sequences, including an increased number of examples regarding solution self-assembly of triblock terpolymers.[14-17] As expected, the higher complexity of these molecular building blocks results in a richer morphology space for self-assembly in solution and in the bulk. Exploring this phase space is an active area of research.[18-21] In terms of stimulus responsiveness, especially ABC triblock terpolymers that combine polyanionic and polycationic blocks have shown great potential, in particular when weak polyelectrolytes are used. In this case, the charge density of the blocks and the formation of interpolyelectrolyte complexes is a function of pH, which is directly reflected in the shape and aggregation number of the corresponding aggregates in solution.

The splitting process of block copolymer micelles into submicelles has so far been only studied in solution.[22-26] Surface-immobilized micelles reported in the literature respond to external triggers such as pH,[27-33] temperature,[33, 34] or solvent[35] mainly by polymer desorption from the surface. This phenomenon is often accompanied by irreversible morphological changes from micellar aggregates to brush-like structures[27, 33] or smaller micelles.[33] For example, stimuli-responsive poly(2-(dimethylamino)ethyl methacrylate)-*block*-poly(*N*-isopropylacrylamide), $DMAEMA_{(corona)}$-*b*-$PNIPAM_{(core)}$, micelles reported

by Sukhishvili and co-workers[33] disintegrated into brush-like layers when the temperature was decreased below the lower critical solution temperature (LCST) of the core-forming block. In addition, exposure to pH below the pK_b of the corona induced changes in the aggregation number resulting in a decrease in micellar diameter. Further factors influencing the reversibility of the stimulus response are the degree of quaternization and the nature of the substrate,[27-30,31] which has been investigated by Biggs and co-workers for pH-responsive poly(2-(dimethylamino)ethyl methacrylate)-*block*-poly(2-(diethylamino)ethyl methacrylate), $PDMAEMA_{(corona)}$-$PDEAEMA_{(core)}$, diblock copolymer micelles. Usually, the micelles reported in the literature are obtained from diblock copolymers containing stimuli-responsive blocks. These systems often lack stability, especially if the stimulus response of the core-forming block is triggered deliberately.

In contrast to solution studies, the properties of triblock terpolymers on surfaces have so far received less attention, although – as for solution behavior - striking differences as compared to diblock copolymer systems are expected. Indeed, we have recently shown that the deposition of micelles of polybutadiene-*block*-poly(methacrylic acid)-*block*-quaternized poly(2-(dimethylamino)ethyl methacrylate) (PB-*b*-PMAA-*b*-PDMAEMAq) can form pH-sensitive coatings for self-regulated bacterial repulsion.[31, 36] The same micellar building blocks can be incorporated into polyelectrolyte multilayers resulting in films with a strong and at the same time fully reversible pH-induced change in swelling and mechanical properties.[37] Both effects could be explained by the structure of the employed triblock terpolymer, enabling the formation and dissolution of *intramicellar* interpolyelectrolyte complexes between the sequentially arranged polyanionic (PMAA) and polycationic (PDMAEMAq) blocks.

In the present work, we demonstrate the response toward changes in pH of surface-immobilized multicompartment micelles formed by an ABC triblock terpolymer featuring both a weak polyanionic and a weak polycationic block. Due to the choice in nature and lengths of the polyacid and polybase block, full *charge reversal* of the micelles is possible upon applying suitable conditions. We find that this results in a well-defined splitting process. Each micelle is turned into a cluster of satellite micelles, which can be preserved in shape by returning to the original pH value. While changes in aggregation number and micelle splitting / budding transitions are well-known for block copolymer micelles in solution, such a defined splitting process has not been observed or controlled on a surface before. In addition, the transient cluster shapes can be stabilized by quenching. We discuss the underlying physicochemical mechanisms of the process as well as the potential of exploiting it for creating surface-immobilized colloidal clusters.

Results and Discussion

We used an ampholytic ABC triblock terpolymer, BMAAD (PB_{800}-*b*-$PMAA_{200}$-*b*-$PDMAEMA_{285}$, the subscripts denoting the degree of polymerization of the corresponding block), with a molecular weight

of ~105 kg/mol (PDI ~ 1.10).[38] It consists of a hydrophobic polybutadiene (B) block, a poly(methacrylic acid) (MAA) middle block, and a poly(2-(dimethylamino)ethyl methacrylate) (D) block. The molecular structure and contour lengths of the blocks are given in Figure 5.1a. The triblock terpolymer is a polyampholyte since both a polyacid, PMAA ($pK_{a,app}$~5.5),[39] and a polybase, PDMAEMA ($pK_{b,app}$~7.8),[40] are present. Both represent weak (annealed) polyelectrolytes rendering the material pH-sensitive. Please note, that the apparent dissociation constants of the triblock terpolymer are similar to those of the homopolymer equivalents.[38]

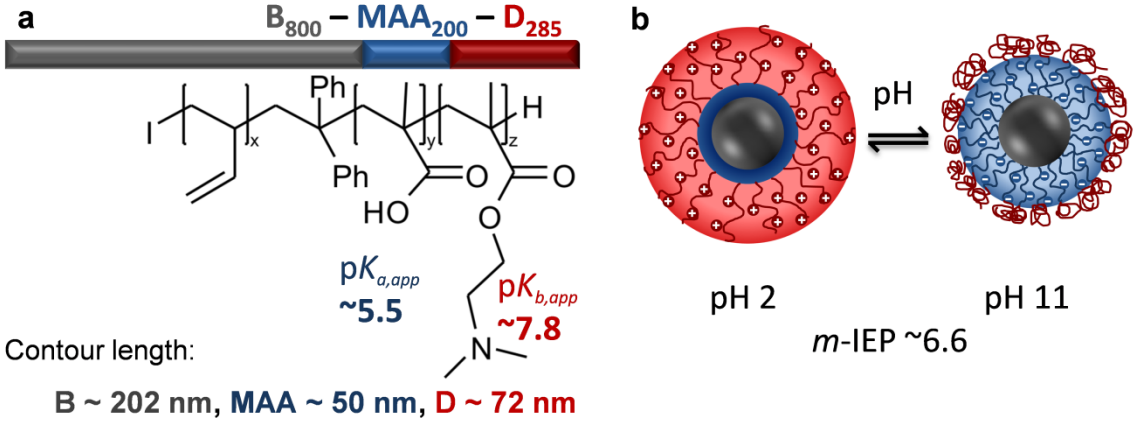

Figure 5.1. Structure of the used BMAAD triblock terpolymer with the contour lengths of the blocks (a) and the corresponding micellar aggregates in aqueous solution below and above the *micellar* isoelectric point (*m*-IEP) (b).

In aqueous solution, the triblock terpolymer forms micellar aggregates (*cf.* Figure 5.1b) due to the hydrophobicity of polybutadiene (B) forming the core. Such micelles show a strong pH dependence concerning their shape, size, and surface charge, which has been investigated previously.[38] Briefly, it was found that at pH 2, well below the *micellar* isoelectric point (*m*-IEP) at pH ~6.6, star-like core-shell-corona micelles are formed. Thereby, the hydrophobic PB core is surrounded by a protonated / uncharged PMAA shell and a positively charged PDMAEMA corona resulting in a positive ξ-potential of + 35 mV. In contrast, at pH 10, the PMAA middle block is negatively charged, while the PDMAEMA block is uncharged, resulting in a negative ξ-potential of -11 mV. It is noteworthy that the pH-induced structural transitions between the shell and the corona accompanied by a charge inversion are fully reversible in solution between pH 2 and 10. Further characteristics such as shape, size, and charge, as determined by cryogenic transmission electron microscopy (cryo-TEM), dynamic light scattering (DLS) and ξ-potential measurements, can be found elsewhere.[38] Please note that the *m*-IEP was determined *via* turbidity titration and has been defined as the pH of maximum turbidity.

The core-shell-corona BMAAD micelles were adsorbed from a pH 2 solution onto bare silica *via* dip coating. Taking into account silica's point of zero charge at pH~2.5[41] we conclude that at pH 2 positively charged micelles are adsorbed onto an either uncharged or slightly positively charged silica surface *via* nonelectrostatic forces, such as hydrophobic interactions or hydrogen bonding between amino and

silanol groups. Electrostatic repulsion between like-charged species on the surface and in solution limited the adsorption to a monolayer following the random sequential adsorption (RSA) model.[42, 43] Similar behavior was observed in our previous work on BMAADq (*i.e.*, quaternized BMAAD) micelles.[31] The characterization of the BMAAD micelles was carried out by atomic force microscopy (AFM) and scanning electron microscopy (SEM) in dry state (*cf.* Figure S5.1). The immobilized micelles are of spherical but slightly flattened shape with an average height h_{AFM}~55 nm and diameter d_{AFM}~140 nm. Contrary to AFM (Figure 5.2a), SEM images show the contrast between the electron rich polybutadiene core with a diameter $d_{SEM,core}$~95 nm and the surrounding shell with a thickness $t_{SEM,shell}$~15 nm. According to the results of the adsorption kinetics (*cf.* Figure S5.1), the BMAAD micelle density reaches a plateau and a maximum surface coverage of ~7 micelles/μm^2, corresponding to ~44–50% (taking into account the expansion of the corona), after approximately 5 min.

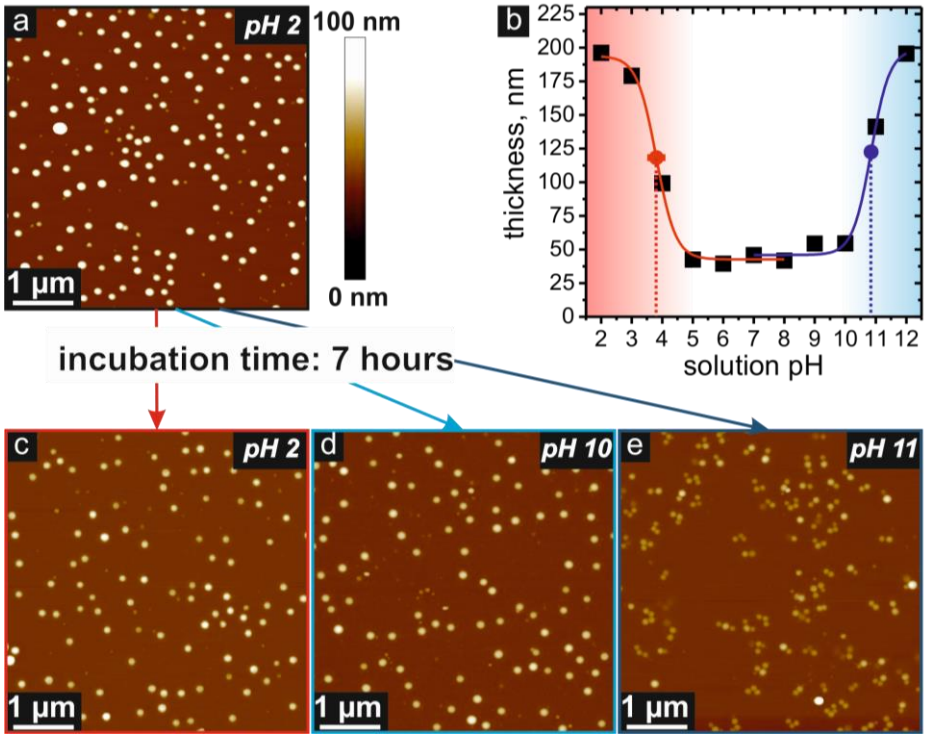

Figure 5.2. AFM height image of surface-immobilized BMAAD micelles deposited from a pH 2 solution on silica (a). pH response of a BMAAD monolayer in the range from pH 2 to 12 measured using *in situ* ellipsometry (b). Effective thickness (black squares) is plotted as a function of pH. Sigmoidal fits (solid lines) with the corresponding pK_{app} values (circles) are indicated by red and blue colors for PDMAEMA and PMAA, respectively. AFM images after an incubation time of 7 h in pH 2 (c), pH 10 (d), and pH 11 (e).

The pH response of surface-immobilized micelles was investigated in a pH range from 2 to 12 using *in situ* ellipsometry. The spot size of the ellipsometric setup used in this experiment is ~20 mm^2. Consequently, the ellipsometric signal cannot resolve the size changes on a single micelle level, but rather averages over the areas covered by not close packed micelles. Thereby, the effective thickness of the micelle monolayer film was measured as a function of solution pH. Qualitatively, the "U-shape" swelling profile in Figure 5.2b is in good agreement with the pH response of BMAAD micelles in

solution.[38] The pronounced increase in film thickness observed in strong acidic and strong basic pH is attributed to the stretching of either the PDMAEMA or the PMAA block due to increasing charge density caused by ionization of the amino and carboxyl groups, respectively. In the range of moderate pH values between pH 5 and 10, surface-immobilized micelles collapse due to the formation of an *intramicellar* interpolyelectrolyte complex (*im*-IPEC) between PMAA and PDMAEMA.

In general, both corona blocks (MAA and D) are weak polyelectrolytes, which respond to external stimuli such as pH by changing their charge density, thereby inducing changes in properties and structure of the micelles. On the surface, the BMAAD micelles exhibit strong swelling and shifts in the apparent pK_a from 5.5 to 10.8 for the polyacid and in the apparent pK_b from 7.8 to 10.2 for the polybase. Similar shifts in the apparent dissociation constants were observed for star polymers, micelles, and surface-anchored brushes and were attributed to the confinement of the polyelectrolyte chains due to architecture.[40, 44-48] Thereby, a stronger shift was observed for an increasing number of arms, chains per area or grafting density. In our previous work, a similar effect was observed for the PMAA middle block in BMAADq micelles, which were incorporated into multilayer films.[37] In the case of BMAAD micelles, these shifts originate from the interaction between weak polybase and weak polyacid blocks.

To examine the morphology changes of the micellar aggregates on the surface as a function of pH, we performed imaging atomic force microscopy experiments. Samples of surface-immobilized BMAAD micelles exemplarily shown in Figure 5.2a were immersed in different pH solutions each and incubated for 7 h. Longer incubation times were avoided in order to keep the impact of alkaline surface etching to a minimum. The impact of pH on the micellar morphology is shown in Figure 5.2c-e (the morphology at additional pH values is reported in Figure S5.2). While Figure 5.2a,c,d indicates an essentially unchanged morphology, after incubation in pH 11 for 7 h (Figure 5.2e) drastic changes are observed. Instead of the initially adsorbed micelles, we found clusters of still well-defined micellar but distinctly smaller objects on the surface. Obviously, surface-immobilized BMAAD micelles respond to an abrupt pH increase by splitting into subunits. Please note that after incubation at pH 12 for 7 h (Figure S5.2c) it was not possible to assess the morphological changes of BMAAD micelles due to an advanced corrosion of the silica surface by alkaline etching.

The splitting kinetics of the micelles at pH 11 was investigated for different incubation times (see Figure S5.3 for detailed images). We find that the splitting process is finished in the time frame of 1 h and that it is followed by a progressive desorption of polymer from the surface, if the samples are incubated at pH 11 for prolonged time. In addition to an internal restructuring of the micelles, the pH-dependent charge density of silica[49] leads to repulsive interactions between the negatively charged PMAA corona and the likewise negatively charged silica surface which facilitates polymer desorption.

To suppress further desorption after splitting, the BMAAD clusters were quenched at pH 2. Thereby, the system returns to initial (adsorption) conditions with less repulsive / more favorable interactions

between the positively charged PDMAEMA corona and the almost uncharged silica surface. Presumably stronger adhesion of the micelles to the substrate at pH 2 kinetically traps the system in the pH 11 morphology. In addition, repulsive interactions between subunit coronas - positively charged PDMAEMA at pH 2 - inhibit their fusion back to a single micelle. Structural changes of the BMAAD micelles during the whole pH-cycle were monitored using *ex situ* AFM measurements on the same spot. Figure 5.3 shows AFM images of initial micelles and after successive exposure to pH 11 and 2. Thus, measurements on the same spot enable a direct comparison between initial micelles and resulting clusters on a single particle level.

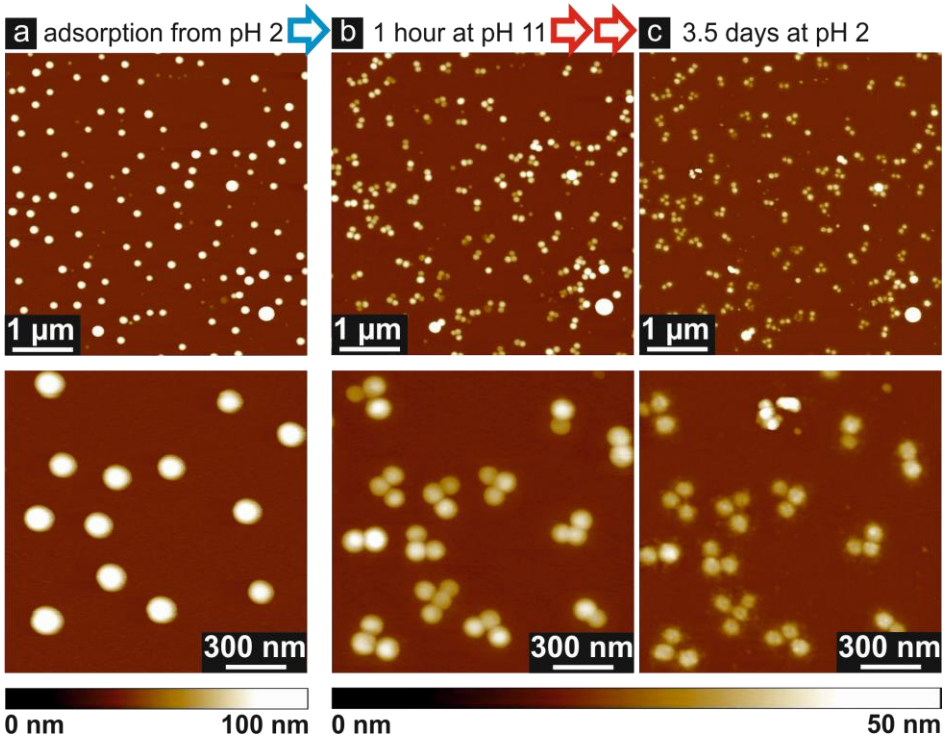

Figure 5.3. *Ex situ* AFM measurements on the same spot of the sample (in dry state) performed after adsorption from pH 2 solution (a), after immersion in pH 11 for 1 h (b), and after a 3.5 days long exposure to pH 2 (c). Larger micelles (*e.g.*,. in the bottom right corner of the overview scans) were used as reference points to find the same spot again after treatment. Upper row, overview scans; bottom row, higher magnification.

The results clearly indicate that the pH-induced structural changes on the surface are irreversible and the micellar cluster structure can be preserved by returning to pH 2. Even after 3.5 days incubation at pH 2 the clusters remained on the surface without merging (*cf.* Figure 5.3b and c). This long-term stability renders a subsequent post-treatment of the clusters *via* wet chemistry possible. An alternative approach for stabilization of the subunits is a postsplitting cross-linking of the hydrophobic PB cores.[50] Please note that a second exposure to pH 11 does not lead to a second splitting but to fuzzy structures (*cf.* Figure S5.4).

For a more quantitative analysis, AFM height images (Figure 5.4a,b) obtained before and after splitting of BMAAD micelles on the same spot of the sample were used. A comparison on a single particle level

given in Figure S5.5 shows a significant decrease in subunit height to ~35% and in subunit diameter to ~75% of the initial micelle size. Furthermore, the data on height and diameter was used to calculate the radius of curvature, contact area (*cf.* Figure S5.5), and volume (Figure 5.5). After splitting, the radius of curvature increases by ~20%, and its distribution becomes broader. In addition, the polymer/silica contact area increases by ~35%. These findings lead to the assumption that BMAAD micelles tend to spread laterally on the silica surface during the splitting process.

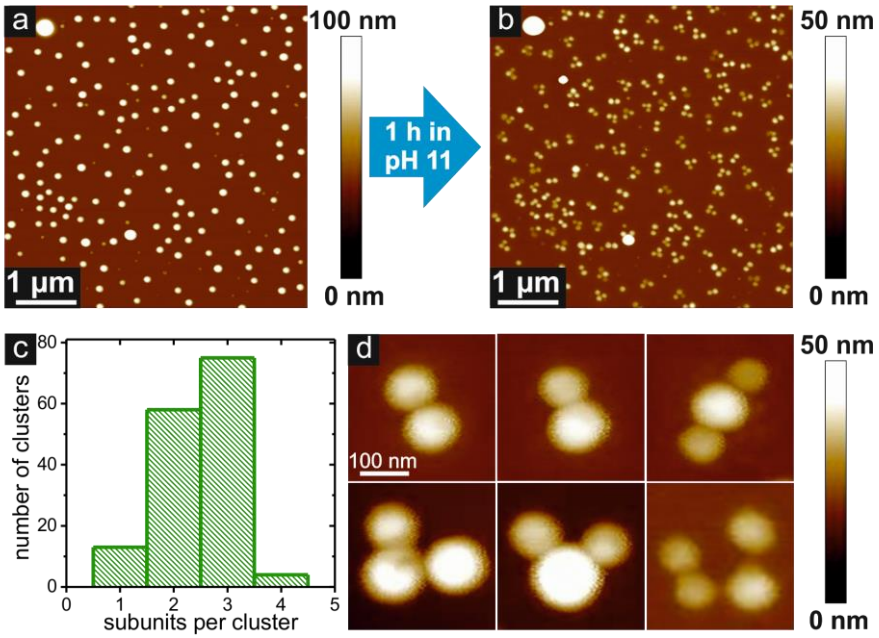

Figure 5.4. *Ex situ* AFM height images on the same spot before (a) and after incubation in pH 11 for 1 h (b). Cluster size (number of subunits per cluster) distribution (c) and AFM height images of typical clusters, depicting different subunit patterns (d).

According to the evaluation in Figure 5.4c, clusters of 2 or 3 micelles are most favorable. A few typical subunit arrays in a cluster are displayed in Figure 5.4d. Interestingly, the average center-to-center distance between subunits is in the range of ~100 nm independent of the cluster size (number of subunits) and pattern, and the mean angle between the subunits in a triplet is ~80° (*cf.* Figure S5.6). Please note that small features as well as large micelles on the surface, present in all AFM and SEM images, were excluded from statistics since those structures were not subject to splitting and are not representative for the whole sample.

Using the data on height and diameter (*cf.* Figure S5.5), the volume distribution of the initial micelles before splitting and the resulting clusters (sum of subunit volumes) were calculated. The results are given in Figure 5.5a. Direct comparison of volumes shows a significant drop from a mean value of $(0.56 \pm 0.15)\times10^{-3}$ µm^3 for micelles to $(0.23 \pm 0.09)\times10^{-3}$ µm^3 for clusters. The overall loss of volume amounts to ~60%, which indicates polymer desorption during the splitting process. Similar observations were made for other surface-immobilized micelles upon changes in the environmental conditions, *e.g.*, as a response to solvent changes,[35] pH, and/or temperature.[32-34]

On the basis of findings for the pH-dependent adsorption behavior of a PDMAEMA homopolymer[51] and PMAA-*b*-PDMAEMA diblock copolymer on silica,[52] strong interactions, which might reduce the effective micelle or cluster volume, both at low and high pH were considered unlikely. In addition, polymer desorption was verified qualitatively *via* DLS and freeze-drying of the pH 11 supernatant (*cf.* Figure S5.7). Moreover, this loss of material helps to understand the observation that the micelle morphology change is not reversible upon pH changes from 2 to 11 and back as shown in Figure 5.3. The triblock terpolymer desorbs irreversibly upon exposure to pH 11. Therefore, the system cannot restore the aggregation number upon returning to pH 2 rendering the morphological changes irreversible.

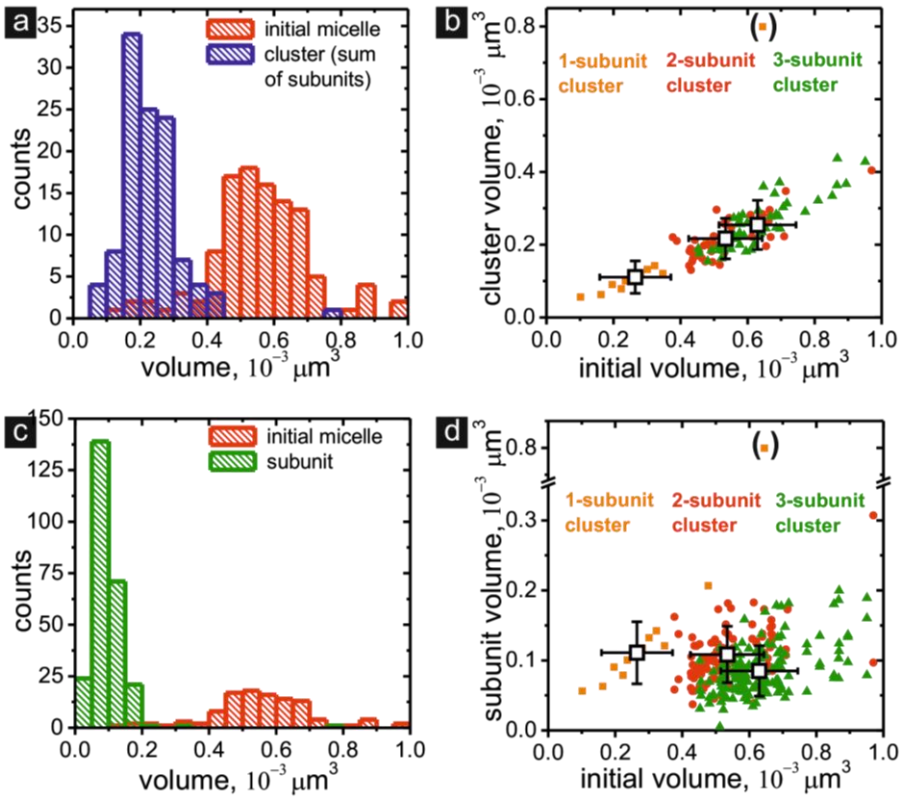

Figure 5.5. Histogram on volume distributions of initial micelles (red) before and the resulting clusters (blue) after splitting (a). The cluster size as a function of the initial micelle volume shows a linear dependence and the number of subunits per cluster (1, orange squares; 2, red circles; 3, green triangles) increases with increasing micelle volume (b). Black open squares (□) represent the mean values and the corresponding standard deviations. Histograms on the PB core volume distributions of the initial micelles (red) before and the resulting subunits (green) after splitting (c). Single subunit volume plotted as a function of the initial micelle volume (d).

The plot of cluster volume as a function of initial micelle volume in Figure 5.5b shows two distinct trends: First, there is a linear dependence between micelle and cluster volume which indicates a constant loss of polymer, independent of the initial micelle size or the resulting cluster size. The slope of the regression line is 0.4 which implies that ~40 vol% of the BMAAD triblock terpolymer is retained on the surface. Second, the larger the initial micelles, the higher is the number of subunits per cluster (*cf.* Figure S5.8a), suggesting an approximately constant subunit volume and thereby a constant aggregation

number after splitting. Comparison between micelles and subunits on a single particle level (Figure 5.5c,d) confirms this assumption. The resulting subunit size is indeed independent of the initial micelle volume. Thus, the combination of micelle splitting and partial polymer desorption leads to subunits of similar dimensions and a mean volume of $(0.094 \pm 0.039) \times 10^{-3}$ μm^3.

The pH-induced structural rearrangements of the BMAAD micelles into subunits are directly related to changes in aggregation number with the aim to minimize the total free energy of the system. Using eq 5.1 the aggregation number N_{agg} can be calculated as a function of the PB core volume V_{core}. Thereby, m_{core} is the mass of the micellar core, m_{PB}^{chain} is the mass of a single PB chain, N_A is the Avogadro constant, M_{PB}^{chain} is the molecular weight of PB, and ρ_{PB} is the density of the micellar PB core.

$$N_{agg} = \frac{m_{core}}{m_{PB}^{chain}} = \frac{N_A \rho_{PB}}{M_{PB}^{chain}} \cdot V_{core} \tag{5.1}$$

Micellar height and diameter, obtained from AFM images (Figure S5.5a,b), include the contribution of the collapsed PMAA shell and PDMAEMA corona in addition to the hydrophobic PB core. To subtract the contribution of shell and corona from the overall detectable volume, a correction factor of 0.5 was introduced. This factor takes into account the differences in degree of polymerization, molecular weight, and density of each block. The mean aggregation numbers amount to 3 540 ± 970 chains per micelle for the initial micelles and to 600 ± 250 for subunits. N_{agg} of the subunits is independent of the initial micelle size and number of subunits per cluster as it is shown in Figure S5.8b.

Considering structural and morphological characteristics of the BMAAD micelles as a function of pH, changes in aggregation number upon changes in the environmental conditions were expected to occur. This effect was reported by Xu *et al.*[53] and Webber *et al.*[29] for micellar systems in solution and observed by Gensel *et al.*[31] and Sakai *et al.*[27] on surfaces. Mean-field theory of pH-induced transitions in diblock copolymer micelles with weak polyelectrolyte blocks was proposed in ref 54. In our case, this unusual pH response by splitting into subunits can be attributed to the dynamic nature of the BMAAD micelles. Such micellar systems are dynamic in terms of being capable of adjusting to changes in the environmental conditions, *e.g.*, external stimuli (salt, pH).[38] The herein used BMAAD micelles are able to undergo changes in size distribution and aggregation number due to a low glass transition temperature of the PB core ($T_g \sim -16$ °C)[55] with a predominant 1,2-microstructure. Hydrophobic bridges and protrusions of the PB core of BMAAD(q) micelles[38, 50] indicate a low interfacial tension between the PB core and the shell. Similar findings were reported for other systems containing PB as core-forming block.[56, 57]

Interestingly, in solution the BMAAD micelles show no significant differences in size and aggregation number between pH 2 and 10, despite the charge inversion.[38, 58] In particular, at both extremes (at pH 2 and 10) the hydrophobic PB core has a diameter of ~68 nm, which corresponds to an estimated aggregation number of ~2 000. Considering the findings on the surface, BMAAD micelles were dialyzed and characterized using cryo-TEM (*cf.* Figure S5.9) to elucidate their behavior in pH 11 solution. Thereby, micelles with distinctly smaller core diameters of ~51 nm (N_{agg} ~940) were found. This observation suggests a decrease in aggregation number similar to splitting on the surface. Consequently, BMAAD micelles exhibit a similar behavior both in solution and on the surface. Besides the charge inversion, no significant changes in the micellar structure were observed in a broad pH range, from pH 2 to 10. In both cases, the splitting occurs only at pH 11. However, in contrast to solution studies, surface-immobilized micelles are considerably stronger affected by an abrupt pH increase to pH 11, which results in clusters of even smaller spherical objects (N_{agg} ~600). The difference between behavior in solution and on a surface to our opinion is caused by three parameters: time frame of the pH change, polymer concentration, and degree of freedom. In solution the pH exchange is performed *via* dialysis of micelles at pH 2 against pH 11 solution as the dialysate. Thus, the pH changes more gradually within 2-3 days due to diffusion of ions through the porous membrane. The overall polymer concentration is approximately constant during this process. Moreover, the micelles are free to move and interact with each other, thereby allowing a dynamic exchange between chains associated into micelles and "free" chains, which assures an equilibrium in addition to splitting. In contrast, a dry sample of surface-immobilized micelles is exposed to a polymer-free solution at pH 11. The micelles experience instantly pH 11 and a strong dilution. Thereby, micelles are inhibited in their movement allowing only *intramicellar* interactions, which result in splitting. Thus, the stimuli-induced restructuring may occur through local rearrangements and binding to neighboring free silica surface as well as through direct dissociation of initial micelles into "free" chain bundles (which desorb into the solution) and the reassembly of the surface-bound residue to subunits at the interface. In addition, for surface-immobilized BMAAD micelles the *intramicellar* repulsion is joined by the repulsion between negatively charged PMAA chains and the negatively charged silica surface that increases its charge density with increasing pH. On the basis of these findings, we conclude that the pH-induced micelle splitting is a surface-assisted effect.

For a theoretical description of the BMAAD micelles, we consider ABC triblock terpolymers with a hydrophobic core-forming C block (PB) and two weak polyelectrolyte blocks B (polyacid PMAA) and A (polybase PDMAEMA). We analyze the aggregation number of the micelles assuming that in both limiting cases (acidic and alkaline conditions) the micelles retain spherical, star-like shape.

At strongly acidic conditions (pH=2), the micelles have a core-shell-corona shape with the central core formed by the hydrophobic block C, surrounded by a spherical shell formed by the collapsed and

uncharged block B, and decorated by a (positively) charged corona formed by the extended blocks A. The degrees of polymerization are denoted as N_A, N_B, N_C of the A, B, and C blocks, respectively. v_C and v_B are the corresponding volumes of the monomer units. If φ_C and φ_B are the volume fractions of polymer in C-core and B-shell, respectively, then R_C and R_B are the corresponding outer radii in a micelle with aggregation number p.

The free energy of the core-shell-corona micelle can be presented as

$$F = F_{\text{corona}} + F_{\text{interface}} \tag{5.2}$$

with $F_{\text{interface}} = 4\pi R_C^2 \gamma_{BC} + 4\pi R_B^2 \gamma_B$ and $F_{corona} = pN_A \ln\left(\frac{pN_A}{R_{corona}^3 - R_B^3}\right)$.

Thereby, $F_{interface}$ accounts for the excess free energy of the core-shell (C/B) and shell-corona interfaces, γ_{BC} and γ_B are the corresponding surface tensions. The free energy of the corona comprises as the main contribution the translational entropy of an ideal gas of counterions confined in the corona. Minimization of the free energy per chain,

$$\frac{\partial}{\partial p}\frac{F_{\text{corona}} + F_{\text{interface}}}{p} = 0 \tag{5.3}$$

leads to the following expression for the aggregation number in the equilibrium micelle

$$p_{core-shell} = \left(\frac{N_C v_C}{\varphi_C} + \frac{N_B v_B}{\varphi_B}\right)^2 N_A^{-3}\left[\gamma_B + \gamma_{BC}\left(\frac{N_C v_C / \varphi_C}{N_C v_C / \varphi_C + N_B v_B / \varphi_B}\right)^{2/3}\right]^3 \tag{5.4}$$

In contrast, at strongly alkaline conditions (pH=11) the block B is fully ionized and negatively charged, whereas block A is uncharged, but remains soluble in water.

The excess free energy of the C-core/corona interface is given as $F_{\text{interface}} = 4\pi R_C^2 \gamma_C$ and the ionized inner part of the corona provides the main contribution to the coronal free energy, $F_{\text{corona}} = pN_B \ln\left(\frac{pN_B}{R_B^3 - R_C^3}\right)$. Thereby, the corona consists of an inner hydrated "shell" formed by fully ionized and strongly extended B-blocks and an outer region formed by nonionized and weakly extended A-blocks.

By applying eq 5.3 we obtain an expression for the aggregation number in a star-like micelle with ionic coronal chains:

$$p_{star} = \left(\frac{N_C v_C}{\varphi_C} \right)^2 \gamma_C^3 N_B^{-3} \tag{5.5}$$

We remark that this is an upper estimate for the aggregation number, an account of repulsive interactions under good solvent conditions between A-blocks would lead to a smaller value.

Hence,

$$\frac{p_{core-shell}}{p_{star}} = \left(1 + \frac{N_B v_B \varphi_C}{N_C v_C \varphi_B} \right)^2 \left(\frac{N_B}{N_A} \right)^3 \left(\frac{\gamma_B + \gamma_{BC} \left(1 + \frac{N_B v_B \varphi_C}{N_C v_C \varphi_B} \right)^{-2/3}}{\gamma_C} \right)^3 \tag{5.6}$$

If this ratio is larger than unity, one can expect splitting of micelles upon switching from acidic to alkaline conditions in solution. A detailed theoretical consideration is given in the Supporting Information.

On the basis of the results and theoretical considerations discussed above, we propose the following explanation for the pH-induced micellar splitting process in three steps (*cf.* Figure 5.6). In addition to stimuli-responsive blocks, BMAAD micelles possess a hydrophobic core-forming block, which is generally impassive to pH changes in aqueous solution and provides a certain degree of micellar stability in a broad pH range (pH 2-10). In the first step, surface-immobilized BMAAD micelles are exposed to pH 11. Thereby, they experience a sudden environmental change: the PDMAEMA corona becomes uncharged, simultaneously the charge density of the PMAA shell rapidly increases. This leads to a charge inversion of the micelles.

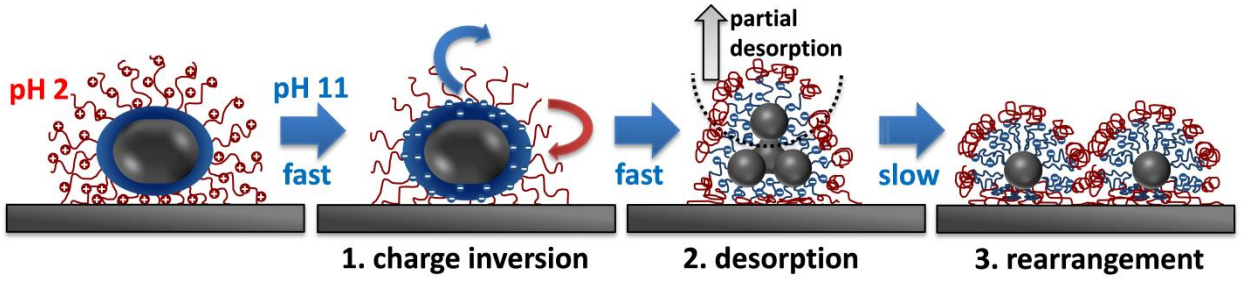

Figure 5.6. Schematic illustration of the splitting of BMAAD micelles into subunit clusters as a response to pH changes from pH 2 to 11.

In the second step, at some point during charge inversion the system becomes unstable, and finally, the instability leads to evolution of the micelles accompanied by polymer desorption. Desorption of the whole micelle in the process is, at least temporarily, inhibited by secondary interactions (*e.g.*, hydrophobic interactions or hydrogen bonding between amino and silanol groups) between PDMAEMA

and the silica surface, and is probably restricted to a removal of polymer chains that are not directly bound to the substrate. Similar observations were reported by Sakai *et al.*[59] and Mahltig *et al.*[35] The reason for destabilization of the micellar structure is an inner (osmotic) pressure due to repulsive interactions between neighboring carboxylic acid groups and strong interchain repulsion inside the PMAA shell. Thereby, the hydrophobic PB core is forced to adjust to the pH response of the shell. This phenomenon was predicted by Borisov *et al.*[54] for star-like micelles in solution. In spite of the thermodynamically unfavorable contact, a sudden pH-induced polymer desorption leads inevitably to exposure of the hydrophobic core (at least in an intermediate state) to the aqueous solution. This behavior is similar to that reported in previous work for BMAADq micelles[31] and for $PDMAEMA_{(corona)}$-$PDEAEMA_{(core)}$ diblock copolymer micelles on silica.[27] As a result, this state is rather short-lived and transfers into the third and last one. Thereby, the driving force is the minimization of the energetically unfavorable PB/water interface leading to concerted rearrangements of the three covalently linked blocks that are partially attached (*via* PDMAEMA) to the silica surface. In contrast to the first two steps, the last one is presumably rather slow. The whole process involves curling up of PB chains into spherical structures, to adopt an energetically more favorable shape, deprotonation and partial collapse of PDMAEMA, and stretching of PMAA out into solution to minimize the repulsion between neighboring charged groups. The splitting seems to be a compromise between the hydrophobicity of PB, trying to minimize the PB/water interface, and the repulsion of ionized PMAA chains, trying to increase the distance between neighboring charged groups. The pH-triggered splitting of BMAAD micelles provides an insight into the delicate balance between competing forces and opens perspectives to surface-supported cluster formation.

Conclusions

In conclusion, multicompartment micelles formed from a triblock terpolymer consisting of a hydrophobic PB block, a weak polyanionic PMAA block, and a weak polycationic PDMAEMA block show an unusual behavior when exposed to pH changes from pH 2 to pH 11 while immobilized on the surface: rather than desorption of the molecular building blocks or spreading into brush-like layers, as found for diblock copolymer micelles under comparable conditions, supramolecular reorganization results in a transition to a second, well-defined state of micellar clusters. We find that the typical aggregation number of the submicelles forming a cluster is ~600 chains and that there is a clear tendency of micelles of larger aggregation numbers to split into a larger number of submicelles. Thus, the process is decreasing the polydispersity of the supramolecular aggregates.

Although this state is transient at pH 11, it can be quenched by returning to the original pH of 2. Thus, the well-defined clusters are stabilized and can be used as supramolecular building blocks or surface-immobilized “colloidal molecules”.[60-62] One interesting perspective, that we will explore in the future, is to use these as templates for the organization of functional inorganic particles, such as plasmonic and / or catalytically active metal nanoparticles. Here, the unique structure of the clusters with a well-defined

intermicellar distance and relative orientation makes them interesting for controlling plasmonic coupling properties[63-66] as well as synergies between different nanoparticles in catalysis. More generally, this is the first example of surface-supported colloidal clusters that are not preformed in solution but rather formed *in situ* opening an avenue toward the formation of hierarchical structures.

Materials and Methods

Materials. The triblock terpolymer consisting of polybutadiene (B), poly(methacrylic acid) (MAA), and poly(2-(dimethylamino)ethyl methacrylate) (D) (subscripts denote the degree of polymerization of the respective block, M_n ~ 105 kg/mol, PDI ~ 1.10) was synthesized *via* sequential living anionic polymerization of butadiene, DMAEMA, and *tert*-butyl methacrylate (*t*BMA), followed by hydrolysis of the P*t*BMA block.[38] Stock solutions of the BMAAD triblock terpolymer micelles were prepared in Milli-Q water at pH~5 and dialyzed against pH 2 or 11 water to obtain micellar solutions with a concentration of 0.38 g/L. Dialysis was performed using molecular porous membranes (Spectra/Por® 3, Roth) with a molecular weight cutoff (MWCO) of 3 500 Da.

Milli-Q water (18.2 MΩ.cm) was used in all aqueous solutions. HCl and NaOH solutions (0.1 and 1 M, Grüssing) were used to adjust the pH of water.

Sample Preparation. Micelles were adsorbed onto silicon wafers (CrysTec) *via* dip coating from a 0.38 g/L polymer solution. The substrates were cleaned using the RCA method[67] (15 min sonication in a 1:1 mixture of water and 2-propanol and subsequent 10 min heating at 70 °C in a 5:1:1 mixture of water, 25% ammonia solution, and 30% hydrogen peroxide solution). Freshly cleaned substrates were dipped into a BMAAD micelle solution (pH 2, 0.38 g/L) for 15 min before rinsing with water and drying in a nitrogen stream. Please note that in order to avoid dehydration, the samples were used in the course of 24 h after preparation. Substrates with adsorbed micelles were immersed in water with different pH values (pH 2–12) and incubated for various periods of time (0.5–7 h). Afterward, they were removed from the aqueous solution and dried with nitrogen.

Ellipsometry. Ellipsometric measurements in air were performed with a Sentech SE 850 spectroscopic ellipsometer at a constant incidence angle of 70°. A home build liquid cell[68] was used for *in situ* ellipsometry in water of different pH at a constant incidence angle of 65°. Measurements were performed after a minimum equilibration time of 20 min.

Atomic Force Microscopy (AFM). AFM images were taken with commercial AFMs (Dimension3100 equipped with a NanoScope V controller and Dimension Icon, both from Bruker AXS Inc.) operating in Tapping Mode™ using Si_3N_4 cantilevers from Olympus with a typical spring constant of ~42 or ~26 N/m and a typical resonance frequency of 300 kHz (OTESPA or OTESPA-R3, Bruker). The average number of adsorbed micelles was determined from at least three 5×5 μm images for each

sample. To study the morphology changes of adsorbed micelles after pH treatment, *ex situ* AFM measurements on the same spot were performed before and after the treatment.

Scanning Electron Microscopy (SEM). SEM measurements were performed on a Gemini Leo 1550 instrument operating at 3 keV. The samples were sputtered with a 1.3 nm thin platinum film prior to measurement.

Cryogenic Transmission Electron Microscopy (cryo-TEM). Cryo-TEM micrographs were obtained from shock vitrified (by liquid ethane, – 179 °C) aqueous micellar solutions.The measurements were performed at a pressure of 10^{-7} - 10^{-8} hPa using a Zeiss/LEO EM 922 Omega instrument (Zeiss NTS GmbH, Oberkochen, Germany) operated at an acceleration voltage of 200 kV.

Dynamic Light Scattering (DLS). The hydrodynamic diameters of the aggregates formed in the pH 11 immersion solution were determined using a Nano-Zetasizer (Malvern Instruments Co, Worcestershire, U.K.).

Acknowledgment

This research was funded by BFHZ, BMBF, SFB840, COST Action CM1101. The authors thank C. Kunert for conducting the SEM experiments, M. Drechsler for cryo-TEM measurements, and O. Grimm for control experiments on PDMAEMA homopolymers. OVB acknowledges support by Russian Science Foundation Grant No. 14-33-00003.

References

1. Park, C.; Yoon, J.; Thomas, E. L., Enabling Nanotechnology with Self Assembled Block Copolymer Patterns. *Polymer* **2003,** *44*, 6725-6760.
2. Cheng, J. Y.; Ross, C. A.; Smith, H. I.; Thomas, E. L., Templated Self-Assembly of Block Copolymers: Top-Down Helps Bottom-Up. *Adv. Mater.* **2006,** *18*, 2505-2521.
3. Paquet, C.; Kumacheva, E., Nanostructured Polymers for Photonics. *Mater. Today* **2008,** *11*, 48-56.
4. Tseng, Y. C.; Darling, S. B., Block Copolymer Nanostructures for Technology. *Polymers* **2010,** *2*, 470-489.
5. Schacher, F. H.; Rupar, P. A.; Manners, I., Functional Block Copolymers: Nanostructured Materials with Emerging Applications. *Angew. Chem. Int. Ed.* **2012,** *51*, 7898-7921.
6. Jeong, S. J.; Kim, J. Y.; Kim, B. H.; Moon, H. S.; Kim, S. O., Directed Self-Assembly of Block Copolymers for Next Generation Nanolithography. *Mater. Today* **2013,** *16*, 468-476.
7. Calandra, P.; Caschera, D.; Liveri, V. T.; Lombardo, D., How Self-Assembly of Amphiphilic Molecules Can Generate Complexity in the Nanoscale. *Colloids Surf., A* **2015,** *484*, 164-183.
8. Stefik, M.; Guldin, S.; Vignolini, S.; Wiesner, U.; Steiner, U., Block Copolymer Self-Assembly for Nanophotonics. *Chem. Soc. Rev.* **2015,** *44*, 5076-5091.
9. Krausch, G.; Magerle, R., Nanostructured Thin Films *via* Self-Assembly of Block Copolymers. *Adv. Mater.* **2002,** *14*, 1579-1583.

10. Orilall, M. C.; Wiesner, U., Block Copolymer Based Composition and Morphology Control in Nanostructured Hybrid Materials for Energy Conversion and Storage: Solar Cells, Batteries, and Fuel Cells. *Chem. Soc. Rev.* **2011,** *40*, 520-535.
11. Mai, Y. Y.; Eisenberg, A., Self-Assembly of Block Copolymers. *Chem. Soc. Rev.* **2012,** *41*, 5969-5985.
12. Stuart, M. A. C.; Huck, W. T. S.; Genzer, J.; Müller, M.; Ober, C.; Stamm, M.; Sukhorukov, G. B.; Szleifer, I.; Tsukruk, V. V.; Urban, M.; Winnik, F.; Zauscher, S.; Luzinov, I.; Minko, S., Emerging Applications of Stimuli-Responsive Polymer Materials. *Nat. Mater.* **2010,** *9*, 101-113.
13. Guragain, S.; Bastakoti, B. P.; Malgras, V.; Nakashima, K.; Yamauchi, Y., Multi-Stimuli-Responsive Polymeric Materials. *Chem. - Eur. J.* **2015,** *21*, 13164-13174.
14. Wyman, I. W.; Liu, G. J., Micellar Structures of Linear Triblock Terpolymers: Three Blocks but Many Possibilities. *Polymer* **2013,** *54*, 1950-1978.
15. Li, Z. B.; Kesselman, E.; Talmon, Y.; Hillmyer, M. A.; Lodge, T. P., Multicompartment Micelles from ABC Miktoarm Stars in Water. *Science* **2004,** *306*, 98-101.
16. Kubowicz, S.; Baussard, J. F.; Lutz, J. F.; Thunemann, A. F.; von Berlepsch, H.; Laschewsky, A., Multicompartment Micelles Formed by Self-Assembly of Linear ABC Triblock Copolymers in Aqueous Medium. *Angew. Chem. Int. Ed.* **2005,** *44*, 5262-5265.
17. Cui, H. G.; Chen, Z. Y.; Zhong, S.; Wooley, K. L.; Pochan, D. J., Block Copolymer Assembly *via* Kinetic Control. *Science* **2007,** *317*, 647-650.
18. Gröschel, A. H.; Walther, A.; Löbling, T. I.; Schacher, F. H.; Schmalz, H.; Müller, A. H. E., Guided Hierarchical Co-Assembly of Soft Patchy Nanoparticles. *Nature* **2013,** *503*, 247-251.
19. Gröschel, A. H.; Müller, A. H. E., Self-Assembly Concepts for Multicompartment Nanostructures. *Nanoscale* **2015,** *7*, 11841-11876.
20. Schacher, F.; Walther, A.; Müller, A. H. E., Dynamic Multicompartment-Core Micelles in Aqueous Media. *Langmuir* **2009,** *25*, 10962-10969.
21. Gröschel, A. H.; Schacher, F. H.; Schmalz, H.; Borisov, O. V.; Zhulina, E. B.; Walther, A.; Müller, A. H. E., Precise Hierarchical Self-Assembly of Multicompartment Micelles. *Nat. Commun.* **2012,** *3*, 10.
22. Nicolai, T.; Colombani, O.; Chassenieux, C., Dynamic Polymeric Micelles *versus* Frozen Nanoparticles Formed by Block Copolymers. *Soft Matter* **2010,** *6*, 3111-3118.
23. Gohy, J. F., Block Copolymer Micelles. In *Block Copolymers II*, Abetz, V., Ed. Springer: Berlin, 2005; pp 65-136.
24. Mok, M. M.; Lodge, T. P., Temperature-Based Fluorescence Measurements of Pyrene in Block Copolymer Micelles: Probing Micelle Core Glass Transition Breadths. *J. Polym. Sci., Part B: Polym. Phys.* **2012,** *50*, 500-515.
25. van Stam, J.; Creutz, S.; De Schryver, F. C.; Jérôme, R., Tuning of the Exchange Dynamics of Unimers between Block Copolymer Micelles with Temperature, Cosolvents, and Cosurfactants. *Macromolecules* **2000,** *33*, 6388-6395.
26. Borisova, O.; Billon, L.; Zaremski, M.; Grassl, B.; Bakaeva, Z.; Lapp, A.; Stepanek, P.; Borisov, O., Synthesis and pH- and Salinity-Controlled Self-Assembly of Novel Amphiphilic Block-Gradient Copolymers of Styrene and Acrylic Acid. *Soft Matter* **2012,** *8*, 7649-7659.
27. Sakai, K.; Smith, E. G.; Webber, G. B.; Baker, M.; Wanless, E. J.; Bütün, V.; Armes, S. P.; Biggs, S., Characterizing the pH-Responsive Behavior of Thin Films of Diblock Copolymer Micelles at the Silica/Aqueous Solution Interface. *Langmuir* **2006,** *22*, 8435-8442.
28. Sakai, K.; Smith, E. G.; Webber, G. B.; Schatz, C.; Wanless, E. J.; Bütün, V.; Armes, S. P.; Biggs, S., Comparison of the Adsorption of Cationic Diblock Copolymer Micelles from Aqueous Solution onto Mica and Silica. *Langmuir* **2006,** *22*, 5328-5333.
29. Webber, G. B.; Wanless, E. J.; Armes, S. P.; Biggs, S., Tunable Diblock Copolymer Micelles-Adapting Behaviour *via* Subtle Chemical Modifications. *Faraday Discuss.* **2005,** *128*, 193-209.
30. Webber, G. B.; Wanless, E. J.; Armes, S. P.; Tang, Y. Q.; Li, Y. T.; Biggs, S., Nano-Anemones: Stimulus-Responsive Copolymer-Micelle Surfaces. *Adv. Mater.* **2004,** *16*, 1794-1798.

31. Gensel, J.; Betthausen, E.; Hasenöhrl, C.; Trenkenschuh, K.; Hund, M.; Boulmedais, F.; Schaaf, P.; Müller, A. H. E.; Fery, A., Surface Immobilized Block Copolymer Micelles with Switchable Accessibility of Hydrophobic Pockets. *Soft Matter* **2011,** *7*, 11144-11153.
32. Erel, I.; Zhu, Z. C.; Zhuk, A.; Sukhishvili, S. A., Hydrogen-Bonded Layer-by-Layer Films of Block Copolymer Micelles with pH-Responsive Cores. *J. Colloid Interface Sci.* **2011,** *355*, 61-69.
33. Xu, L.; Zhu, Z. C.; Sukhishvili, S. A., Polyelectrolyte Multilayers of Diblock Copolymer Micelles with Temperature-Responsive Cores. *Langmuir* **2011,** *27*, 409-415.
34. Zhu, Z. C.; Sukhishvili, S. A., Temperature-Induced Swelling and Small Molecule Release with Hydrogen-Bonded Multilayers of Block Copolymer Micelles. *ACS Nano* **2009,** *3*, 3595-3605.
35. Mahltig, B.; Müller-Buschbaum, P.; Wolkenhauer, M.; Wunnicke, O.; Wiegand, S.; Gohy, J. F.; Jérôme, R.; Stamm, M., Highly Regular Polyampholytic Structures Adsorbed Directly from Solution. *J. Colloid Interface Sci.* **2001,** *242*, 36-43.
36. Gensel, J.; Borke, T.; Pazos-Pérez, N.; Fery, A.; Andreeva, D. V.; Betthausen, E.; Müller, A. H. E.; Möhwald, H.; Skorb, E. V., Cavitation Engineered 3D Sponge Networks and Their Application in Active Surface Construction. *Adv. Mater.* **2012,** *24*, 985-989.
37. Gensel, J.; Dewald, I.; Erath, J.; Betthausen, E.; Müller, A. H. E.; Fery, A., Reversible Swelling Transitions in Stimuli-Responsive Layer-by-Layer Films Containing Block Copolymer Micelles. *Chem. Sci.* **2013,** *4*, 325-334.
38. Betthausen, E.; Drechsler, M.; Förtsch, M.; Schacher, F. H.; Müller, A. H. E., Dual Stimuli-Responsive Multicompartment Micelles from Triblock Terpolymers with Tunable Hydrophilicity. *Soft Matter* **2011,** *7*, 8880-8891.
39. Dautzenberg, H.; Jaeger, W.; Kötz, J.; Philipp, B.; Seidel, C.; Stscherbina, D., *Polyelectrolytes*. Carl Hanser: München, 1994.
40. Plamper, F. A.; Ruppel, M.; Schmalz, A.; Borisov, O.; Ballauff, M.; Müller, A. H. E., Tuning the Thermoresponsive Properties of Weak Polyelectrolytes: Aqueous Solutions of Star-Shaped and Linear Poly(*N,N*-dimethylaminoethyl methacrylate). *Macromolecules* **2007,** *40*, 8361-8366.
41. Longtin, R.; Maroni, P.; Borkovec, M., Transition from Completely Reversible to Irreversible Adsorption of Poly(amido amine) Dendrimers on Silica. *Langmuir* **2009,** *25*, 2928-2934.
42. Evans, J. W., Random and Cooperative Sequential Adsorption. *Rev. Mod. Phys.* **1993,** *65*, 1281-1329.
43. Feder, J., Random Sequential Adsorption. *J. Theor. Biol.* **1980,** *87*, 237-254.
44. Burkhardt, M.; Martinez-Castro, N.; Tea, S.; Drechsler, M.; Babin, I.; Grishagin, I.; Schweins, R.; Pergushov, D. V.; Gradzielski, M.; Zezin, A. B.; Müller, A. H. E., Polyisobutylene-*block*-Poly(methacrylic acid) Diblock Copolymers: Self-Assembly in Aqueous Media. *Langmuir* **2007,** *23*, 12864-12874.
45. Currie, E. P. K.; Sieval, A. B.; Fleer, G. J.; Stuart, M. A. C., Polyacrylic Acid Brushes: Surface Pressure and Salt-Induced Swelling. *Langmuir* **2000,** *16*, 8324-8333.
46. Parnell, A. J.; Martin, S. J.; Dang, C. C.; Geoghegan, M.; Jones, R. A. L.; Crook, C. J.; Howse, J. R.; Ryan, A. J., Synthesis, Characterization and Swelling Behaviour of Poly(methacrylic acid) Brushes Synthesized Using Atom Transfer Radical Polymerization. *Polymer* **2009,** *50*, 1005-1014.
47. Plamper, F. A.; Becker, H.; Lanzendorfer, M.; Patel, M.; Wittemann, A.; Ballauff, M.; Müller, A. H. E., Synthesis, Characterization and Behavior in Aqueous Solution of Star-Shaped Poly(acrylic acid). *Macromol. Chem. Phys.* **2005,** *206*, 1813-1825.
48. Tomlinson, M. R.; Cousin, F.; Geoghegan, M., Creation of Dense Polymer Brush Layers by the Controlled Deposition of an Amphiphilic Responsive Comb Polymer. *Polymer* **2009,** *50*, 4829-4836.
49. Kirby, B. J.; Hasselbrink, E. F., Zeta Potential of Microfluidic Substrates: 1. Theory, Experimental Techniques, and Effects on Separations. *Electrophoresis* **2004,** *25*, 187-202.

50. Betthausen, E.; Drechsler, M.; Förtsch, M.; Pergushov, D. V.; Schacher, F. H.; Müller, A. H. E., Stimuli-Responsive Micellar Interpolyelectrolyte Complexes - Control of Micelle Dynamics *via* Core Crosslinking. *Soft Matter* **2012,** *8*, 10167-10177.
51. Shin, Y. W.; Roberts, J. E.; Santore, M., The Influence of Charge Variation on the Adsorbed Configuration of a Model Cationic Oligomer onto Colloidal Silica. *J. Colloid Interface Sci.* **2001,** *244*, 190-199.
52. Walter, H.; Harrats, C.; Müller-Buschbaum, P.; Jérôme, R.; Stamm, M., Adsorption of Ampholytic Diblock Copolymers from Dilute Aqueous Solution at the Solid/Liquid Interface. *Langmuir* **1999,** *15*, 1260-1267.
53. Xu, L.; Zhu, Z. C.; Borisov, O. V.; Zhulina, E. B.; Sukhishvili, S. A., pH-Triggered Block Copolymer Micelle-to-Micelle Phase Transition. *Phys. Rev. Lett.* **2009,** *103*, 4.
54. Zhulina, E. B.; Borisov, O. V., Self-Assembly in Solution of Block Copolymers with Annealing Polyelectrolyte Blocks. *Macromolecules* **2002,** *35*, 9191-9203.
55. Schacher, F.; Yuan, J. Y.; Schoberth, H. G.; Müller, A. H. E., Synthesis, Characterization, and Bulk Crosslinking of Polybutadiene-*block*-Poly(2-vinyl pyridine)-*block*-Poly(*tert*-butyl methacrylate) Block Terpolymers. *Polymer* **2010,** *51*, 2021-2032.
56. Synatschke, C. V.; Schacher, F. H.; Förtsch, M.; Drechsler, M.; Müller, A. H. E., Double-Layered Micellar Interpolyelectrolyte Complexes-How Many Shells to a Core? *Soft Matter* **2011,** *7*, 1714-1725.
57. Walther, A.; Müller, A. H. E., Formation of Hydrophobic Bridges between Multicompartment Micelles of Miktoarm Star Terpolymers in Water. *Chem. Commun.* **2009**, 1127-1129.
58. Rinkenauer, A. C.; Schallon, A.; Guenther, U.; Wagner, M.; Betthausen, E.; Schubert, U. S.; Schacher, F. H., A Paradigm Change: Efficient Transfection of Human Leukemia Cells by Stimuli-Responsive Multicompartment Micelles. *ACS Nano* **2013,** *7*, 9621-9631.
59. Sakai, K.; Smith, E. G.; Webber, G. B.; Baker, M.; Wanless, E. J.; Bütün, V.; Armes, S. P.; Biggs, S., pH-Responsive Behavior of Selectively Quaternized Diblock Copolymers Adsorbed at the Silica/Aqueous Solution Interface. *J. Colloid Interface Sci.* **2007,** *314*, 381-388.
60. Li, F.; Josephson, D. P.; Stein, A., Colloidal Assembly: The Road from Particles to Colloidal Molecules and Crystals. *Angew. Chem. Int. Ed.* **2011,** *50*, 360-388.
61. Blaaderen, A. v., Chemistry. Colloidal Molecules and Beyond. *Science* **2003,** *301*, 470-471.
62. Glotzer, S. C., Some Assembly Required. *Science* **2004,** *306*, 419-420.
63. Hanske, C.; Tebbe, M.; Kuttner, C.; Bieber, V.; Tsukruk, V. V.; Chanana, M.; König, T. A. F.; Fery, A., Strongly Coupled Plasmonic Modes on Macroscopic Areas *via* Template-Assisted Colloidal Self-Assembly. *Nano Lett.* **2014,** *14*, 6863-6871.
64. Fan, J. A.; Bao, K.; Sun, L.; Bao, J. M.; Manoharan, V. N.; Nordlander, P.; Capasso, F., Plasmonic Mode Engineering with Templated Self-Assembled Nanoclusters. *Nano Lett.* **2012,** *12*, 5318-5324.
65. Pazos-Pérez, N.; Wagner, C. S.; Romo-Herrera, J. M.; Liz-Marzán, L. M.; de Abajo, F. J. G.; Wittemann, A.; Fery, A.; Alvarez-Puebla, R. A., Organized Plasmonic Clusters with High Coordination Number and Extraordinary Enhancement in Surface-Enhanced Raman Scattering (SERS). *Angew. Chem. Int. Ed.* **2012,** *51*, 12688-12693.
66. Höller, R. P. M.; Dulle, M.; Thomä, S.; Mayer, M.; Steiner, A. M.; Förster, S.; Fery, A.; Kuttner, C.; Chanana, M., Protein-Assisted Assembly of Modular 3D Plasmonic Raspberry-like Core/Satellite Nanoclusters: Correlation of Structure and Optical Properties. *ACS Nano* **2016**, **DOI:** 10.1021/acsnano.5b07533
67. Kern, W.; Puotinen, D. A., Cleaning Solutions Based on Hydrogen Peroxide for Use in Silicon Semiconductor Technology. *RCA Review* **1970,** *31*, 187.
68. Elbs, H.; Krausch, G., Ellipsometric Determination of Flory-Huggins Interaction Parameters in Solution. *Polymer* **2004,** *45*, 7935-7942.

Supporting Information

Surface Immobilization – Adsorption Kinetics

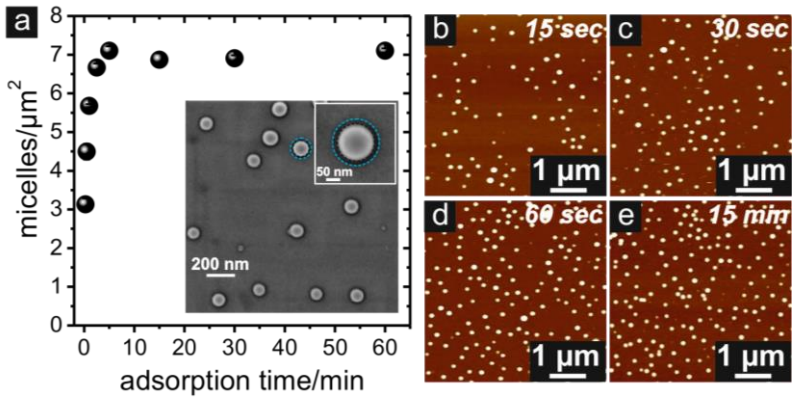

Figure S5.1. Micelle density on a silica surface as a function of adsorption time, inset: SEM image (PB core: black dashed line, PMAA shell: blue dashed line) (a) and exemplarily the corresponding AFM height images (*z*-scale: 0-100 nm) after 15, 30, 60 sec, and 15 min adsorption time (b-e).

pH-Response – Incubation at pH 10.5 and pH 12

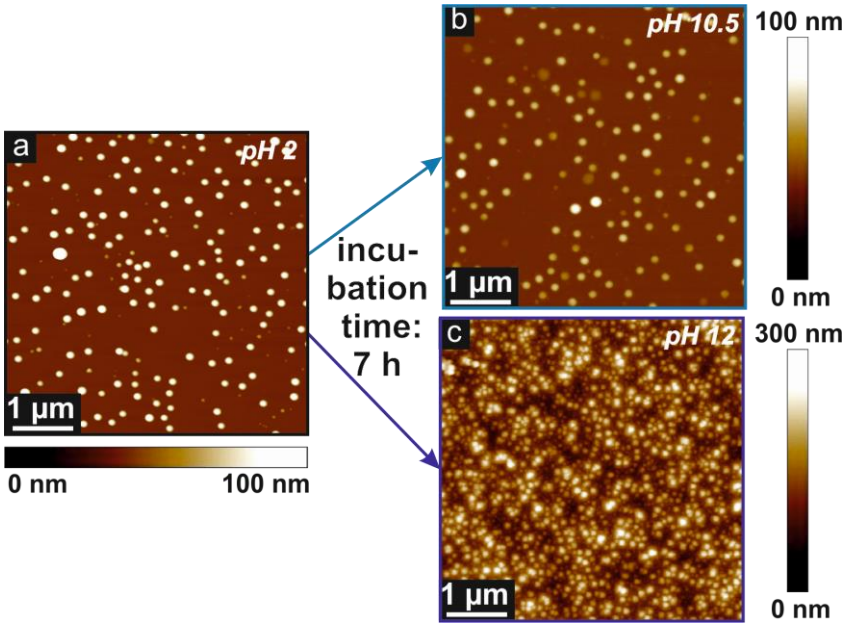

Figure S5.2. AFM height images of a reference sample (exemplarily) with surface-immobilized BMAAD micelles adsorbed from pH 2 solution (a) and samples after immersion/incubation at pH 10.5 (b) and pH 12 (c).

Splitting Kinetics

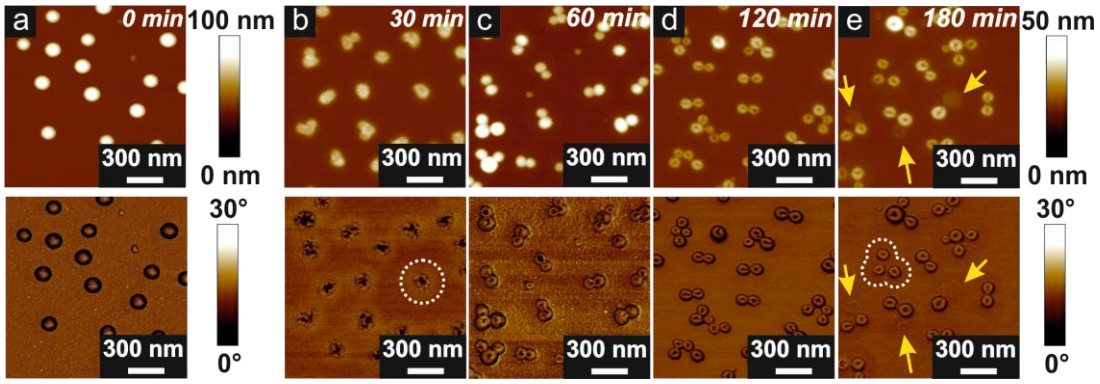

Figure S5.3. AFM height (top row) and phase (bottom row) images of BMAAD micelles adsorbed from pH 2 before (a) and after exposure to pH 11 for 30, 60, 120, and 180 min (b-e), respectively. The "finger prints" of the corona in the phase images are highlighted by dashed white lines (b,e) and the "finger prints" of desorbed subunits are pointed out by yellow arrows (e).

Successive Exposure to Basic and Acidic Solutions

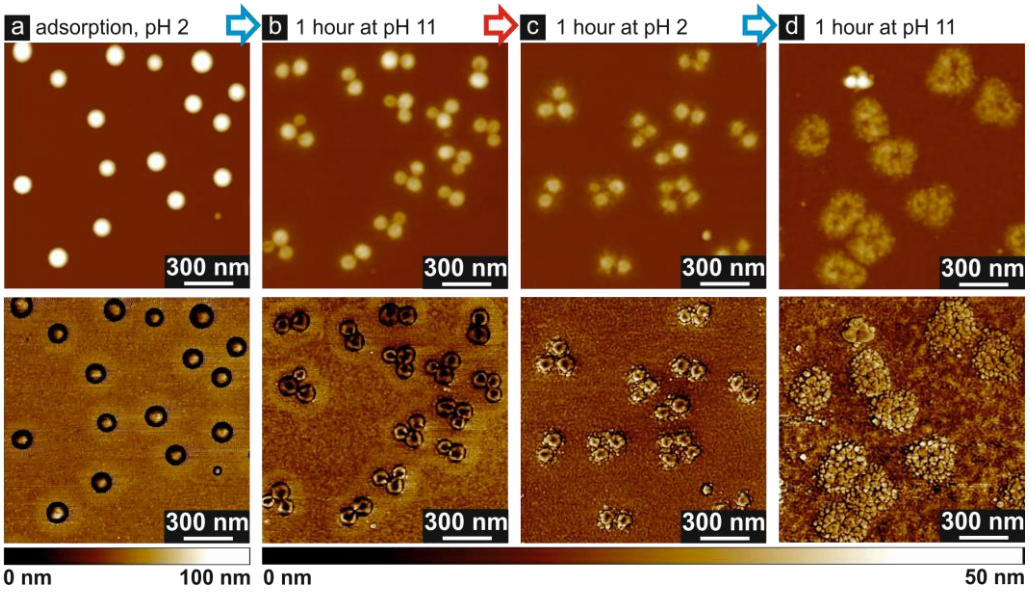

Figure S5.4. AFM height (top row) and phase (bottom row; *z*-ranges: (a) 0-30°, (b) 0-10°, (c) 0-10°, (d) 0-30°) images of surface-immobilized BMAAD micelles in dry state directly after adsorption from pH 2 solution (a), and after subsequent exposure to pH 11 (b), pH 2 (c) and again pH 11 (d), each for the duration of 1 hour.

Diameter, Height, Radius of Curvature and Surface Area

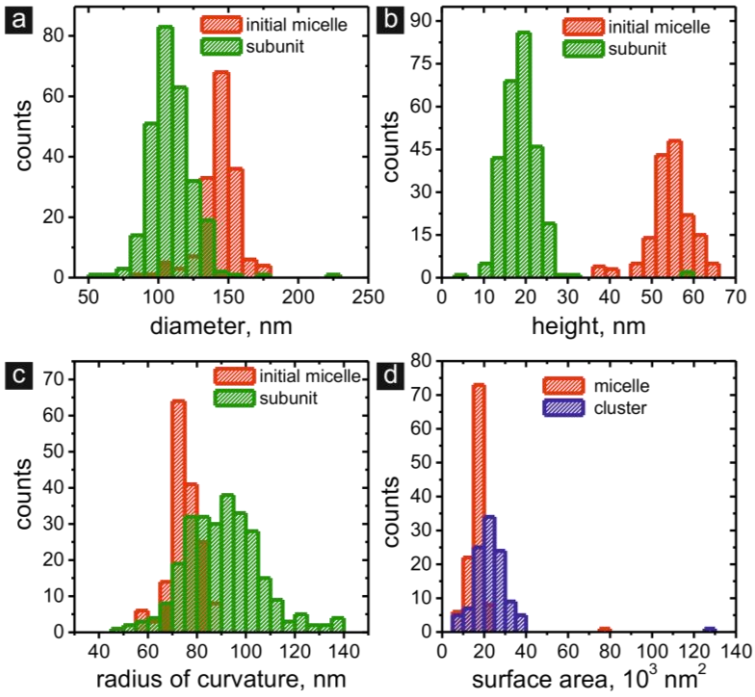

Figure S5.5. Distributions of AFM raw data such as diameter (a) and height (b) of the initial micelles before splitting (red) as well as of the resulting subunits (green) after splitting. Using the raw data the distributions of the radius of curvature (c) and contact area between the micelles or clusters (= sum of subunits, blue) and the silica substrate (d) can be calculated.

Distances Within the Clusters

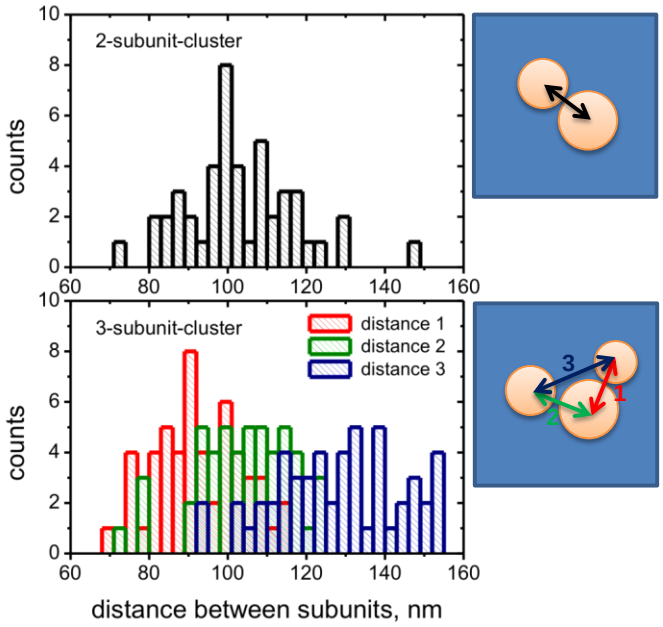

Figure S5.6. Distributions of center-to-center distances in 2-subunit and 3-subunit clusters with schemes illustrating the corresponding distances.

Polymer Desorption During Splitting

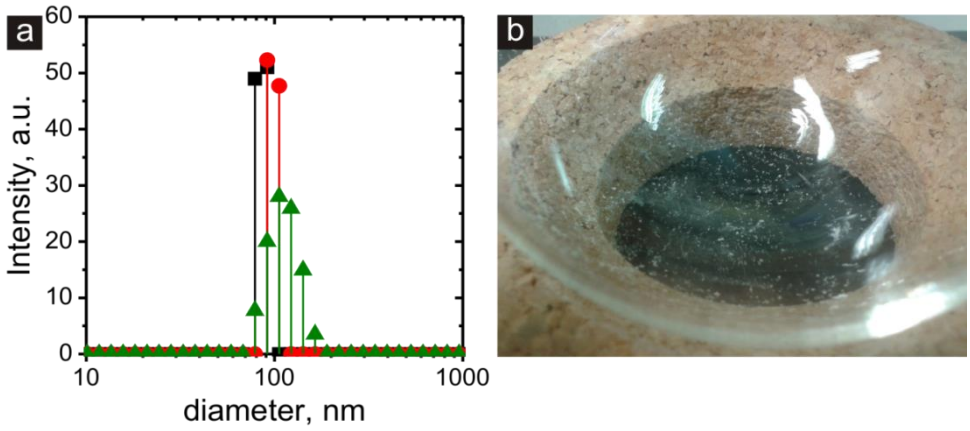

Figure S5.7: Hydrodynamic diameters (DLS) of micellar aggregates detected in the supernatant after incubation of surface-immobilized BMAAD micelles for one hour at pH 11 (a). Freeze-drying of the supernatant (collected from 3 samples) resulted in a white powder (b) which corresponds to the polymer desorbed from the surface.

Cluster Size and Aggregation Number

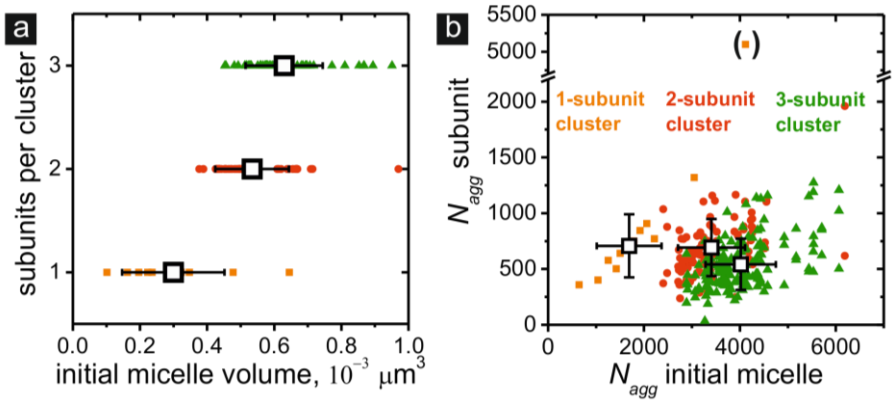

Figure S5.8. Cluster size (= number of subunits per cluster) as a function of the initial micelle volume (a) and aggregation number of subunits after splitting as a function of the initial micelle aggregation number (b). Different colors correspond to a different number of subunits per cluster (1: orange squares (■), 2: red circles (●), 3: green triangles (▲)). Black open squares (□) represent the mean values and the corresponding standard deviations.

Cryo-TEM in pH 2 and 11

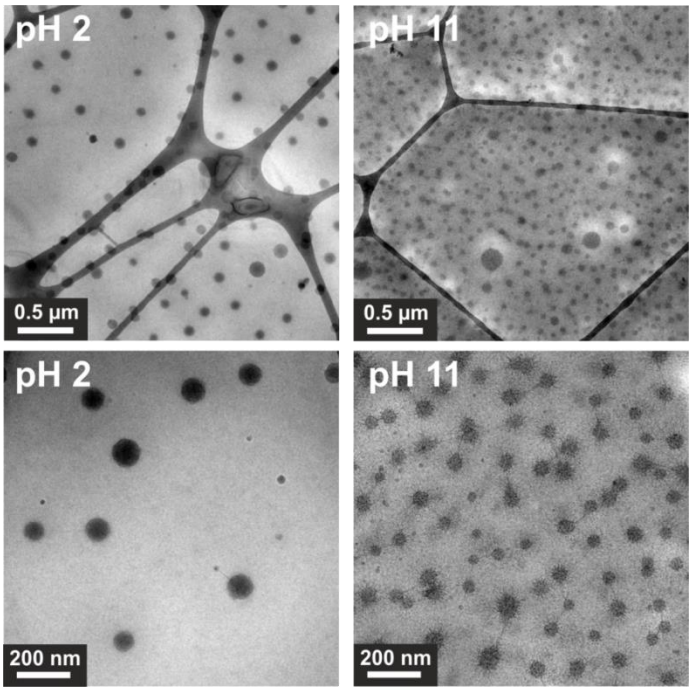

Figure S5.9. Cryo-TEM micrographs of BMAAD micelles in pH 2 solution and after dialysis against pH 11.

Theoretical Consideration of Micelles Splitting

Consider ABC triblock terpolymers with degrees of polymerization N_A, N_B, N_C of A, B and C blocks, respectively. Block C is hydrophobic and forms a dense core of the micelle. v_C and v_B are the volumes of C and B monomer units, respectively. Blocks B and A are weak polyacid and weak polybase, respectively. We analyze the aggregation number in micelles assuming that in both limiting cases (acidic and alkaline conditions) the micelles retain spherical star-like shape, that is, the radius of the dense core is smaller than that of the hydrated corona.

Acidic conditions:

At strongly acidic conditions (pH=2) block B (that is, PMAA) is uncharged and collapsed due to the intrinsic hydrophobicity, whereas block A (PDMAEMA) is fully ionized (positively charged), the fraction of charged monomer units $\alpha \cong 1$.

The micelles have a core-shell-corona shape with the central core formed by hydrophobic block C surrounded by a spherical shell formed by collapsed and uncharged block B and decorated by (positively) charged corona formed by extended blocks A.

Let φ_C and φ_B be the volume fractions of C and B monomers in the core and in the shell, respectively. Then $R_C = \left(\frac{3}{4\pi} \frac{pN_C v_C}{\varphi_C} \right)^{1/3}$ and $R_B = \left(\frac{3p}{4\pi} \left[\frac{N_C v_C}{\varphi_C} + \frac{N_B v_B}{\varphi_B} \right] \right)^{1/3}$ are the outer radii of the C-core and of the B-shell in a micelle with aggregation number p, respectively.

The free energy (in $k_B T$ units) of the core-shell-corona micelle can be presented as

$$F = F_{\text{corona}} + F_{\text{interface}} \tag{S5.1}$$

The term

$$F_{\text{interface}} = 4\pi R_C^2 \gamma_{BC} + 4\pi R_B^2 \gamma_B \tag{S5.2}$$

accounts for the excess free energy of the core-shell (C/B) and shell-corona interfaces, γ_{BC} and γ_B are the corresponding surface tensions (in $k_B T$ units).

Then eq. S5.2 can be presented in the form

$$F_{\text{interface}} = (36\pi)^{1/3} p^{2/3} \left(\frac{N_C v_C}{\varphi_C} + \frac{N_B v_B}{\varphi_B} \right)^{2/3} \left[\gamma_B + \gamma_{BC} \left(\frac{N_C v_C / \varphi_C}{N_C v_C / \varphi_C + N_B v_B / \varphi_B} \right)^{2/3} \right] \tag{S5.3}$$

The free energy of the corona comprises as the main contribution translational entropy of ideal gas of counterions confined in the corona,

$$F_{corona} = pN_A \ln \left(\frac{pN_A}{R_{corona}^3 - R_B^3} \right) \tag{S5.4}$$

(where we have omitted *p*-independent terms). Minimization of the free energy per chain,

$$\frac{\partial}{\partial p} \frac{F_{\text{corona}} + F_{\text{interface}}}{p} = 0 \tag{S5.5}$$

leads to the following expression for the aggregation number in the equilibrium micelle

$$p_{core-shell} = \left(\frac{N_C v_C}{\varphi_C} + \frac{N_B v_B}{\varphi_B} \right)^2 N_A^{-3} \left[\gamma_B + \gamma_{BC} \left(\frac{N_C v_C / \varphi_C}{N_C v_C / \varphi_C + N_B v_B / \varphi_B} \right)^{2/3} \right]^3 \tag{S5.6}$$

(a numerical coefficient is omitted).

Alkaline conditions

At strongly alkaline conditions (pH=11) the block B is fully ionized and negatively charged whereas block A is uncharged, but remains soluble in water.

The excess free energy of the C-core/corona interface assumes the simple form:

$$F_{\text{interface}} = 4\pi R_C^2 \gamma_C \tag{S5.7}$$

The corona consists of inner hydrated "shell" formed by fully ionized and strongly extended B-blocks, and outer region formed by nonionized and weakly extended A-blocks. The ionized inner part of the corona provides the main contribution to the coronal free energy,

$$F_{\text{corona}} = pN_B \ln\left(\frac{pN_B}{R_B^3 - R_C^3}\right) \tag{S5.8}$$

By applying eq. S5.5 we obtain an expression for the aggregation number in a star-like micelle with ionic coronal chains

$$p_{star} = \left(\frac{N_C v_C}{\varphi_C}\right)^2 \gamma_C^3 N_B^{-3} \tag{S5.9}$$

We remark that this is an upper estimate for the aggregation number, an account of repulsive interactions under good solvent conditions between A-blocks would lead to a smaller value.

Hence,

$$\frac{p_{core-shell}}{p_{star}} = \left(1+\frac{N_B v_B \varphi_C}{N_C v_C \varphi_B}\right)^2 \left(\frac{N_B}{N_A}\right)^3 \left(\frac{\gamma_B + \gamma_{BC}\left(1+\frac{N_B v_B \varphi_C}{N_C v_C \varphi_B}\right)^{-2/3}}{\gamma_C}\right)^3 \tag{S5.10}$$

If this ratio is larger than unity, one can expect splitting of micelles upon switching from acidic to alkaline conditions in solution.

6 Patterned Thermoresponsive Microgel Coatings for Noninvasive Processing of Adherent Cells

Reprinted with permission from

Patterned Thermoresponsive Microgel Coatings for Noninvasive Processing of Adherent Cells, Katja Uhlig, Thomas Wegener, Jian He, Michael Zeiser, Johannes Bookhold, Inna Dewald, Neus Godino, Magnus Jaeger, Thomas Hellweg, Andreas Fery, and Claus Duschl

Biomacromolecules **2016** *17* (3), 1110-1116

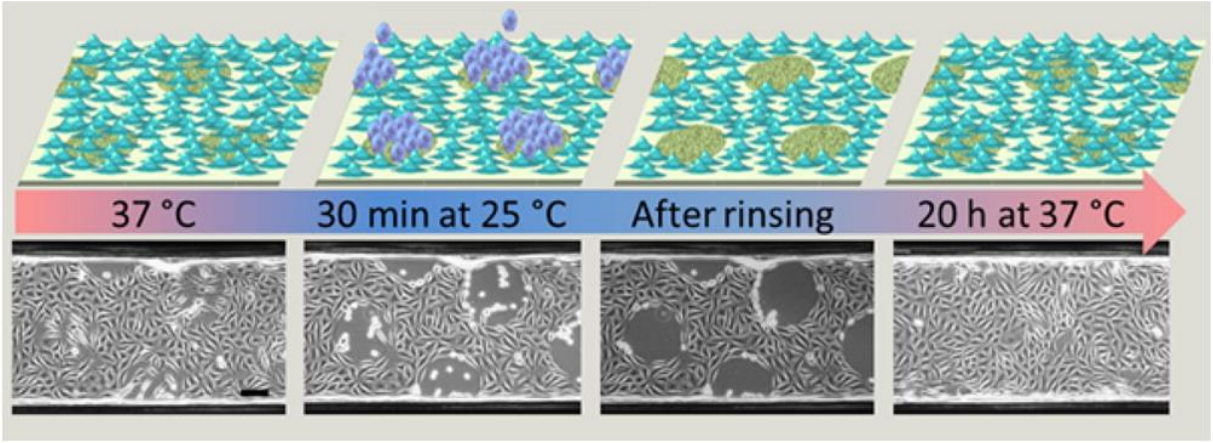

Abstract

Cultivation of adherently growing cells in artificial environments is of utmost importance in medicine and biotechnology to accomplish in vitro drug screening or to investigate disease mechanisms. Precise cell manipulation, like localized control over adhesion, is required to expand cells, to establish cell models for novel therapies and to perform noninvasive cell experiments. To this end, we developed a method of gentle, local lift-off of mammalian cells using polymer surfaces, which are reversibly and repeatedly switchable between a cell-attractive and a cell-repellent state. This property was introduced through micropatterned thermoresponsive polymer coatings formed from colloidal microgels. Patterning was obtained through automated nanodispensing or microcontact printing, making use of unspecific electrostatic interactions between microgels and substrates. This process is much more robust against ambient conditions than covalent coupling, thus lending itself to up-scaling. As an example, wound healing assays were accomplished at 37 °C with highly increased precision in microfluidic environments.

Introduction

The promises of novel therapeutic approaches, diagnostic tools, and test systems that utilize cells for assessing the efficacy or the toxicity of compounds are about to show their first benefits.[1, 2] However, substantial obstacles are still limiting a broad application of cell-based systems. These limitations do not necessarily lie in a limited understanding of basic aspects of the biological context. They rather result from an inability to ensure and maintain the quality and reliability levels of cell material that are mandatory for clinical applications and pharmaceutical research. A key aspect in this context is the noninvasive treatment and reliable and reproducible processing of adherent cells.

For improving the reliability and accuracy of cell assays as well as for cell expansion, the control of cell adhesion is crucial. This includes the thorough detachment of cells from their substrate. Crude mechanical scratching or the use of enzyme solutions, which both heavily impair cell viability,[3] are still standard methods for removing adherent cells from the culture surface. A much more gentle approach that does not affect the quality of the cells makes use of surface coatings from thermoresponsive polymers.[4, 5] Such coatings mediate protein, and therefore cell, adhesion above the lower critical solution temperature (LCST), where the polymer is in a collapsed state. Below the LCST, the polymer changes to a hydrated and expanded configuration, thus disallowing protein binding and resulting in cell repulsion.[6-10]

The most popular thermoresponsive polymer poly(*N*-isopropylacrylamide) (PNIPAM) has a LCST of 32 °C. Hence, cell cultivation on PNIPAM coatings is straightforward at 37 °C, and decreasing the temperature below the LCST initiates cell detachment from the substrate for further use. Okano et al. pioneered this concept over the last two decades, focusing on applications in regenerative medicine.

Various coating techniques have been reported using grafting-from approaches, like surface-initiated ATRP (atom transfer radical polymerization) or electron beam-induced graft polymerization,[11, 12] or grafting-to approaches using covalent coupling on gold substrates.[13] However, the fabrication of these coatings requires expensive equipment, e.g., specialized gaseous atmospheres, and lacks the flexibility necessary for adapting the coating properties to the wide range of adhesion behaviors of the cell types of interest.

Recently, we introduced thermoresponsive PNIPAM microgels as a coating material.[14] Thermoresponsive microgel coatings show a number of advantages over layer formats where the polymer is tethered directly to the substrate.[15, 16] The microgel that we employed for coating has a diameter of several hundreds of nanometers. This size is sufficient to ensure firm immobilization to common surface materials through nonspecific electrostatic and van der Waals interaction. A thin poly(ethylenimine) (PEI) base serves to stabilize the layer. This allows the use of very simple immobilization methods, such as dipping the substrate into a microgel solution, spraying or spin-coating suitable solutions, and hence increases the flexibility for producing a wide range of coating patterns.

As an example, we address one challenging requirement for establishing new cell assays: enabling the localized and reproducible control of cell adhesion without inflicting cell injury. This need is very prominent for popular cell tests like the wound healing assay.[17] Here, collective cell migration is studied under a variety of conditions, e.g., the effect of drug candidates.[18, 19] A cell-free area representing the wound is generated within a cell monolayer to observe its resettlement. Next to standard procedures, like local cell scratching, several protocols for selective cell detachment have been suggested: Kolesnikova et al. applied a laser-induced patterning of a confluent cell layer growing on gold nanoparticles.[20] Pasparakis et al. exposed a cell layer to light through a structured mask to locally ablate a cell adhesion-mediating coating.[21] Besides light-triggered cell detachment, electrochemical triggers were also reported. Surfaces of Raghavan et al., for example, can be switched from a cell-repellent to a cell-attractive state.[22] Although these cell detachments were localized, they are not reversible and partly cell invasive.

Here, we demonstrate the fabrication of patterned thermoresponsive microgel coatings employing automated nanodispensing and microcontact printing (μCP). We utilized both methods to generate spots with a feature size of 200 μm and show the selective control of cell adhesion on coated versus uncoated areas. In contrast to other methods, clear boundaries between cell-populated and bare areas can be produced with high definition and without producing ill-defined cell debris. Finally a cell assay is described that assesses the migration activity of cells, thus demonstrating the considerable potential of patterned thermoresponsive microgel coatings for designing novel tools for the analysis of adherent cells.

Materials and Methods

Microgel Synthesis. *N*-isopropylacrylamide (NIPAM; Sigma-Aldrich 97%) was recrystallized in n-hexane. Acrylic acid (AA; Merck 99%) was freed from the stabilizer 4-methoxyphenol using a column packed with aluminum oxide, basic (Alox B, Macherey & Nagel). The radical initiator ammonium persulfate (APS; Sigma-Aldrich, ≥ 99%) and the cross-linker *N*,*N*′-methylenebis(acrylamide) (BIS; Sigma-Aldrich, 99%) were used without further purification. Water was purified using an Arium pro VF system (Satorius Stedim).

The homopolymer microgel of NIPAM (MZ140) and the copolymer microgel of NIPAM and acrylic acid (MZ160) with a monomer ratio of 99:1 were synthesized through a precipitation reaction. All syntheses were performed in a 250 mL three-neck flask equipped with a reflux condenser, a mechanical stirrer and a nitrogen inlet. For the synthesis of the homopolymer microgel MZ140 and the copolymer microgel MZ160, the thermoresponsive compounds NIPAM (10.568 mmol, 1.196 g) and BIS (0.98 mmol, 0.151 g) (total amount of thermoresponsive compounds 11.548 mmol) were dissolved in 150 mL purified water. The solution was heated up to 70 °C under continuous stirring and purged with nitrogen. In the case of the copolymer synthesis, 1 mol % acrylic acid (0.116 mmol, 0.036 g) was added after 50 min. All polymerization reactions were initiated after 1 h of heating and stirring under nitrogen gas flow by the addition of APS (0.41 mmol, 0.096 g) dissolved in 1 mL water. The polymerization reaction proceeded for 4 h at 70 °C. Afterward, the reaction medium was cooled to room temperature and stirred overnight. Both microgels were cleaned from reaction byproducts and impurities through five successive centrifugation, decantation and redispersion steps using purified water. The sample names and the related chemical composition of the microgels are shown in Table 6.1.

Table 6.1. Monomer Content of the Microgels

Sample name	m_{NIPAM}/g	m_{BIS}/g	c_{BIS}/mol %	m_{AA}/g	c_{AA}/mol %
MZ140	1.196	0.151	8.486	0	0
MZ160	1.196	0.151	8.486	0.0096	1.133

Photon Correlation Spectroscopy (PCS). Particle sizes and volume phase transition temperatures were measured at a fixed scattering angle of $\theta = 60°$ using a diode LASER (Toptica Photonics AG) with a wavelength of $\lambda = 661.4$ nm and a fast correlator (ALV-6010, ALV GmbH) with a thermostat bath (Haake Phoenix II, Thermo Scientific). All measurements were performed on a highly diluted sample with a concentration of $c \leq 0.001$ wt % in cylindrical quartz cuvettes (Hellma GmbH & Co. KG) with

an outer diameter of 10 mm. The samples were thermally equilibrated for 15 min prior to the measurement.

Local Microgel Coating

Inkjet Printing. The microgel spots were deposited using a nanoplotter (NP2.1, GeSiM, Germany) equipped with a piezo dispenser (Nano-Tip A, GeSiM, Germany). For each spot, 300 pL were dispensed with a distance of 500 µm to cover an area of 1 cm^2. Two different kinds of target substrates were used for microgel dispensing: (1) Glass coverslips (20×20 mm^2, Menzel, Germany) were cleaned with 5 % Hellmanex III (Hellmanex Analytics, Germany) for 5 h followed by rinsing with deionized water. Subsequently, the glass substrates were dipped into 1 % poly(ethylenimine) solution (PEI, Sigma-Aldrich, Germany) for 10 s followed by a drying step using an air stream. (2) Cyclo olefin polymer substrates (COP or Zeonex) were purchased from ibidi (ibiTreat COP). The COP substrates were modified by the manufacturer for cell culture purposes. The static contact angles of COP and PEI-modified glass substrates were measured with a contact angle measuring system G10 (Krüss Surface Science, Germany).

Microcontact Printing. The microcontact printing of the microgel was performed using the µCP3 in combination with a poly(dimethylsiloxane) stamp (all GeSiM, Germany). The stamp structure consisted of a pillar array with 200 µm diameter each and a pillar-to-pillar distance of 83 µm. For inking, the stamp was put into a reservoir with 1.4 wt % microgel suspension and incubated for 300 s. Afterward, the stamp was dried with an air stream and then pressed to a PEI-modified glass substrate for 120 s.

AFM Analysis. Atomic force microscopy (AFM) images of dried samples were obtained using a commercial AFM (Dimension 3100 equipped with a NanoScope V controller from Bruker AXS Inc., USA) operating in tapping mode using standard Si_3N_4 cantilevers from Olympus with a typical spring constant of ~42 N m^{-1} and a typical resonance frequency of 300 kHz (OTESPA, Bruker). All images were processed and analyzed using NanoScope software (Version 7.30).

Microfluidic Device. The microchannels were self-produced by assembling a sandwich consisting of a 3 mm thick poly(methyl methacrylate) (PMMA, Modulor, Germany) plate, a structured double-side sticky pressure-sensitive adhesive (PSA) foil (3M, U.S.A.) and for sealing a glass substrate with microgel patterns as bottom. Due to the huge pattering area of 1 cm^2, an accurate positioning of the channel and the patterns was not needed. A micromill (MDX-40A, Roland DG, Germany) was used to drill the holes for the corresponding tubing connection into the PMMA plate of 40 mm × 22 mm. The microfluidic features were created by cutting the 86 µm thick PSA foil with a cutting plotter (CE5000–40 Graphtec CraftRobo Pro, U.S.A.). PMMA, PSA, and microgel-modified glass substrate were assembled and laminated at 60 °C (DH-360, laminator, Linea, Germany). The channel was 500 µm wide, 1 cm long and had three inlets. The tubing (Teflon FEP, ID 0,020 × 10, Techlab, Germany) was connected to the channel, valves (Omnifit, CHM, Germany) and a 1 mL syringe (ILS, Germany).

Cell Culture. L929 mouse fibroblasts (ACC 2, DSMZ, Germany) were cultivated in Dulbecco's modified Eagle medium (DMEM) containing HEPES (25 mM), fetal calf serum (FCS; 10 %), penicillin/streptomycin (1 %), and l-glutamine (2 mM, all Biochrom, Germany), and CHO-K1 (ACC 110, DSMZ Germany) was cultivated in Ham's F12 supplemented with FCS (10 %) and penicillin/streptomycin (1 %, all Biochrom, Germany) at 37 °C and 5% CO_2.

About 3×10^4 cells cm^{-2} were seeded on the thermoresponsive microgel surface. The samples were stored in the incubator for 1 or 2 days. After this time, the substrates were cooled down to room temperature (~22 °C), i.e., below the LCST of the microgels, which made the pattern cell-repellent. To observe the morphology of the cells, the samples were quickly transferred from the incubator to an optical microscope at room temperature, equipped with a 10×/0.25 objective and a Nikon Digital Sight DS-L1 (Nikon, Germany). After 30 min under microscopic observation, the cells were gently rinsed with a 1 mL pipet.

Cell Assays in Microfluidic Setup. The microsystems were incubated with cell medium overnight. Afterward, air bubbles were flushed out of the system with additional medium. L929 mouse fibroblasts (2×106 ml^{-1}) were injected through a side channel and cultivated in situ for 1 day in an incubator. After 30 min under microscopic observation at ~22 °C, different flow velocities were applied through the main channel using a 1 mL glass syringe (ILS, Germany) driven by a syringe pump (SP230IWZ, WPI, UK).

Cell Migration Observation. All cell migration observations were performed with a fully automated setup (Cell-R, Olympus, Germany) equipped with a 10×/0.3 objective and an incubation chamber (Air Conditioning Unit, Evotec, Germany). For assaying the inhibition, locally defined areas were first created by cooling and rinsing a cell monolayer on a polymer substrate as described above. Subsequently, locostatin (dissolved in DMSO, both Sigma-Aldrich, Germany) was added to a final concentration of 42 μM resulting in 1.2 % DMSO. As a control an identical substrate was incubated with 1.2 % pure DMSO to preclude an effect on the cell behavior. For analyzing the cell survival rate in samples treated with and without locostatin, a propidium iodide staining (Sigma-Aldrich, Germany) using 10 μg mL^{-1} was performed after 400 min.

Results and Discussion

For noninvasive processing of adherent cells, we locally deposited two different thermoresponsive microgels that were negatively charged. The colloidal microgels MZ140 and MZ160 have cross sections of approximately 300 nm above the LCST and 150 nm below the LCST. They differ in the content of acrylic acid. MZ160 has more negative charges due to the presence of 1.1 mol % acrylic acid. The presence of acrylic acid resulted in a LCST of ~35 °C for MZ160, which was 2° higher than the LCST of MZ140 at ~33 °C.

First, we established two different protocols to pattern surfaces with microgels using either spotting or microcontact printing. Structured thermoresponsive coatings were created by dispensing 300 pL droplets of MZ140 microgel suspension (0.5 wt %) on PEI-modified glass and on COP substrates in a 353 μm grid using an inkjet printer. The deposited microgel spots were visualized by phase contrast microscopy. On PEI-modified glass, the spots were approximately 200 μm in diameter (Figure 6.1A), while on COP they were 25 % smaller (Figure 6.1E). The difference in size of the microgel spots is related to the wettability of the substrate. Water contact angle measurements on COP substrates resulted in (68 ± 2)° and in (31 ± 1)° on PEI-modified glass substrates. COP is more hydrophobic than PEI-modified surfaces; therefore, the contact area of the aqueous microgel suspension is smaller, leading to smaller microgel spots. The distance of the spots was arbitrary, and the dispensing volume, i.e., spot size, can be varied depending on the application. Alternatively, the microgels were locally deposited by microcontact printing. We employed a PDMS stamp structured with 200 μm diameter pillars arranged in a 283 μm grid. Various patterns can be obtained, depending on the stamp design. The stamp had been wetted with a 1.4 wt % microgel suspension of MZ140 and was transferred to a PEI-modified glass cover slide. The printed microgel pattern corresponded well with the employed stamp design (Figure 6.1I). To investigate the cell adhesion on the thermoresponsive spots, L929 mouse fibroblasts and CHO epithelial cells were cultured for 2 days on either spotted or printed surfaces while the cell morphology was monitored (Figure 6.1B,F,J and Supporting Information (SI) Figure 6.1A). The cells grew homogeneously, establishing a monolayer throughout the whole surface. After the temperature had been decreased below the LCST to 22 °C for 30 min, the microgel spots could be identified due to the local change in the morphology of the fibroblasts (Figure 6.1C,K and SI Figure 6.1B). The fibroblasts rounded up on the microgel spots, induced by changes in physicochemical properties of the microgel as it cooled below its LCST.[14] Cells on the PEI-modified glass remained in the elongated morphology, indicating that the loss of adherence was not simply due to a direct temperature effect on the cells. In contrast to the cell behavior of L929 mouse fibroblasts on the microgel coating, the CHO epithelial cells on the microgel spots remained in the elongated state, despite the temperature reduction to 22 °C (Figure 6.1G). Subsequently, the surfaces were gently rinsed using a 1 mL pipet. As a result, both the fibroblasts and the epithelial cells were flushed only from the microgel spots (Figure 6.1D,H,L and SI Figure 6.1C). Cells on the COP and on the PEI-coated glass remained on the substrate after rinsing and maintained their spread morphology. Remarkably, the CHO cells were also detached locally upon rinsing, although there had been no visible change in the morphology of these cells on the microgel spots. A possible explanation is that cell–cell contacts between the epithelial cells preserved the cell layer in spite of the overall loss of adhesion to the then repellent microgel substrate. This stabilization was, however, insufficient to withstand the shear force generated by rinsing. By contrast, fibroblasts do not develop cell–cell contacts, thus the morphology change was clearly observable. There was no apparent difference between the microgels MZ140 and MZ160. The use of both microgel suspensions resulted in efficient local cell detachment of fibroblasts and epithelial cells. Therefore, we used both

microgels for the following experiments. Both techniques, spotting and printing, resulted in coatings that were fully functional with regard to controlling cell adhesion. Spotting is a very robust method that yields a high reproducibility of surface functionality. It is, however, necessarily limited in the geometric features that can be obtained. By contrast, microcontact-printed microgel patterns did not always result in functional coatings, indicating a lower reproducibility (data not shown).

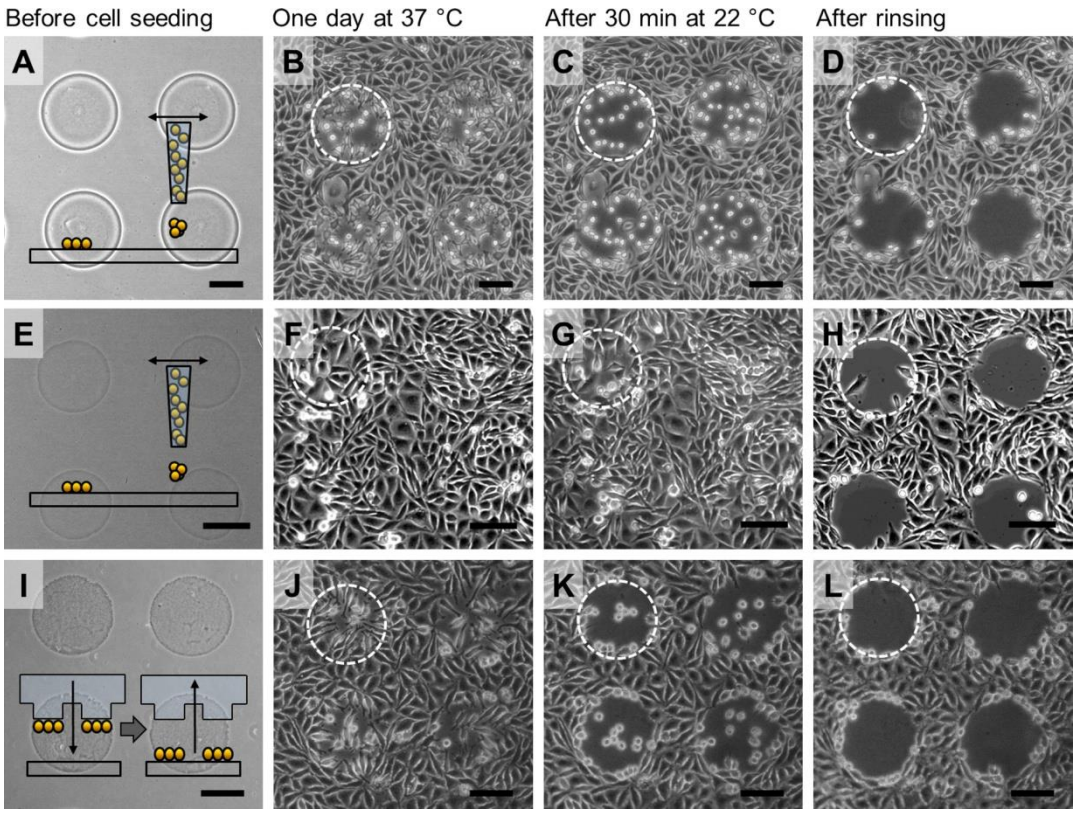

Figure 6.1. Phase contrast images of (A,E) spotted and (I) printed (μ-CP) thermoresponsive microgel suspensions (MZ140) on PEI-coated glass cover slides (A,I) and COP (E). (A–H) 0.5 wt % and (I–L) 1.4 wt % microgel suspensions were employed. The position of one microgel spot is indicated exemplarily by dashed white circles. After 2 days at 37 °C, L929 mouse fibroblasts (B, J) and CHO-K1 epithelial cells (F) adhered homogeneously on the surface. After having been exposed to room temperature (~22 °C) for 30 min, the fibroblasts on the microgel spots changed their morphology from an elongated to a round shape (C,K), while cells on the surrounding PEI-coated regions remained in the elongated shape. The CHO cells maintained their elongated morphology on both the microgel coating and the COP substrate (G). All cells could locally be removed from the microgel patterns by rinsing (D,H,L). The scale bars are 100 μm.

Cell detachment requires a certain minimum microgel density on the surface. In order to quantify this, the surface topography was investigated by AFM. The concentration of the microgel MZ160 suspensions used for spotting were varied (0.2 wt %, 0.1 wt % to 0.05 wt %). As mentioned above, this microgel has the same diameter as MZ140. Afterward, cell tests and AFM measurements were performed to correlate the microgel density with cell detachment functionality (SI Figure 6.1). The results were then related to AFM measurements of a substrate generated by microcontact printing. Representative AFM images obtained from both coating techniques are shown in Figure 6.2. Spotting a 0.2 wt % microgel suspension resulted in a mixture of multi- and monolayers. The microgels were

heterogeneously distributed. Due to the high concentration of the microgel suspension, the particles tended to form aggregates configured in multilayers. These aggregates are visible as regions with high topography in the micrometer range (Figure 6.2, upper row). Less concentrated suspensions mostly produced monolayers. The average microgel distance was found to be $d_{\mu gel}$ = (0.914 ± 0.001) µm for 0.1 wt % and $d_{\mu gel}$ = (0.961 ± 0.001) µm for 0.05 wt %. Although these values merely differ by 5 %, the cell tests remarkably revealed that the cell detachment functionality upon temperature reduction was substantially decreased for a concentration of 0.05 wt % (SI Figure 6.1). In contrast to the multilayer formation at high microgel concentrations achieved by spotting, microcontact printing of MZ140 led to the generation of microgel monolayers. Reducing microgel vacancies again requires a minimum microgel density. Using 1.4 wt % resulted in an average microparticle distance of $d_{\mu gel}$ = (832 ± 1) nm. This surface coverage was found to be sufficient for successful cell detachment after cooling of the substrate to room temperature (Figure 6.1F–H). Repeated microgel hydration and dehydration caused by temperature shifts below and above the LCST did not influence the microgel distribution on the surface as shown by Schmidt et al.[15, 16]

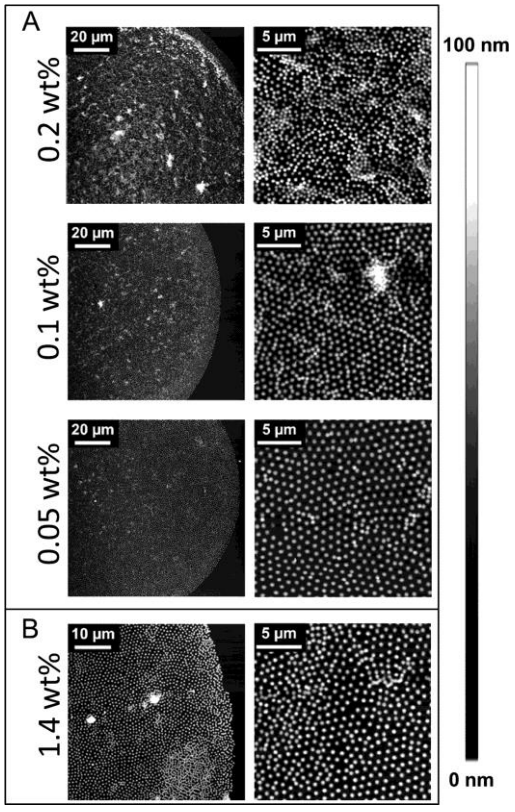

Figure 6.2. (A) AFM images of thermoresponsive microgel spots deposited on PEI-coated glass cover slides using an inkjet spotter. The concentration of the microgel (MZ160) suspension was reduced from 0.2 wt % (top row) to 0.1 wt % (middle row) and 0.05 wt % (bottom row). A concentration of 0.2 wt % resulted in a heterogeneous microgel coating composed of microgel multilayers and monolayers. At lower concentrations (0.1 and 0.05 wt %), homogeneous monolayers were obtained with an average microgel distance of $d_{\mu gel}$ = (0.914 ± 0.001) µm for 0.1 wt % and $d_{\mu gel}$ = (0.961 ± 0.001) µm for 0.05 wt %. (B) AFM images of thermoresponsive microgel (MZ140) spots deposited on PEI-coated glass cover slides using microcontact printing.

The inking suspension had a concentration of 1.4 wt %. For large parts, homogeneous monolayers with an average microgel distance of $d_{\mu gel}$ = (832 ± 1) nm were obtained.

To demonstrate the broad applicability of patterned thermoresponsive coatings, we integrated them into a microfluidic cell assay. First, we seeded L929 mouse fibroblasts for 1 day in a microchannel at 37 °C (Figure 6.3, first row). The cells grew homogeneously as a monolayer throughout the channel. Subsequently, we reduced the temperature to 22 °C for 30 min. Cells on the microgel spots decreased their cell adhesion area and assumed a rounded morphology. Cells on the PEI coating remained in the adhered state and maintained a spread morphology. Application of a laminar shear flow flushed away cells from microgel patterns, resulting in defined cell-free areas. In an additional experiment, the cell medium was supplemented with a viability marker (calcein AM) after local cell detachment (SI Figure 6.2). Almost all cells were stained, indicating an unimpaired viability and thus a particularly gentle local cell patterning.

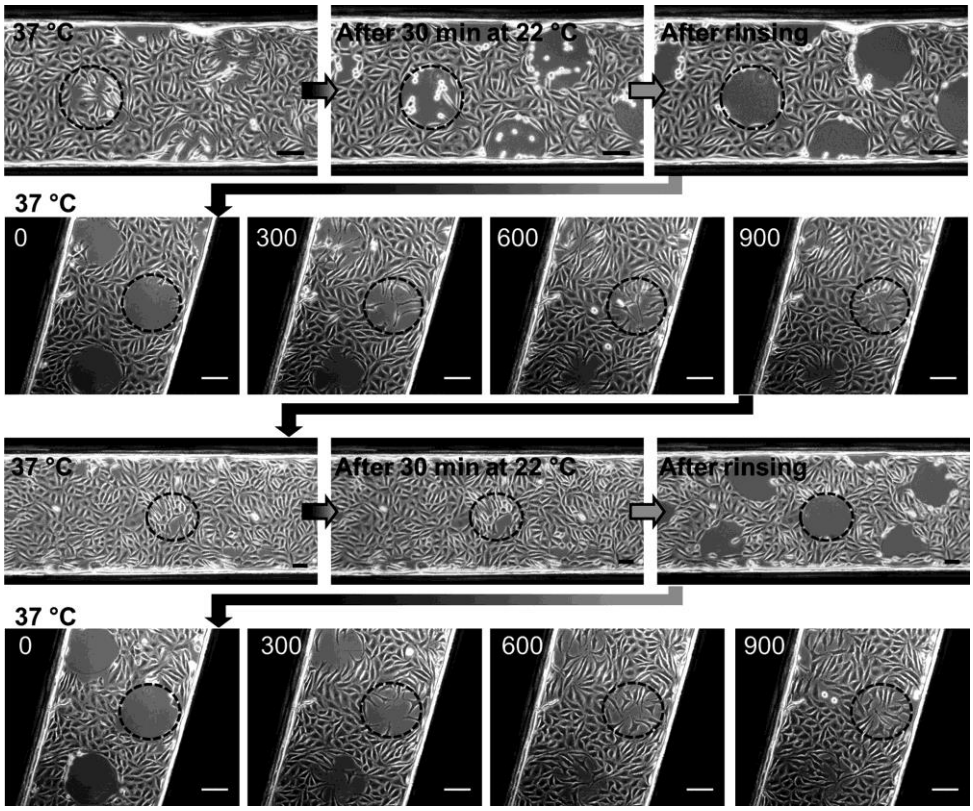

Figure 6.3. Phase contrast images of L929 mouse fibroblasts cultivated in a microchannel on a PEI-coated glass slide with microgel spots (MZ160, c = 0.5 wt %). All images correspond to one continuous experiment. Exemplary, one microgel-coated area per picture is indicated by a dashed black circle. The scale bars are 100 µm. (First row) Mouse fibroblasts exposed to (left) 37 °C, (center) 30 min at 22 °C, and (right) after exposure to a shear flow. Cells were locally removed from the microgel spots. (Second row) Time lapse at 37 °C of the cells migrating onto the previously created cell-free thermoresponsive microgel spots at 0, 300, 600, and 900 min. When the temperature was increased to 37 °C, cells started to migrate to the newly generated open space and form a closed cell monolayer after 900 min. (Third row) Temperature decrease from 37 °C (left) to 22 °C (center), and application of a shear flow again removed the cells from the microgel spots (right). (Fourth row) Resettlement of the initially cell-free spots over a course of 900 min after temperature increase to 37 °C. Brightness of the images has been adjusted in the second and forth lines for better visualization.

The temperature-dependent cell adhesion-mediating properties of thermoresponsive polymers enable a reversible switching from a cell-attractive to a cell-repellent and back to cell-attractive state. For validation, we incubated the microchannel with the previously patterned cell sheets at 37 °C and observed the cell behavior (Figure 6.3, second row, and SI Figure 6.3). Within 15 h, the mouse fibroblasts resettled the cell-free areas and formed a homogeneous monolayer. Using the recovered cell layer, the temperature was again decreased to 22 °C (Figure 6.3, third row). The cells did not round up after 30 min. This may have been due to the increased cell number. Thus, the L929 fibroblasts started to form cell–cell contacts contrary to their native behavior and were able to maintain their spread morphology. Nevertheless, application of a shear flow locally detached the fibroblasts from the microgel spots. Finally, we increased the temperature once more to 37 °C and again observed a cell overgrowth of the spots (Figure 6.3, fourth row).

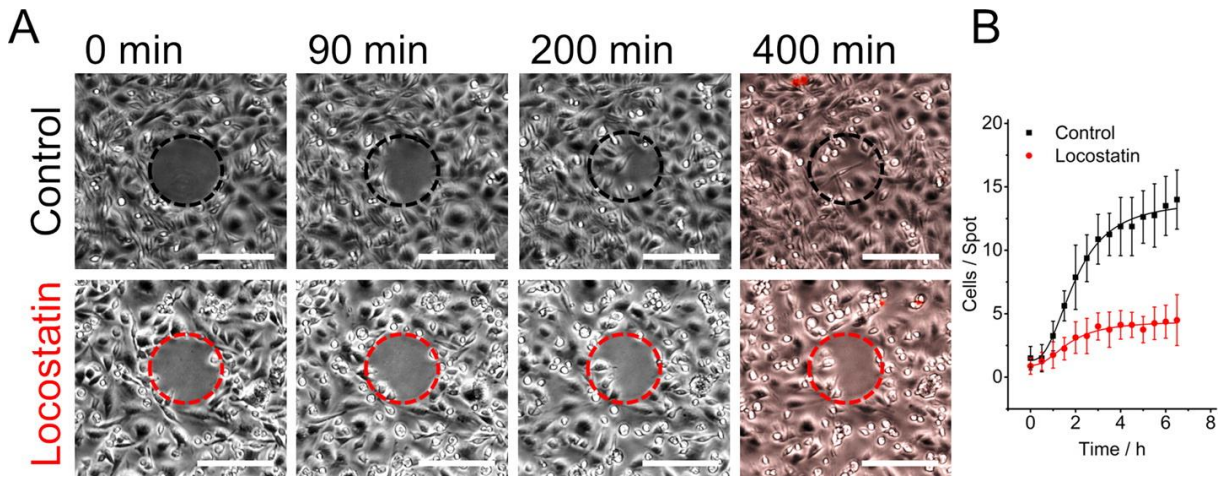

Figure 6.4. (A) Time lapse microscopy of CHO epithelial cells migrating on thermoresponsive microgel spots (MZ140, c = 0.5 wt %, indicated by a dashed circle) without (first row) and with 42 µM locostatin (second row). Before recording the resettlement of the free areas through migration, the cells were locally removed from the spots by rinsing after 30 min at to 22 °C and the temperature was increased to 37 °C again. After 400 min, the dead cells were stained with propidium iodide. A merge of the phase contrast image and the fluorescence image is shown in the last column. There is no observable difference of dead cell (red staining) numbers with regard to no addition and locostatin addition. The scale bars are 200 µm. (B) With locostatin, the number of cells on the functional spots was significantly lower than in the control without locostatin at every time point beyond 1 h (B, evaluation of n = 8 spots).

To prove the claim just outlined, a wound healing assay was performed using a cell migration-inhibiting compound, viz. locostatin. This small, organic and cell permeable molecule acts on the Raf kinase inhibitor protein (RKIP) and, thus, inhibits the cell migration of epithelial cells.[23] We cultured CHO-K1 epithelial cells on substrates with locally structured thermoresponsive polymers, removed cells from the spots by temperature reduction below the LCST and rinsing as detailed above. Subsequently, we observed the resettlement of the spots at 37 °C in samples with and without locostatin (Figure 6.4). A nearly complete coverage of the cell monolayer was achieved after 400 min on the control surface, whereas the samples treated with locostatin showed still plenty of free space on the spots at this time. The extent of cell recovery was analyzed by quantification of cells on the spots as a function of time

(Figure 6.4 B). The decelerating effect of locostatin could be measured after 90 min at the earliest. Locostatin also induced a change in the cell morphology in comparison to the control: The CHO cells started to round up during the incubation. To quantify toxic effects of locostatin, a propidium iodid staining was performed after 400 min, to visualize the dead cells. In both samples, the survival rates were similar, i.e., about 95 %, suggesting that locostatin had no toxic effect under the given experimental conditions.

In summary, we show that thermoresponsive microgel coatings are highly suitable for wound healing assays. The surface-induced cell detachment is a very mild procedure. Cells that were either detached or remained on the surface showed no signs of stress induced by the thermoresponsive microgel, as verified by calcein live staining (SI Figure 6.2). Furthermore, our patterning techniques allow for a well-defined geometry with sharp microgel coating edges as visualized in Figure 6.2. This enables a precise local cell detachment and, thus, strongly improves assay-to-assay comparability. These benefits set our method apart from other wound-forming techniques using destructive approaches, e.g., electric current or laser ablation of cells. These procedures inevitably also damage cells near to the detaching area, thus influencing the test result. Cell scratching similarly harms cells and results in undefined removal. In particular, our combination of thermoresponsive microgels with microfluidics enables an easy exchange of medium and test compounds, evidently also in an alternating manner to allow for time-dependent dosing.

Conclusion

We established an easy-to-process, robust, and flexible locally structured thermoresponsive polymer coating for defined spatially resolved cell detachment that can be induced by a temperature trigger. The coating principle is based on electrostatic interactions of a negatively charged microgel with a positively charged substrate like PEI-coated glass or synthetic materials like COP. For locally patterned deposition, spotting of microgel suspensions of picoliter volumes or microcontact printing were successfully applied. Both coating strategies resulted in a spatially defined cell detachment upon temperature shifting. We identified a lower limit of surface coverage by systematically varying the average microgel distance and correlating it with cell detachment efficiency. The establishment of a wound healing assay and its integration into microfluidics indicates the versatility and practicality of thermoresponsive microgels.

As a future perspective, we plan to also establish cocultures of different cell lines based on locally patterned thermoresponsive coatings. Due to the flexibility in designing different geometries and dimensions, we believe that microgel-based thermoresponsive coatings may become a crucial element in novel powerful assays.

Acknowledgment

We thank Beate Morgenstern for her excellent cell culture assistance. This work is part of the project "ThermoCell" (13N11980) which was financed by the BMBF.

References

1. Wade, R. J.; Bassin, E. J.; Gramlich, W. M.; Burdick, J. A. *Adv. Mater.* **2015**, *27* (8) 1356– 1362
2. Saha, K.; Mei, Y.; Reisterer, C. M.; Pyzocha, N. K.; Yang, J.; Muffat, J.; Davies, M. C.; Alexander, M. R.; Langer, R.; Anderson, D. G.; Jaenisch, R. *Proc. Natl. Acad. Sci. U. S. A.* **2011**, *108* (46) 18714– 18719
3. Hodges, G. M.; Livingston, D. C.; Franks, L. M. *J. Cell Sci.* **1973**, *12* (3) 887– 902
4. Mendes, P. M. *Chem. Soc. Rev.* **2008**, *37* (11) 2512– 2529
5. da Silva, R. M. P.; Mano, J. F.; Reis, R. L. *Trends Biotechnol.* **2007**, *25* (12) 577– 583
6. Lutz, J.-F.; Weichenhan, K.; Akdemir, Ö.; Hoth, A. *Macromolecules* **2007**, *40*, 2503– 2508
7. Okano, T.; Yamada, N.; Sakai, H.; Sakurai, Y. J. *Biomed. Mater. Res.* **1993**, *27*, 1243– 1251
8. Okano, T.; Yamada, N.; Okuhara, M.; Sakai, H.; Sakurai, Y. *Biomaterials* **1995**, *16* (4) 297– 303
9. Wischerhoff, E.; Uhlig, K.; Lankenau, A.; Börner, H. G.; Laschewsky, A.; Duschl, C.; Lutz, J.-F. *Angew. Chem., Int. Ed.* **2008**, *47* (30) 5666– 5668
10. Uhlig, K.; Wischerhoff, E.; Lutz, J.-F.; Laschewsky, A.; Jäger, M. S.; Lankenau, A.; Duschl, C. *Soft Matter* **2010**, *6*, 4262– 4267
11. Mizutani, A.; Kikuchi, A.; Yamato, M.; Kanazawa, H.; Okano, T. *Biomaterials* **2008**, *29* (13) 2073– 2081
12. Idota, N.; Tsukahara, T.; Sato, K.; Okano, T.; Kitamori, T. *Biomaterials* **2009**, *30* (11) 2095– 2101
13. Uhlig, K.; Boerner, H. G.; Wischerhoff, E.; Lutz, J.-F.; Jaeger, M. S.; Laschewsky, A.; Duschl, C. *Polymers* **2014**, *6* (4) 1164– 1177
14. Schmidt, S.; Zeiser, M.; Hellweg, T.; Duschl, C.; Fery, A.; Möhwald, H. *Adv. Funct. Mater.* **2010**, *20* (19) 3235– 3243
15. Schmidt, S.; Motschmann, H.; Hellweg, T.; von Klitzing, R. *Polymer* **2008**, *49* (3) 749– 756
16. Schmidt, S.; Hellweg, T.; von Klitzing, R. *Langmuir* **2008**, *24* (21) 12595– 12602
17. Yao, X.; Peng, R.; Ding, J. *Adv. Mater.* **2013**, *25* (37) 5257– 5286
18. Friedl, P.; Gilmour, D. *Nat. Rev. Mol. Cell Biol.* **2009**, *10* (7) 445– 457
19. Rørth, P. *Annu. Rev. Cell Dev. Biol.* **2009**, *25* (1) 407– 429
20. Kolesnikova, T. A.; Kohler, D.; Skirtach, A. G.; Möhwald, H. *ACS Nano* **2012**, *6* (11) 9585– 9595
21. Pasparakis, G.; Manouras, T.; Selimis, A.; Vamvakaki, M.; Argitis, P. *Angew. Chem.* **2011**, *123* (18) 4228– 4231
22. Raghavan, S.; Desai, R. A.; Kwon, Y.; Mrksich, M.; Chen, C. S. *Langmuir* **2010**, *26* (22) 17733– 17738
23. Bement, W. M. *Chem. Biol.* **2005**, *12* (9) 953– 954

Supporting Information

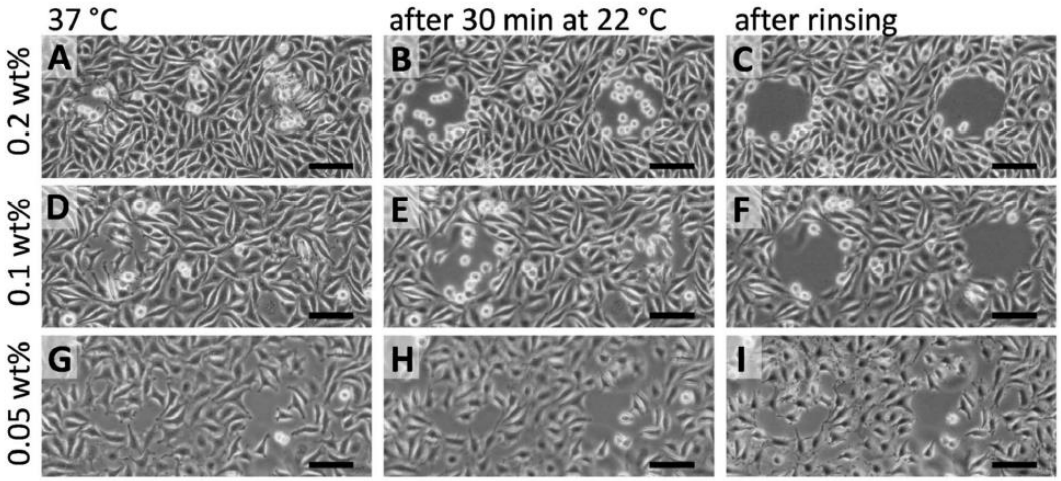

SI Fig. 6.1: Phase contrast images of L929 mouse fibroblasts cultivated on PEI-coated glass cover slides with thermoresponsive microgels spots (MZ160). The concentration of the microgel suspension was varied during spotting (ink-jet); from 0.2 wt % (A-C) to 0.1 wt % (D-F) and 0.05 wt % (G-I). After one day of cell culture at 37 °C, the cells adhered and spread on the PEI-coated area and on the microgel (A, D and G). When having been exposed to room temperature (~22 °C) for 30 min, the cells changed their morphology from an elongated to a round shape on the microgel deposited with the highest concentration of 0.2 wt % (B). On spots generated from a microgel suspension of 0.1 wt %, the cells reduced their adhesion area (E). Cells located on spotted microgel with the lowest concentration of 0.05 wt % remained spread (H). The cells could locally be removed from the microgel by rinsing (C, F), except for those on microgel spots formed from 0.05 wt % (I). These cells remained on the microgel surfaces, similar to those growing on the PEI coating. The scale bars are 100 µm.

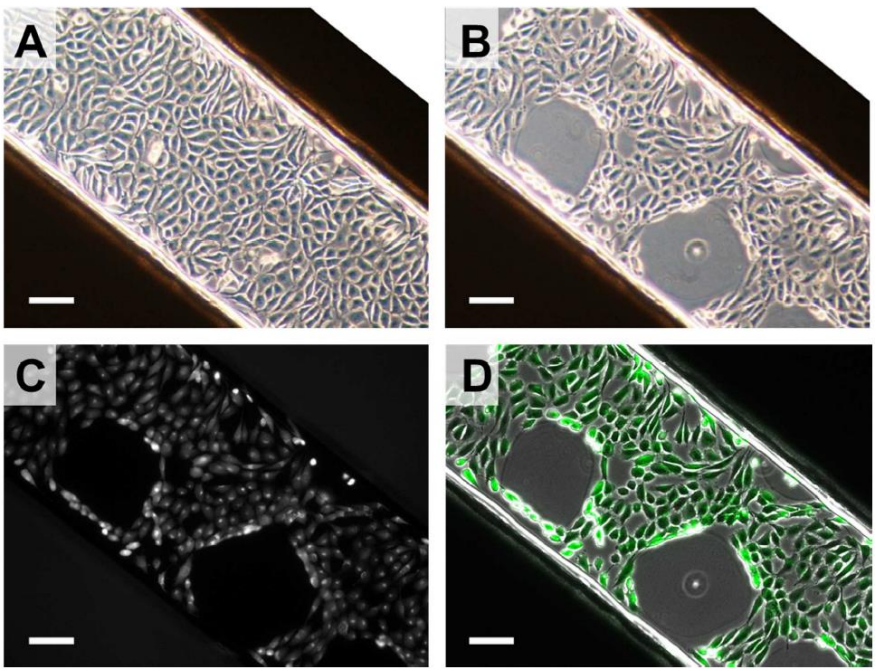

SI Fig. 6.2: Microscopy images of L929 mouse fibroblasts cultivated on PEI-coated glass cover slides with thermoresponsive microgels spots (MZ140, 0.5 wt %, prepared by spotting) in a microchannel. (A) After two days of cell culture at 37 °C, the

cells adhered and spread on the PEI-coated area and on the microgel. (B) When having been exposed to room temperature (~22 °C) for 30 min and flushing, the cells could locally be removed from the microgel. Afterwards, a life staining with calcein was performed to investigate the cell viability. All cells are stained as shown in the fluorescence image (C) and in the overlay (D), indicating a particularly gentle generation of a wound in a cell monolayer. The scale bars are 100 µm.

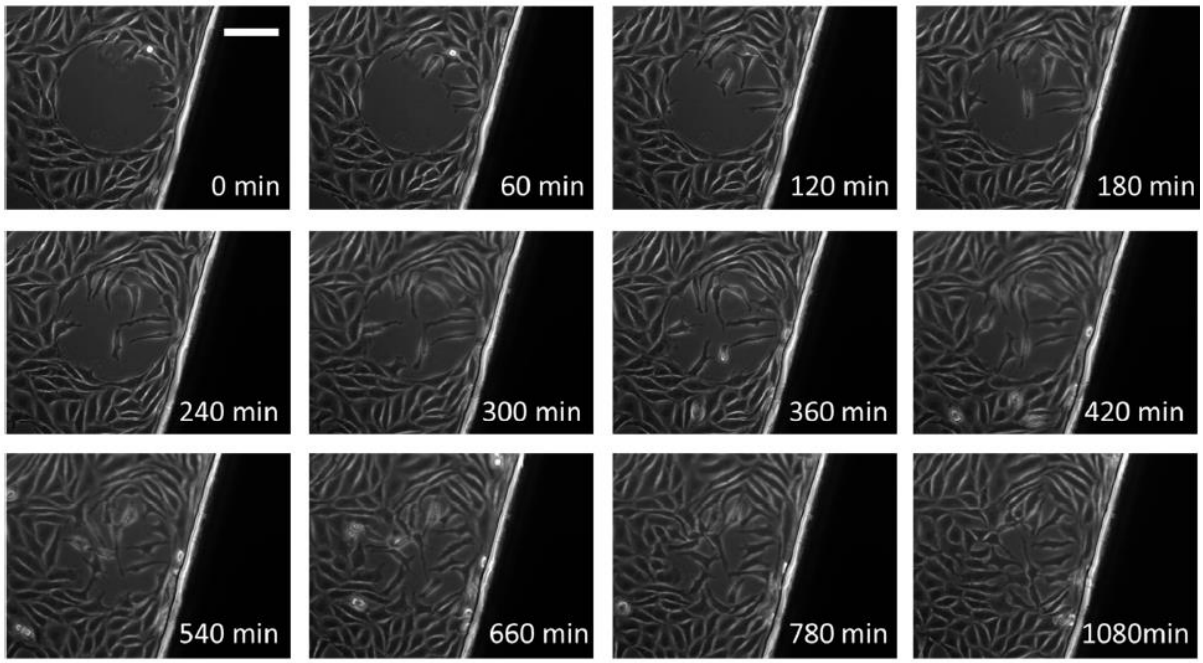

SI Fig. 6.3. More detailed time series of Figure 6.3, second row. Time lapse at 37 °C of the cells migrating onto the previously created cell-free thermoresponsive microgel spots at different time points within 18 h. When the temperature was increased to 37 °C, cells started to migrate to the newly generated open space and form a closed cell monolayer. The scale bar is 100 µm.

7 Impact of Compartmentalization on the Salt-Induced Swelling in Block Copolymer Micelle Multilayers

Inna Dewald, Julia Gensel, Johann Erath, Alexandra Leluk, Eva Betthausen, Oleg V. Borisov, Axel H.E. Müller, Felix H. Schacher, Andreas Fery.

Unpublished Work

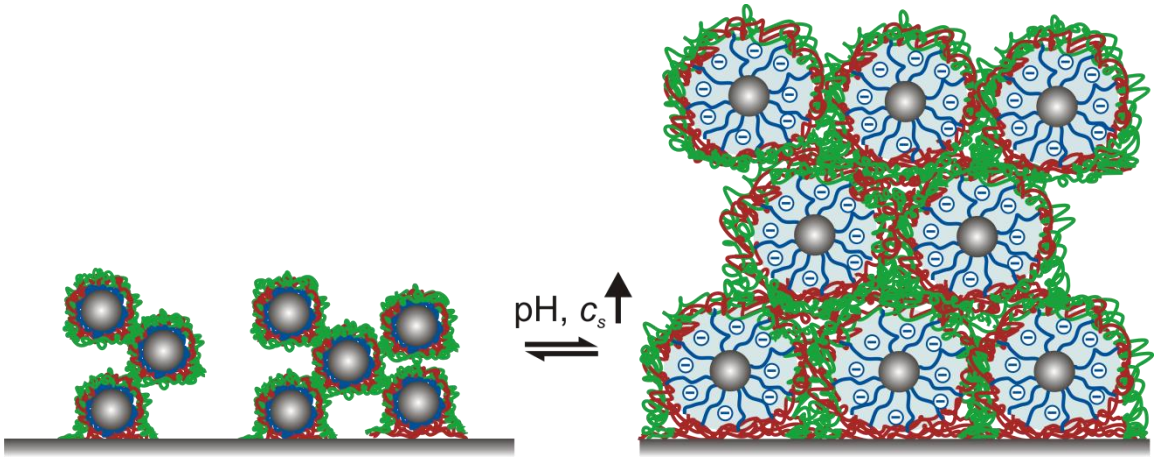

Introduction

After the introduction by Iler[1] and Decher,[2-3] the layer-by-layer (LbL) technique gained a considerable popularity, especially for the formation of polyelectrolyte multilayers (PEMs). Due to its simplicity and versatility the process is adaptable with regard to the substrate and the incorporated material. Currently, much research in the field of functional coatings is driven by requirements for specific applications, such as reversible response to external signals and the integration of discrete compartments with the ability to incorporate and release cargo molecules on demand. In view of this trend, the incorporation of supramolecular aggregates from block copolymers, such as micelles or vesicles, into multilayer films provides several advantages in terms of stability and functionality.[4-5]

Since the first reports by Kataoka,[6-7] a broad range of different multilayer systems based on diblock copolymer micelles were described in the literature. Usual combinations are micelle/micelle[8-17] and micelle/polyelectrolyte[18-30] multilayer systems. To meet the requirements of a controlled drug release from micellar compartments within the film, block copolymer micelles with either pH-responsive[12, 14-15, 24] or temperature-responsive[27-31] cores were used as building blocks. The key feature of these constructs is the separation of functionality and cohesion. The first report of a repeatable load-and-release experiment from multilayers containing micelles with a temperature-responsive core was published by Sukhishvili and coworkers.[27] They assembled poly(*N*-vinylpyrrolidone)-*block*-poly(*N*-isopropylacrylamide), $PNIPAM_{(core)}$-*b*-$PVPON_{(corona)}$ with poly(methacrylic acid), PMAA, in an alternating fashion. The authors demonstrated experimentally a 25-fold higher loading capacity for a hydrophobic dye molecule within the micelle containing films, as compared to the corresponding PVPON/PMAA films. Even higher loading capacities were reached by replacing PMAA with tannic acid.[31] Thereby, the stimulus-responsive core-forming block introduces stimuli-responsive reservoirs, whereas the corona block ensures the cohesion within the resulting films via electrostatic interactions or hydrogen bonding.

In contrast to block copolymer micelles, the incorporation of triblock copolymer micelles into multilayer films is limited to a few publications.[32-34] In the case of an ABA block structure, with the stimulus-responsive B-block located in the micellar core, the connectivity within the core on both sides provides the multilayer film with a higher stability and a controlled swelling.[33] Using micelles from an ABC triblock terpolymer instead, may introduce an additional compartment into the film. In our previous study we used core-shell-corona micelles from polybutadiene-*block*-poly(methacrylic acid)-*block*-quaternized poly(2(dimethylamino)ethyl methacrylate) ($PB_{(core)}$-*b*-$PMAA_{(shell)}$-*b*-$PDMAEMAq_{(corona)}$)[35] for the assembly into micelle/poly(sodium 4-styrene sulfonate) (PSS) multilayers.[34] Maintaining their structure in the resulting micelle/PSS films, the PB-*b*-PMAA-*b*-PDMAEMAq micelles introduced three compartments to the film – the hydrophobic PB core, the stimulus-responsive PMAA shell, and the interpolyelectrolyte complex (IPEC) between PSS and PDMAEMAq corona. Thus, every compartment assumes a function – the cohesion inside the PB core maintains the integrity of micelles inside the film,

the pH-sensitive PMAA shell introduces functionality by means of brush-like swelling transitions, and the ionically crosslinked PDMAEMAq/PSS IPEC secures the stability of the multilayers in spite of strong conformational changes of the shell.

In the present work, we investigate the multilayer assembly of multicompartment micelles from the ABC triblock terpolymer BMAADq (PB-*b*-PMAA-*b*-PDMAEMAq) with PSS, and demonstrate the response of the resulting films to changes in the environmental ionic strength at a given pH. Thereby, the importance of the environmental conditions during assembly is highlighted and two strategies for keeping the micellar aggregates intact are presented. The micelle multilayers respond to changes in the ionic strength by exhibiting characteristic features of both polyelectrolyte brushes and polyelectrolyte multilayers. This behavior is a result of film partitioning into three compartments, whereby the *non-monotonous* swelling is associated with the brush-like PMAA shell and the salt-induced *annealing* of micelle/PSS multilayers is attributed to the IPEC between Dq corona and PSS. Furthermore, the comparison of micelle/PSS films with Dq/PSS films in terms of their swelling behavior reveals that the stimulus response of both compartments can be triggered separately, depending on pH and salt concentration.

Results and Discussion

We used an amphiphilic ABC triblock terpolymer, BMAADq (PB_{800}-*b*-$PMAA_{200}$-*b*-$PDMAEMAq_{285}$, subscript denoting degree of polymerization), with a molecular weight of ~110 kg/mol (PDI = 1.10)[35] and poly(sodium 4-styrene sulfonate) (PSS, 70 kg/mol) for multilayer construction. The chemical structures of both polymers are given in Figure 7.1a,b.

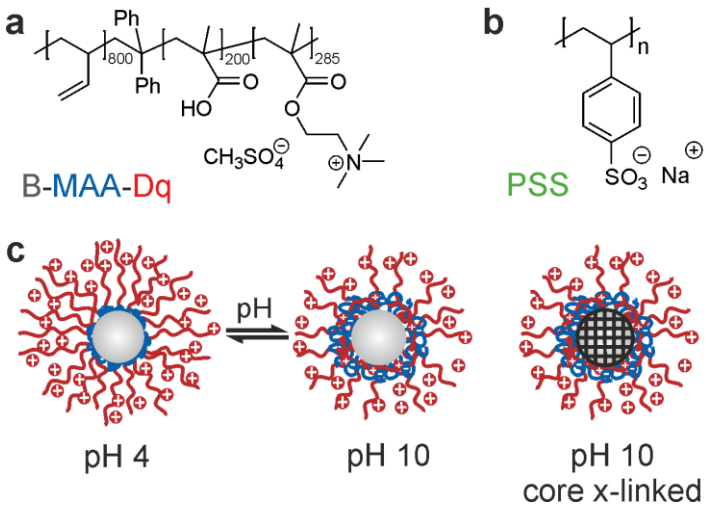

Figure 7.1. Chemical structures of the BMAADq triblock terpolymer (a) and PSS (b), and schematic illustrations of the micellar structures in aqueous solutions at pH 4 and 10 (c).

The triblock terpolymer consists of a hydrophobic polybutadiene (B) block, a pH-sensitive poly(methacrylic acid) (MAA) middle block, and a third block of quaternized poly(2-(dimethylamino)ethyl methacrylate) (Dq). In aqueous solution, the triblock self-assembles into core-

shell-corona micelles due to the hydrophobicity of the PB block. However, the morphology-determining factor is the pH-response of the weak (annealed) PMAA shell ($pK_{a,app}$ ~5.5)[36] as depicted in Figure 7.1c. At pH 4 the polyacid chains are protonated / uncharged and form a thin shell of phase separated PMAA around the hydrophobic PB core. Thereby, the strong PDMEAMAq corona blocks are fully charged and stretched out into solution. In contrast, at pH 10 the negatively charged PMAA chains interact with the positively charged PDMEAMAq corona, which results in the formation of an *intramicellar* interpolyelectrolyte complex (*im*-IPEC). Due to a higher degree of polymerization of the PDMEAMAq block, compared to PMAA, the excess PDMEAMAq provides the micelles with positive net charge and stability, even at high pH values. These pH-induced structural changes of the shell and the corona are fully reversible in solution between pH 4 and pH 10 and are accompanied by small changes in core size and thereby in aggregation number. Crosslinking of the PB core inhibits these changes and ensures constant aggregation numbers.[37]

Multilayer Buildup. For multilayer construction, the positively charged non-crosslinked BMAADq micelles at pH 4 and 10, and micelles with crosslinked cores at pH 10 were assembled with negatively charged PSS in an alternating manner using the layer-by-layer (LbL) approach.[2-3] Please note that the pH of the PSS solution was adjusted to pH 4 and 10 according to pH of the micellar solution. The characterization of surface-immobilized micelles on a single particle level can be found elsewhere.[38] The film growth was monitored in dry state using spectroscopic ellipsometry and atomic force microscopy (AFM). Figure 7.2 shows the evolution of the film thickness as a function of deposition steps, and the impact of assembly conditions on the surface topography.

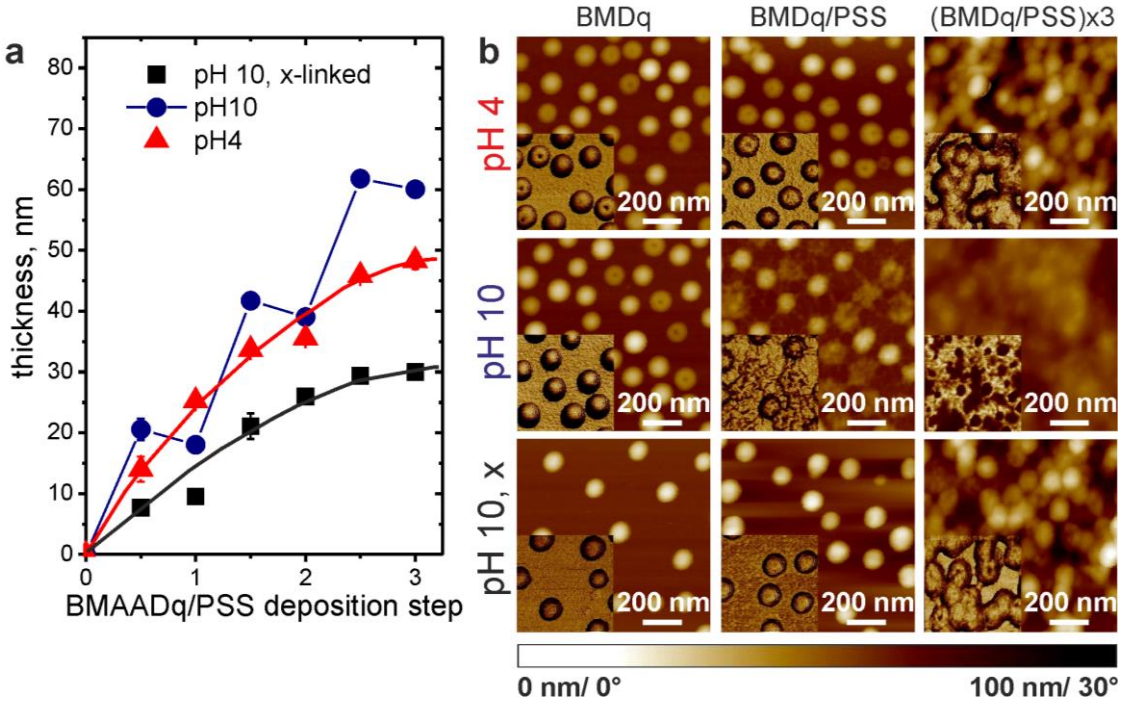

Figure 7.2. Film growth behavior as a function of deposition pH and crosslinking of PB core. Ellipsometric thickness in dry state plotted as a function BMAADq/PSS deposition steps (a). Solid lines are guides to the eye. The AFM height and phase (inset) images show the impact of adsorption conditions on the micellar structure (b).

At pH 4 the film thickness of micelle/PSS multilayers increases steadily with increasing number of deposition steps and the micelles are intact after deposition of PSS on top. In this state, the PMAA shell is uncharged / collapsed and the PDMAEMAq corona chains are free to form a complex with PSS. In contrast, at pH 10 the film thickness increases in a zig-zag manner. Since the increase or decrease is a function of the terminating layer, this behavior can be attributed to the *odd-even effect*.[39] Thereby, the value increases with every deposition of BMAADq micelles and decreases a fraction with the following PSS deposition. The corresponding AFM images show a partial disassembly already after the first exposure to PSS at pH 10, which advances with increasing number of deposition steps, until the initially spherical micellar morphology becomes almost unrecognizable. This phenomenon occurs for two reasons: First, at pH 10 the main part of the PDMAEMAq corona is complexed by the PMAA chains in the *im*-IPEC. The subsequent addition of PSS leads to a competition for PDMAEMAq as binding partner. Thereby, the incoming PSS irreversibly substitutes PMAA from the weakly bound PMAA/Dq complex by the formation of a strong PSS/Dq complex.[40-41] Second, the low glass transition temperature of the PB core ($T_g \sim -16$ °C)[42] and the low interfacial tension between the core and the shell[35, 37] facilitate structural rearrangements inside the otherwise impassive hydrophobic core.[43] These rearrangements, imposed on the core by changes in the shell, can be suppressed by crosslinking the PB core, thereby preserving micellar integrity in the presence of PSS at alkaline pH.[37] However, the corresponding x-BMAADq/PSS films grow slowly and require additional steps in preparation. Thus, further experiments were performed using multilayer films assembled in pH 4, whereby micellar integrity is ensured due to suitable assembly conditions.

Stimulus Response. The presence of polyelectrolytes in the multilayer system renders the films responsive toward external triggers such as pH and ionic strength. The pH-dependent swelling of $(BMAADq/PSS)_{x3}$ films has been investigated in a previous study.[34] Briefly, the IPEC between Dq corona and PSS – both strong polyelectrolytes with pH-independent charge density – ensures the pH-independent stability of the multilayer films *via* ionic crosslinks. Due to assembly at pH 4, the pH-responsive PMAA block is not a component of the multilayer-forming IPEC, but is covalently attached to both the micellar core and the corona in the IPEC. Thus, the internal architecture of BMAADq micelles during the LbL assembly facilitates the formation of a highly swellable, double-end-tethered brush-like shell with a $pK_{a,app}$ at pH ~9.5. The swelling in alkaline pH is attributed to the deprotonation of PMAA and the subsequent stretching of the chains due to repulsive interactions between neighboring charged groups. Cycling experiments confirmed a reversible swelling transition, whereby the Dq/PSS matrix flexibly adjusts to volumetric changes in the shell, thereby maintaining the micellar integrity inside the multilayers.

In contrast to the preceding study, the focus of this work is on the response of $(BMAADq/PSS)_3$ films to changes in ionic strength. Taking into account the findings for the pH-dependent swelling, the salt-dependent swelling of the film was investigated at three different pH conditions. A representative AFM

height image of a 3-bilayer film, before any treatment, is presented in Figure 7.3a. The pH conditions – pH 3, ~6.5 (Milli-Q water), 10.5 – were chosen with regard to the corresponding state of the micelle/PSS films. The changes in the film thickness as a function of the increasing ionic strength were monitored using *in situ* ellipsometry (Figure 7.3b). Considering the influence of the nature and valence of a salt on the swelling,[44] sodium chloride (NaCl) was chosen due to its properties as an inert and monovalent salt to adjust the external salt concentration.

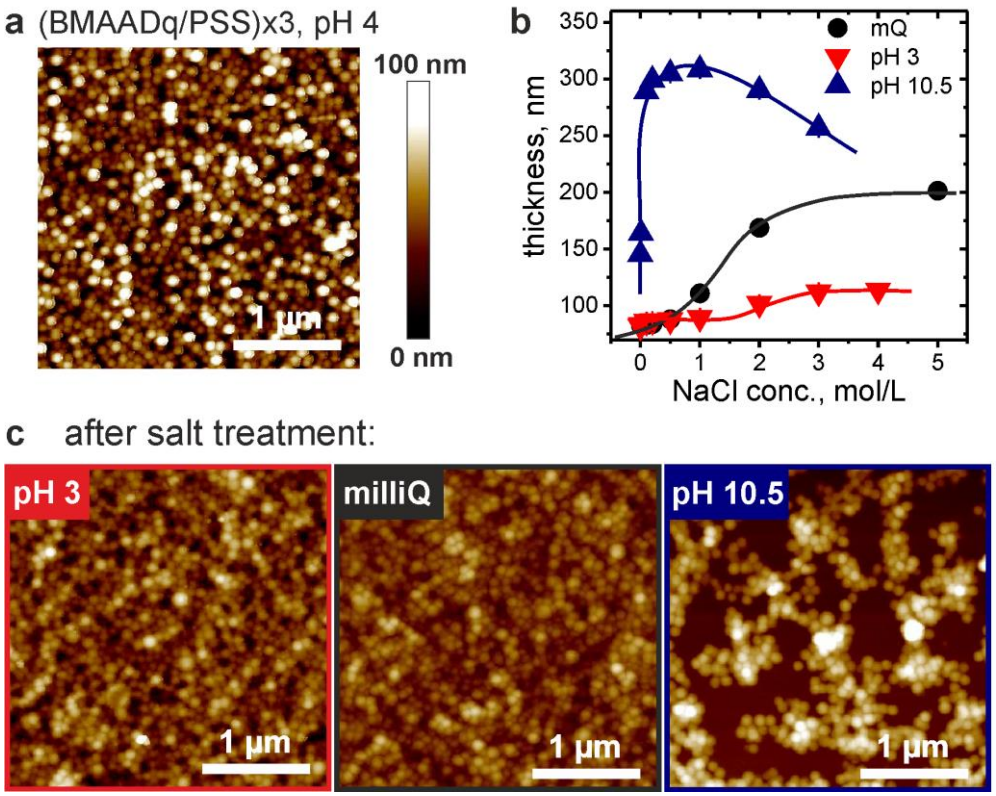

Figure 7.3. A representative AFM height image of a 3-bilayer film, deposited at pH 4 (a). *In situ* ellipsometry measurements show the changes in the effective film thickness of $(BMAADq/PSS)_{x3}$ films exposed to aqueous solutions at pH 3, ~6.5 (mQ), 10.5, and different concentrations of NaCl (b). AFM height images show the corresponding samples after the treatment with pH and salt (c).

Figure 7.3b shows that the thickness of $(BMAADq/PSS)_{x3}$ films increases with increasing concentration of added salt. However, the extent of the swelling depends mainly on the pH conditions. Whereas at pH 3 the changes in film thickness are very subtle, the changes observed in pH~6.5 are more pronounced. In both cases, the films start to swell at salt concentrations around 1 mol/L. Below 1 M NaCl, the film thickness *d* is ~80 nm and increases with increasing salt concentrations until a plateau is reached at ~110 nm at pH 3 and ~200 nm at pH~6.5. In contrast, at pH 10.5 (> $pK_{a,app}$ ~9.5) the LbL film is already swollen with a starting thickness of ~145 nm. The additional salt, even at low concentrations, leads to further increase in film thickness, until a maximum of *d* ~310 nm is reached at ~1 M NaCl. Further increase in salt concentration leads to a decrease in film thickness. This behavior is in agreement with the theoretically predicted trends for brush-like systems.[45] This will be discussed later in the section "Brush-Like Swelling".

Micellar Integrity. The AFM images in Figure 7.3c show that the micellar integrity is maintained in the multilayer films even after a harsh treatment at high pH and high salt concentrations. To assess changes in film thickness and refractive index after the salt-treatment, ellipsometry measurements were performed on dry films. Additionally, the corresponding porosity *P* (volume fraction of the pores) of the films before and after exposure to different pH and salt was calculated using eq 7.1.[46] The refractive indices n_i are indexed with *f* for the dense film without pores (n_f =1.51)[34] and with *x* for porous films.

$$P = 1 - \frac{n_x^2 - 1}{n_f^2 - 1} \cdot \frac{n_f^2 + 2}{n_x^2 + 2} \tag{7.1}$$

After exposure to pH 3 and ~6.5 and salt concentrations up to 5 M NaCl, the dry thickness of both films decreased by ~30-45%, the refractive index increased by ~10-15%, and the porosity decreased by ~30%. These changes indicate the formation of more compact films due to a salt-induced *annealing effect*. In analogy to polyelectrolyte multilayers (PEMs),[47] the micelle/PSS multilayer buildup is a non-equilibrium process, yielding non-equilibrium structures. Normally, in the case of an assembly without additional salt, such films contain only few salt counterions and the internal charges are compensated intrinsically by matched numbers of positive and negative polymer repeat units.[47] Introduction of extrinsic charges leads to a scenario where PE charges are compensated by salt ions, which facilitates local rearrangements. Because of bond restrictions and connectivity, motions of polyelectrolyte segments are coupled. During the rearrangement process adjacent repeat units undergo a quasi-concerted localized reshuffling, which culminates in a net polymer motion. Rapid surface smoothing occurs especially in solutions of high salinity.[48] Thereby, the high salt concentration enhances the mobility of charge-paired polyelectrolyte chains by freeing up segments and "lubricating" the motion of one charged polymer against the other. This effect provides the micelles in the LbL films with a considerable mobility. At pH 10.5, micelle desorption occurred while treating the sample with a 4 M NaCl solution (data not included). Nevertheless, despite extreme conditions the micellar structure remained intact indicating a high robustness and resilience of the incorporated micelles in the LbL films.

Brush-Like Swelling. In view of the findings in our previous work on the pH-pendent swelling of BMAADq/PSS multilayers, the results in Figure 7.3b are well in line with the assumption of PMAA exhibiting a brush-like behavior. First, the extreme shift in the apparent pK_a of ~9.5[34] determined for the PMAA shell of incorporated micelles with respect to a linear PMAA homopolyer with a p$K_{a,app}$ of ~5.5.[49] In general, constraints due to the end-grafting of the polymer chains lead to a specific stimulus response, which differs from the response of polymer chains in dilute solution.[50] As a result counterion condensation occurs to avoid an accumulation of charges in the limited space and to minimize Coulombic repulsion of neighboring charges. Thus, dissociation of the acidic groups within a brush layer is suppressed and the p$K_{a,\,app}$ shifts to higher pH values.[51-52] Second, especially the salt-induced swelling of $(BMAADq/PSS)_{x3}$ at pH 10.5 (Figure 7.3b) points toward the *anomalous salt effect*, which

entails a non-monotonous swelling, typical for weak PE brush systems.[53-60] Thereby, at low ionic strength sodium ions induce dissociation of acidic groups and replace protons, which can leave the brush layer without violating the electroneutrality condition. The increased charge density results in electrostatic repulsion between neighboring COO^--groups and a measurable swelling of the brush in the osmotic brush (OB) regime (Figure 7.4a). In contrast, above a critical ionic strength this effect becomes overcompensated by charge screening and the brush shrinks in the salted brush (SB) regime.[61-62] The maximum thickness of ~310 nm at ~1 M NaCl corresponds to the crossover from the OB regime to the SB regime. The fact, that a maximum film thickness is reached at lower pH values, indicates a shift in apparent pK_a to lower pH with increasing salt concentration. The results are in good agreement with experiments performed on weak brushes grafted from a planar solid substrate.[52, 58] A similar swelling behavior at pH 10 with a transition at 1 M NaCl was reported for surface-grafted PAA brushes of higher grafting densities,[58] and spherical PAA brushes in KCl.[61] In general, the transition from the osmotic to the salted brush regime depends on the grafting density σ of a brush, whereby the transition point shifts to higher ionic strength with increasing σ.[58] In the case of BMAADq micelles, the apparent grafting density of PMAA chains can be estimated from the aggregation number of the polymer $N_{agg} \approx 1800$[34-35] divided by the surface area of the PB core $A = 4\pi R_{core}^2$, with $R_{core} = 32\,nm$ being the radius of the PB core at pH 4, which amounts to $\sigma_{app} \approx 0.14\,nm^{-2}$. Since the micelles are monodisperse, shifts in the apparent pK_a due to changes in the grafting density can be neglected.[63]

Theoretical Considerations. The pH- and salt-responsive swelling behavior of multilayers formed upon LbL co-assembly of BMAADq micelles to strong polyelectrolytes such as the linear polyanion PSS was qualitatively analyzed on the basis of a scaling approach. At low porosity the degree of swelling of the layer coincides with the degree of swelling of an individual micelle encapsulated into the shell of interpolyelectrolyte complex (IPEC) formed by the outer cationic block and linear polyion. The elastic response of the complexed micelle arises due to combination of conformational entropy penalty in the extended pH-sensitive anionic arms and excess interfacial energy of the IPEC shell. $F_{shell}(R)/k_BT \cong \gamma R^2$, where R is the shell radius, k_B is the Boltzmann constant and T is the temperature. The surface tension coefficient is $\gamma/k_BT \sim l_B^{2/3}$ at low salt and $\gamma/k_BT \sim c_{salt}^{-2}$ at high salt concentration, where l_B is the Bjerrum length. Here, we have omitted numerical factors. Therefore, at low salt concentration the size of an individual micelle with the IPEC shell can be expressed as $R \cong \alpha^{1/2} L_{PMAA}(1+16\pi\gamma \cdot L_{PMAA}/3p)^{-1/2}$ where L_{PMAA} is the contour length and α is the pH-dependent degree of ionization of the PMAA block. The account of the finite size of the collapsed PB core provides non-power law corrections to the latter expression. Furthermore, analysis of swelling behavior as a function of salt concentration accounts for the effects of salt on both degree of ionization of the PMAA blocks and the elasticity of the IPEC shell. However, the latter is relatively weak in the

range of low salt concentration where the former is expected to demonstrate abnormal swelling upon an increase in salt concentration, similar to that predicted earlier for star-shaped weak polyelectrolytes.[64]

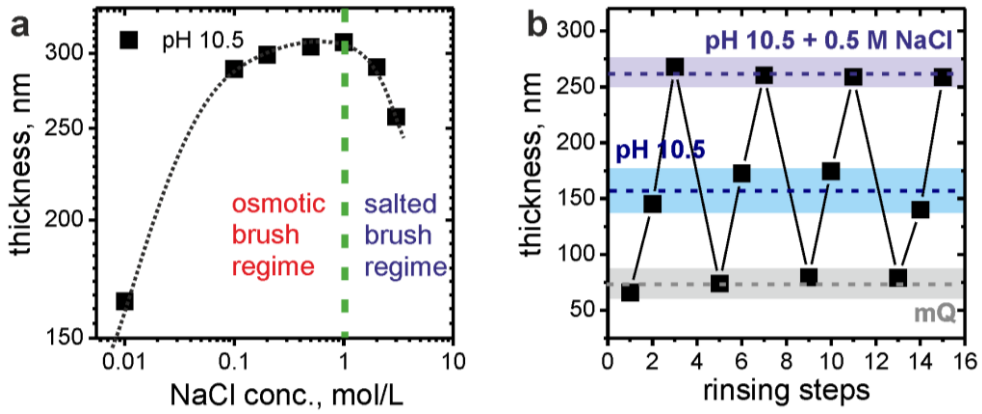

Figure 7.4. Log-log plot of changes in the ellipsometric film thickness of a $(BMAADq/PSS)_{x3}$ film at pH 10.5 as a function of salt concentration (a) and the corresponding cycling experiment showing the reversibility and reproducibility of the swelling (b).

Reversible Stimulus Response. Furthermore, to examine the reversibility of the salt-induced swelling of the brush-like component (PMAA) in the multilayer in alkaline conditions, a 3-point cycling experiment was performed. Thereby, starting with Milli-Q water, first the pH was increased to pH 10.5 and subsequently the salt concentration increased to 0.5 M NaCl. At the end of a cycle the ellipsometry cell was rinsed several times with Milli-Q water. The PMAA domains responded to changes in pH and ionic strength by changing between ionized and non-ionized states which result in swelling and shrinking of the micelle/PSS multilayers. The results in Figure 7.4b show an increase in film thickness with increasing pH and ionic strength, whereby the switching is reversible within the osmotic brush regime for at least 3 cycles.

Mechanical Properties. The BMAADq/PSS multilayers swell upon pH-increase as well as upon an increase of the external salt concentration and allow thereby an enormous uptake of water up to > 90%, especially for high pH values and for elevated salt concentrations. The water uptake of the film inevitably leads to changes in its mechanical properties. To assess these changes quantitatively, the AFM colloidal probe technique, introduced by Butt[65] and Ducker[66], was used. The data was accumulated by recording force-distance curves on a $(BMAADq/PSS)_3$ multilayer film. The subsequent transformation by subtracting the effect of the cantilever deflection resulted in force-indentation curves, which contain only the contribution of the film. Five representative force-indentation curves – one for each salt concentration – are given in Figure 7.5a. For the fits data were used with upper force threshold set to 60 nN. Moreover, measurements on the same spot of the sample confirmed that no plastic deformation of the film occurs.

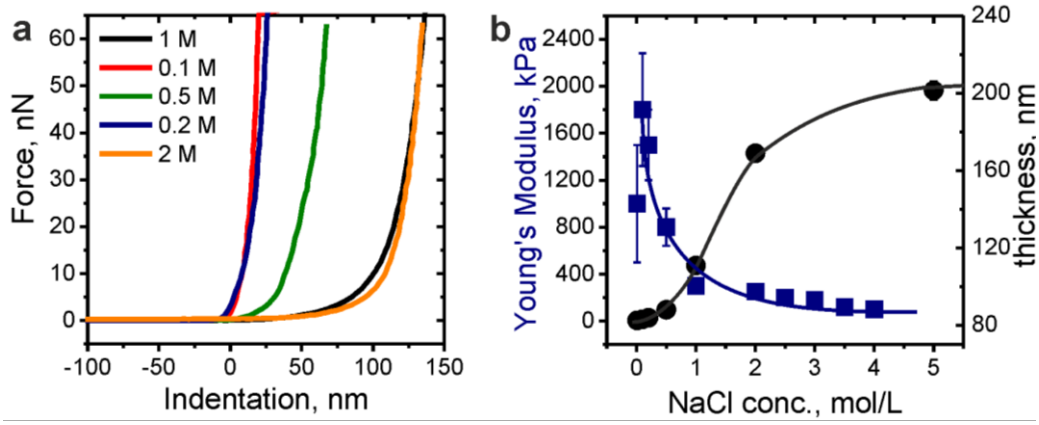

Figure 7.5. Representative force-indentation curves measured on a $(BMAADq/PSS)_{x3}$ film at different ionic strengths (a) and the resulting Young's modulus and the ellipsometric film thickness as a function of NaCl concentration (b).

Since the measurements were performed in liquid, in contact mode, the adhesion is negligible. Therefore, the mechanical properties of the system were evaluated using the linear elasticity theory. The indentation of a sphere into a linear elastic plane can be described by the Hertzian power law,[67] which was used to calculate the elastic modulus of the film (eq 7.2).

$$F = \frac{4}{3} \cdot \frac{E}{1-\nu^2} \cdot R^{1/2} \cdot \delta^{3/2} \tag{7.2}$$

Thereby, F is the force applied by a spherical probe with radius R, ν is the Poisson ratio, E the elastic modulus, and δ the indentation of the film. For the analysis only data below 20 nN were used to avoid the effects of substrate. Furthermore, since the Hertz model does not account for the inhomogeneity of the systems, the obtained values should be viewed only as rough estimates. The obtained data for the elastic modulus and the corresponding film thickness are summarized in Figure 7.5b. Thereby, the values are averaged over at least 36 data points. The resulting Young's modulus exhibits inverse proportionality to the film thickness in its swollen state as a function of the external salt concentration c_s. The modulus decreases with increasing ionic strength by 1 order of magnitude. At $c_s \leq 1$ M the modulus of the film is rapidly decreasing with increasing salt concentration from ~1800 kPa down to ~300 kPa, while the film starts to swell slowly. In contrast, at concentrations beyond 1 M the coating swells even further until it is highly swollen and soft, meanwhile the modulus decreases to low kPa values. In that region the modulus is decreasing more slowly from ~300 kPa down to ~100 kPa. A similar salt softening effect was observed for polyelectrolyte multilayer capsules.[68]

Decoupling the Response of Compartments. Considering the ability of both the PE brushes and PEMs to respond to changes in the ionic strength by swelling suggests that in the first approximation both the PMAA shell and the Dq/PSS IPEC may contribute to the overall swelling of BMAADq/PSS films as a function of ionic strength (Figure 7.6a). Judging from the strong swelling of the PMAA shell as a function of pH,[34] and a rather weak response of comparable PEM films from chemically similar polyelectrolytes,[48] the contribution of the brush is expected to be more pronounced. To verify this

assumption, the swelling behavior of $(Dq/PSS)_{x5}$ multilayer films was investigated as a function of ionic strength. Since both PEs are permanently charged, independent of the environmental pH, the measurement was performed for different salt concentration in Milli-Q water. To compare the data for $(Dq/PSS)_{x5}$ with the results of the $(BMAADq/PSS)_{x3}$ the obtained ellipsometric thickness was normalized by the value in Milli-Q water, without additional salt. The corresponding plots of the swelling degree as a function of the salt concentration are summarized in Figure 7.6b.

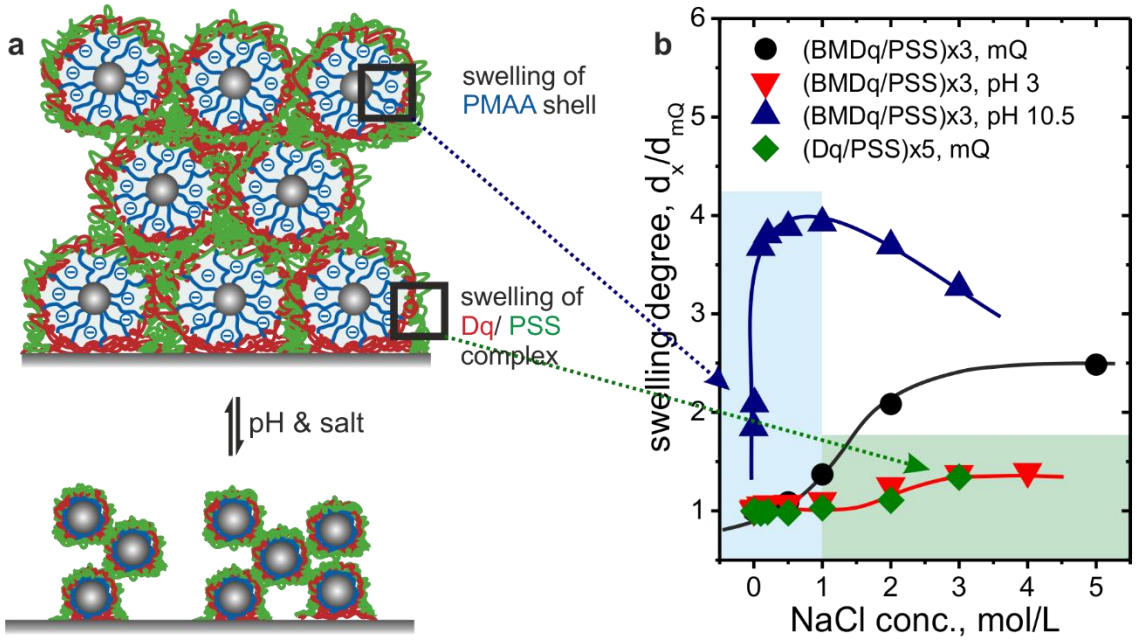

Figure 7.6. Schematic illustration of the BMAADq/PSS multilayer film in a collapsed (uncharged MAA block) and a swollen (charged MAA shell) state (a). Swelling degree of BMAADq/PSS and Dq/PSS films as a function of pH and NaCl concentration (b). The solid lines are guides to the eye.

Remarkably, the swelling profile of the $(Dq/PSS)_{x5}$ film correlates very well with the one of $(BMAADq/PSS)_{x3}$ at pH 3. This observation suggests, that at pH values well below the $pK_{a,app}$ ~9.5 of the incorporated micelles, the PMAA shell remains protonated and collapsed even at elevated salt concentrations. Thus, the slight increase in the swelling degree at ≥1 M is attributed to the contribution of the Dq/PSS IPEC. In contrast, at pH values above the $pK_{a,app}$ the already swollen films swell even further with increasing salt concentration until a maximum at 1 M is reached. Since no contribution of the complex is expected at low salt concentrations, the swelling can be attributed to the brush-like behavior of the PMAA shell. For moderate pH conditions in the presence of additional salt ions, the contribution of both the shell and the PE complex is expected, as shown for the swelling degree in Milli-Q water (pH~6.5). Thus, the stimulus response of both components can be triggered independently by choosing appropriate pH conditions and salt concentrations.

Conclusions

In conclusion, triblock terpolymer BMAADq micelles with a hydrophobic PB core, a pH-sensitive PMAA shell and a permanently charged Dq corona present promising building blocks for the fabrication of stable and stimulus-responsive coatings. The cationic micelles were incorporated into multilayer films using the strong polyanion PSS as the counterpart in the LbL assembly. The multilayer buildup was investigated for different pH conditions. We found that the performance and stability of BMAADq/PSS multilayer films strongly depends on the pH-dependent structural features of the micelles during assembly. Assembly at pH 4, or alternatively crosslinking the PB core prior to incorporation, provided the films with a pH-independent stability and ensured micellar integrity in the LbL films. The resulting BMAADq/PSS multilayer were investigated with respect to their pH- and salt-dependent swelling behavior, mechanical properties and film porosity. Depending on the environmental pH and ionic strength, the films exhibit a *brush-like* and / or *PEM-like* behavior. Especially at high pH, the micelle/PSS films exhibit a non-monotonous swelling behavior as a function of ionic strength, similar to the *anomalous salt effect* of weak PE brushes. After the exposure to solutions with high ionic strength, the films showed a significantly reduced porosity, which corresponds to the *annealing effect* known for PEMs. The combination of both brush-specific and PEM-specific properties is a consequence of film compartmentalization due to the core-shell-corona structure of the BMAADq micelles: (1) The hydrophobic PB core ensures micellar integrity. (2) The brush-like PMAA shell provides a stimuli responsive compartment with high swelling degrees at high pH and low ionic strength <1 M. (3) In contrast, the IPEC between Dq corona and PSS provides mainly the film stability via ionic crosslinks, but contributes also to a small extent to the swelling at high ionic strengths above 1 M. Thus, by the choice of the stimulus and the range of operation, the swelling of both PE compartments, the PMAA shell and the Dq/PSS IPEC, can be triggered independently. The decoupling of the swelling behavior in two compartments opens new perspectives for the surface-mediated drug co-delivery.

Materials and Methods

Materials. The triblock terpolymer consinsting of a polybutadiene (B), a poly(methacrylic acid) (MAA) and a quaternized poly(2-(dimethylamino)ethyl methacrylate) (Dq) block, $B_{800}MAA_{200}Dq_{285}$ (M_n ~110 000 g/mol; PDI = 1.10) was synthesized *via* sequential living anionic polymerization followed by a postmodification of the third block by quaternization in a dioxane-water mixture (1:1).[35] In order to obtain micellar structures, the solution was dialyzed against a buffer solution (pH 4, VWR, AVS Titronium). Crosslinking of the PB core in BMAADq micelles was performed directly after the quaternization reaction in a dioxane/water mixture (1:1, v/v) by the addition of a UV photoinitiator, Lucirin TPO (2,4,6-tri-methylbenzoylphosphine oxide, BASF). 25 wt% Lucirin TPO, calculated according to the weight fraction of polybutadiene, were added to the polymer solution. After stirring for 1 hour, the mixture was dialyzed against pH 10 buffer solution light. Afterward, the micellar solution

was irradiated with a UV lamp (Hoehnle UVAHAND 250 GS, equipped with a quartz glass filter) under continuous stirring for 30 min.[37]

Poly(sodium 4-styrene sulfonate) (PSS, M_w = 70 000 g/mol) and quaternized poly(2-(dimethylamino)ethyl methacrylate) (Dq) were purchased from Sigma-Aldrich. In order to adjust the pH and ionic strength, HCl or NaOH solutions (0.1 M or 1 M, Grüssing) and NaCl (Grüssing) were used, respectively.

Sample Preparation. The fabrication of multilayer films was performed using the LbL technique.[3] Thereby, freshly cleaned silicon wafers (CrysTec) were dipped alternately into a BMAADq micelles buffer solution (pH 4, VWR, AVS Titrinorm, ionic strength ~0.05 M) with a concentration of ~0.46 M and an aqueous PSS solution (1 mg/mL, adjusted to pH 4 with 0.1 M HCl), each for 15 min. After every assembly step the excess of the deposited polymer was removed by rinsing the substrate with Milli-Q water. Finally, the films were dried in a nitrogen stream before characterization. Dq/PSS multilayers were prepared in the same way at pH 4, whereby micelles were replaced by Dq.

The substrates were cleaned using RCA method.[69] Thereby, silicon wafers were sonicated for 15 min in a 1:1 mixture of water and 2-propanol, and subsequently heated at 70 °C in a 5:1:1 mixture of water, ammonia (25%), and hydrogen peroxide (30%) for 10 min.

Ellipsometry. Ellipsometry measurements were performed with a Sentech SE 850 spectroscopic ellipsometer. For measurements in air, a constant incidence angle of 70° was set. Ellipsometric studies in water of different pH values and ionic strengths were performed in a home build liquid cell[70] at a constant incidence angle of 65°. Thereby, the pH solutions were changed *in situ* and the measurements conducted after a minimum equilibration time of 15 minutes. All measurements were performed in the spectral range 400 – 800 nm. Besides, a simple model of one-layer-film was used. The fitting of the data was performed using a Cauchy model.[71]

Atomic Force Microscopy. Atomic force microscopy (AFM) imaging was performed with a commercial AFM (Dimension 3100 equipped with a NanoScope V controller, both from Bruker AXS Inc., USA) operating in TappingMode™. Si_3N_4 cantilevers from Olympus with a typical spring constant of ~42 N/m and a typical resonance frequency of 300 kHz (OMCL-AC160TS) were used. The force measurements were performed on an Asylum MFP 3D AFM (Mannheim, Germany), in a droplet of MilliQ water with defined NaCl concentrations using the colloidal probe (CP) technique. Colloidal glass (SiO_2) particles (Polysciences, Germany) were used as force sensors. They were glued onto pre-calibrated cantilevers (force constant ~0.1 N/m, NSC 12, tipless, noAl, Micromash, Estonia) using an epoxy resin (UHU schnellfest, Germany), micromanipulator (MP-285, Shutter Instrument, USA) and an inverted microscope (Axiovert 200, Zeiss, Germany). The calibration of the cantilevers, or more precisely the determination of the spring constant of cantilever was performed using the thermal noise method introduced by Hutter and Bechhoefer.[72] All measurements of the presented data were performed

using a cantilever with a force constant of 0.285 N/m and a CP with R = 10.6 µm. The optical lever sensitivity was detected prior to the records of the data by reference measurements on a hard substrate (glass slide), for each ionic strength. The data was obtained from force mapping (36 data points on a 50 µm x 50 µm map).

Acknowledgment

This research was funded by BFHZ, SFB840, COST Action CM1101. OVB acknowledges support by Russian Science Foundation Grant No. 14-33-00003.

References

1. Iler, R. K., Multilayers of Colloidal Particles. *J. Colloid Interface Sci.* **1966,** *21*.
2. Decher, G.; Hong, J. D.; Schmitt, J., Buildup of Ultrathin Multilayer Films by a Self-Assembly Process. 3. Consecutively Alternating Adsorption of Anionic and Cationic Polyelectrolytes on Charged Surfaces. *Thin Solid Films* **1992,** *210*, 831-835.
3. Decher, G., Fuzzy Nanoassemblies: Toward Layered Polymeric Multicomposites. *Science* **1997,** *277*, 1232-1237.
4. Zhu, Z. C.; Sukhishvili, S. A., Layer-by-layer Films of Stimuli-Responsive Block Copolymer Micelles. *J. Mater. Chem.* **2012,** *22*, 7667-7671.
5. Dewald, I.; Fery, A., Polymeric Micelles and Vesicles in Polyelectrolyte Multilayers: Introducing Hierarchy and Compartmentalization. *Adv. Mater. Interfaces* **2017**, *4*, 1600317 (1-11).
6. Emoto, K.; Iijima, M.; Nagasaki, Y.; Kataoka, K., Functionality of Polymeric Micelle Hydrogels with Organized Three-Dimensional Architecture on Surfaces. *J. Am. Chem. Soc.* **2000,** *122*, 2653-2654.
7. Emoto, K.; Nagasaki, Y.; Kataoka, K., A Core-Shell Structured Hydrogel Thin Layer on Surfaces by Lamination of a Poly(ethylene glycol)-*b*-Poly(D,L-lactide) Micelle and Polyallylamine. *Langmuir* **2000,** *16*, 5738-5742.
8. Qi, B.; Tong, X.; Zhao, Y., Layer-by-Layer Assembly of Two Different Polymer Micelles with Polycation and Polyanion Coronas. *Macromolecules* **2006,** *39*, 5714-5719.
9. Bo, Q.; Tong, X.; Zhao, Y.; Zhao, Y., A micellar route to layer-by-layer assembly of hydrophobic functional polymers. *Macromolecules* **2008,** *41*, 3562-3570.
10. Cho, J.; Hong, J.; Char, K.; Caruso, F., Nanoporous Block Copolymer Micelle/Micelle Multilayer Films with Dual Optical Properties. *J. Am. Chem. Soc.* **2006,** *128*, 9935-9942.
11. Hong, J.; Bae, W. K.; Lee, H.; Oh, S.; Char, K.; Caruso, F.; Cho, J., Tunable Superhydrophobic and Optical Properties of Colloidal Films Coated with Block-Copolymer-Micelles/Micelle-Multilayers. *Adv. Mater.* **2007,** *19*, 4364-4369.
12. Biggs, S.; Sakai, K.; Addison, T.; Schmid, A.; Armes, S. P.; Vamvakaki, M.; Bütün, V.; Webber, G., Layer-by-Layer Formation of Smart Particle Coatings Using Oppositely Charged Block Copolymer Micelles. *Adv. Mater.* **2007,** *19*, 247-250.
13. Smith, E. G.; Webber, G. B.; Sakai, K.; Biggs, S.; Armes, S. P.; Wanless, E. J., Direct Visualization of a Self-Organized Multilayer Film of Low Tg Diblock Copolymer Micelles. *J. Phys. Chem. B* **2007,** *111*, 5536-5541.
14. Sakai, K.; Webber, G. B.; Vo, C.-D.; Wanless, E. J.; Vamvakaki, M.; Bütün, V.; Armes, S. P.; Biggs, S., Characterization of Layer-by-Layer Self-Assembled Multilayer Films of Diblock Copolymer Micelles. *Langmuir* **2008,** *24*, 116-123.

15. Addison, T.; Cayre, O. J.; Biggs, S.; Armes, S. P.; York, D., Polymeric Microcapsules Assembled from a Cationic/Zwitterionic Pair of Responsive Block Copolymer Micelles. *Langmuir* **2010,** *26*, 6281-6286.

16. Hong, J.; Park, H., Fabrication and Characterization of Block Copolymer Micelle Multilayer Films Prepared Using Dip-, Spin- and Spray-Assisted Layer-by-Layer Assembly Deposition. *Colloids Surf., A* **2011,** *381*, 7-12.

17. Hong, J.; Cho, J.; Char, K., Hollow Capsules Prepared from all Block Copolymer Micelle Multilayers. *J. Colloid Interface Sci.* **2011,** *364*, 112-117.

18. Ma, N.; Zhang, H. Y.; Song, B.; Wang, Z. Q.; Zhang, X., Polymer Micelles as Building Blocks for Layer-by-Layer Assembly: An Approach for Incorporation and Controlled Release of Water-Insoluble Dyes. *Chem. Mater.* **2005,** *17*, 5065-5069.

19. Ma, N.; Wang, Y. P.; Wang, Z. Q.; Zhang, X., Polymer Micelles as Building Blocks for the Incorporation of Azobenzene: Enhancing the Photochromic Properties in Layer-by-Layer Films. *Langmuir* **2006,** *22*, 3906-3909.

20. Ma, N.; Wang, Y.; Wang, B.; Wang, Z.; Zhang, X.; Wang, G.; Zhao, Y., Interaction between Block Copolymer Micelles and Azobenzene-Containing Surfactants: From Coassembly in Water to Layer-by-Layer Assembly at the Interface. *Langmuir* **2007,** *23*, 2874-2878.

21. Zhao, Y.; Bertrand, J.; Tong, X.; Zhao, Y., Photo-Cross-Linkable Polymer Micelles in Hydrogen-Bonding-Built Layer-by-Layer Films. *Langmuir* **2009,** *25*, 13151-13157.

22. Zhu, Y.; Tong, W.; Gao, C.; Möhwald, H., Assembly of Polymeric Micelles into Hollow Microcapsules with Extraordinary Stability against Extreme pH Conditions. *Langmuir* **2008,** *24*, 7810-7816.

23. Kang, E.; Lee, S. C.; Park, K., Layer-by-layer Assembly of Poly(lactic-co-glycolic acid)-*b*-Poly(l-lysine) Copolymer Micelles. *NanoBiotechnology* **2007,** *3*, 96-103.

24. Addison, T.; Cayre, O. J.; Biggs, S.; Armes, S. P.; York, D., Incorporation of Block Copolymer Micelles into Multilayer Films for Use as Nanodelivery Systems. *Langmuir* **2008,** *24*, 13328-13333.

25. Kim, B.-S.; Park, S. W.; Hammond, P. T., Hydrogen-Bonding Layer-by-Layer Assembled Biodegradable Polymeric Micelles as Drug Delivery Vehicles from Surfaces. *ACS Nano* **2008,** *2*, 386-392.

26. Kim, B.-S.; Smith, R. C.; Poon, Z.; Hammond, P. T., MAD (Multiagent Delivery) Nanolayer: Delivering Multiple Therapeutics from Hierarchically Assembled Surface Coatings. *Langmuir* **2009,** *25*, 14086-14092.

27. Zhu, Z.; Sukhishvili, S. A., Temperature-Induced Swelling and Small Molecule Release with Hydrogen-Bonded Multilayers of Block Copolymer Micelles. *ACS Nano* **2009,** *3*, 3595-3605.

28. Erel, I.; Zhu, Z.; Zhuk, A.; Sukhishvili, S. A., Hydrogen-Bonded Layer-by-Layer Films of Block Copolymer Micelles with pH-Responsive Cores. *J. Colloid Interface Sci.* **2011,** *355*, 61-69.

29. Xu, L.; Zhu, Z.; Sukhishvili, S. A., Polyelectrolyte Multilayers of Diblock Copolymer Micelles with Temperature-Responsive Cores. *Langmuir* **2011,** *27*, 409-415.

30. Zhuk, A.; Xu, L.; Ankner, J. F.; Sukhishvili, S. A., Selective Water Uptake within Micelle-Containing Layer-by-Layer Films of Various Architectures: A Neutron Reflectometry Study. *Soft Matter* **2013,** *9*, 410-417.

31. Zhu, Z. C.; Gao, N.; Wang, H. J.; Sukhishvili, S. A., Temperature-Triggered On-Demand Drug Release Enabled by Hydrogen-Bonded Multilayers of Block Copolymer Micelles. *J. Controlled Release* **2013,** *171*, 73-80.

32. Tan, W. S.; Cohen, R. E.; Rubner, M. F.; Sukhishvili, S. A., Temperature-Induced, Reversible Swelling Transitions in Multilayers of a Cationic Triblock Copolymer and a Polyacid. *Macromolecules* **2010,** *43*, 1950-1957.

33. Tan, W. S.; Zhu, Z. C.; Sukhishvili, S. A.; Rubner, M. F.; Cohen, R. E., Effect of Block Copolymer Architecture on the Thermally Induced Swelling of Micelle-Containing Multilayer Thin Films. *Macromolecules* **2011,** *44*, 7767-7774.

34. Gensel, J.; Dewald, I.; Erath, J.; Betthausen, E.; Müller, A. H. E.; Fery, A., Reversible Swelling Transitions in Stimuli-Responsive Layer-by-Layer Films Containing Block Copolymer Micelles. *Chem. Sci.* **2013,** *4*, 325-334.
35. Betthausen, E.; Drechsler, M.; Förtsch, M.; Schacher, F. H.; Müller, A. H. E., Dual Stimuli-Responsive Multicompartment Micelles from Triblock Terpolymers with Tunable Hydrophilicity. *Soft Matter* **2011,** *7*, 8880-8891.
36. Dautzenberg, H.; Jaeger, W.; Kötz, J.; Philipp, B.; Seidel, C.; Stscherbina, D., *Polyelectrolytes*. Carl Hanser Verlag: München, 1994.
37. Betthausen, E.; Drechsler, M.; Förtsch, M.; Pergushov, D. V.; Schacher, F. H.; Müller, A. H. E., Stimuli-Responsive Micellar Interpolyelectrolyte Complexes - Control of Micelle Dynamics *via* Core Crosslinking. *Soft Matter* **2012,** *8*, 10167-10177.
38. Gensel, J.; Betthausen, E.; Hasenöhrl, C.; Trenkenschuh, K.; Hund, M.; Boulmedais, F.; Schaaf, P.; Müller, A. H. E.; Fery, A., Surface Immobilized Block Copolymer Micelles with Switchable Accessibility of Hydrophobic Pockets. *Soft Matter* **2011,** *7*, 11144-11153.
39. von Klitzing, R., Internal Structure of Polyelectrolyte Multilayer Assemblies. *PCCP* **2006,** *8*, 5012-5033.
40. Jomaa, H. W.; Schlenoff, J. B., Accelerated Exchange in Polyelectrolyte Multilayers by "Catalytic" Polyvalent Ion Pairing. *Langmuir* **2005,** *21*, 8081-8084.
41. Kabanov, V. A., Polyelectrolyte Complexes in Solution and in Bulk. *Russ. Chem. Rev.* **2005,** *74*, 3.
42. Schacher, F.; Yuan, J. Y.; Schoberth, H. G.; Müller, A. H. E., Synthesis, Characterization, and Bulk Crosslinking of Polybutadiene-*block*-Poly(2-vinyl pyridine)-*block*-Poly(*tert*-butyl methacrylate) Block Terpolymers. *Polymer* **2010,** *51*, 2021-2032.
43. Dewald, I.; Gensel, J.; Betthausen, E.; Borisov, O. V.; Müller, A. H. E.; Schacher, F. H.; Fery, A., Splitting of Surface-Immobilized Multicompartment Micelles into Clusters upon Charge Inversion. *ACS Nano* **2016,** *10*, 5180-5188.
44. Biesalski, M.; Johannsmann, D.; Rühe, J., Electrolyte-Induced Collapse of a Polyelectrolyte Brush. *J. Chem. Phys.* **2004,** *120*, 8807-8814.
45. Fleer, G. J., Polyelectrolyte Brushes and Polyelectrolyte Adsorption Lasers. *Ber. Bunsen-Ges. Phys. Chem. Chem. Phys.* **1996,** *100*, 936-942.
46. Born, M.; Wolf, E., *Principles of Optics*. Chambridge University Press: Cambridge, 1999.
47. Jomaa, H. W.; Schlenoff, J. B., Salt-Induced Polyelectrolyte Interdiffusion in Multilayered Films: A Neutron Reflectivity Study. *Macromolecules* **2005,** *38*, 8473-8480.
48. Dubas, S. T.; Schlenoff, J. B., Swelling and Smoothing of Polyelectrolyte Multilayers by Salt. *Langmuir* **2001,** *17*, 7725-7727.
49. Ruiz-Pérez, L.; Pryke, A.; Sommer, M.; Battaglia, G.; Soutar, I.; Swanson, L.; Geoghegan, M., Conformation of Poly(methacrylic acid) Chains in Dilute Aqueous Solution. *Macromolecules* **2008,** *41*, 2203-2211.
50. de Gennes, P. G., Conformations of Polymers Attached to an Interface. *Macromolecules* **1980,** *13*, 1069-1075.
51. Currie, E. P. K.; Sieval, A. B.; Fleer, G. J.; Stuart, M. A. C., Polyacrylic Acid Brushes: Surface Pressure and Salt-Induced Swelling. *Langmuir* **2000,** *16*, 8324-8333.
52. Parnell, A. J.; Martin, S. J.; Dang, C. C.; Geoghegan, M.; Jones, R. A. L.; Crook, C. J.; Howse, J. R.; Ryan, A. J., Synthesis, Characterization and Swelling Behaviour of Poly(methacrylic acid) Brushes Synthesized Using Atom Transfer Radical Polymerization. *Polymer* **2009,** *50*, 1005-1014.
53. Israels, R.; Leermakers, F. A. M.; Fleer, G. J., On the Theory of Grafted Weak Polyacids. *Macromolecules* **1994,** *27*, 3087-3093.
54. Pincus, P., Colloid Stabilization With Grafted Polyelectrolytes. *Macromolecules* **1991,** *24*, 2912-2919.

55. Zhulina, E. B.; Birshtein, T. M.; Borisov, O. V., Theory of Ionizable Polymer Brushes. *Macromolecules* **1995,** *28*, 1491-1499.
56. Balastre, M.; Li, F.; Schorr, P.; Yang, J. C.; Mays, J. W.; Tirrell, M. V., A Study of Polyelectrolyte Brushes Formed from Adsorption of Amphiphilic Diblock Copolymers Using the Surface Forces Apparatus. *Macromolecules* **2002,** *35*, 9480-9486.
57. Ballauff, M.; Borisov, O., Polyelectrolyte Brushes. *Curr. Opin. Colloid Interface Sci.* **2006,** *11*, 316-323.
58. Bhat, R. R.; Tomlinson, M. R.; Wu, T.; Genzer, J., Surface-Grafted Polymer Gradients: Formation, Characterization, and Applications. In *Surface-Initiated Polymerization II*, Springer: Berlin, 2006; Vol. 198, pp 51-124.
59. Biesalski, M.; Johannsmann, D.; Rühe, J., Synthesis and Swelling Behavior of a Weak Polyacid Brush. *J. Chem. Phys.* **2002,** *117*, 4988-4994.
60. Biesalski, M.; Ruhe, J.; Johannsmann, D., Segment Density Profiles of Polyelectrolyte Brushes Determined by Fourier Transform Ellipsometry. *J. Chem. Phys.* **1999,** *111*, 7029-7037.
61. Guo, X.; Ballauff, M., Spherical Polyelectrolyte Brushes: Comparison between Annealed and Quenched Brushes. *Phys. Rev. E* **2001,** *64*, 9.
62. Rühe, J.; Ballauff, M.; Biesalski, M.; Dziezok, P.; Gröhn, F.; Johannsmann, D.; Houbenov, N.; Hugenberg, N.; Konradi, R.; Minko, S.; Motornov, M.; Netz, R. R.; Schmidt, M.; Seidel, C.; Stamm, M.; Stephan, T.; Usov, D.; Zhang, H., Polyelectrolyte Brushes. In *Polyelectrolytes with Defined Molecular Architecture I*, Schmidt, M., Ed. Springer: Berlin Heidelberg, 2004; Vol. 165.
63. Geoghegan, M.; Ruiz-Pérez, L.; Dang, C. C.; Parnell, A. J.; Martin, S. J.; Howse, J. R.; Jones, R. A. L.; Golestanian, R.; Topham, P. D.; Crook, C. J.; Ryan, A. J.; Sivia, D. S.; Webster, J. R. P.; Menelle, A., The pH-Induced Swelling and Collapse Atom Transfer Radical Polymerization. *Soft Matter* **2006,** *2*, 1076-1080.
64. Borisov, O. V.; Zhulina, E. B.; Leermakers, F. A. M.; Ballauff, M.; Müller, A. H. E., Conformations and Solution Properties of Star-Branched Polyelectrolytes. In *Self Organized Nanostructures of Amphiphilic Block Copolymers I*, Müller, A. H. E.; Borisov, O., Eds. Springer: Berlin, 2011; Vol. 241, pp 1-55.
65. Butt, H. J., Measuring Electrostatic, Van der Waals, and Hydration Forces in Electrolyte-Solutions with an Atomic Force Microscope. *Biophys. J.* **1991,** *60*, 1438-1444.
66. Ducker, W. A.; Senden, T. J.; Pashley, R. M., Direct Measurement of Colloidal Forces Using an Atomic Force Microscope. *Nature* **1991,** *353*, 239-241.
67. Hertz, H., Über die Berührung fester elastischer Körper. *Journal für die reine und angewandte Mathematik* **1881,** *92*, 156-171.
68. Heuvingh, J.; Zappa, M.; Fery, A., Salt Softening of Polyelectrolyte Multilayer Capsules. *Langmuir* **2005,** *21*, 3165-3171.
69. Kern, W.; Puotinen, D. A., Cleaning Solutions Based on Hydrogen Peroxide for Use in Silicon Semiconductor Technology. *RCA Review* **1970,** *31*, 187.
70. Elbs, H.; Krausch, G., Ellipsometric Determination of Flory-Huggins Interaction Parameters in Solution. *Polymer* **2004,** *45*, 7935-7942.
71. Fujiwara, H., *Spectroscopic Ellipsometry: Principles and Applications*. Wiley: Chichester, 2007.
72. Hutter, J. L.; Bechhoefer, J., Calibration of Atomic-Force Microscope Tips. *Rev. Sci. Instrum.* **1993,** *64*, 1868-1873.

Danksagung

An dieser Stelle möchte ich all jenen danken, die diese Arbeit ermöglicht und zu ihrem Gelingen beigetragen haben.

An erster Stelle möchte ich mich bei meinem Doktorvater Prof. Dr. Andreas Fery bedanken. Vielen Dank für das spannende Thema, die – sowohl wissenschaftlich als auch menschlich – lehrreiche Betreuung, und die Möglichkeit an zahlreichen Konferenzen teilzunehmen und nebenbei ein wenig die Welt zu bereisen. Danke auch für die Motivation und die Unterstützung!

Auch bei Julia Gensel und Johann Erath, von denen ich in der Zeit vor der Promotion viel gelernt habe, möchte ich mich ganz herzlich bedanken! Vielen Dank für eure Hilfsbereitschaft und Euer Wissen, dass ihr mit mir geteilt habt! Außerdem möchte ich mich bei Munish Chanana bedanken, der mich im ersten Jahr meiner Promotion begleitet hat und stets einen Rat und eine witzige Geschichte parat hatte.

Liebe Sybille, vielen Dank für alles – die tolle Deko, die familiäre Atmosphäre am Lehrstuhl und dafür, dass Du dich so liebevoll um alle kümmerst!

An dieser Stelle möchte ich auch all meinen Kooperationspartnern für die erfolgreiche Zusammenarbeit danken. Mein besonderer Dank geht an die AG Müller: Eva Betthausen und Felix Schacher möchte ich für die Mizellen danken, die diese Arbeit erst möglich gemacht haben!
Bei unseren Technikern und wissenschaftlichen Angestellten Petra Zippelius, Carmen Kunert, Markus Hund und Wolfgang Häfner möchte ich mich ebenfalls bedanken. Vielen Dank für eure Hilfsbereitschaft!
Ich danke auch allen Praktikanten und HiWis. Ein besonderer Dank geht dabei an Olga Isakin: Vielen Dank für die tolle Zusammenarbeit und dein Engagement während der Masterarbeit!

Liebe PC II – vielen Dank für diese schöne Zeit! Gemeinsame Kaffeepausen, Grillen auf der Terrasse, diverse Freizeitaktivitäten, aber auch die „Telefonkonferenzen“ haben die Zeit am Lehrstuhl unglaublich bereichert! Vielen Dank dafür! An dieser Stelle möchte ich einen besonderen Dank an zwei sehr lieb gewonnene Kollegen, Pavel Cherepanov und Inga Melnyk aussprechen: Дорогие мои, спасибо вам за то что не даете забыть русский язык, за наши совместные отпуски, всякие другие глупости и просто весело проведенное время! Bei allen meinen Bürokollegen Mareen Müller, Olga Isakin, Anja Steiner, Yannic Brasse, Christoph Hanske, Maximilian Seuß, Jens Neubauer und Benedikt Neugirg möchte ich mich für die angenehme Arbeitsatmosphäre sowie für zahlreiche wissenschaftliche

Diskussionen und Tipps bedanken! Bei Ben und der AG Papastavrou, insbesondere Nicolas Helfricht, möchte ich mich für das letzte Jahr bedanken. Ohne euch wäre es nach dem Dresden-Umzug am Lehrstuhl ziemlich trist geworden.

Bei Pavel, Ben, Nico, Inga, Jens, Yannic, Julia und Julia Rattke möchte ich mich für das Korrekturlesen von Abschnitten meiner Arbeit bedanken.

Ein ganz besonderer Dank gilt aber meinen Eltern und meinem Bruder, die mich immer nach Kräften unterstützt, mir immer den Rücken gestärkt haben und ohne die so vieles nicht möglich gewesen wäre. Любимые мама и папа! Спасибо вам за все - за ваше терпение, доверие и лубовь! Спасибо за вашу помошь в трудные моменты и полезный совет в любой ситуации!

(Eidesstattliche) Versicherungen und Erklärungen

(§ 8 Nr. 6 PromO BayNAT)

Hiermit erkläre ich mich einverstanden, dass die elektronische Fassung der Dissertation unter Wahrung meiner Urheberrechte und des Datenschutzes einer gesonderten Überprüfung hinsichtlich der eigenständigen Anfertigung meiner Dissertation unterzogen werden kann.

(§ 8 Nr. 8 PromO BayNAT)

Hiermit erkläre ich an Eides statt, dass ich diese Arbeit selbständig verfasst und keine anderen als die von mir angegebenen Quellen und Hilfsmittel benutzt habe.

(§ 8 Nr. 9 PromO BayNAT)

Hiermit erkläre ich, dass ich nicht bereits anderweitig ohne Erfolg versucht habe, eine Dissertation einzureichen oder mich der Doktorprüfung zu unterziehen.

(§ 8 Nr. 10 PromO BayNAT)

Hiermit erkläre ich, dass ich keine Hilfe von gewerblichen Promotionsberatern bzw. -vermittlern in Anspruch genommen habe und diese auch künftig nicht in Anspruch nehmen werde.

Bayreuth, den

.....

Inna Dewald